Technical Report C89-02
March 1990



# TECHNICAL REPORT FOR THE PERIOD 1 OCTOBER 1987 - 30 SEPTEMBER 1989

Center Staff





SPONSORED BY:
DEFENSE ADVANCED RESEARCH PROJECTS AGENCY

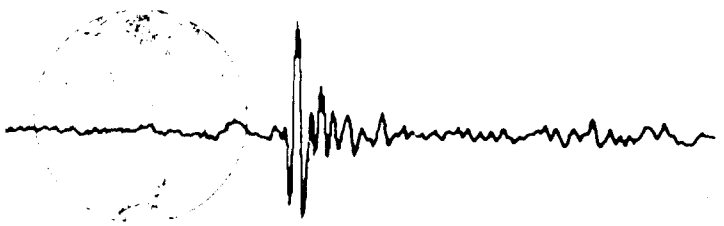

Center for Seismic Studies
1300 N. 17th Street, Suite 1450
Arlington, Virginia 22209-3871
Telephone: (703) 276-7900

Technical Report C89-02
March 1990

# TECHNICAL REPORT FOR THE PERIOD 1 OCTOBER 1987 - 30 SEPTEMBER 1989

Center Staff

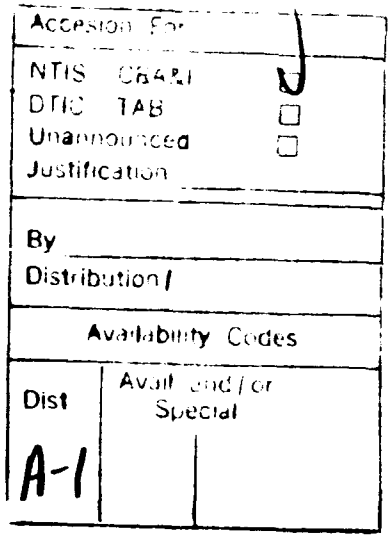


APPROVED FOR PUBLIC RELEASE
DISTRIBUTION UNLIMITED



Sponsored by:
DEFENSE ADVANCED RESEARCH PROJECTS AGENCY
Monitored by:
Defense Supply Service - Washington
Under Contract No. MDA903-87-C-0037

Science Applications International Corp.
1300 N. 17th Street, Suite 1450
Arlington, VA 22202

UNCLASSIFIED
SECURITY CLASSIFICATION OF THIS PAGE

# REPORT DOCUMENTATION PAGE

Form Approved
OMB No 0704-0188
Exp Date Jun 30, 1986

| | |
|---|---|
| 1a REPORT SECURITY CLASSIFICATION<br>UNCLASSIFIED | 1b RESTRICTIVE MARKINGS<br>None |
| 2a SECURITY CLASSIFICATION AUTHORITY | 3 DISTRIBUTION / AVAILABILITY OF REPORT<br>Unlimited |
| 2b DECLASSIFICATION / DOWNGRADING SCHEDULE | |
| 4 PERFORMING ORGANIZATION REPORT NUMBER(S)<br>Technical Report C89-02<br>SAIC-90/1167 | 5 MONITORING ORGANIZATION REPORT NUMBER(S)<br>- |
| 6a NAME OF PERFORMING ORGANIZATION<br>Science Applications International Corporation<br>6b OFFICE SYMBOL (If applicable) | 7a NAME OF MONITORING ORGANIZATION<br>Defense Supply Service-Washington |
| 6c ADDRESS (City, State, and ZIP Code)<br>Center for Seismic Studies<br>1300 N. 17th Street, Suite 1450<br>Arlington, VA 22209 | 7b ADDRESS (City, State, and ZIP Code)<br>Room 1D245, The Pentagon<br>Washington, DC 20310 |
| 8a NAME OF FUNDING / SPONSORING ORGANIZATION Defense Advances Research Projects Agency<br>8b OFFICE SYMBOL (If applicable)<br>NMRO | 9 PROCUREMENT INSTRUMENT IDENTIFICATION NUMBER<br>MDA903-87-C-0037 |
| 8c ADDRESS (City, State, and ZIP Code)<br>1400 Wilson Boulevard<br>Arlington, VA 22209 | 10 SOURCE OF FUNDING NUMBERS<br>PROGRAM ELEMENT NO / PROJECT NO. / TASK NO / WORK UNIT ACCESSION NO |

11 TITLE (Include Security Classification)
Technical Report for the Period 1 October 1987 - 30 September 1989

12 PERSONAL AUTHOR(S) A. Ryall, J. Coyne, A. Henson, H. Israelsson, V. Ryaboy

| 13a TYPE OF REPORT | 13b TIME COVERED | 14 DATE OF REPORT (Year, Month, Day) | 15 PAGE COUNT |
|---|---|---|---|
| Technical | FROM 1/10/87 TO 10/9/89 | 1990 March | 215 |

16 SUPPLEMENTARY NOTATION

| 17 COSATI CODES | | | 18 SUBJECT TERMS (Continue on reverse if necessary and identify by block number) |
|---|---|---|---|
| FIELD | GROUP | SUB-GROUP | Seismology, Seismic Identification, Nuclear Monitoring, Mantle Structure, Polarization Analysis, High Frequency Seismic Waves, Regional Seismic Waves, |
| | | | |
| | | | |

19 ABSTRACT (Continue on reverse if necessary and identify by block number)

This report describes research conducted by the Center for Seismic Studies during the period 1 October 1987 through 30 September 1989. Section 1 is a preliminary report on high frequency waves recorded by several seismic stations in the U.S.S.R. This work is continuing on another contract. Section 2 covers results of several studies, including the development of an improved crustal and upper mantle model for the Baltic shield and western U.S.S.R. using data from mining blasts recorded at NORESS; an analysis of the relative ability of 3-component and array stations to determine azimuth of seismic sources; a study of the design requirements of seismic networks for global monitoring using observations from the 1984 GSE Technical Test as the basis; and a study of the effect of source radiation patterns on the detectability of P, pP and sP. Section 3 contains four short summaries of work partly supported under this contract, but which have been or will be fully reported elsewhere. Section 4 describes software developed under this project which has been made available to other researchers through normal Center support functions. Keywords:

| 20 DISTRIBUTION / AVAILABILITY OF ABSTRACT | 21 ABSTRACT SECURITY CLASSIFICATION |
|---|---|
| ☒ UNCLASSIFIED/UNLIMITED ☐ SAME AS RPT ☐ DTIC USERS | UNCLASSIFIED |

| 22a NAME OF RESPONSIBLE INDIVIDUAL | 22b TELEPHONE (Include Area Code) | 22c OFFICE SYMBOL |
|---|---|---|
| Ralph W. Alewine | (202) 694-3622 | DARPA/NMRO |

DD FORM 1473, 84 MAR — 83 APR edition may be used until exhausted. All other editions are obsolete.

SECURITY CLASSIFICATION OF THIS PAGE
UNCLASSIFIED

# Table of Contents

## FOREWORD

This report describes work conducted by the Center for Seismic Studies research staff under contract MDA903-87-C-0037, over the period 1 October 1987 to 30 September 1989. This effort was undertaken in response to redirection of the *Intelligent Array System (IAS)* development contract by DARPA, and included the tasks described in the following paragraphs. Accomplishments under each of these tasks are summarized in this Foreword, and described in detail in the papers that make up the remainder of this Technical Report.

A. Refine the Detection and Post-Detection Algorithms.

One study under this task, to evaluate a Soviet technique for determining event size using comb-filtered seismic recordings at regional distance ranges, was not undertaken. The need for this investigation was obviated by the success of Norwegian seismologists in using measurements of Lg waves recorded at NORESS for consistent determinations of magnitude for explosions at the Soviet Eastern Kazakh test site. Additional effort was directed toward other tasks that emerged as more important, particularly work to refine the structural model of the earth's crust and upper mantle in the region east of the NORESS array, described under Task B.

A second element under this task was to study high-frequency characteristics of regional events recorded by stations operated jointly by the National Resources Defense Council and the Soviet Academy of Sciences in eastern Kazakh. Work done under this element by Anne Henson was directed toward the use of three-dimensional spectrogram plots as a post-detection analyst tool for discriminating between regional earthquakes and mine blasts. The results of this analysis were quite promising, and are summarized in Section 1.1. A full report on this investigation, which was partly supported by an AFGL contract to study high-frequency propagation, is contained in Center report C89-01.

B.Improve the Capability to Locate Events with a Network of Arrays and Single Stations.

Under this task, Vlad Ryaboy conducted a detailed study of NORESS recordings of approximately 150 mine explosions along a profile from NORESS to Helsinki to Leningrad. The events were 250-1,300 km from NORESS and had local magnitude in the range 2.0-3.5. Event locations and origin times were constrained by the University of Helsinki's regional seismic network bulletins. Combined analysis of the explosion signals together with results of gravity and other geophysical investigations taken from the literature indicate the presence of a pronounced low-velocity layer in the upper mantle beneath the Baltic shield, in the depth range 105-135 km. This conclusion is important in two respects. First,

accurate knowledge of crust-upper mantle structure is essential in order to obtain accurate location of events recorded by the various new arrays in Scandinavia and Germany, and the model obtained in this study represents an improvement over previous structural models available for the Baltic shield and western USSR. Second, low-velocity layers in the upper mantle have a drastic effect on the propagation of high-frequency seismic signals, and the particular model obtained in this study offers a possible explanation for the observation by Ringdal and Mykkeltveit that the high-frequency content of regional seismic signals decreases abruptly at distances of 700-800 km. A detailed report on Ryaboy's investigation is given in Section 2.1. Results of this study have been reported at the DARPA/AFGL and DARPA/AFTAC seismic research symposia, respectively in May and November 1989, and at the western AGU meeting in December 1989. The study will also be presented at the NORSAR symposium in February 1990, and submitted to the Bulletin of the Seismological Society of America for possible publication.

In the area of three-component analysis related to event location, Anne Henson has reviewed methods proposed by various authors for extracting polarization characteristics of seismic signals, and has also conducted an observational investigation to compare the accuracy of three-component analysis at single stations with results of analyzing array data. The review of polarization methods, presented in Section 2.2, leads to the recommendation that the eigensystem deconvolution method proposed by Jurkevics (1988) is preferred to other methods, because it operates in the time domain, provides information on S-type phases as well as P-waves, and has been adapted for array processing of 3-component and array stations for estimating azimuth and wave slowness. The conclusions of this study, described in detail in Section 2.3, indicate that the capability depends critically on signal-to-noise ratio (SNR). For sufficient SNR, however, both methods compare favorably, with only a slightly better performance for the frequency-wavenumber method used to process data from the array. Results of this study were presented as a report to the UN Conference on Disarmament, Group of Scientific Experts, in July 1989, and will be presented at the NORSAR symposium in February 1990 and subsequently submitted to the Bulletin of the Seismological Society of America for possible publication.

Under an element of Task B to quantify the observability of depth phases in a global monitoring system, Hans Israelsson has conducted a detailed investigation aimed at the design of networks for global monitoring of test ban treaties. Three major requirements are assumed for monitoring networks -- geographical uniformity, balance between seismological functions, and monitoring capabilities superior to other existing networks. From these requirements, Israelsson characterizes the major seismological functions for a network, defines station selection procedures, and evaluates the capabilities of the various functions in relation to

number and types of seismic stations in the network. Recommendations of this study, which is included in Section 2.4, focus on the use of array stations to improve sensitivity in key regions, use of master event techniques for event location, incorporation of a sufficient number of stations to accurately determine depth of detected events, and use of long-period data for Ms magnitude determination. The study relies on observations from the 1984 GSE Technical Test as the basis for capability estimates.

In a second paper related to depth determination, Israelsson has completed a preliminary study of depth estimation based on an approach developed by Pearce (1977, 1980), which utilizes amplitude ratios of reflected to direct arrivals -- pP/P and sP/P. Israelsson attempts to account for the effect of source radiation patterns on the observability of depth phases pP and sP, and in a summary given in Section 2.5, he examines this problem from both theoretical as well as observational points of view.

C. Acquire the Knowledge Necessary to Identify Events.

Work under this task is described in several reports. In the first, Israelsson studied waveforms recorded by the NORESS high-frequency element from 137 small events in a mining district in Sweden, and developed a case-based approach using cluster analysis to group the events by correlation analysis. The latter utilized the covariance matrix of three-component recordings, following the method developed by Jurkevics (1987). The study, summarized in the Proceedings of the May 1989 DARPA/AFGL Seismic Research Symposium, was partly supported by an AFGL contract to analyze high-frequency signals, and a complete report on the method and results is given in Center report C89-01. In the present report, Section 3.1 gives a summary of this study.

In Section 3.2, Henson summarizes results of an investigation of spectrogram characteristics of regional events recorded by NORESS and the NRDC seismic network in eastern Kazakh. This study was partly supported by the AFGL contract to investigate high-frequency propagation, and is reported in detail as part of Center report C89-01. Results of the analysis, presented at the DARPA/AFGL Seismic Research Symposium in May 1989, indicate that spectrograms can be extremely useful as an analyst tool for discriminating ripple-fired mine blasts from earthquakes.

In Sections 3.3 and 3.4, respectively, Israelsson summarizes a study on the usefulness of the mb-Ms method of event identification and work done to improve the automatic association program used in the 1984 GSE Technical Test. The main conclusion of the Ms study is that use of maximum likelihood techniques for estimating mb and Ms could eliminate the gap between detection and identification thresholds, but in order to apply such techniques the detection

threshold for surface waves would have to be lowered below the theoretical threshold of about Ms 3.5. As a result, substantial improvements in use of mb-Ms estimates for small events are not envisioned. In Section 3.4, Israelsson describes an approach to reduce the number of spurious events in the output of the automatic association program. This approach sets up rules for identifying multiple and split events, so that these events can be flagged for interpretation by the analyst.

Section 3.5 summarizes a demonstration presented at the October 1987 International Data Center (IDC) Workshop, under GSE auspices. The demonstration was designed to show how supplementary waveform data might have been used to resolve problems that the Stockholm, Moscow and Washington IDC's failed to reconcile during the 1984 GSE Technical Test. The demonstration involved assembly of a set of analysis software tools that have since been distributed to other agencies involved in nuclear monitoring research. The tools have also been distributed to other countries, including Finland and the USSR.

In addition to the research reports summarized above, a number of classified reports were prepared by Alan Ryall at DARPA's request. These dealt with matters related to the ongoing Nuclear Testing Talks with the USSR, and with the Joint Verification Experiment that took place in 1988. Using support under this contract, Ryall also participated as a member of the US Delegation to the Nuclear Testing Talks, travelling to Geneva and the USSR on DOD invitational travel orders on several occasions in 1987 and 1988.

D. Implement the Seismology and Graphics Software.

Under this task, the Center research staff was to collect, modify, document and install software appropriate for interactive analysis of seismic data on Sun workstations at the Center, and to test these programs to determine which of them might be integrated into an analysis concept incorporating the expert system. Section 4.1 of this report summarizes software that John Coyne, working with the Teledyne-Geotech group at the Center (primarily Mary Ann Brennan) has installed for the use of Center researchers.

Alan Ryall

## 1.1 SUMMARY OF STUDY OF HIGH-FREQUENCY CHARACTERISTICS OF EVENTS RECORDED BY THE NRDC NETWORK

### 1.1.1 Introduction

The use of 3-D spectrogram plots to characterize regional events has been investigated and reported elsewhere (Suteau-Henson, 1989). Part of that study uses events recorded at the NORESS array, and addresses the question of how events can be characterized by comparison with previous events at the same location. It is summarized in Section 3.2 of this report. Here, we summarize the part of that study concerning the high-frequency characteristics of events recorded by the NRDC network in Eastern Kazakhstan near the Semipalatinsk Test Site.

Analysis of such events enables us to study spectral characteristics (such as spectral complexity and modulations) for data recorded at a single station without the benefits of array-averaging. Spectrograms are built from high-frequency spectra covering the entire event. This technique is described elsewhere (Suteau-Henson, 1989, and Section 3.2 of this report). The dataset includes calibration shots recorded by the NRDC network, recordings of the Soviet nuclear explosion "JVE2" at the same sites, and a set of unidentified events in that area.

### 1.1.2 Results

We used the spectrogram technique to study events (mostly local) recorded at one or two single stations of the NRDC network, located in Eastern Kazakhstan near the Soviet Test Site, and consisting of three three-component stations at Karkaralinsk (KKL), Karasu (KSU) and Bayanaul (BAY). Station KSU was not used, because of a pronounced resonance peak due to near-receiver structure. The NRDC short-period data have a Nyquist frequency of 125 Hz, but we found that the useful frequency range was limited to half of that.

*Figure 1* (top) shows the spectrogram at station BAY for one of three known H.E. calibration shots. These are single explosions, and, as expected, no spectral modulations are observed. Since no array-averaging could be performed, the non-stationarity of the noise produces many noise peaks after noise correction. Also, the scatter in the spectrograms is much larger than for NORESS events (see Section 3.2). We also obtained spectrograms for a nuclear explosion, the JVE2 event at the Soviet Test Site, recorded with instruments of the University of Nevada-Reno. One is shown in *Figure 1* (bottom). As expected, no spectral modulations are observed. Above ≈ 30 Hz, the spectral amplitude above noise level remains roughly constant, instead of continuing to decay, as it does for the calibration shots. The character of the data above 30 Hz seems to indicate an instrument-related artifact, correlated with the actual signal, so we cannot ascertain that the source of the JVE2 event was

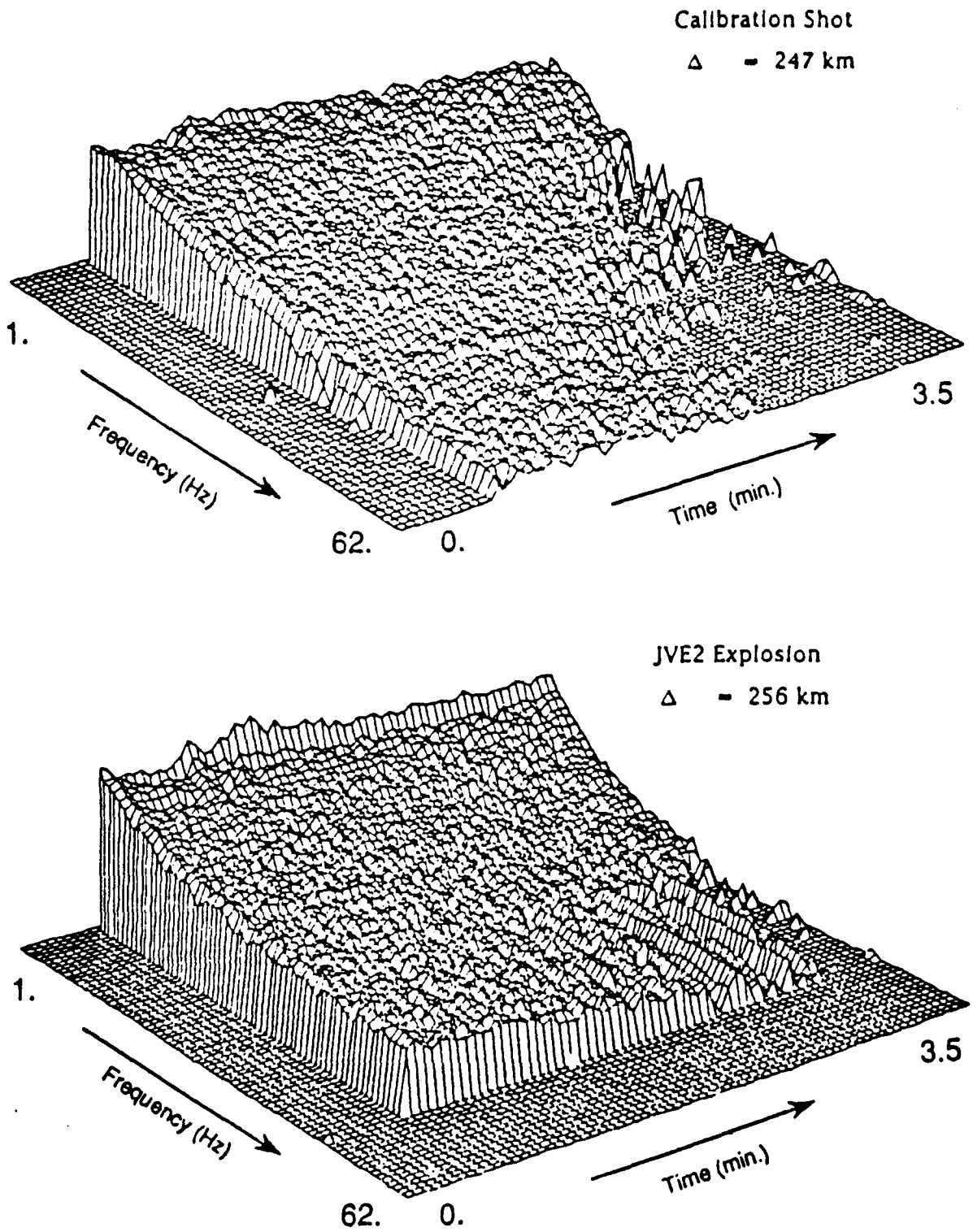


*Figure 1.* Spectrograms of two single explosions at NRDC station BAY. Top: Calibration shot. Bottom: JVE2 nuclear explosion at Semipalatinsk Test Site, recorded by the University of Nevada-Reno (the data have a Nyquist frequency of 50 Hz).

particularly rich in higher frequencies.

Finally, we analyzed a set of unidentified events recorded at the NRDC stations. *Figure 2* (top) shows the spectrogram for a presumed local mine blast, at station BAY. This and some other presumed explosions show spectral modulations (similar at all stations that detected), but others do not. Hedlin *et al.* (1988) report observing such modulations for presumed explosions, indicating ripple-firing. The spectrogram at station BAY for a presumed earthquake at ≈ 1100 km (*Figure 2*, bottom) has no complex character, as expected.

### 1.1.3 Conclusions

The high-frequency characteristics of events (mostly local) recorded at NRDC stations have been studied using spectrograms. The scatter in the spectrograms is larger than at NORESS (see Section 3.2), due to lack of array-averaging. In spite of that, distinctive spectral modulations are often observed for presumed mine blasts. They are similar at different stations and indicate ripple-firing. Single explosions, such as three HE calibration shots and the JVE2 nuclear explosion (recorded with UNR instruments), as well as a regional presumed earthquake, do not show spectral modulations, as expected.

Anne Suteau-Henson

### References

Hedlin, M. A. H., J. B. Minster and J. A. Orcutt, 1988. "The Time and Time-Frequency Characteristics of Quarry Blasts and Chemical Explosions Recorded in Kazakhstan U.S.S.R. (abstract)," *EOS, Trans. Am. Geophys. Union*, Vol. 69, p. 1331.

Suteau-Henson, A., 1989. "Characterization of Earthquakes and Explosions Recorded at NORESS and the NRDC Stations," in *Center for Seismic Studies Report, C89_01.*

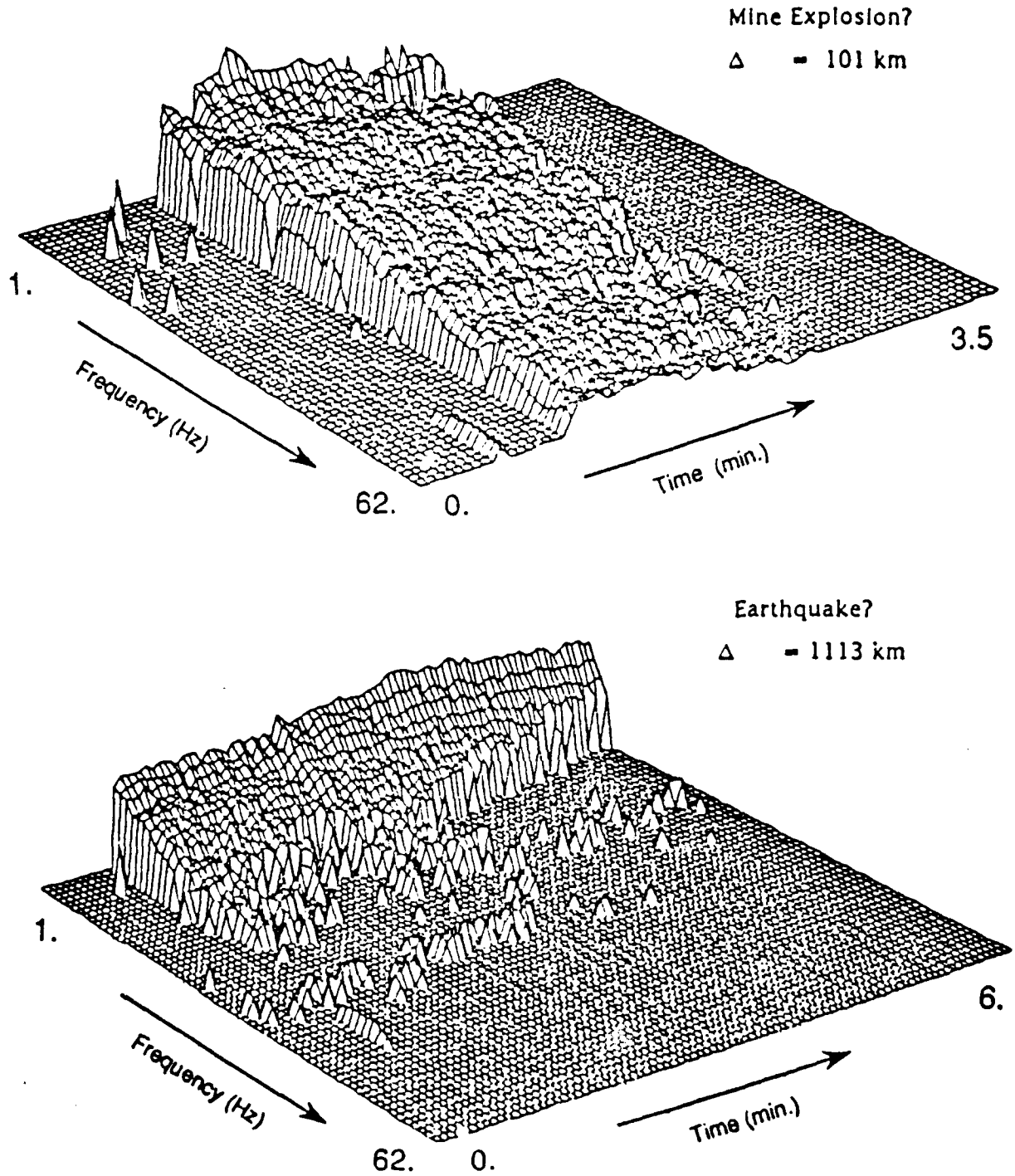


*Figure 2.* Spectrograms of two unidentified events at NRDC station BAY. Top: Presumed local mine explosion (times beyond the end of the recorded data are masked). Bottom: Presumed regional earthquake.

## 2.1 UPPER MANTLE STRUCTURE ALONG A PROFILE FROM OSLO (NORESS) TO HELSINKI TO LENINGRAD, BASED ON EXPLOSION SEISMOLOGY


### ABSTRACT

Waveforms from the NORESS array have been analyzed for 147 industrial explosions which occurred during the 1985-1988 period, and were located along a profile running east from Oslo (NORESS) to Helsinki to Leningrad (*OHL profile*). The events were 250-1,300 km from NORESS and had local magnitude in the range 2.0-3.5. Event locations and origin times constrained by the University of Helsinki's regional seismic network provide a reliable basis for traveltime estimation at NORESS. We also used data recorded by NORSAR in 1979 for three shots on the *FENNOLORA* north-south, long-range seismic profile, which were near the OHL profile. Analysis of mantle P-wave signals from the explosions showed that first arrivals could be traced continuously to a distance of 750-800 km, where there is a cutoff and shift of approximately 2.0-2.5 seconds in the traveltime curve, and an increase in average apparent velocity. Interpretation of the observed traveltimes and waveforms for this profile suggests increasing P-wave velocity in the uppermost mantle below the Moho from 8.1 to 8.55 km/sec in the depth range 40-105 km, a low-velocity zone (velocity 8.0 km/sec) from approximately 105 to 135 km depth, and velocity almost constant or increasing very slowly from 8.65 to 8.66 km/sec in the range 135-200 km. Combined analysis of the seismic data with a Bouguer gravity map indicates the presence in the upper mantle of a high-velocity, high-density body of linear extent approximately 200-300 km, east of the NORESS array. It is postulated that this body may represent the root of an ancient volcanic system, in which lighter, silicic constituents were depleted during the eruptive phase.


### 2.1.1 Introduction

Many problems of geology and geophysics require quantitative data on lateral and vertical inhomogeneities in the upper mantle. In monitoring a low-threshold test ban treaty, for example, accurate knowledge of upper-mantle structure would be critical for accurate location of events recorded at far-regional distances (1,000 km or more) by a single station or array, and for estimating magnitude or yield of seismic events from amplitudes of the recorded waves. In the same area, accurate knowledge of crust-upper mantle structure are also important in considerations related to the design of networks aimed at achieving specific monitoring capabilities.

Velocity structure of the upper mantle below the Baltic shield has been the subject of intensive investigations based on recorded body and surface waves from explosions and earthquakes. These studies indicate that, on average, the upper

mantle in this region is characterized by relatively high velocity compared with neighboring areas (Herrin and Taggart, 1968; Vinnik and Ryaboy, 1981; Husebye and Hovland, 1982; Calcagnile, 1982; Nolet *et al.*, 1986; Bannister *et al.*, 1989), although there is not total agreement between results of different investigations.

As an example, reference models of the lithosphere used in processing data for the NORSAR/NORESS and Helsinki bulletins do not contain upper-mantle low-velocity layers, but instead incorporate a medium of constant velocity below the Moho. These models are based on average traveltimes of distant events from different azimuths. Velocity sections constructed by Masse and Alexander (1974) and Given and Helmberger (1980) do contain a low-velocity layer, but in the Masse-Alexander model the low-velocity layer was borrowed from Masse's investigation of the Canadian shield (Masse, 1973). These studies, together with one by King and Calcagnile (1976) were based on observations of Soviet nuclear explosions at shot-receiver distances more than 900-1,000 km, and as a result cannot be used reliably to infer upper-mantle structure for depths less than 100-150 km. S-wave velocity sections of the upper mantle constructed for the Baltic shield from surface-wave studies contain a low-velocity layer underlying a high-velocity lid, at a depth of approximately 100 km according to Nolet *et al.* (1986), or 75-135 km according to Calcagnile (1982).

The most detailed P-wave velocity sections of the upper mantle are those for the *Blue Road* and *FENNOLORA* long-range profiles (*Figure 1*; Lund, 1979a, 1979b; Mueller and Ansorge, 1986; Stangl *et al.*, 1986; Fuchs *et al.*, 1987; Guggisberg and Berthelsen, 1987). These models were based on very detailed field observations along reversed and overlapping profiles. The main feature of the models is laminar structure of the Moho, with alternating high- and low-velocity layers in the upper mantle, determined from a number of breaks in the $P_n$ traveltime curves, with the more distant branches successively shifted to later times (*i.e.*, delayed).

To evaluate these results, we studied NORESS recordings of 147 mining and other industrial explosions, detonated during the period 1985-1988 along an east-west profile from Oslo (NORESS) to Helsinki to Leningrad (*Figure 1*; *OHL* profile). We also used data recorded by the NORSAR array in 1979 for three shots on the *FENNOLORA* north-south profile, which were near the OHL profile. It should be noted that the *FENNOLORA* database is larger and more detailed, but that the data for the OHL profile have the advantage of better signal-to-noise ratio (*SNR*). This is critical in identifying weak mantle waves recorded as first arrivals at far-regional distance ranges.

In the following sections we describe the analysis of NORESS explosion recordings, the wave field observed on the profile, construction of the upper mantle velocity section, and comparison of results with other geophysical and geological data.

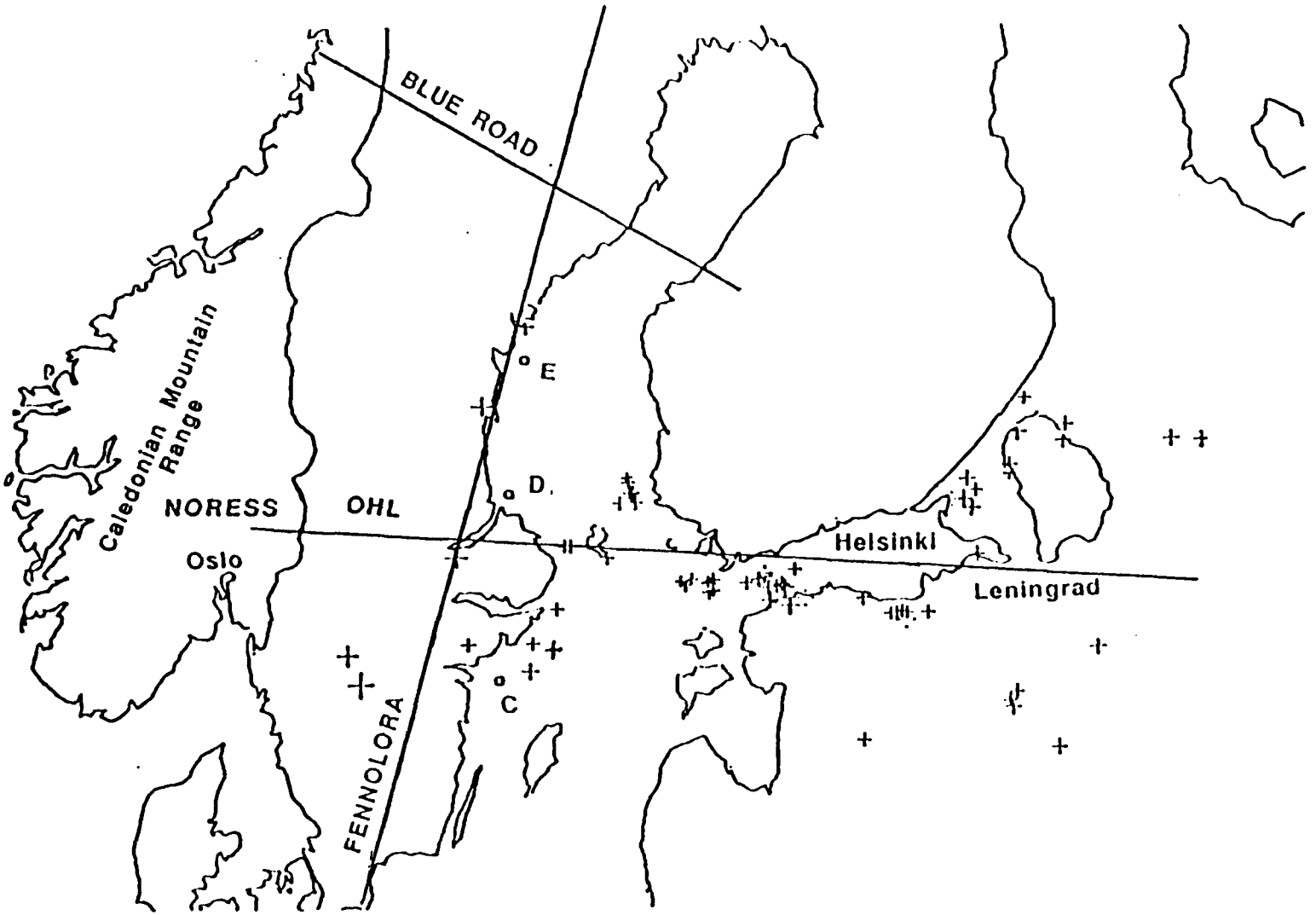


*Figure 1.* Location map of NORESS array and shot points used in this study. Crosses -- location of mine blasts (size of crosses proportional to event magnitude) for the Oslo-Helsinki-Liningrad (OHL) profile; squares -- shotpoints C, D, E for FENNOLORA profile; solid lines -- FENNOLORA and Blue Road long-range seismic profiles, and OHL profile.

### 2.1.2 Profile Location and Event Analysis

The events used in this study are located on or near a 1,300 km-long profile from the NORESS array to Helsinki to Leningrad (*OHL* on *Figure 1*). This profile mainly crosses a complex of basement rocks about 1,600-1,900 m.y. old (*Svecofennides*), while the NORESS array is located north of the Oslo Graben, near the boundary between the 400-m.y. old *Caledonides* and the Precambrian Baltic shield (*Figure 2*). On the eastern part of the profile several events are located on the northwestern part of the Russian plate, where the sedimentary layer is rather thin (300-500 m or less; Litvinenko and Platonenkova, 1978).

These events were listed and identified as possible explosions in the NORESS and Helsinki seismological bulletins (Appendix I). The events were in the range of epicentral distance from 250 to 1,300 km, and had magnitude (*ML*) 2.0-3.5. For distance less than 450 km, we reanalyzed NORSAR recordings for three of the 1979 *FENNOLORA* shots (C, D and E), which were near the OHL profile (Mereu et al., 1983). The *FENNOLORA* explosions had magnitude less than 2.0 based on the listings in the International Seismological Centre Bulletin (1982).

A comparison of locations and estimated origin times in the NORESS and Helsinki bulletins shows large discrepancies, up to several tens of kilometers in location and several seconds in origin time (Appendix I). According to the Helsinki bulletin, events identified as repeated explosions at the same mine occurred at several points of the profile. Traveltimes for such events typically agreed within 0.3-0.5 second, and a value ±0.5 second can be used as a conservative estimation of the average origin-time error listed in the Helsinki bulletin. This conclusion can also be confirmed by the scatter in observed traveltimes of $P_n$ waves from an average curve (see *Figure 11* and accompanying discussion) which has an RMS deviation less than ±0.5 second. A comparison of traveltimes for the same events listed in the NORESS bulletin gave discrepancies up to several seconds.

Statistical analysis of Appendix I was carried out using various methods, and the results of this analysis helped to better understand the origin of discrepancies between the two bulletins. It was found that differences between origin time (T) and epicentral distance (DIST) are not entirely random, but are also influenced by systematic factors, and cannot be approximated by a normal distribution. On the other hand, the difference between NORESS backazimuths calculated from locations in the Helsinki and NORESS bulletins does approximate a normal distribution (*Figure 3*). The analysis also showed a negative, statistically significant relation between T and DIST (coefficient of linear correlation equal to -0.80).

Based on the above considerations plus the proximity of the Helsinki network to the events, we concluded that location parameters in the Helsinki bulletin had less error than those based only on NORESS recordings. As a result, we used Helsinki

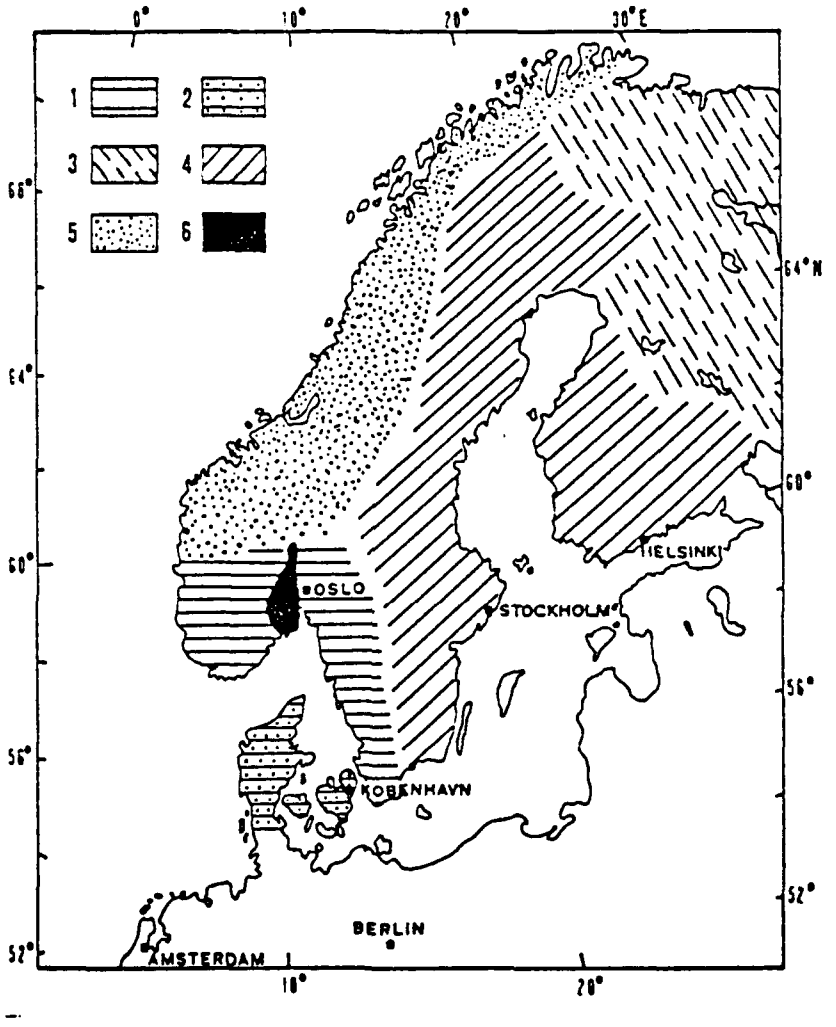


*Figure 2.* Tectonic sketch map of Baltic Shield. 1 -- *Sveconorwegian* (900-1200 m.y.); 2 -- platform, partly *Sveconorwegian*; 3 -- *Svecokarelides* (2200-2800 m.y.); 4 -- *Svecofennides* (1600-1900 m.y.); 5 -- *Caledonides* (400 m.y.); 6 -- Oslo Graben (300 m.y.). Adapted from Calcagnile (1982).

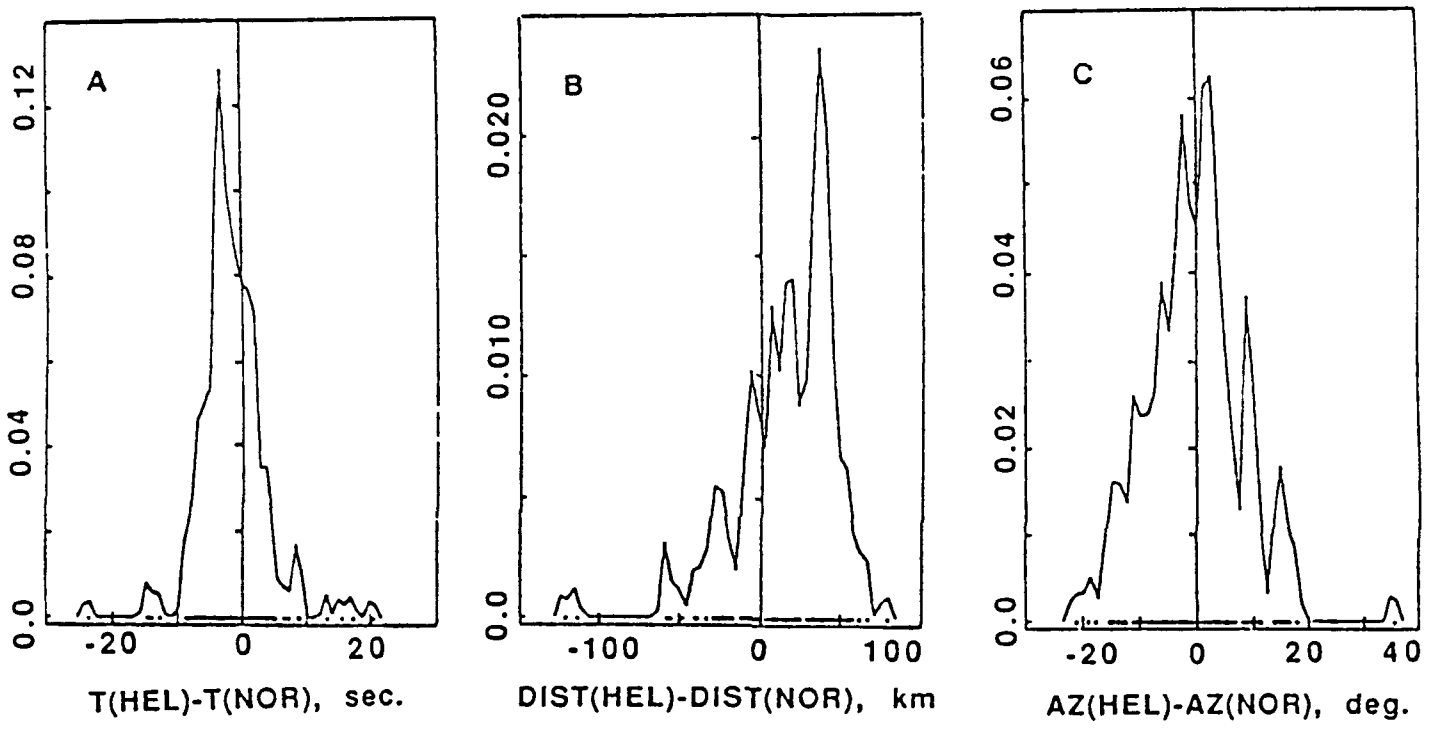


*Figure 3.* Density plots A, B, and C of differences between origin times (T), epicentral distances (DIST), and azimuths (AZ), respectively, from Helsinki (HEL) and NORESS (NOR) bulletins, for 147 explosions detonated along the Oslo-Helsinki-Leningrad profile. One can see that density plots A and B are non-symmetric, while plot C is nearly symmetric about the vertical axis. The modes of the density plots are -3.21 sec. (A), 37.50 km (B), and 2.20 deg. (C).

bulletin locations and origin times as the basis for interpretation. As a final note, approximately half of the original 147 events were excluded from interpretation because of poor signal-to-noise ratio.

### 2.1.3 Crustal Thickness

Misunderstanding upper-mantle velocity structure (*e.g.*, in reference velocity models used in the bulletins) can be a major source of error in locating events and estimating their origin times at far-regional distance. Therefore a new contour map of Moho depth and schematic map of $P_n$ velocity for the Baltic shield and neighbouring geological units has been compiled from the most reliable data, namely from published deep seismic refraction profiles (Azbel *et al.*, 1989; Dahlman *et al.*, 1971; Galdin *et al.*, 1988; Guggisberg and Berthelsen, 1987; Korhonen and Porkka, 1981; Litvinenko and Platonenkova, 1978; Lund, 1979a, 1979b, 1980; Lund and Slunga, 1981; Luosto *et al.*, 1984, 1985, 1989; Mueller and Ansorge, 1986; Mykkeltveit, 1980; Prodehl, 1984; Prodehl and Kaminski, 1984; Sellevoll and Warrick, 1971; Weinrebe, 1981). We also used maps of Moho depth variations beneath Fennoscandia and adjacent regions, published earlier (Bungum *et al.*, 1980; Calcagnile, 1982; Fluh and Berthelsen, 1986; Glaznev *et al.*, 1989; Meissner *et al.*, 1987; Sellevoll, 1973; Semov, 1987). A location map of seismic profiles used in compiling the crustal thickness map is shown on *Figure 4*. Velocity sections of the crust were constructed for these profiles based on various approaches to interpretation, but in general the discrepancy in Moho depth did not exceed 2-3 km at points where the seismic profiles crossed, which is not considered important for a map of crustal thickness with 5-km contour intervals.

*Figure 4* shows that crustal thickness beneath Fennoscandia and adjacent geological provinces varies from about 30 to 55 km. The crust generally thickens from the coast to the Baltic shield interior. On average the crust below the *Caledonides* and Russian plate is thinner than that of the Baltic shield. Comparison of *Figures 2 and 4* indicates that there is no simple correlation between $P_n$ velocity and crustal thickness, surface geology or age. In the oldest part of the eastern Baltic shield the *Svecokarelides* (2200-2800 m.y.) are characterized by crustal thickness of 35 to 45 km, increasing to 50-55 km beneath younger *Svecofennides* (1600-1900 m.y.). In southern areas of Sweden and Finland one can see relatively narrow zones of sharp crustal thickening up to 50-55 km and more (*Figure 4*). $P_n$ velocities vary from 7.8-8.0 up to 8.3-8.5 km/sec. The most frequently obtained values of $P_n$ velocities for Fennoscandia are 8.1-8.2 km/sec.

For the OHL profile, crustal thickness beneath the NORESS array and at distances greater than 400 km from NORESS is about 40 km. In contrast, the Moho beneath *FENNOLORA* shots C, D, and E, and several other events is larger -- up to 50-55 km (*Figure 1, Figure 4*). As a result, $P_n$ traveltime corrections were made to account for variations in crustal structure along the profile.

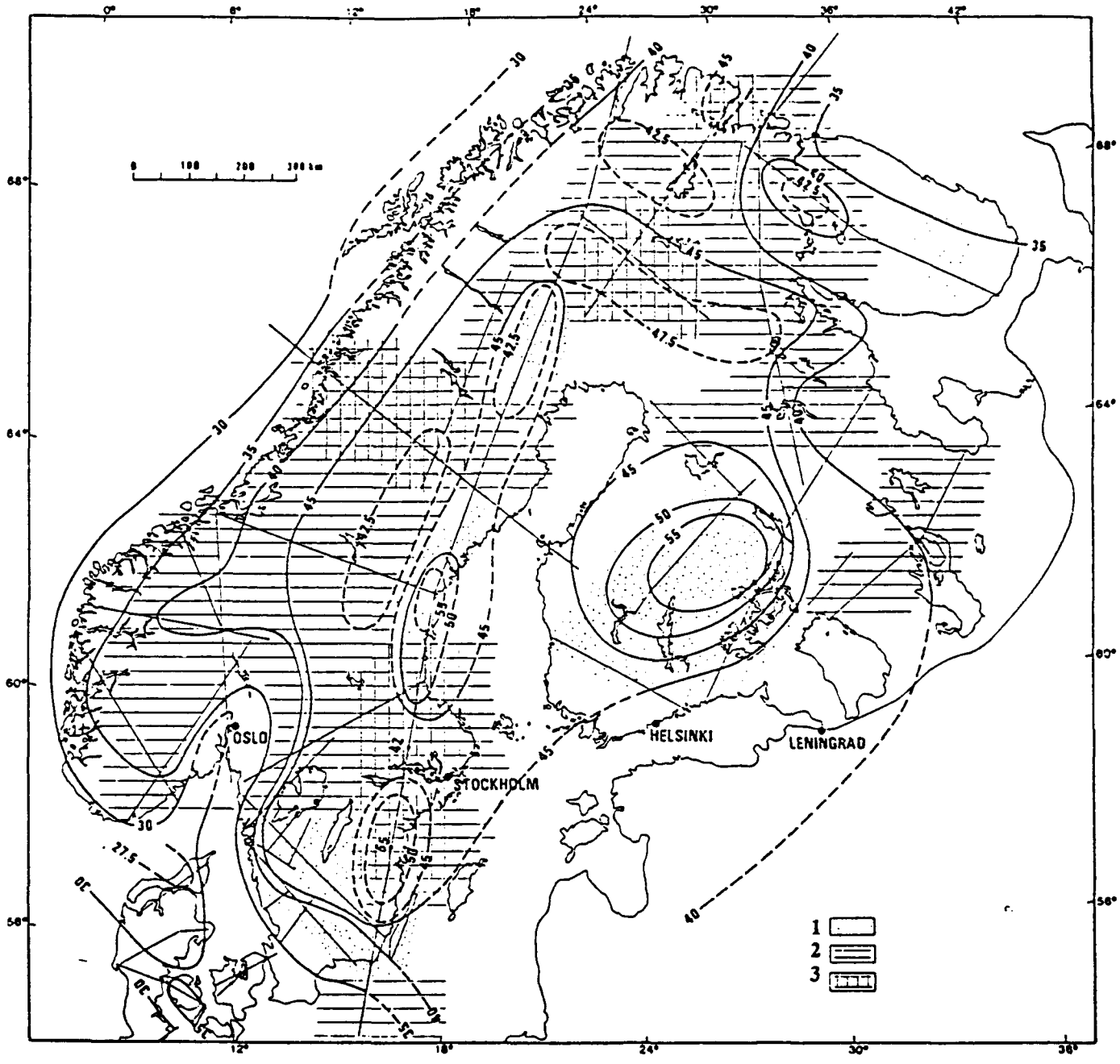


*Figure 4.* Coutour map of crustal thickness (km) and schematic map of *Pn* velocity for the Baltic Shield and adjacent areas, based on DSS data. Lines of equal Moho depth are represented by thick solid lines for reliable data, and dashed lines for unreliable data. Values of *Pn* velocity (km/s) are: 1 -- 7.8-8.0; 2 -- 8.1-8.2; 3 -- 8.3-8.5. Thin solid lines denote DSS profiles. The crustal thickness varies from as little as 30-35 km near the coast to 50-55 km within the interior areas. *Pn* wave velocity varies from 7.8-8.0 km/s up to 8.3-8.5 km/s (the most frequently observed values are 8.1-8.2 km/s). There is no direct relation between variations of the crustal thickness and *Pn* velocity.

### 2.1.4 P-Waves From The Upper Mantle

Our study of NORESS and NORSAR recordings of explosions at far-regional distances confirmed an observation of previous authors, that the $P_n$ wave of classical seismology has a very complicated structure and consists of several wave groups (Nersesov and Rautian, 1964; Ryaboy, 1979; 1989a; Fuchs, 1986; Fuchs *et al.*, 1987; Lund, 1979a, 1979b; Mueller and Ansorge, 1986). First arrivals of mantle P-waves on the OHL profile are typically characterized by small amplitudes and relatively high frequency (5-8 Hz), and these are followed by secondary arrivals with substantially larger (factor of 5-10 or more) amplitudes and lower frequency (2-4 Hz). In general, analysis of the weak first arrivals was possible only by filtering and beamforming of signals. *Figures 5-8* show examples of NORESS recordings of mantle P-waves, with phases designated by $P_{n1}$, $P_{n2}$ (first arrivals) and $P1$, $P2$ (later arrivals). Note that because of unknown but varying shot size and conditions at the shotpoint, a detailed study of changes in amplitude and frequency of the signals with distance was not possible.

A number of shots detonated during the 1979 *FENNOLORA* project were recorded by the NORSAR array. These explosions usually had magnitude less than 2.0, based on listings in the *Bulletin of the International Seismological Centre.* A detailed analysis of records of the *FENNOLORA* explosions was published by Mereu *et al.* (1983). Three of the shots were located in the area where the *FENNOLORA* and OHL profiles crossed. Comparison of NORSAR $P_n$ traveltimes for the *FENNOLORA* shots (*C, D* and *E* in *Figure 1*) showed that they were later than NORESS arrivals for the same distance range on the OHL profile.

To better understand this contradiction we reanalyzed NORSAR recordings of shots C, D and E. Mereu *et al.* showed that beams constructed for a group of NORSAR subarrays did not show a marked improvement in SNR over single-element traces because of lost coherency, and as a result they analyzed filtered single-element signals. In contrast, we applied beamforming to each of seven NORSAR subarrays, and constructed record sections consisting of filtered beams. Beaming even a small number of traces in this way improved SNR and made it possible to correlate weak first arrivals (*Figure 9*). Sometimes there was adequate SNR without beamforming, as illustrated by the single sensor (01B2) trace included in *Figure 9* (406.3 km distance). The $P_n$ first arrivals in *Figure 9* are approximately 1.0-1.5 seconds earlier than for the single-element records used by Mereu *et al.* We conclude that in analyzing single-element traces, one could mistakenly interpret larger secondary arrivals as primary arrivals, because the latter would be weak and buried in noise.

The same explanation may apply to a comparison of $P_n$ traveltimes for the Swedish seismological network, for *FENNOLORA* explosions ($M_L < 2.0$) and regional earthquakes ($M_L \approx 3.0$–$3.5$) referred to zero focal depth. According to Bath (1981,

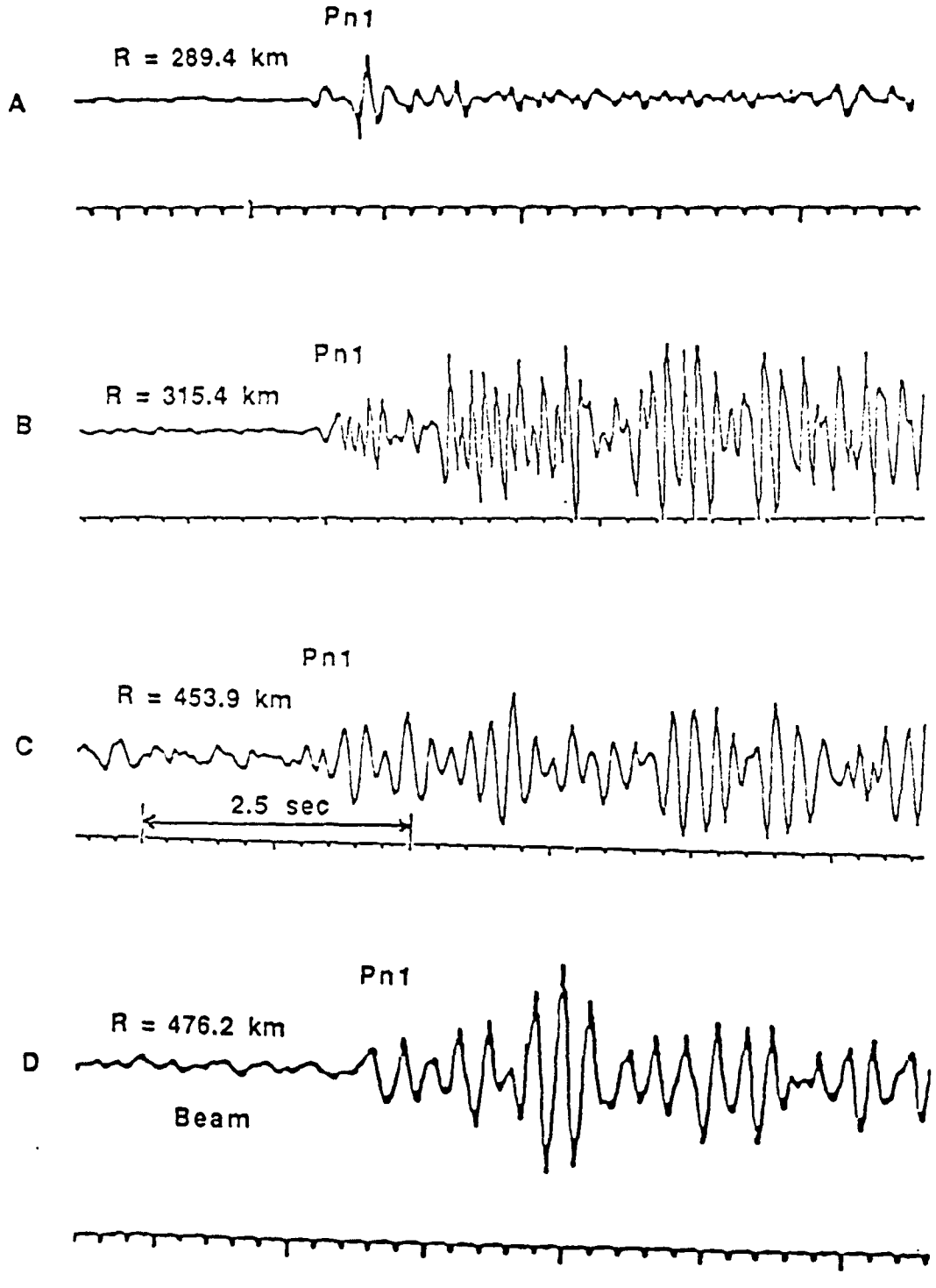


*Figure 5.* NORESS recordings of mantle waves $P_{n1}$ from explosions. A, B, and C are single sensors, D is an array beam. A -- event 86195, magnitude M = 4.1, no filter; B -- event 86025, M = 3.2, filter: 3-12 Hz; C -- event 86133a, M = 2.5, filter: 4-12 Hz; D -- event 87362b, M = 2.6, filter: 2-15 Hz.

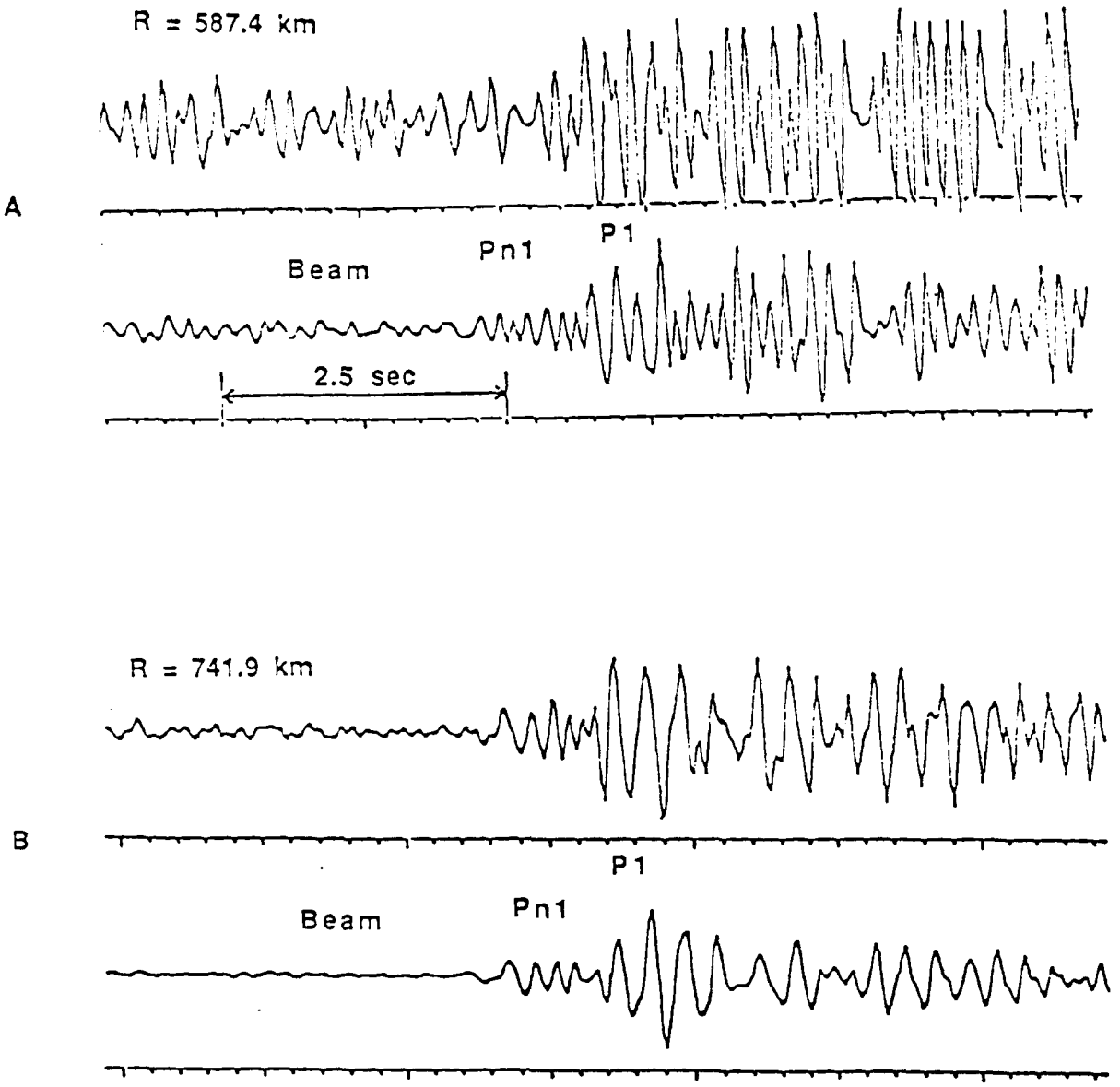


*Figure 6.* NORESS recordings of mantle waves from two explosions (single sensor and array beam). A -- event 87274b, M = 2.4, filter: 3-12 Hz; B -- event 87147, M = 2.9, filter: 3-12 Hz. Two groups of mantle waves can be correlated as first ($P_{n1}$) and second ($P1$) arrivals. $P_{n1}$ is usually characterized by smaller amplitudes and higher frequencies compared with later arrivals. The figure also illustrates signal to-noise ratio improvement through beamforming.

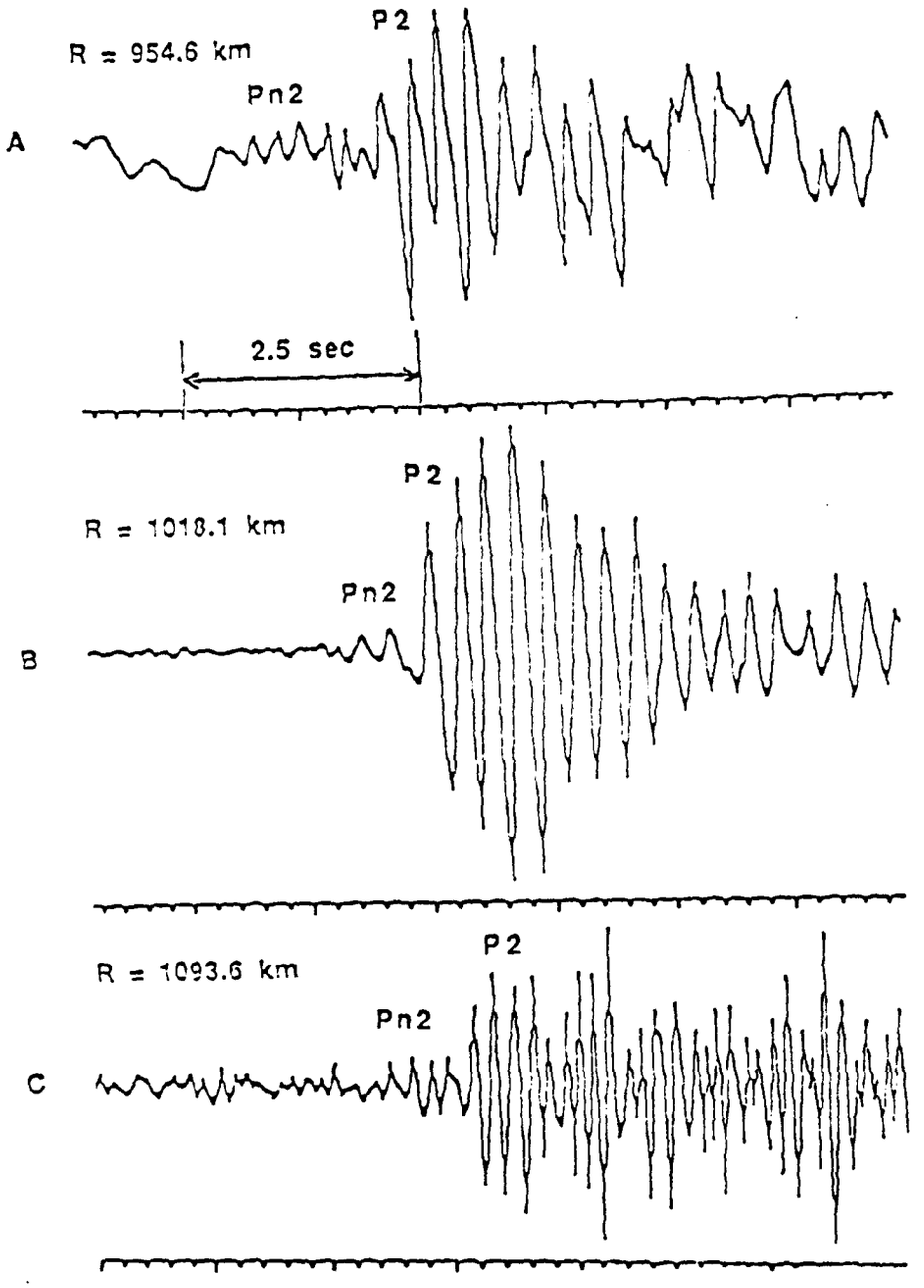


*Figure 7.* NORESS recordings for: A -- event 86086 (M = 3.5, no filter); B -- event 86163 (M = 3.7, filter: 2-15 Hz); C -- event 87359 (M = 3.0, filter: 4-10 Hz). These records were obtained by applying beamforming. The distances are beyond the range where $P_{n1}$ disappears and the first arrivals are delayed relative to an extension of the $P_{n1}$ traveltime curve. Two groups of mantle waves can be correlated as first ($P_{n2}$) and secondary ($P2$) arrivals.

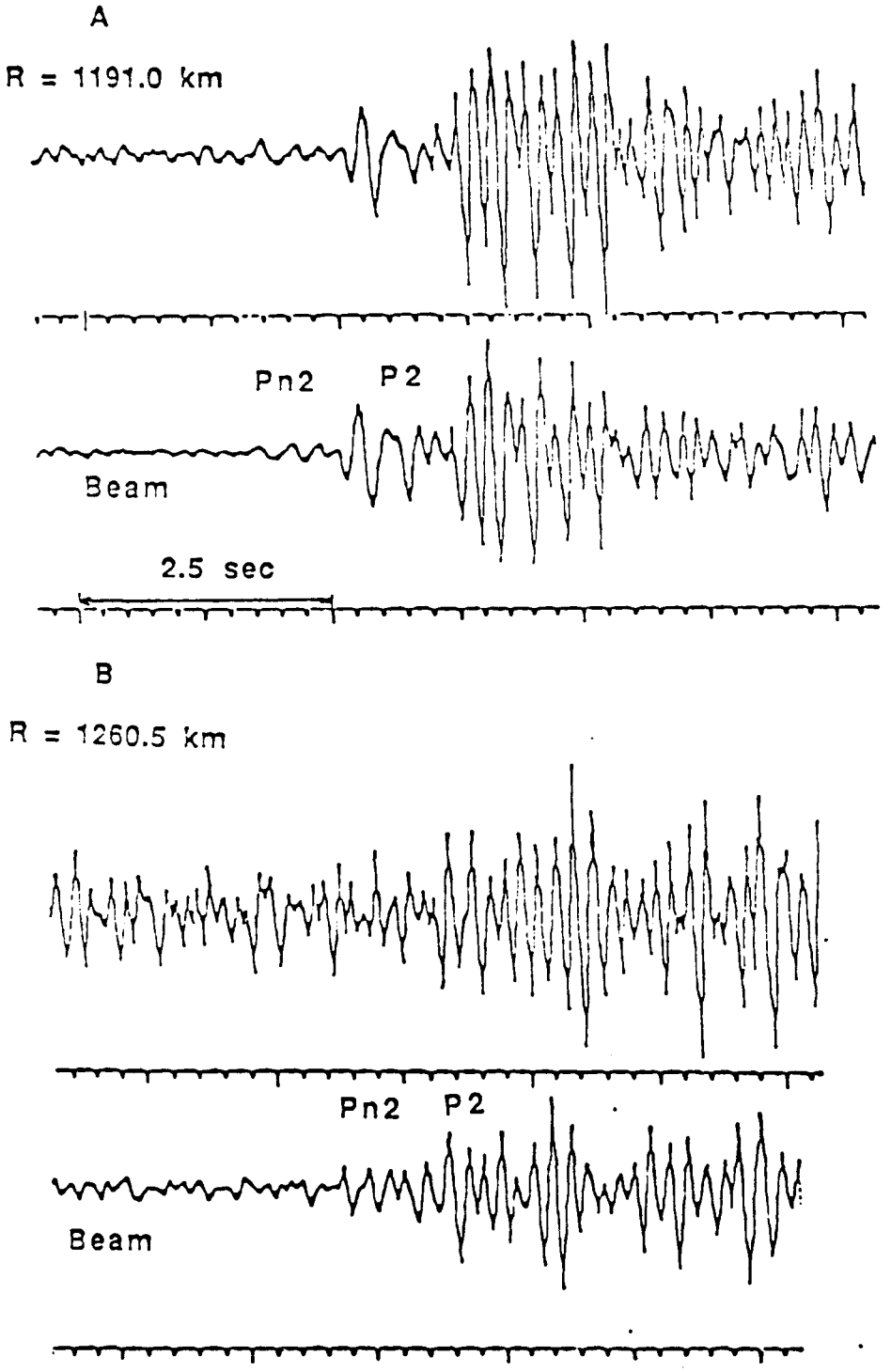


*Figure 8.* NORESS recordings (single sensor and array beam) for: A -- event 86364 (M = 3.4, filter: 3-12 Hz); B -- event 87045 (M = 2.5, filter: 4-10 Hz). The figure also illustrates signal to-noise ratio improvement through beamforming.

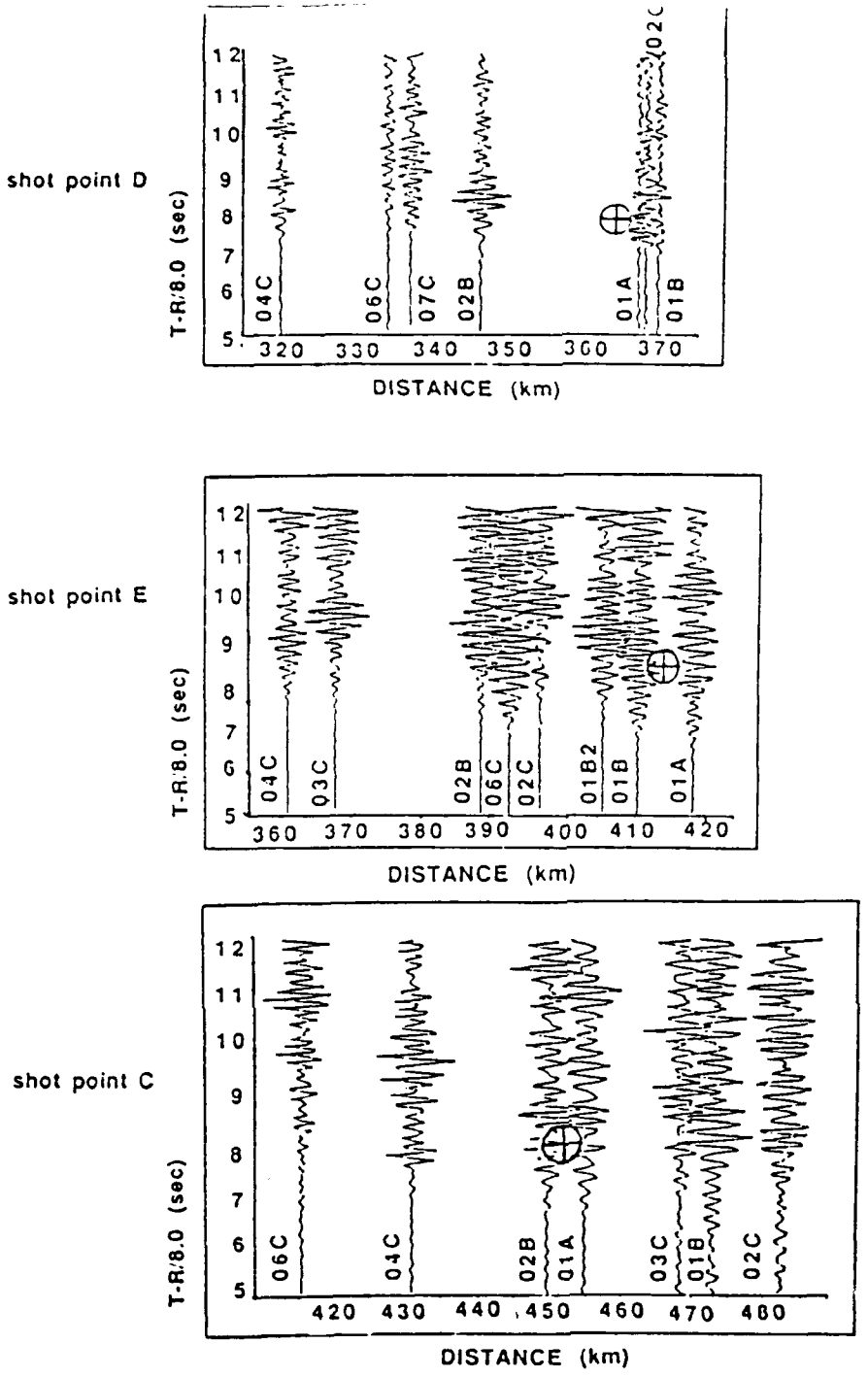


*Figure 9.* Trace-normalized record sections from shotpoints D, E, and C (FENNOLORA experiment, 1979) recorded at the NORSAR array. The sections are arranged in order of increasing shotpoint distance, and consist of filtered beams (filter: 2-10 Hz) constructed for each of seven subarrays of the NORSAR array. For shot point E we also included in the section the recording of the vertical sensor 01B2 (R = 406.3 km), because good signal-to-noise ratio was observed for this single sensor. Note that first *Pn* arrivals are approximately 1.0-1.5 sec. earlier than data of Mereu et al. (1983) shown by circle with cross. Reduction velocity of the time axis is 8.0 km/s.

*Table 2*) $P_n$ traveltimes for earthquakes are consistently earlier (up to 1.0-1.4 second for epicentral distance 1,000-1,400 km). This discrepancy can be explained by better SNR for the larger-magnitude earthquakes; the weak first arrivals from *FENNOLORA* explosions were probably buried in noise.

A record section was constructed for upper-mantle signals recorded by NORESS for the OHL profile, using SPZ traces (mainly beams) with good SNR, plotted at the appropriate epicentral distance (*Figure 10*). The NORSAR subarray 06C beams for *FENNOLORA* shots C, D, and E were also plotted on the record section (NORESS is located within subarray 06C). All traces in *Figure 10* were bandpass-filtered (3-8 Hz for NORSAR and 3-12 Hz for NORESS data). Note that in detailed analysis of the signals we tried various filters on each trace, and in general the best filter selection produced better SNR than the standard settings used to construct *Figure 10*. For this reason, we have also included a traveltime plot (*Figure 11*) showing first arrivals measured on filtered traces that had the best SNR. Traveltimes for several of the explosions (including the *FENNOLORA* shots) were corrected to account for differences in crustal thickness (up to 50-55 km beneath shot points, compared with approximately 40 km beneath NORESS array and most of the explosions on the OHL profile). For different shot points these corrections varied from -0.6 to -0.8 sec.

Upper-mantle traveltime curves constructed for the OHL profile are shown in *Figures 10 and 11*. In both figures $P_{n1}$ arrivals can be followed continuously to about 800-850 km, with average apparent velocity 8.2-8.5 km/sec. Note that in the distance range 300-500 km the apparent velocity of $P_{n1}$ is locally high, 8.5-8.6 km/sec (*Figure 11*). This observation is based on NORSAR recordings of the *FENNOLORA* shots, for which the location and origin time of the events are accurately known. A second intensive arrival $P1$ is observed following $P_{n1}$ over the same distance range (*Figure 10*).

Beyond 800-850 km there is a shift of 2.0-2.5 seconds in the traveltime curve, with $P_{n1}$ and $P1$ dying out and a later phase $P_{n2}$ appearing as the first arrival, followed by another intensive phase $P2$. The apparent velocity of $P_{n2}$ is high, 8.6-8.8 km/sec. This break and shift of the $P_n$ traveltime curve is similar to traveltimes observed for nuclear explosions recorded in adjoining areas of the eastern European platform (Vinnik and Ryaboy, 1981; Ryaboy *et al.*, 1987), but the 2-second shift in that region was observed at smaller distance (550-650 km) in that study. On the *FENNOLORA* profiles the $P_n$ traveltime branch is delayed in the range 700-800 km, but the magnitude of this shift usually does not exceed 1.0-1.5 sec. If other $P_n$ traveltime shifts exist for the OHL profile at distances less than 700-800 km, they are not evident on the record section, and the magnitude of each shift has to be less than 0.5-1.0 second.

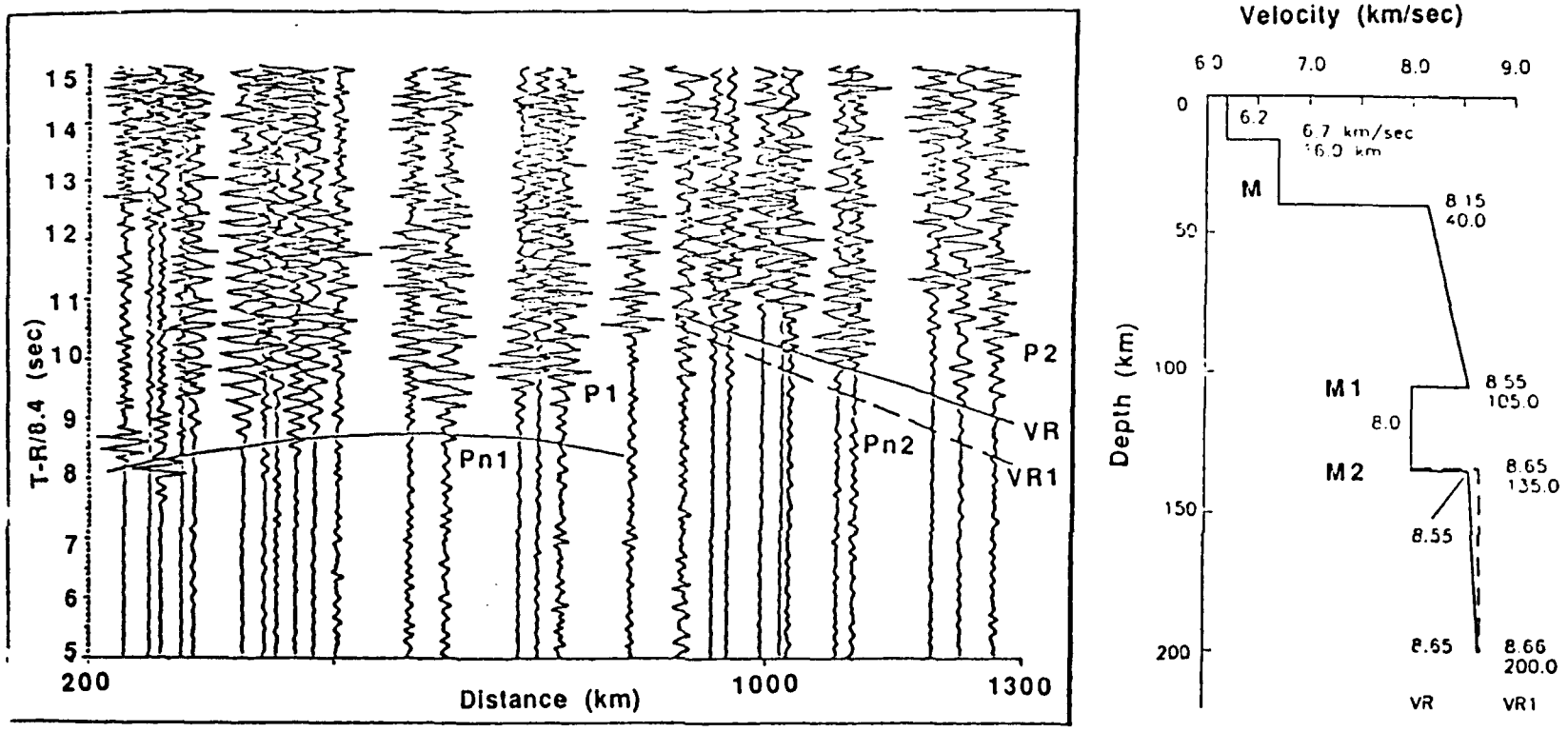


*Figure 10.* Trace-normalized record section for the Oslo- Helsinki-Leningrad profile and theoretical traveltime curves of waves refracted in the upper mantle. Reduction velocity is 8.4 km/s, and records are bandpass-filtered between 3 and 10 Hz. Velocity models VR and VR1 used to calculate traveltime curves are shown to the right. Note the delayed traveltime branch beyond 800-850 km for first arrivals. The intensive wave group P1 sharply attenuates at approximately the same distance range.

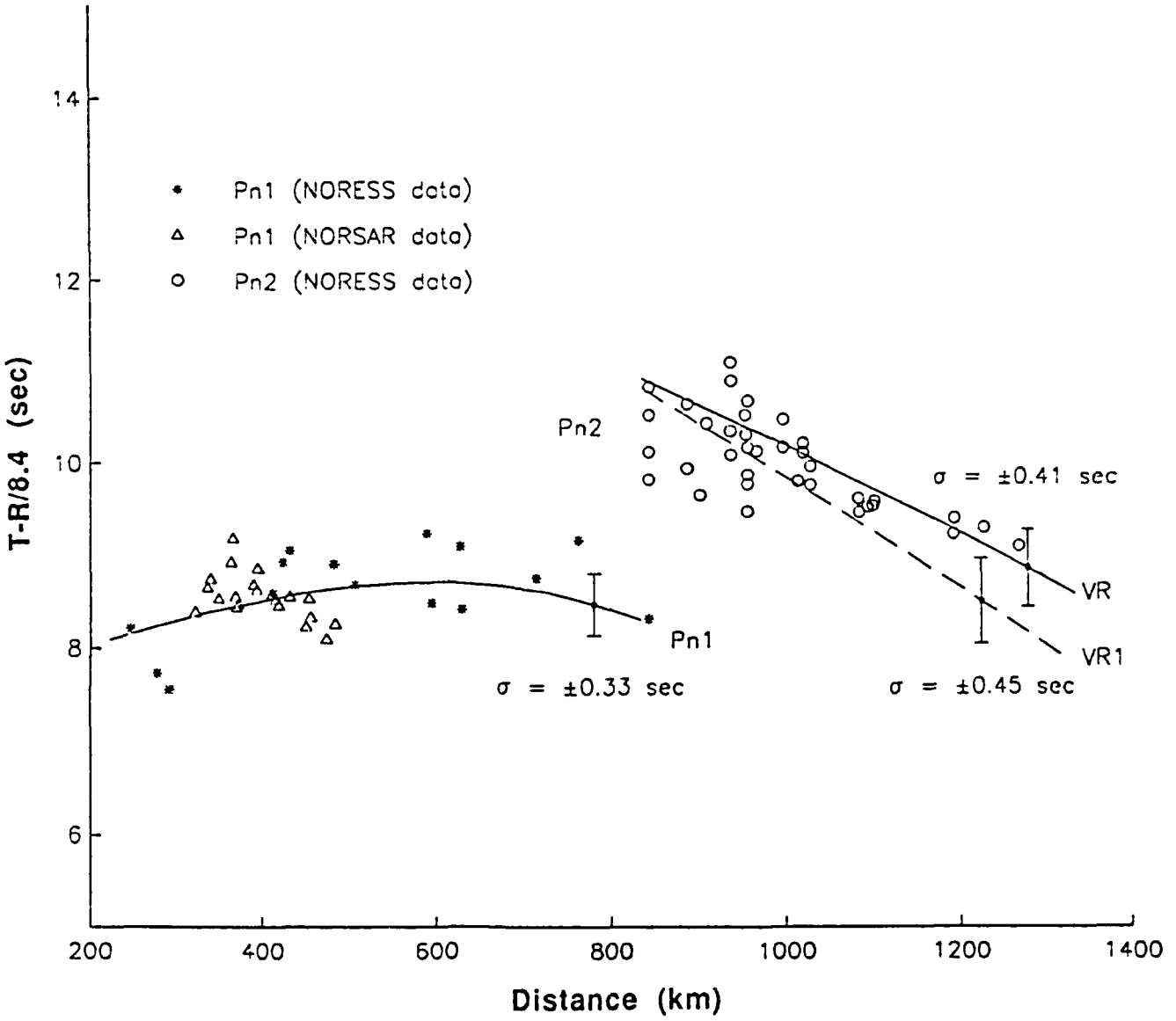


*Figure 11.* Comparison of observed and theoretical traveltimes of $P_n$ ($P_{n1}$ and $P_{n2}$) for the Oslo-Helsinki-Leningrad profile. Velocity models used in the calculations of the traveltime curves of waves refracted in the upper mantle are shown in Figure 10. Vertical bars are standard deviations of the observed traveltimes of $P_{n1}$ and $P_{n2}$ waves from the calculated traveltimes.

### 2.1.5 Upper-Mantle Velocity Structure of The Southeastern Baltic Shield

Interpretation of the break and shift in the traveltime curve at 800-850 km is critical in interpreting $P_n$ traveltimes for the OHL profile. With the data available to us, we cannot uniquely resolve this problem since interpretation could be based either on laterally homogeneous or two-dimensional models. For example, since we do not have observations along reversed and overlapping profiles, we might assume that there are no pronounced lateral velocity changes in the upper mantle beneath the profile, and interpret the traveltime curve and record section on the basis of laterally homogeneous layers. In that case, the delayed traveltime branch could be completely explained by a low velocity layer in the upper mantle. This conclusion would agree with results of upper-mantle studies along long-range DSS profiles on the East-European platform (Vinnik and Ryaboy, 1981). However, this interpretation can be checked by comparing the DSS results with gravity data, and such a comparison will be presented in the next section.

Inversion of the traveltime curves to obtain a velocity section was accomplished by an iterative process of comparing theoretical traveltime curves and synthetic waveforms with the observed data. The theoretical curves and seismograms were calculated by the WKBJ method (Chapman *et al.*, 1988), using spherical earth models with the two-layered crustal velocity model used in processing data for the NORESS Bulletin. In this modeling the first arrivals $P_{n1}$ and $P_{n2}$ are refracted waves travelling in two relatively high-velocity layers of the upper mantle, separated by a low-velocity layer which accounts for the traveltime delay beyond 800-850 km. The intensive waves $P1$ and $P2$ are probably reflected waves from the top of the low-velocity layer ($P1$) and boundaries below the base of this layer ($P2$). Possible solutions of the problem were sought among the simplest velocity models, with the requirement that calculated and observed traveltimes agree to within ±0.5 sec. *Figure 12* shows the theoretical traveltime curves and synthetic seismograms calculated for velocity sections that best fit the data (VR, VR1).

The average deviation of the theoretical traveltime curves from observed $P_{n1}$ and $P_{n2}$ first arrivals is less than ±0.5 sec. Upper-mantle velocity models VR and VR1 are only representative of an aggregate of models consistent with the observed $P$-traveltimes. These velocity models give a comparable fit to traveltimes of $P_{n1}$ and $P_{n2}$, but model VR1 has a smaller velocity gradient below the bottom of the low velocity layer and fits the small observed amplitudes of $P_{n2}$ better than model VR (*Figure 12*).

Thus, a laterally homogeneous velocity model of the upper mantle for the OHL profile consists of two layers characterized by increasing velocity with depth, separated by a low-velocity layer. In the lid, between depths of 40 and 105 km, the velocity increases from 8.1 to 8.55 km/sec; from 105 to 135 km depth the velocity is 8.0 km/sec; and from 135 to 200 km the velocity increases very slowly (is almost

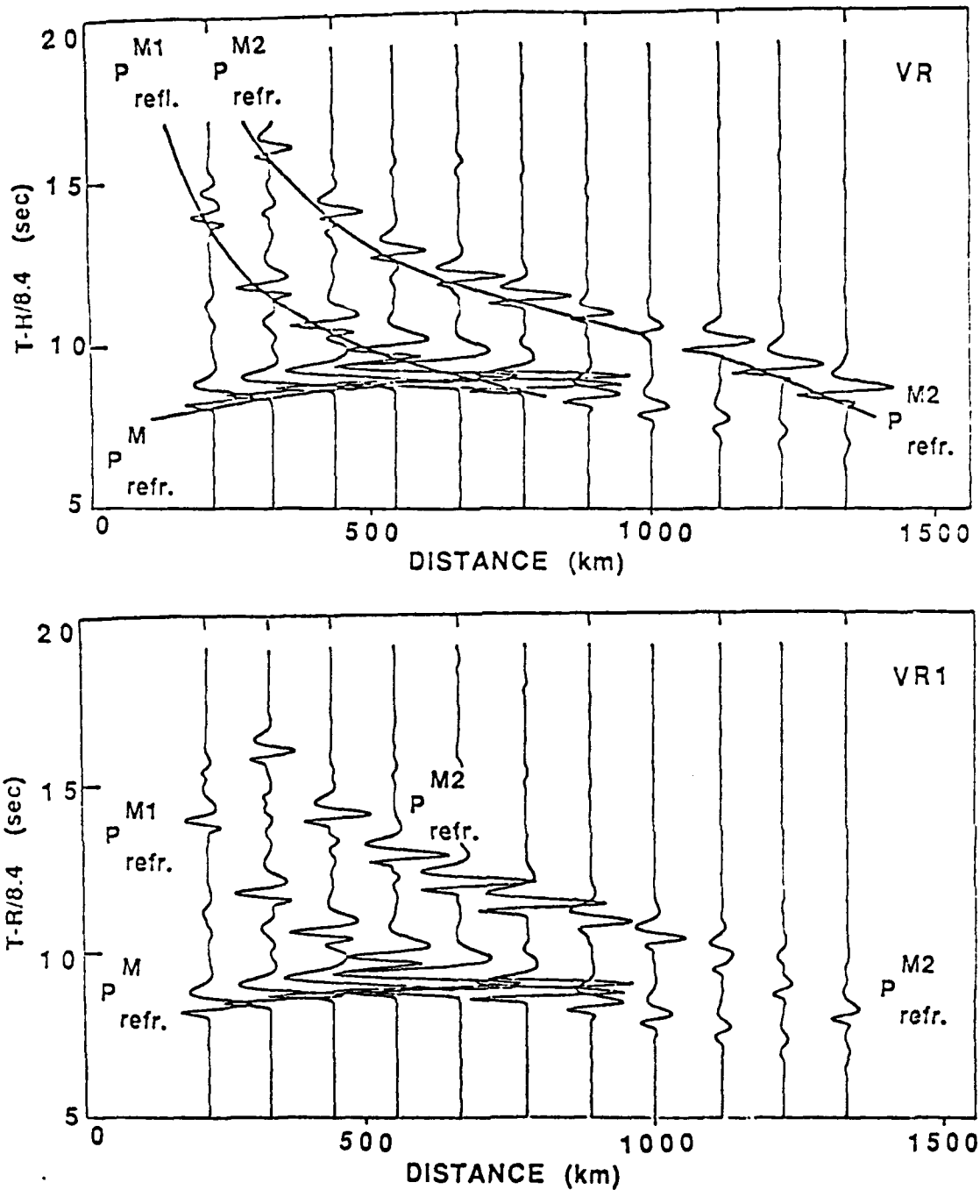


*Figure 12.* Synthetic seismograms and traveltime curves of upper-mantle P-waves. Velocity models used in the calculations (VR and VR1) are shown in Figure 10. $P^{M}_{refr}$ is a wave refracted in the upper layer of the mantle between boundaries M and M1, $P^{M1}_{refl}$ is a wave reflected from boundary M1, $P^{M2}_{refr}$ is a wave refracted in the upper mantle beneath boundary M2, $P^{M2}_{refl}$ is a wave reflected from boundary M2. The amplitudes of the $P^{M2}_{refr}$-wave are significantly smaller for model VR1 (Bottom) that for VR (Top), due to decreasing velocity gradient below boundary M2.

constant) from 8.65 to 8.66 km/sec. There is of course a tradeoff between the thickness of the low-velocity layer and its velocity. Additional low-velocity layers could be included in this velocity section, but the layer thicknesses must be less than 5-10 km.

### 2.1.6 Combined Seismic and Gravity Interpretation

Gravity anomalies due to density variations in the upper mantle can be analyzed by subtracting calculated crust/upper-mantle effects from the total Bouguer gravity field. This approach was used in studying upper mantle structure of Northern Eurasia (Vol'vovskii *et al.*, 1962; Ryaboy, 1979; Bur'yanov *et al.*, 1983). Joint analysis of seismic and gravity data is described in this section for the southern Baltic Shield, undertaken to study possible lateral inhomogeneities within the upper mantle.

A comparison of crustal thickness (*Figure 4*) with Bouguer gravity anomalies (*Figure 13*) for Fennoscandia indicates that in western areas, beneath the Caledonian Mountains, a significant depression of the Moho up to depths 40-45 km coincides with a very strong negative Bouguer anomaly (up to -80 to -100 mgal). The Baltic Shield is characterized by a relatively smooth gravity field, with variations of the Bouguer gravity anomalies from -(20-40) to +(20-40) mgal. At the same time there are both small and extended zones of sharp crustal thickening up to 50-55 km beneath the Baltic Shield. One of these zones is crossed by the OHL profile in southern Sweden, and a second one is in an area adjacent to the profile in southern Finland. Such variations in crustal thickness *should* lead to strong negative gravity anomalies, -(100-150) mgal, but such anomalies are absent on the Bouguer gravity map. This suggests that crustal thickening is compensated by density variations in the crust and/or upper mantle.

To consider this problem further, we calculated the gravity influence of the crust along a profile from the North Sea to Leningrad, the central and eastern parts of which coincide with the OHL profile, and the western part with the *Flora-Asnes* seismic profile (Sellevoll and Warrick, 1971). The North Sea-Leningrad line also crosses several seismic profiles in southern Sweden (*FENNOLORA*), southern Norway, southern Finland, and northwestern USSR (Dahlman *et al.*, 1971; Guggisberg *et al.*, 1984; Guggisberg and Berthelsen, 1987; Luosto *et al.*, 1984, 1985; Litvinenko and Platonenkova, 1978). Crustal velocity-depth sections compiled from seismic data for the east-west North Sea-Leningrad profile are shown in *Figures 14 and 15*. Crustal thickness along the profile varies from about 30-40 km beneath the Caledonian Mountains to 45-55 for the Baltic Shield, while the mean crustal velocity increases from approximately 6.4-6.5 to 6.65-6.70 km/sec. Thickening below the Baltic Shield is mainly in the lower crust (layers with velocities 6.6 km/sec and more). One can see that increasing Moho depth in the central part of the profile up to 50-55 km accompanies an *increase* in the Bouguer gravity anomaly, from -(60-80) mgal to zero

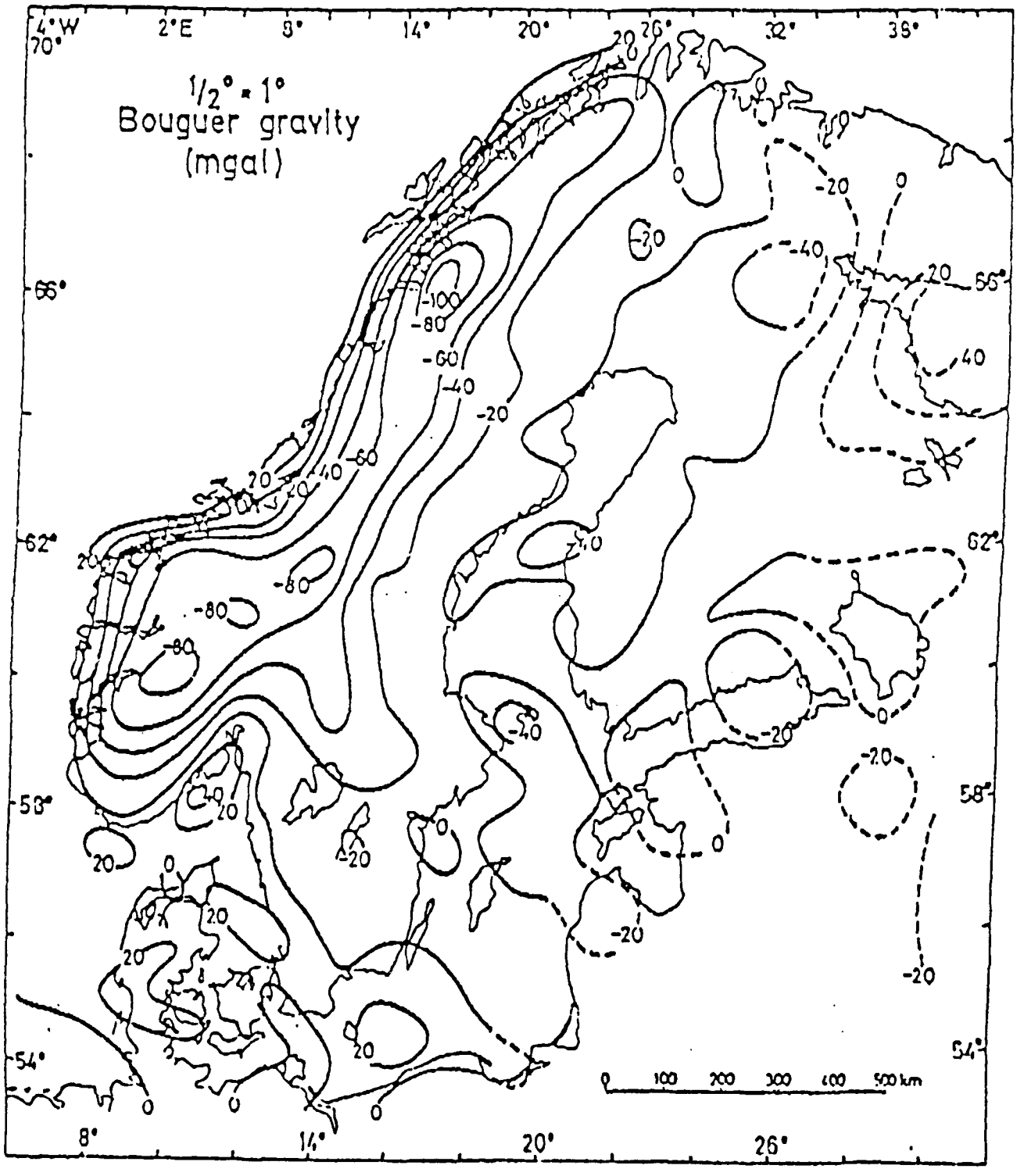


*Figure 13.* Bouguer gravity anomaly map (adapted from Balling, 1984). Contours are at 20 mgal intervals.

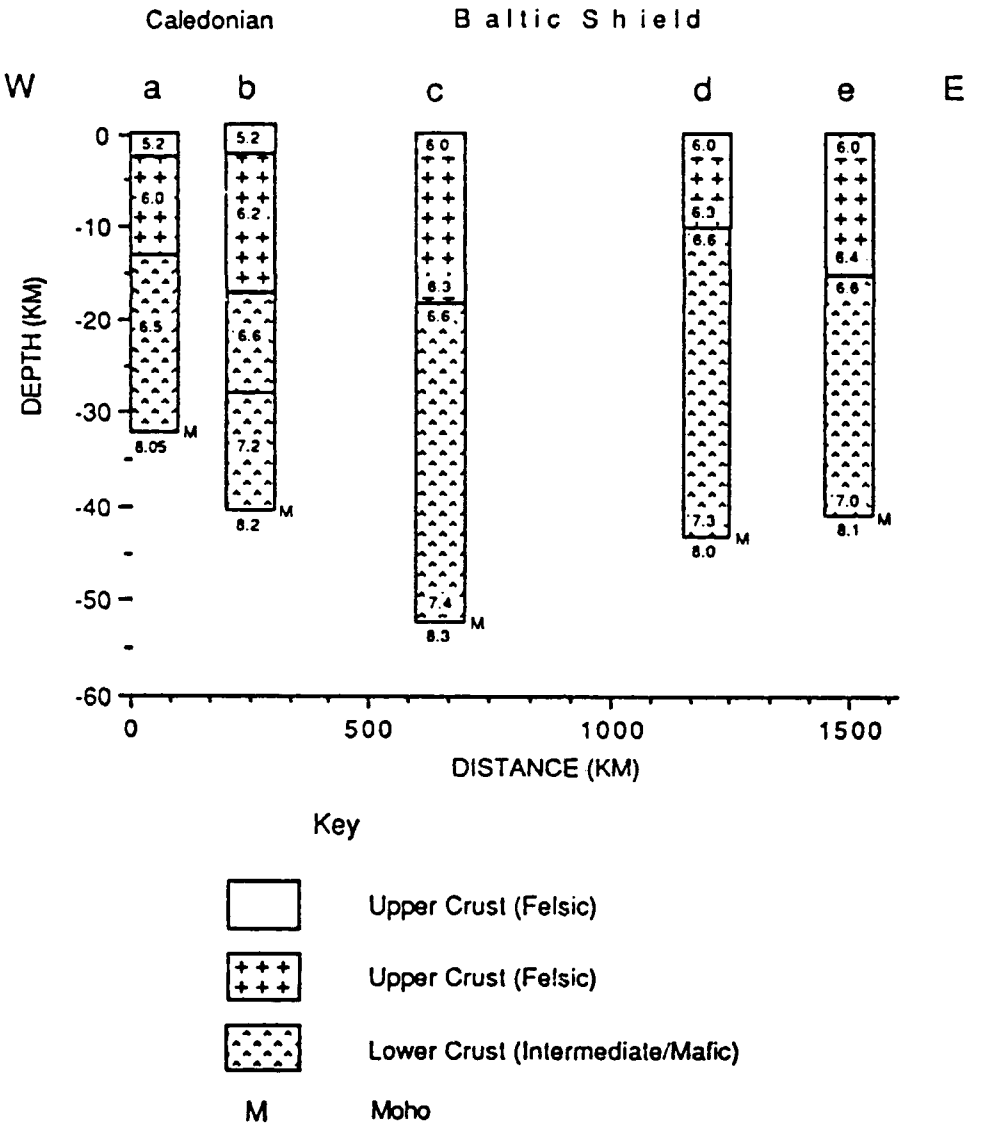


*Figure 14.* Representative seismic velocity-depth sections for a profile from the North Sea to Helsinki to Leningrad. The lower part of the crust is relatively thinner beneath the Caledonian Mountains (a,b) compared with the Baltic Shield (c,d,e). Sources: a -- Sellevoll and Warrick (1971); b -- Dahlman et al. (1971); c -- Guggisberg and Berthelsen (1987); d -- Luosto et al. (1985); e -- Litvinenko and Platonenkova (1978).

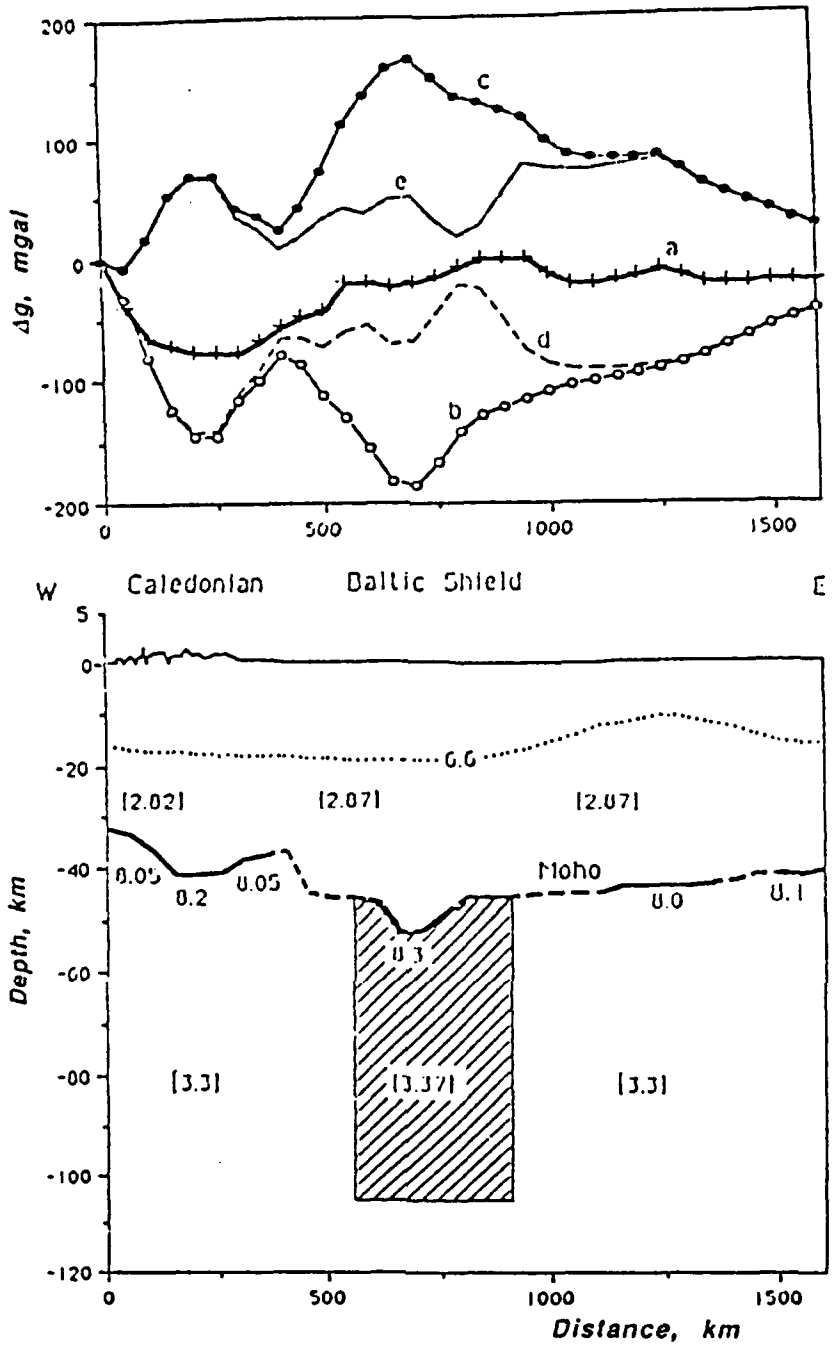


*Figure 15.* Comparison of seismic and gravity data for the North Sea-Leningrad profile. Top -- gravity curves: a -- observed Bouguer gravity anomalies; b -- theoretical influence of the earth's crust; c -- difference between curves a and b (residual gravity anomalies); d -- theoretical influence of the crust and upper mantle; e -- difference between curves a and d. Bottom -- cross-section showing velocity and density. Dotted line -- approximate location of 6.6 km/s line; numbers below Moho are $P_n$ velocity (km/s); numbers in brackets are average density (gm/cc); shaded area -- high-velocity, high-density body in the lower lithosphere.

(*Figure 15*). A similar correlation has also been observed for other regions of Eurasia (Vol'vovskii *et al.*, 1962).

To calculate the gravity influence of the crust we estimated values of mean crustal density along the profile, based in turn on variations in mean crustal velocity from the seismic data (*Figure 14*) and the velocity ($V$)-density ($\rho$) relationship, constructed as a result of statistical analysis of numerous laboratory measurements, $\rho = 0.60 + 0.34\ V$ (Krasovskii, 1979). Calculations show that the transition from the Caledonian Mountains to the Baltic Shield is accompanied by an increase in mean density of the earth's crust from 2.82 to 2.87 g/cc. The average density of the upper mantle was assumed to be 3.3 g/cc.

The gravity field constructed from the density model (*Figure 15*) was calculated using a program of J. Leutgert (written communication, 1989). The difference between observed Bouguer gravity and the theoretical anomaly due to the crust is more than 100 mgal in that part of the profile where Moho depths are 50-55 km (*Figure 15*). Based on available seismic data, we cannot explain such large deviations by lateral variations in crustal structure. We conclude, therefore, that the discrepancy between observed and calculated gravity curves is caused by lateral density variation in the upper mantle. A high-density body (density contrast of +0.07 g/cc relative to the surrounding material) of linear extent 300-600 km is located within the mantle lid, east of the NORESS array. The effect of such a body would explain the observed gravity, within a precision of ±30 mgal. This amount of scatter can easily be explained by the influence of small-scale lateral density inhomogeneities in the crust and upper mantle along the profile.

The interpretation of a high-velocity body in the upper mantle east of NORESS satisfies both the observation of increased $P_n$ velocity and the mean velocity of the lower lithosphere up to 100 km depth in southeastern Sweden, along both the OHL (NORSAR data in *Figure 11*) and *FENNOLORA* (Guggisberg and Berthelsen, 1987) profiles, and it also agrees with observations of teleseismic data (Husebye *et al.*, 1986). Had we used some other velocity-density relationship in the interpretation, the parameters (linear dimension, thickness, density contrast) of the high-density body might have changed, but probably not the main conclusion concerning the existence of such a body in the lower lithosphere. On the basis of the seismic and gravity data analyzed in this study we cannot reliably estimate the depth of penetration of this body in the upper mantle.

### 2.1.7 Discussion and Conclusions

Analysis of record sections of mine blasts recorded by seismic arrays such as NORESS is an effective way to study upper mantle structure on long-range profiles, provided there is some local network control on the location and origin time of the

explosions. There are tradeoffs between this method and traditional seismic profiling based on single-element recording of small chemical explosions, with the main advantages of our method being that (1) beamforming of weak signals improves SNR, and (2) the mine explosions tend to be larger than chemical explosions usually used in seismic profiling. These factors can be critical in identifying weak mantle waves recorded as first arrivals at far-regional distances. Our work suggests that, in earlier studies, larger secondary arrivals may have been interpreted as primary arrivals because the latter were weak and buried in noise.

A laterally homogeneous velocity section of the upper mantle was constructed for the OHL profile to depths of 200 km, based on interpretation of traveltimes and waveforms of the first arrivals. This section consists of two layers that have velocity increasing with depth, separated by a rather pronounced low-velocity layer in the depth range of approximately 105-135 km (*Figure 10*, model VR1). Other low-velocity layers (if they exist) must be thinner, and cannot be reliably detected with the data on hand. The upper-mantle velocity section constructed for this case is the simplest one that quantitatively fits the traveltimes and qualitatively explains the amplitudes of the first arrivals. This model also gives a qualitative fit to the more intensive second arrivals at far-regional distances.

Comparison of our results with other geophysical and geological data suggests that low-velocity layer in the upper mantle approximately coincides with a frequency-dependent low-Q layer found by Der *et al.* (1986), with the top of a shear-wave low-velocity layer determined by Calcagnile (1982) and Nolet *et al.* (1986) on the basis of surface waves, and with a layer of reduced viscosity determined by Artyushkov (1979) from observations of post-glacial rebound. Deep geoelectrical studies carried out in various areas of the Baltic Shield (Kaikkonen *et al.*, 1983; Jones,1982) and neighbouring Russian plate (Vanyan *et al.*, 1977; Vanyan and Shilovskiy, 1983) generally show a gradual decrease in resistivity with depth. On the background of this decrease, a high-conductivity layer was detected in the upper mantle below Sweden and Finland at depths of about 100-200 km (Jones, 1982). The calculated thickness of this layer was about 40 km and its depth varied beneath different geological units of the Baltic Shield. At the same time the geothermal estimate of upper-mantle temperature is less than the solidus for upper-mantle material (Smirnov, 1970, 1980; Chermac, 1982; Milanovsky, 1984), and a petrological study of mantle xenoliths (Dobretsov, 1980; Luts, 1974) showed that beneath the East European and Siberian platforms the upper mantle is crystalline.

Our combined interpretation of seismic and Bouguer gravity data for the OHL profile indicates that a high-density, high-velocity body probably exists in the lower lithosphere below the Moho, in an area where the crust thickens to 50-55 km (Moho root) approximately 300-600 east of NORESS. This conclusion agrees with the observation of increased $P_n$ velocity on the *FENNOLORA* profile in southeastern Sweden (Guggisberg and Berthelsen, 1987), and with the mean velocity of the lower

lithosphere up to depth 100 km determined by Husebye *et al.* (1986) from teleseismic data. One might also hypothesize a high-density body in the upper mantle beneath southern Finland, where the crust thickens up to 50-55 km (*Figure 4*). However, increased $P_n$ velocity was not observed in that area, either because there is no high-density body or because its top is well below the Moho. The effect on the velocity model of the high-velocity body beneath the OHL profile is primarily to decrease the velocity gradient in the uppermost mantle, relative to that for the laterally homogeneous model (*Figure 10*). The most important feature of the model, namely the low-velocity layer, is reliably determined and stable, although values of its parameters can vary somewhat.

The results discussed above can be qualitatively explained on the basis of a model of solid crystalline state of the lower lithosphere and asthenosphere beneath ancient platforms of Northern Eurasia (Ryaboy, 1985). Mantle rocks below the Baltic Shield from about 100 to 200 km depth probably have high subsolidus temperature (Milanovsky, 1984). According to theoretical results and data obtained in laboratories, the mantle rocks here are crystalline and have very specific physical and rheological properties. Namely, they can flow slowly, and are characterized by slightly decreased values (up to 3-5 %) of velocity of P- and S-waves, electrical resistivity, and Q (Mizutani and Kanamori, 1964; Sato and Sacks, 1989; Sato *et al.*, 1989). These variations fit rather well with results of previous studies of geophysical properties of the lithosphere at 100-200 km depth below the Baltic Shield.

An interesting feature of the deep structure of the Baltic Shield in southeastern Sweden and southern Finland is the possible correlation of crustal thickening (to 50-55 km) with the presence of high-density, high-velocity bodies in the lower lithosphere. Comparison with surface geology indicates that this thickening occurs beneath *Svecofennide* units that were tectonically active over a long period during Proterozoic time, when numerous eruptions of felsic and mafic volcanic rocks occured in the area (Hain, 1977; Boyd *et al.*, 1985; Grigor'eva *et al.*, 1989). Major- and trace-element studies indicate that the observed batholiths consist of basic rocks that originated in the upper mantle as products of partial melting (Patchett *et al.*, 1981; Wilson *et al.*, 1985). Thus, the depressed Moho and deeper high-density bodies may represent residual roots of ancient Proterozoic volcanoes, with the deep high-velocity zones consisting of mantle rocks depleted of silicic constituents during the eruptive phase. This picture is similar to a high-velocity body postulated on the basis of teleseismic data in the upper mantle beneath the Silent Canyon caldera in southern Nevada, which Spence (1974) has explained by extrusion of volatile magmatic components. Analogous structures have also been observed in the late Oligocene Questa caldera in north-central New Mexico (Lipman, 1983), and the late Proterozoic Salma caldera in the Arabian Shield (Kellog, 1985).

We can hypothesize that similar high-density bodies should exist in the lower lithosphere of other ancient shields, particularly where crustal thickening has been

observed in areas lacking pronounced negative gravity anomalies. Examples of such areas are the Ukrainian, Voronezh (Sollogub, 1986; Semov, 1987), and Canadian (Mooney and Braile, 1989) Shields. For example, thickening of the crust up to 50 km beneath Lake Superior (Canadian Shield) is accompanied by a rather pronounced Bouguer gravity high (Gravity Anomaly Map Committee, 1987). A thin low-velocity layer was also found in the upper mantle of the Canadian Shield (Masse, 1973) at approximately the same depth range as under the OHL profile.

The lower-lithosphere/asthenosphere model presented here opens new possibilities for resolving geodynamic problems relative to the Baltic Shield. In the area of seismic verification of test ban treaties, the low-velocity zone together with high-velocity bodies in the lower lithosphere would significantly influence propagation of seismic signals recorded at far-regional and teleseismic distance ranges (McLaughlin *et al.*, 1989; Barker and Murphy, 1989). In particular, our velocity model of the upper mantle offers a possible explanation for observations by NORSAR scientists, that the high-frequency content of regional seismic signals decreases abruptly at distances of 700-800 km (Loughran, 1987, 1988; Mykkeltveit, 1988). An important goal of further investigations of deep structure of the Baltic Shield will be to study lateral variations of the upper-mantle velocity model described in this paper.

Vladislav Ryaboy

## ACKNOWLEDGEMENTS

The author is grateful to Alan Ryall, Ken Olsen, Walter Mooney and Jan Kutina for their constant helpfulness during this work and for their valuable criticism. Alan Ryall also made a very valuable contribution in editing the manuscript, and John Coyne helped with software and calculations used in this study.

## References


Artyushkov, Ye. V., 1979. *Geodinamika (Geodynamics)*, Nauka (Science) Publisher House (in Russian), Moscow. p. 327.

Azbel, I. Ya., A. F. Buyanov, V.T. Ionkis, N.V. Sharov, and V.P. Sharova, 1989. "Crustal Struture of the Kola Peninsula from Inversion of Deep Seismic Sounding Data," *Tectonophysics*, Vol. 162, No. 1/2, pp. 87-100.

Balling, N., 1984. "Gravity and Isostasy in the Baltic Shield," in *First EGT Workshop: The Northern Segment*, European Science Foundation, Strasbourg, pp. 53-68.

Bannister, S. C., B. O. Ruud, and E. S. Husebye, 1989(in press). "Tomographic Estimates of Sub-Moho Seismic Velocities in Fennoscandia and Structural Implications," *Tectonophysics.*

Barker, B. W. and J. R. Murphy, 1989. "A Lithospheric Velocity Anomaly Beneath Shagan River Test Site: Part 1. Detection and Location with Network Magnitude Residuals," *Seismological Research Letters*, Vol. 60, No. 1, p. 5.

Bath, M., 1981. "Average Crustal Travel Times in Sweden Re-examined," *Pure and Applied Geophysics*, Vol. 119, No. 6, pp. 1116-1124.

Boyd, R., H. Papunen, A. Vorma, V. Zagorodny, and W. Robonen, 1985. *General Geological Map of the Baltic Shield (1:2 500 000 scale)*, Geological Survey of Finland, Bulletin 333, p. 1.

Bungum, H., S. Pirhonen, and E. S. Husebye, 1980. "Crustal Thickness in Fennoscandia," *Geophys. J. R. astr. Soc.*, Vol. 63, pp. 759-774.

Bur'yanov, V. B., V. V. Gordienko, S. N. Kulik, and N. M. Loginov, 1983. *Kompleksnoe Geofizicheskoye Izucheniye Tektonosfery Kontinentov (Complex Geophysical Study of the Tectonosphere of Continents)*, Naukova Dumka Publisher House (in Russian), p. 76.

Calcagnile, G., 1982. "The Lithosphere-Astenosphere System in Fennoscandia," *Tectonophysics*, Vol. 90, pp. 19-35.

Chapman, C. H., chu Jen-Yi, and D. G. Luness, 1988. "The WKBJ Seismogram Algorithm," in *Seismological Algorithms. Computational Methods and Computer Programs*, pp. 47-74.

Chermac, V., 1982. "Geothermal Model of the Lithosphere and Chart of the Thickness of the Lithosphere in the Territory of the USSR," *Izv. Akad. Nauk SSSR, Fizika Zemli (in*

*Russian)*, No. 1, pp. 25-38.

Dahlman, O., A. Vogel, C. E. Lund, R. Kanestrom, K. Haugland, and S. Gregersen, 1971. "The Trans-Scandinavian Seismic Profiles of 1969," in *Proceedings of the Colloquium of Deep Seismic Sounding in Northern Europe Held in Uppsala on December 1 and 2, 1969*, pp. 55-98.

Der, Z. A., A. C. Lees, and V. F. Cormier, 1986. "Frequency Dependence of Q in the Mantle Underlying the Shield Areas of Eurasia, Part III: The Q Model," *Geophys. Journ. astr. Soc.*, Vol. 87, pp. 1103-1112.

Dobretsov, N. L., 1980. *Vvedenie v global'nuyu petrologiyu (Introduction to Global Petrology)*, Nauka (Science) Publisher House (in Russian), p. 200.

Fluh, E. R. and A. Berthelsen, 1986. "Tectonic Evaluation and Crustal Structure in Denmark, and Southwest Sweden," in *Proceedings of the Third Workshop on the European Geotraverse (EGT) Project*, pp. 41-51.

Fuchs, K., 1986. "Structure, Physical Properties and Lateral Heterogeneities of the Subcrustal Lithosphere from Long-Range Deep Seismic Sounding Observations on Continents," *Tectonophysics*, Vol. 56, No. 197, pp. 1-15.

Fuchs, K., L. P. Vinnik, and C. Prodehl, 1987. "Exploring Heterogeneities of the Continental Mantle by High Resolution Seismic Experiments," in *Composition, Structure and Dyn. mics of the Lithosphere-Asthenosphere System. Geodynamics Series*, Vol. 16, pp. 137-154.

Galdin, N. E., A. V. Egorkin, S. K. Zuganov, L. I. Kagalova, and N. M. Chernishov, 1988. "Glubinnoe Stroenie Zemnoi Kori Kol'skogo Poluostrova Vdol' Regional'nogo profilia MOVZ-GCZ Pechenga-Umbozero- Pulon'ga-Ruch'i (Deep Structure of the Earth's Crust Beneath the Kola Peninsula Along the MCWE-DSS Long-Range Profile Pechenga-Umbozero-Pulon'fa-Ruch'i) (in Russian)," *Geotektonika (Geotectonics)*, Vol. 4, pp. 30-44.

Given, J. W. and D. V. Helmberger, 1980. "Upper Mantle Structure of Northwestern Eurasia," *Journ. of Geophys. Res.*, Vol. 85, No. B12, pp. 7183-7196.

Glaznev, V. N., A. B. Raevsky, and N. V. Sharov, 1989. "A Model of the Deep Structure of the Northeastern Part of the Baltic Shield Based on Joint Interpretation of Seismic, Gravity, Magnetic and Heat flow Data," *Tectonophysics*, Vol. 162, pp. 151-164.

Gravity Anomaly Map Committee, 1987. *Gravity Anomaly Map of North America, Scale 1:5,000,000*, The Geological Society of America.

Grigor'eva, L. V., V. V. Ivanikov, and N. F. Shinkarev, 1989. "Tektonicheskoe Razvitie Baltiiskogo Shita V Proterozoe (Tectonic evolution of the Baltic Shield in Proterozoic) (in Russian)," *Geotektonika (Geotectonics)*, Vol. 1, pp. 37-47.

Guggisberg, B., J. Ansorge, and St. Mueller, 1984. "Structure of the Upper Mantle Under Southern Scandinavia from Fennolora Data," in *Proceedings of the First Workshop on the European Geotraverse (EGT). The Northern Segment*, pp. 49-52.

Guggisberg, B. and A. Berthelsen, 1987. "A Two-Dimensional Velocity Model for the Lithosphere Beneath the Baltic Shield and Its Possible Tectonic Significance," *Terra Cognita*, Vol. 7, pp. 631-638.

Hain, V. E., 1977. *Regional'naya Geotektonika (Regional Geotectonics)*, Nedra (Interior) Publisher House (in Russian), p. 359.

Herrin, E. and J. Taggart, 1968. "Regional Variations In *P* Travel Times," *Bull. Seism. Soc. Am.*, Vol. 58, pp. 1325-1337.

Husebye, E. S. and J. Hovland, 1982. "On Upper Mantle Seismic Heterogeneities Beneath Fennoscandia," *Techonophysics*, Vol. 90, pp. 1.

Husebye, E. S., J. Hovland, A. Christoffersson, K. Astrom, R. Slunga, and C.E. Lund, 1986. "Tomographical Mapping of the Lithosphere and Asthenosphere Beneath Southern Scandinavia and Adjacent Areas," *Tectonophysics*, Vol. 128, pp. 229-250.

International Seismological Centre, 1982. *Regional Catalogue of Earthquakes (July-December, 1979)*, No. 16.

Jones, A. G., 1982. "Observations of the Electrical Asthenosphere Beneath Scandinavia," *Tectonophysics*, Vol. 90, pp. 37-55.

Kaikkonen, P., L. L. Vanyan, S. E. Hjelt, A. P. Shilovsky, K. Pajunpaa, and P. P. Shilovsky, 1983. "A Preliminary Geoelectrical Model of the Karelian Megablock of the Baltic Shield," *Phys. Earth Planet. Inter.*, Vol. 32, pp. 301-305.

Kellogg, K. S., 1985. "Root Zone of the Late Proterozoic Salma Caldera, Northeastern Arabian Shield, Kingdom of Saudi Arabia," *Journ. Geophys. Res.*, Vol. 90, No. B13, pp. 11,253-11,262.

King, D. W. and G. Calcagnile, 1976. "*P*-wave Velocities in the Upper Mantle Beneath Fennoscandia and Western Russia," *Geophys. Journ. R. astr. Soc.*, Vol. 46, pp. 407-432.

Korhonen, H. and M. Porkka, 1981. "The Structure of the Baltic Shield Region on the

Basis of DSS and Earthquake Data," *Pure and Applied Geophysics*, Vol. 119, No. 6, pp. 1093-1099.

Krasovskii, S. S., 1979. "O Zavisimosti Mexhdu Plotnost'u i skorost'u uprugih voln porod konsolidirovannoi zemnoi kori i verhnei mantii (On Relationship Between Seismic Velocity and Density of Rocks of the Earth Crust and Upper Mantle)," in *Gravitatsionnaia Model Zemnoi Kori i Verhnei Mantii (Gravity Pattern of the Earth Crust and Upper Mantle)*, Naukova Dumka Publisher House (in Russian), pp. 33-48.

Lipman, P. W., 1983. "The Miocene Quest Caldera, Northern New Mexico: Relation to Batholith Emplacement and Associated Molybdenum Mineralization," in *The Genesis of Rocky Mountain Ore Deposits: Changes with Time and Tectonics, Proceedings of the Denver Region Exploration Geologists Society Symposium*, pp. 133-148.

Litvinenko, I. V. and L. N. Platonenkova, 1978. "Stroenie Zemnoi Kori i Verhnei Mantii Vostochnoi Chasti Baltiiskogo Shita (Structure of the Earth Crust and Upper Mantle in the Eastern Baltic Shield)," in *Stroenie Zemnoi Kori i Verhnei Mantii Tsentralnoi i Vostochnoi Evropi (Structure of the Earth Crust and Upper Mantle in the Central and Eastern Europe)*, Naukova Dumka Publisher House (in Russian), pp. 127-135.

Loughran, L. B., 1987. *NORSAR Semiannual Technical Summary*, 1 October 1986 - 31 Mar 1987, p. 124.

Loughran, L. B., 1988. *NORSAR Semiannual Technical Summary*, 1 October 1987 - 31 Mar 1988, p. 105.

Lund, C. E., 1979a. "The Fine Structure of the Lower Lithosphere Underneath the Blue Road Profile in Northern Scandinavia," *Tectonophysics*, Vol. 56, pp. 111-122.

Lund, C. E., 1979b. "Crustal Structure Along the Blue Road Profile in Northern Scandinavia," *Geol. Foren. Stockholm Forh.*, Vol. 101, No. 1, pp. 191-204.

Lund, C. E., 1980. "Fennoscandian Long-Range Project, 1979-Fennolora," in *Proceedings of the 17th Assembly of the European Seismological Commission*, Vol. 15, pp. 511-515.

Lund, C. E. and R. Slunga, 1981. "Crustal and Upper-Mantle Structure of the Baltic Shield Investigated by a Combined Interpretation of Deep-Seismic-Sounding Data and Surface-Wave Analysis," *Pure and Applied Geophysics*, Vol. 119, No. 6, pp. 1100-1106.

Luosto, U., E. H. Flueh, C. E. Lund, and Working Group, 1989. "The Crustal Structure Along the POLAR Profile from Seismic Refraction Investigations," *Tectonophysics*, Vol. 162, No.1/2, pp. 51-86.

Luosto, U., H. Korhonen, I. P. Kosminskaya, S. M. Zverev, C. E. Lund, N. V. Sharov, E. Lanne, A. Tupperainen, V. M. Ilmola, and A. N. Foursov, 1985. *First Results from the DSS Study on the Baltic Profile in SE Finland,* Institute of Seismology, University of Helsinki, p. 21.

Luosto, U., E. Lanne, H. Korhonen, A. Guterh, M. Grad, R. Materzok, and E. Perchuc, 1984. "Deep Structure of the Earth's Crust on the SVEKA Profile in Central Finland," *Annales Geophysicae,* Vol. 2, No. 5, pp. 559-570.

Luts, B. G., 1974. *Petrologiya Glubinnyh zon Kontinental'noi kori i Verhnei Mantii (Petrology of Deep Continental Crust and Upper Mantle),* Nauka (Science) Publisher House (in Russian), p. 304.

Masse, R. P., 1973. "Compressional Velocity Distribution Beneath Central and Eastern North America," *Bull. Seism. Soc. Am.,* Vol. 63, pp. 911-935.

Masse, R. P. and S. S. Alexander, 1974. "Compressional Velocity Distribution Beneath Scandinavia and Western Russia," *Geophys. Journ. R. astr. Soc.,* Vol. 39, pp. 587-602.

McLaughlin, K. L., J. R. Murphy, and B. W. Barker, 1989. " A Lithospheric Velocity Anomaly Beneath Shagan River Test Site: Part 2. Imaging and Inversion with Amplitude Transmission Tomography," *Seismological Research Letters,* Vol. 60, No. 1, p. 5.

Meissner, R., T. H. Wever, and E. R. Fluh, 1987. "The Moho in Europe - Implications for Crustal Development," *Annales Geophysicae,* Vol. 5B, No. 4, pp. 357-364.

Mereu, R. F., S. Mykkeltveit, and E. S. Husebye, 1983. "Fennolora Recordings at NORSAR," *Journ. of Geophys. Res.,* Vol. 52, pp. 119-130.

Milanovsky, S. Yu., 1984. "Deep Geothermal Structure and Mantle Heat Flow Along the Barents Sea - East Alps Geotraverse," *Tectonophysics,* Vol. 103, pp. 175-192.

Mizutani, H. and H. Kanamori, 1964. "Variation of Elastic Wave Velocity and Attenuative Property Near the Melting Temperature," *Journ. of Physics of the Earth,* Vol. X11, No. 2, pp. 43-49.

Mooney, W. D. and L. W. Braile, 1989. "The Seismic Structure of the Continental Crust and Upper Mantle of North America," in *The Geology of North America,* Vol. A, pp. 39-52.

Mueller, St. and J. Ansorge, 1986. "Long-Range Seismic Refraction Profiles in Europe," in *Reflection Seismology: A global Perspective. Geodynamics Series.,* AGU, Washington, Vol.13, pp. 167-182.

Mykkeltveit, S., 1980. "A Seismic Profile in Southern Norway," *Pure and Applied Geophysics*,, Vol. 118, pp. 1310-1325.

Nersesov, I. L. and T. G. Rautian, 1964. "Kinematika i Dinamika Seismicheskih voln Na Rasstoianiah Do 3500 km Ot Epitsentra (Kinematics and Dynamics of Seismic Waves to Distances of 3,500 km from the Epicenter)," in *Eksperimental'naia Seismika (Experimental Seismology)*, Nauka (Science) Publisher House (in Russian), pp. 63-87.

Nolet, G., B. Dost, and H. Paulssen, 1986. "Preliminary Results from the EGT's NARS Project," in *Proceedings of the Third Workshop on the European Geotraverse (EDT) Project*, European Science Foundation, pp. 223-226.

Patchett, P. J., O. Kouvo, C. E. Hedge, and M. Tatsumoto, 1981. "Evolution of Continental Crust and Mantle Heterogeneity; Evidence from Hf Isotopes," *Contrib. Mineral. Petrol.*, Vol. 78, pp. 279-297.

Prodehl, C., 1984. "Structure of the Earth's Crust and Upper Mantle," *Landdt-Bornstein New Series*, Vol. V2, pp. 97-206.

Prodehl, C. and V. Kaminski, 1984. "Crustal Structure Under the Fennolora Profile," in *Proceedings of the First Workshop on the European Geotraverse (EGT). The Northern Segment*, European Science Foundation, pp. 43-68.

Ryaboy, V. Z., 1966. "Kinematic and Dynamic Characteristics of Deep Waves Associated with Boundaries in the Crust and Upper Mantle," *Izv. (Bull.) Acad. Sci. USSR, Geophys. Ser., AGU Transl.*, Vol. 3, pp. 177-184.

Ryaboy, V. Z., 1979. *Struktura Verkhney Mantii Territorii SSR po Seismicheskim Dannym (The Upper Mantle Structure of the Territory of the USSR According to Seismic Data)*, Nedra Publisher House (in Russian), p. 245.

Ryaboy, V. Z., 1985. "Lower Lithosphere and Asthenosphere of Central and Eastern Regions of Northern Eurasia Based on Seismic Data," *Izvestiya Academy of Sciences, USSR, Physics of the Solid Earth (English edition)*, Vol. 21, No. 2, pp. 100-110.

Ryaboy, V. Z., 1989a. *Upper Mantle Structure Studies by Explosion Seismology in the USSR*, DELPHIC Associates, p. 154.

Ryaboy, V. Z., Ju. A. Burmakov, L. N. Nikitina, and S. V. Potap'ev, 1987. "Osnovnie Cherti Skorostnogo Stroenia Verhnei Mantii (The Main Features of the Upper Mantle Velocity Structure)," in *Glubinnoe Stroenie Slaboseismichnih Regionov SSSR (Deep Structure of the Nonseismic Regions of the USSR Territory)*, Nauka (Science) Publisher House (in Russian), pp. 86-116.

Sato, H. and I. S. Sacks, 1989. "Anelasticity and Thermal Structure of the Oceanic Upper Mantle: Temperature Calibration with Heat Flow Data," *J. Geophys. Res.*, Vol. 94, No. B5, pp. 5705-5715.

Sato, H., I. S. Sacks, and T. Murase, 1989. "The Use of Laboratory Velocity Data for Estimating Temperature and Partial Melt Fraction in the Low-Velocity Zone: Comparison with Heat Flow and Electrical Conductivity Studies," *J. Geophys. Res.*, Vol. 94, No. B5, pp. 5689-5704.

Sellevoll, M. A., 1973. "Mohorovicic Discontinuity Beneath Fennoscandia and Adjacent Parts," *Tectonophysics*,No. 20, pp. 359-366.

Sellevoll, M. A. and R. E. Warrick, 1971. "A Refraction Study of the Crustal Structure in Southern Norway," *Bull. Seism. Soc. Am.*,Vol. 61, No. 2, pp. 457-471.

Semov, V. N., 1987. "Zakonomernosti Stroenia i Morfologia Poverhnosti Moho (Some Regularities of Structure and Morphology of the Moho Discontinuity)," in *Glubinnoe Stroenie Slaboseismichnih Regionov SSR (Deep Structure of the Nonseismic Regions of the USSR Territory)*, Nauka (Science) Publisher House (in Russian), pp. 71-80.

Smirnov, Ya. B., 1970. "Values of Geothermal Research for Studying the Earth's Crust and Upper Mantle," in *Problemy Stroyeniya Zemnoy Kory i Verkhnei Mantii (Problems of the Structure of the Earth's Crust and Upper Mantle)*, Nauka (Science) Publisher House (in Russian), pp. 250-265.

Smirnov, Ya. B., 1980. *Teplovoye Pole Territorii SSR (Heat Field in the Territory of the USSR)*, GUGK (in Russian), p. 150.

Sollogub, V. B., 1986. *Litosfera Ukrainy (Lithosphere of the Ukraine)*, Naukova Dumka (Science) Publisher House (in Russian), p. 183.

Spence, W., 1974. "*P*-wave Residual Differences and Inferences on an Upper Mantle Source for the Silent Canyon Volcanic Centre, Southern Great Basin, Nevada," *Geophys. Journ. astr. Soc.*, Vol. 38, pp. 505-523.

Stangl, R., K. Fuchs, and C. Prodehl, 1986. "The Structure of the Upper Mantle Below Scandinavia--An Interpretation of the Travel Time and Amplitude Data with the Aid of the Reflectivity Method," *Teilproject*, Vol. B1, pp. 683-507.

Vanyan, L. L., M. N. Berdichevsky, E. B. Fainberg, and M. V. Fiskin, 1977. "The Study of the Asthenosphere of the East European Platform by Electromagnetic Sounding," *Phys. Earth Planet. Inter.*, Vol. 14, pp. P1-P2.

Vanyan, L. L. and P. P. Shilovsky, 1983. *Glubinnaya Elektroprovodnost' Okeanov i Kontinentov (Depth Electroconductivity of the Oceans and Continents)*, Nauka (Science) Publisher House (in Russian), p. 86.

Vinnik, L. P. and V. Z. Ryaboy, 1981. "Deep Structure of the East European Platform According to Seismic Data," *Phys. Earth Planet. Inter.*, Vol. 25, pp. 27-37.

Vol'vovskii, I. S., V. Z. Ryaboy, and V. I. Shraibman, 1962. "O Prirode Regionalnih Gravitatsionnih Anomalii Buharo-Hivinscoi Provintsii i Sopredelnih Raionov (On Nature of Regional Gravity Anomalies of Buhar-Hiva Region and Adjacent Areas)," *Izvestiya Academy of Sciences, USSR, Geophysical Series (in Russian)*, No. 5, pp. 644-651.

Weinrebe, W., 1981. "Joint Interpretation of Earthquake Travel-Time Residuals and Seismic Measurements Along the 'Blue Norma' Profile in Northern Scandinavia," *Pure and Applied Geophysics*, Vol. 119, No. 6, pp. 1107-1115.

Wilson, M. R., P. J. Hamilton, and A. E. Fallick et al., 1985. "Granites and Early Proterozoic Crustal Evolution in Sweden: Evidence from Sm-Nd, U-Pb and O Isotope Systematics," *Earth Plan. Sci. Lett.*, Vol. 72, pp. 376-388.

## APPENDIX I.
## PROFILE OSLO - HELSINKI - LENINGRAD
## DISCREPANCY BETWEEN CHARACTERISTICS OF EVENTS ACCORDING TO THE HELSINKI AND NORESS BULLETINS

| No. | Date | Origin time From Helsinki Bulletin | Distance from NORESS | Azimuth | Discrepancy (HEL-NOR) Origin time | Distance | Azimuth |
|---|---|---|---|---|---|---|---|
| | | h. m. sec. | km | deg. | sec. | km | deg. |
| 1 | 102985 | 12.01.25.0 | 734.5 | 97.0 | -3.0 | 39.9 | 2.8 |
| 2 | 103185 | 2.55.49.8 | 411.9 | 53.6 | 1.0 | 4.9 | 4.6 |
| 3 | 103185 | 14.11.26.0 | 951.6 | 82.6 | -0.4 | 20.2 | 1.9 |
| 4 | 110185 | 16.04.24.0 | 994.9 | 79.7 | 3.2 | -6.4 | 8.4 |
| 5 | 111285 | 12.22.07.0 | 760.5 | 94.5 | -8.9 | 35.7 | 9.1 |
| 6 | 111385 | 12.07.48.0 | 935.9 | 92.6 | -2.2 | 18.3 | -14.1 |
| 7 | 111485 | 12.52.29.0 | 935.3 | 82.8 | -3.0 | 17.2 | 35.3 |
| 8 | 111585 | 12.02.11.0 | 954.6 | 91.5 | -4.1 | 34.2 | -8.8 |
| 9 | 111585 | 13.53.37.0 | 994.9 | 79.7 | 0.4 | -5.3 | -19.3 |
| 10 | 112285 | 12.58.24.0 | 842.3 | 92.9 | -3.4 | 22.0 | 2.8 |
| 11 | 112385 | 13.06.18.0 | 760.5 | 94.5 | 2.6i | -8.6 | -0.7 |
| 12 | 112585 | 13.06.27.0 | 954.6 | 91.5 | -5.4 | 40.4 | -9.7 |
| 13 | 112785 | 12.18.29.0 | 1082.8 | 77.3 | -2.2 | 39.9 | 2.3 |
| 14 | 120285 | 12.05.58.0 | 954.6 | 91.5 | -3.8 | 34.0 | 5.8 |
| 15 | 120585 | 12.25.14.0 | 1012.3 | 80.2 | -4.6 | 52.6 | -1.0 |
| 16 | 120685 | 13.38.33.0 | 734.5 | 97.0 | -2.8 | 32.1 | -21.6 |
| 17 | 120785 | 13.18.18.0 | 886.8 | 93.5 | -4.2 | 42.4 | -15.0 |
| 18 | 121085 | 13.42.41.7 | 621.1 | 95.7 | -1.8 | 21.7 | 2.5 |
| 19 | 121185 | 12.14.19.0 | 954.6 | 91.5 | -3.9 | 35.9 | 6.5 |
| 20 | 121185 | 12.51.11.0 | 908.7 | 93.1 | -6.5 | 40.3 | -1.6 |
| 21 | 121385 | 12.08.48.0 | 954.6 | 91.5 | -3.9 | 41.6 | 1.4 |
| 22 | 122485 | 13.13.11.0 | 760.5 | 94.5 | -1.1 | 16.4 | -5.8 |
| 23 | 122585 | 12.04.25.0 | 965.0 | 81.2 | -4.6 | 37.8 | -0.3 |
| 24 | 122585 | 14.18.01.0 | 966.4 | 81.8 | -12.9 | 57.3 | 14.4 |
| 25 | 122685 | 13.07.12.0 | 951.6 | 82.6 | -2.3 | 20.1 | -3.0 |
| 26 | 122785 | 12.16.08.0 | 954.6 | 91.5 | 1.8 | -2.5 | -2.8 |
| 27 | 122785 | 14.49.08.0 | 1011.0 | 79.6 | -4.7 | 36.5 | -0.9 |
| 28 | 122885 | 11.47.24.6 | 920.1 | 105.0 | -0.9 | 29.0 | -0.9 |
| 29 | 10386 | 14.58.41.0 | 1026.9 | 74.5 | -3.5 | 40.9 | -10.5 |
| 30 | 11386 | 12.05.38.3 | 705.6 | 94.5 | 1.3 | -8.3 | -0.2 |
| 31 | 11486 | 12.02.24.0 | 954.6 | 91.5 | -4.8 | 41.6 | 1.4 |
| 32 | 11586 | 12.05.55.0 | 954.6 | 91.5 | -6.8 | 60.7 | 1.9 |
| 33 | 11786 | 12.11.59.0 | 935.9 | 92.6 | -0.4 | 7.4 | -10.6 |
| 34 | 12386 | 12.26.27.0 | 954.6 | 91.5 | 0.3 | 0.9 | -4.3 |
| 35 | 12586 | 23.13.24.2 | 315.4 | 64.6 | 1.5 | -8.0 | -11.6 |
| 36 | 20686 | 12.22.04.0 | 935.9 | 92.6 | -2.5 | 20.0 | -7.1 |
| 37 | 21486 | 12.10.21.0 | 954.6 | 91.5 | -2.0 | 3.0 | 8.9 |
| 38 | 21686 | 15.04.09.1 | 1099.3 | 96.1 | -4.4 | 42.1 | -3.5 |
| 39 | 21786 | 12.12.38.0 | 935.9 | 92.6 | -6.3 | 36.8 | -2.2 |
| 40 | 30586 | 12.13.19.0 | 842.3 | 92.9 | -1.8 | 35.0 | -1.5 |
| 41 | 31186 | 12.02.28.0 | 935.9 | 92.6 | -1.2 | 7.9 | -12.9 |
| 42 | 32186 | 13.01.52.0 | 760.5 | 94.5 | 2.0 | -58.4 | 9.2 |
| 43 | 32586 | 12.30.24.0 | 954.6 | 91.5 | -4.1 | 38.2 | 10.0 |
| 44 | 32786 | 12.23.55.0 | 954.6 | 91.5 | 1.4 | -2.5 | -2.8 |
| 45 | 41486 | 14.54.31.2 | 712.4 | 95.7 | -2.7 | 17.8 | 1.6 |
| 46 | 41686 | 11.01.00.0 | 954.6 | 91.5 | 1.3 | -25.9 | 6.5 |
| 47 | 41786 | 13.31.12.0 | 1030.5 | 89.0 | -6.0 | 55.5 | 3.9 |

| No. | Date | Origin time From Helsinki Bulletin | Distance from NORESS | Azimuth | Discrepancy (HEL-NOR) Origin time | Distance | Azimuth |
|---|---|---|---|---|---|---|---|
| | | h. m. sec. | km | deg. | sec. | km | deg. |
| 48 | 42286 | 11.03.17.0 | 954.6 | 91.5 | -1.6 | 6.3 | -7.3 |
| 49 | 42986 | 16.55.31.3 | 695.1 | 93.0 | -3.5 | 46.9 | -1.2 |
| 50 | 42986 | 17.31.45.9 | 696.2 | 93.4 | -3.3 | 46.4 | -4.9 |
| 51 | 51186 | 11.14.35.0 | 935.9 | 92.6 | -3.5 | 24.9 | 11.0 |
| 52 | 51386 | 9.43.15.9 | 453.9 | 114.6 | 8.8 | -29.3 | 14.5 |
| 53 | 51386 | 10.39.52.8 | 453.6 | 114.0 | 1.6 | -29.6 | 13.9 |
| 54 | 51686 | 15.02.25.0 | 1026.9 | 74.5 | -4.0 | 40.0 | -3.3 |
| 55 | 52086 | 11.09.49.0 | 935.9 | 92.6 | -1.0 | 6.1 | -2.3 |
| 56 | 52986 | 11.01.39.0 | 912.0 | 93.8 | 5.0 | -55.9 | -6.0 |
| 57 | 53086 | 11.02.47.0 | 954.6 | 91.5 | -2.2 | 19.7 | 1.8 |
| 58 | 60486 | 9.06.31.0 | 1018.1 | 77.0 | -0.1 | 32.7 | 5.1 |
| 59 | 61286 | 9.30.54.0 | 1018.1 | 77.0 | -1.1 | 8.3 | -8.4 |
| 60 | 61386 | 14.41.01.5 | 716.5 | 94.1 | -1.9 | 34.2 | -3.3 |
| 61 | 61786 | 12.02.54.8 | 442.4 | 119.8 | 17.2 | -114.3 | 17.3 |
| 62 | 62486 | 11.08.54.0 | 954.6 | 91.5 | -5.7 | 44.9 | 5.7 |
| 63 | 62586 | 12.33.17.0 | 1082.8 | 77.3 | -5.8 | 44.7 | 1.7 |
| 64 | 70886 | 12.06.23.4 | 984.0 | 86.7 | 0.9 | -11.2 | -3.4 |
| 65 | 71486 | 13.50.34.1 | 289.4 | 151.7 | 1.6 | -1.7 | 3.9 |
| 66 | 71486 | 14.30.27.0 | 994.9 | 79.7 | 1.3 | -11.5 | -15.7 |
| 67 | 71686 | 11.26.48.0 | 886.8 | 93.5 | -0.2 | 10.3 | 13.2 |
| 68 | 72686 | 1.40.08.3 | 349.7 | 123.2 | -2.0 | 14.3 | 4.7 |
| 69 | 73186 | 14.23.16.1 | 728.3 | 94.1 | -1.1 | 28.9 | -9.7 |
| 70 | 73186 | 15.05.37.0 | 742.0 | 95.9 | -3.8 | 61.9 | 11.0 |
| 71 | 80786 | 11.07.56.0 | 954.6 | 91.5 | -8.0 | 53.8 | -7.8 |
| 72 | 81886 | 8.25.07.0 | 760.5 | 94.5 | 3.3 | -24.6 | 4.7 |
| 73 | 91286 | 13.27.49.3 | 673.4 | 94.6 | -2.1 | 16.9 | -0.4 |
| 74 | 91886 | 15.12.05.2 | 495.1 | 85.0 | 0.0 | 9.7 | -13.7 |
| 75 | 91886 | 16.41.37.5 | 499.4 | 84.9 | 8.8 | -58.9 | 4.7 |
| 76 | 91886 | 16.47.58.5 | 497.3 | 85.1 | 4.5 | -34.0 | -4.8 |
| 77 | 92086 | 22.15.03.1 | 275.3 | 104.5 | 3.8 | -27.1 | -18.0 |
| 78 | 92686 | 11.02.49.2 | 1084.0 | 76.3 | -4.9 | 46.4 | 4.9 |
| 79 | 100286 | 15.06.30.0 | 908.7 | 93.1 | -6.6 | 33.6 | -6.1 |
| 80 | 100486 | 13.44.02.0 | 1026.9 | 74.5 | -3.4 | 15.2 | -15.5 |
| 81 | 101486 | 13.43.56.0 | 1018.1 | 77.0 | -1.2 | 17.6 | 3.2 |
| 82 | 102586 | 13.53.36.0 | 908.7 | 93.1 | -6.8 | 38.2 | -0.8 |
| 83 | 110286 | 7.47.59.0 | 245.2 | 151.4 | -3.5 | 30.3 | -10.5 |
| 84 | 110386 | 15.00.55.8 | 1192.0 | 98.4 | -3.5 | 35.6 | -5.7 |
| 85 | 112786 | 21.39.36.4 | 423.3 | 95.3 | 6.2 | -18.2 | -11.2 |
| 86 | 112786 | 21.50.22.3 | 415.4 | 95.3 | 7.1 | -40.9 | -5.9 |
| 87 | 111186 | 15.21.52.0 | 965.0 | 81.2 | -2.7 | 28.1 | -4.3 |
| 88 | 112186 | 9.47.51.9 | 490.7 | 82.8 | -1.8 | -8.9 | -2.4 |
| 89 | 112386 | 11.16.19.9 | 597.9 | 96.0 | -6.8 | 36.0 | -2.8 |
| 90 | 122386 | 13.51.08.0 | 842.3 | 92.9 | -2.3 | 31.9 | -4.8 |
| 91 | 122686 | 12.02.07.0 | 760.5 | 94.5 | -3.6 | 35.7 | 0.1 |
| 92 | 123086 | 6.09.57.5 | 1191.0 | 91.0 | 3.6 | -19.1 | -12.8 |
| 93 | 11587 | 12.29.38.0 | 760.5 | 94.5 | -3.2 | 30.2 | 9.2 |
| 94 | 12087 | 11.34.38.2 | 952.6 | 81.0 | -3.1 | 29.6 | 9.3 |
| 95 | 12087 | 13.13.13.0 | 1026.9 | 74.5 | -3.8 | 42.1 | 1.3 |
| 96 | 13087 | 13.44.55.0 | 1082.8 | 77.3 | -3.6 | 43.5 | 0.4 |
| 97 | 21487 | 10.27.54.8 | 1268.4 | 76.5 | -3.9 | 14.5 | -8.3 |
| 98 | 22187 | 9.42.42.0 | 1226.6 | 76.6 | 8.4 | -49.1 | -8.0 |
| 99 | 22687 | 13.52.48.0 | 842.3 | 92.9 | -5.0 | 51.4 | -1.9 |
| 100 | 30287 | 12.30.41.0 | 760.5 | 94.5 | 1.9 | -13.3 | 9.6 |

| No. | Date | Origin time From Helsinki Bulletin | Distance from NORESS | Azimuth | Discrepancy (HEL-NOR) Origin time | Distance | Azimuth |
|---|---|---|---|---|---|---|---|
| | | h. m. sec. | km | deg. | sec. | km | deg. |
| 101 | 31387 | 10.47.50.0 | 912.0 | 93.8 | -7.3 | 30.3 | -4.5 |
| 102 | 31387 | 12.39.00.0 | 886.8 | 93.5 | 3.4 | -4.4 | -11.6 |
| 103 | 41687 | 11.29.50.0 | 908.7 | 93.1 | -7.3 | 42.1 | 3.0 |
| 104 | 42187 | 11.47.57.0 | 935.9 | 92.6 | -0.8 | 6.5 | 2.7 |
| 105 | 50787 | 11.21.05.3 | 431.3 | 107.5 | 2.7 | -22.0 | 17.8 |
| 106 | 51287 | 12.25.56.0 | 951.6 | 82.6 | 15.4 | -34.3 | -2.4 |
| 107 | 52187 | 7.22.41.3 | 481.2 | 86.6 | 4.7 | 8.9 | 1.3 |
| 108 | 52587 | 11.50.11.0 | 954.6 | 91.5 | 1.9 | -3.5 | -7.8 |
| 109 | 52787 | 11.05.14.0 | 954.6 | 91.5 | -6.3 | 52.5 | 1.3 |
| 110 | 52787 | 11.41.05.0 | 742.0 | 95.9 | 4.4 | 3.2 | 0.8 |
| 111 | 60887 | 12.51.01.2 | 734.5 | 91.7 | 2.7 | -23.3 | 1.5 |
| 112 | 61687 | 10.24.48.5 | 721.9 | 93.8 | 0.1 | 15.5 | 3.6 |
| 113 | 61687 | 10.31.55.6 | 723.8 | 93.8 | -0.5 | 23.8 | -0.2 |
| 114 | 62587 | 8.23.47.0 | 742.0 | 95.9 | 1.1 | 28.3 | 3.0 |
| 115 | 63087 | 13.00.14.0 | 964.0 | 83.2 | -5.6 | 34.5 | -1.7 |
| 116 | 63087 | 17.30.37.0 | 994.9 | 79.7 | -3.5 | 35.4 | -10.4 |
| 117 | 70287 | 11.02.31.0 | 935.9 | 92.6 | 0.9 | -7.2 | 2.3 |
| 118 | 70687 | 12.02.08.0 | 954.6 | 91.5 | -9.1 | 66.4 | -3.5 |
| 119 | 71687 | 10.29.24.4 | 901.8 | 93.2 | -6.5 | 35.2 | 3.1 |
| 120 | 72287 | 10.27.38.0 | 935.3 | 82.8 | 1.2 | -27.2 | -11.4 |
| 121 | 72287 | 10.28.40.0 | 760.5 | 94.5 | -7.4 | 41.2 | 0.0 |
| 122 | 81287 | 11.25.05.8 | 688.6 | 93.9 | 0.3 | 14.0 | 9.0 |
| 123 | 82887 | 11.05.18.0 | 760.5 | 94.5 | 0.1 | 13.9 | 9.3 |
| 124 | 82887 | 12.37.54.0 | 842.3 | 92.9 | 0.6 | 6.6 | -2.5 |
| 125 | 90487 | 11.46.41.0 | 842.3 | 92.9 | 1.3 | 13.3 | -6.0 |
| 126 | 90987 | 10.02.11.0 | 504.2 | 86.6 | -3.1 | 10.1 | 1.3 |
| 127 | 91687 | 20.16.55.0 | 1026.9 | 74.5 | -1.4 | 9.8 | -15.4 |
| 128 | 91787 | 13.28.38.8 | 424.0 | 115.4 | -14.2 | 36.4 | 16.2 |
| 129 | 92587 | 12.22.23.0 | 908.7 | 93.1 | -14.9 | 47.8 | 9.0 |
| 130 | 100187 | 9.21.10.8 | 493.0 | 83.5 | 13.1 | -122.0 | -6.1 |
| 131 | 100187 | 10.02.33.0 | 587.2 | 96.7 | 0.1 | 5.1 | 10.9 |
| 132 | 100187 | 10.25.05.4 | 593.1 | 97.1 | -1.3 | 20.9 | 3.3 |
| 133 | 101487 | 14.09.41.2 | 712.0 | 95.9 | -1.8 | 24.1 | 6.4 |
| 134 | 111087 | 12.05.32.9 | 631.5 | 96.6 | 0.3 | -7.7 | 15.4 |
| 135 | 111187 | 7.20.47.1 | 627.3 | 97.1 | -4.7 | 1.5 | 7.6 |
| 136 | 111187 | 10.51.53.0 | 628.1 | 95.3 | -2.8 | 31.6 | 1.0 |
| 137 | 111187 | 11.09.00.0 | 1018.1 | 77.0 | -23.9 | 23.2 | -2.7 |
| 138 | 111187 | 11.36.21.2 | 623.9 | 96.0 | 3.2 | 78.2 | -3.2 |
| 139 | 111887 | 10.25.19.0 | 1018.1 | 77.0 | -0.7 | 16.9 | -9.1 |
| 140 | 122587 | 14.08.47.3 | 1093.7 | 96.9 | -2.8 | 38.2 | 2.5 |
| 141 | 122887 | 12.30.37.3 | 1101.5 | 97.2 | -7.5 | 56.2 | 14.7 |
| 142 | 122887 | 14.08.14.0 | 476.2 | 95.8 | 8.6 | -39.1 | 15.7 |
| 143 | 11588 | 12.25.48.0 | 842.3 | 92.9 | -8.6 | 65.9 | -6.6 |
| 144 | 12288 | 11.22.34.0 | 842.3 | 92.9 | 0.0 | -1.6 | -13.9 |
| 145 | 12388 | 9.37.13.9 | 895.6 | 93.4 | -8.4 | 49.4 | 8.3 |
| 146 | 22388 | 12.48.29.0 | 1030.5 | 89.0 | -3.5 | 47.9 | 3.3 |
| 147 | 30588 | 10.51.10.0 | 842.3 | 92.9 | -5.1 | 38.9 | -5.8 |

## 2.2. REVIEW OF METHODS FOR POLARIZATION ANALYSIS

### 2.2.1. Introduction

In this Report we review methods for extracting polarization characteristics and computing the slowness vector from three-component instruments, either in single stations or in arrays. First, we give an overview of a theoretical study comparing the expected performance of various sensor configurations (including vertical-component and three-component arrays) for estimating direction parameters. Then, we evaluate the two most promising methods for particle-motion analysis of three-component data: method (1) uses a Maximum Likelihood estimator , method (2), an eigensystem decomposition. They have recently been used to analyze data similar to those that will be processed by the NMRD systems. We investigate the results obtained when applying these methods to short-period local/regional data, short-period teleseismic data, and broadband teleseismic data. Then, we summarize how polarization attributes can be extracted from three-component data, and help locate events. Finally, based on this review, we recommend the use of method (2) in the NMRD systems, for phase identification, association and event location.

### 2.2.2. Theoretical Investigation of Uncertainty in Direction Estimation

Harris (1982) compares the performance of small arrays and three-component stations in estimating the wavefield direction. His study is a theoretical investigation into the uncertainty of direction estimates in the presence of noise. He uses the Cramer-Rao bound (CRB), which gives a lower bound on this uncertainty. The CRB provides reasonable estimates of performance for:

- sparse arrays of small aperture,
- waves arriving at moderate incidence angles,
- high signal-to-noise ratio (SNR).

The following assumptions are made, for simplicity:

- additive, spatially uncorrelated noise,
- simple signal model, free of refraction and scattering effects.

This study is limited to the case of a plane incident P wave. The particle motion measured at the free surface is linearly polarized, and oriented along the azimuth. The apparent incidence angle, $inc_a$, is easily derived from the true incidence angle, *inc*, for given compressional and shear velocities. For most regional and teleseismic P waves, the incidence angle is between 0 and 60°, in which case $inc_a$ is very close to *inc*.

Harris illustrates his method for a specific array geometry (a seven-element uniform array of either vertical or three-component instruments), assuming monochromatic signal and noise. We extend his study by comparing the performance of a NORESS-type array of vertical elements (hereafter referred to as "vertical array"), the array of three-component elements at NORESS, and a three-component single station, equipped with short-period instruments. The array consists of 25 vertical elements, and 4 three-component stations (one at the hub and three on the C-ring). Following Harris, we assume an incidence angle of 45°, which is typical of a regional P wave, and a full-aperture wavelength, corresponding to an apparent velocity of 8 km/s and a frequency of about 2.7 Hz. For such an incident P wave, the uncertainty on the azimuth estimation is:

- 2.7 times larger for a three-component station than for the three-component array,
- 2.7 times larger for the three-component array than for the vertical array,
- 7.1 times larger for a three-component station than for the vertical array.

The main conclusions of Harris' investigation are:

- *The bounds for arrays are smaller than the bounds for three-component stations. Therefore, arrays perform better in estimating direction parameters.*
- *An array of vertical instruments provides a relatively low cost-benefit ratio for estimating the azimuth.*
- *Since arrays also perform better than three-component stations in estimating incidence angles, they have an edge in identifying P waves.*
- *The difference in performance between arrays and 3-C stations significantly increases as the SNR decreases.*

In the following sections we describe methods for deriving polarization attributes that can be used for phase identification, association and event location.

### 2.2.3. Maximum Likelihood Method for Single-Site Polarization Analysis and Event Location

Christoffersson *et al.* (1988) use a Maximum Likelihood (ML) method to decompose the wavefield from three-component single stations. They must use simplified models of the wavefield, since the number of independent parameters that can be observed at a single site is six for power and six for phase angles. Since they apply this technique in the time domain, the number of independent parameters is actually only six.

Various estimators of particle motion have been proposed, based on the covariance matrix for the three-component time series within a given time window. As opposed to the Principal Component estimator that focuses on the diagonal elements of the covariance matrix (see next section), other estimators put weight on the off-diagonal elements. Christoffersson *et al.* select the ML estimator, because it enables them to test the validity of models for seismic signals, assuming white Gaussian noise.

For standard particle-motion models of P, S, Love and Rayleigh waves, they calculate the $\chi^2$ probability that the observed wavefield fits a given model. They define a time-azimuth grid, and for each point in that grid, they measure the following parameters that can be used to identify the type of phase arrivals:

- the probability of a given wave type times the probability that the energy in that wave type is positive,
- an estimate of apparent wave velocity, converted from an estimated apparent incidence angle via standard formulas (for given crustal velocities).

The apparent incidence angle can be derived for P, and to a lesser extent, for SV. In general, the ML method does not work well for SH, Rayleigh and Love waves, because of complex polarization characteristics and interference effects. One solution proposed by the authors is to ignore transverse motions. This makes it easier to separate P-type from S-type arrivals at regional distances, at the price of loss in azimuth resolution. Shear waves are difficult to analyze with single sites because only simplistic particle-motion models can be used. Using arrays of three-component instruments would make it possible to model more complex wavefields. Also, the constraint of no correlation between SV and SH motions could be lifted.

In conclusion, *the ML method applied to single-site data works well for P waves only.* Results obtained using this technique will be given in Section 2.2.5.

### 2.2.4. Polarization Analysis for Single Stations and Arrays, Using Eigensystem Decomposition

Jurkevics (1988) proposes a method that can be used with either single stations or arrays. It is a "Principal Component" estimator, based on an eigensystem decomposition of the wavefield. Like the ML method, it is a time-domain technique, but a frequency decomposition is also performed. Besides, it can be used for arrays of three-component sensors, as well as for single stations. In the following, we will refer to it as APMA (Array Particle Motion Analysis). The output is a set of attributes describing the particle-motion characteristics as a function of time and frequency.

For a given seismic phase the assumption is made that the particle motion in each frequency band is purely polarized over the duration of the selected time window.

The polarization ellipsoid is computed, using an eigensystem decomposition. Then, "polarization attributes" can be estimated: rectilinearity, planarity, P-wave azimuth, P-wave incidence angle, three-component amplitude, ratio of horizontal to vertical amplitude (H/V), ratio of radial to transverse amplitude, incidence angle of the short axis of the polarization ellipsoid, etc.

When this technique is used for an array of three-component stations, the covariance matrices at individual sensors are averaged. Assuming that the noise and local scattering effects are uncorrelated between array elements, the estimation variance varies as 1/M, where M is the number of array elements. Jurkevics shows that time shifting windows to account for travel time differences between sensors before averaging the covariance matrices is not necessary, as long as the windows have a substantial overlap. This is the case for regional seismograms recorded on the NORESS C-ring, over the entire short-period band (up to 15 Hz). Therefore, no *a priori* knowledge of slowness (from f-k analysis) is required.

The most stable estimates are obtained using wide frequency bands. In practice a set of frequency bands covering the range of interest (for example, 0.5-1.0 Hz, 1-2 Hz, 2-4 Hz, 4-8 Hz, and 8-16 Hz, for short-period data) is selected. The data are bandpass filtered in each band. For a given arrival, a subset of frequency bands, for which the SNR is large enough, is selected. For a time window around the arrival the covariance matrices are computed in each of the selected bands and averaged over the bands, using "spectral balancing" (the sum is weighted by the inverse of the trace of the matrix, so that the result is not dominated by the band with the largest spectral amplitude). The resulting wide-band covariance matrix is used to measure polarization attributes.

The window lengths can be fixed or vary with frequency. Some criteria must be used to select the window in which to extract the polarization attributes for each type of seismic phase. For example, in interactive analysis, Jurkevics selects the time of largest amplitude and rectilinearity for Pn, while the Sn and Lg windows are such that the three-component amplitude is at least 40% of its peak value within the estimation window. Also, polarization measurements can be made over a selected pre-event noise or coda window for comparison.

In summary, *the APMA method can be applied to either single stations or arrays of three-component sensors. It provides both time- and frequency-domain information. Many polarization attributes can be measured.*

### 2.2.5. Results from Polarization Analysis

The techniques briefly described in the previous sections have been used to extract polarization attributes, identify phases, and/or calculate event locations. In this section we review the results obtained for short-period local/regional events, and

short-period and broadband records of teleseismic events.

*Local/Regional Events*

Ruud *et al.* (1988) apply the ML method of Christoffersson *et al.* (1988) to these three classes of data, using single sites only. For 21 short-period recordings at NORESS site A0 of local/regional P waves with SNR ranging from 1.5 to 200, their results can be summarized as follows:

- Most azimuth errors are less than 10°, but some occasional large offsets in azimuth are observed, probably due to local structural effects and/or signal complexity.
- The results are sensitive to the selection of frequency bands, and window length and positioning: small variations in these parameters can induce a change in azimuth and velocity estimates of 5° and 0.5 km/s, respectively.
- There is generally good agreement between Pn azimuth estimates obtained from three-component data and from NORESS array data (using semblance processing). However, the latter are better, more stable and more robust because of noise reduction.
- The major source of mislocation for local/regional events comes from the azimuth estimates; the mislocation seldom exceeds 50 km.

Jurkevics (1988) analyzes a large set of local/regional events at NORESS with a wide range of SNR levels, using the three-component array data. The analysis is performed in three frequency bands, centered at 4, 6 and 10 Hz, respectively. Useful polarization information is extracted not only for P phases, but also for Sn and Lg:

- Using the four-sensor array at NORESS, useful information can be obtained down to an SNR as low as 1.
- Pn and Sn have well defined polarization for all short-period frequencies.
- The standard deviation in the Pn azimuth error is about 10° at 4 Hz, 12° at 6 Hz, and 14° at 10 Hz.
- For Pn with SNR larger than 3, the incidence angle decreases when frequency increases (from 45° at 4 Hz to 30° at 10 Hz).
- The Lg azimuth errors are larger than for Pn and a strong function of frequency.
- Sn and Lg can be distinguished using polarization attributes, but there is an overlap at 10 Hz, due to a lack of high-frequency components in Lg.

- Sn is mostly horizontal, with radial and transverse components of similar amplitudes.
- Lg is dominant in a vertical plane perpendicular to the direction of propagation, with comparable transverse and vertical components.

In the US/GSE/49 Report (1987), the APMA technique is used to evaluate azimuth determination from three-component stations. Three RSTN stations, RSSD, RSON and RSNY, are used. The focus of this study is on teleseismic data, but a few regional Pn phases are analyzed for comparison. Wide-band estimates are obtained. The conclusions are similar to those for short-period teleseismic P waves (see next Subsection). However, better accuracy in azimuth is obtained, due to more favorable incidence angles.

*Short-Period Recordings of Teleseismic Events*

Ruud *et al.* (1988) draw the following conclusions from their analysis of short-period teleseismic P waves at NORESS:

- Relatively low signal frequency and sufficient SNR are necessary to obtain reasonable estimates. For 7 Central Asia earthquakes with $m_b$ 4.9 and above, the azimuth error at site A0 is less than 8°.
- Significant differences in the $\chi^2$ probability patterns are observed in the azimuth-time plane for the same event at NORESS sites A0 and C2. This shows the sensitivity of the technique to complex receiver structure.
- Poor distance estimates contribute the most to location errors.
- Similar events, such as nuclear explosions at a given test site, have similar $\chi^2$ probability patterns at a given recording site. Therefore, exploiting probability pattern information could lead to improved event locations relative to those derived from the slowness vector only.

In the US/GSE/49 Report (1987), the ground motion polarization of teleseismic P waves is measured. The following attributes are estimated in four frequency bands: amplitude, rectilinearity and incidence angle. The azimuth is measured for the purest motion in the frequency band with the highest SNR. The main results are as follows:

- The azimuth estimate is remarkably robust down to SNR close to 1.
- The results are greatly affected by the complicated geology at RSSD. The geology is relatively homogeneous at RSNY and RSON, resulting in better estimates. In particular, there is a correlation between rectilinearity and geological complexity.

- There is a coherent relationship between incidence angle and epicentral distance at RSNY and RSON.

*Broadband Recordings of Teleseismic Events*

Ruud *et al.* (1988) draw the following conclusions:

- The azimuth estimation from broadband teleseismic P waves is very accurate. This is based on broadband recordings at the NORESS hub of 6 events with $m_b \geq 6.2$, for which the azimuth errors are less than about 2°. Such accuracy is attributed to the fact that long-wavelength signals should not be affected by local structure.
- The identification of secondary phases is easy on the basis of estimated apparent velocities.

The US/GSE/49 Report (1987) includes a study of azimuth estimation using recordings of Rayleigh waves. Three attributes are calculated: amplitude, planarity and ratio of largest to smallest horizontal axis, in three frequency bands. Then, the azimuth is estimated for the purest motion. The following observations are made:

- The azimuths are close to the great circle path, but have large standard deviations.
- Although there is more scatter than for estimates from short-period teleseismic P, the Rayleigh azimuths are less sensitive to local geology.
- There is only a slight correlation between SNR and Rayleigh azimuth error.
- RSSD has the largest errors in planarity, due to its complex receiver structure.
- The limitations of this technique for azimuth estimation appear to be due to perturbation by Love waves.

Next, we give a summary of how three-component data can be used for phase identification, association and event location.

### 2.2.6. Phase Characterization and Event Location Using Three-Component Data

The first step is to obtain reliable estimates of polarization characteristics. The information that can be extracted for specific phase types is described below. Note that the following factors will generally affect the uncertainty of the estimates:

- The quality of the results depends on proper selection of the time window and frequency bands, to include the most purely polarized motions.

- The errors on the estimates generally increase with decreasing SNR, although some phase types appear more sensitive than others.
- Structural complexities at the receiver increase the bias and variance of the estimates, especially for high-frequency body waves.

*P Phases*

- For high SNR and mostly homogeneous structure, P phases have almost rectilinear polarization. Therefore, the azimuth and apparent incidence angle can easily be measured. The azimuth can be used for phase association and event location.
- From the apparent incidence angle, apparent velocity (or slowness) can be estimated, assuming known crustal velocities. Apparent velocity can be used to identify the phase type (for example, discriminate between Pn and Pg). For teleseismic events the apparent velocity can then be converted to epicentral distance via travel time tables. However, the observed incidence angle is frequency-dependent in the short-period range, and it can vary significantly from site to site due to effects of receiver structure. Therefore, it is necessary to calibrate each station using a set of reference events. For all these reasons, estimates based on measurement of apparent incidence angle are not as reliable as azimuth estimates.
- The most stable results are obtained at relatively low frequencies, because of the sensitivity of high-frequency signals to complex local structure. In particular, at teleseismic distances azimuth and velocity estimates are less accurate for short-period than for broadband recordings, because of the effects of small-scale source and receiver heterogeneities. Estimates could be improved by correcting any systematic bias due to receiver structure, through proper site calibration.

*Shear Waves and Surface Waves*

- The polarization of shear waves is more complex. SV and SH motions usually arrive in the same time windows and have similar frequency contents. The assumption of no correlation between the two is not valid except in special cases. Also, SV may have elliptical rather than linear polarization due to SV-P conversions. Effects of heterogeneities and/or anisotropy make shear waves even more difficult to interpret in terms of simple particle-motion models. Therefore, they cannot be used to reliably estimate the azimuth.

- However, an Lg azimuth can be measured using the minimum Lg horizontal motion (with a ± 180° ambiguity). This estimate will not be as reliable as that from Pn, because of the greater complexity of Lg motion, and also because noise has a more significant effect on measurement of a direction of minimum motion.

- Although regional S waves cannot be interpreted in terms of simple particle-motion models, they appear to have distinctive polarization characteristics. These can help distinguish Sn from Lg.

- Azimuth estimates can also be obtained from broadband recordings of teleseismic Rayleigh waves. Pure Rayleigh waves have elliptical motion, in the vertical plane aligned with the great-circle path. Although not accurate enough for event location, such estimates could be used as supportive evidence for association of a Rayleigh phase with a given event.

*Event Location*

Once polarization characteristics of the various seismic phases have been extracted, they can be used in an event location scheme:

- At local/regional distances, as well as for broadband recordings of teleseismic events, useful input parameters to an event location will be the phase type, azimuth and apparent velocity (if available from polarization analysis and/or other processing), and arrival time.

- For short-period teleseismic P waves, the incidence angle can be used to estimate distance. However, errors in incidence angle produce larger location errors than do errors in azimuth. Therefore, the major source of mislocation is the distance estimate.

- Three-component location errors increase with decreasing SNR.

In summary,

- *Azimuth estimates from P waves can be used in phase association and event location.*

- *Azimuth estimates from short-period Lg waves and broadband Rayleigh waves can be used only for phase association.*

- *Three-component stations and arrays have much poorer performance in estimating slowness than vertical arrays, especially for shear waves.*

- *Slowness estimates from P waves can be used in phase identification, and in event location (with large uncertainty) when no other method for distance estimation is available.*

- *No reliable direction estimates can generally be obtained from S-type body waves.*

### 2.2.7. Method Selected for the NMRD Systems

The APMA method of Jurkevics (1988) is preferred to that of Christoffersson *et al.* (1988) for the following reasons:

- Polarization attributes are obtained as a function of time *and frequency.*
- The method is developed for *arrays of three-component elements,* as well as single stations.
- A systematic study of the effects of noise on polarization has been performed, providing useful information on the uncertainty that can be expected at any SNR level, and a way to estimate errors.
- The method does not require specific models for S-type phases. Particle-motion characteristics can be derived directly from the measured polarization ellipsoid.
- As a result, for local/regional events, useful information is obtained not only for P phases, but also for Sn and Lg.
- Azimuth estimates with potential usefulness for phase association have been obtained from broadband Rayleigh waves.
- A prototype for an analysis module based on this method has already been implemented as part of the automated processing of array data in the Intelligent Array System (developed by SAIC Geophysics Division), with promising results.

One advantage of the ML method, however, is that $\chi^2$ probabilities are calculated, providing a statistical measure for the error on the estimates. It might be useful to add similar statistics to the APMA method.

In the NMRD systems the APMA method could be used to analyze any kind of three-component data (short-period or broadband, local/regional or teleseismic, from single stations, three-component arrays, or a set of three-component stations within a NORESS-type array). Only detection times, not results from f-k, spectral or other signal analysis, should be used in polarization analysis. All polarization attributes that are potentially useful for phase identification, association and event location should be computed and stored, for further use by an expert system or a human analyst. A new database relation will be created to store the polarization attributes. It will be linked to the "detection" relation through the "arrival id".

Each attribute performs one or more functions in the analysis process. These functions are identified below, along with examples of relevant attributes:

- *parameter extraction* (SNR, rectilinearity, three-component amplitude): select the time window and/or frequency bands in which to extract the polarization attributes for a given arrival.
- *error estimation* (SNR, rectilinearity, planarity): estimate errors on the measured attributes.
- *phase identification* (rectilinearity, incidence angle, H/V, short-axis incidence angle): identify the phase (for example, discriminate Pn from Pg and Sn from Lg).
- *phase association* (azimuth): associate a phase with an event.
- *event location* (azimuth, incidence angle): locate the event a given arrival belongs to.

Automated polarization analysis using the APMA method will be tested on a preliminary set of NORESS and ARCESS array data. Results from beamforming, f-k and polarization analysis will be compared. The correlations between various attributes, and their potential for discriminating between P-type and S-type phases will be studied as a function of SNR.

Anne Suteau-Henson

**References**

Christoffersson, A., E. S. Husebye, and S. F. Ingate, 1988. "Wavefield decomposition using ML-probabilities in modelling single-site 3-component records," *Geophys. J.*, 93, 197-213.

Harris, D. B., 1982. "Uncertainty In Direction Estimation: A Comparison Of Small Arrays And Three-Component Stations," *Technical Report UCID-19589-82*, Lawrence Livermore National Laboratory, October 8, 1982.

Jurkevics, A. 1988. "Polarization Analysis Of Three-Component Array Data," *Bull. seism. Soc. Am.*, 78, 1725-1743.

Ruud, B. O., E. S. Husebye, S. F. Ingate, and A. Christoffersson, 1988. "Event Location At Any Distance Using Seismic Data From A Single, Three-Component Station," *Bull. seism. Soc. Am.*, 78, 308-325.

United States Delegation, 1987. "A Recommendation For Inclusion Of Azimuth As A Reportable Parameter For Three-Component Stations," *Technical Report US/GSE/49*, July 27, 1987.

## 2.3. ESTIMATING AZIMUTH AND SLOWNESS FROM THREE-COMPONENT AND ARRAY STATIONS

### 2.3.1. Introduction

The capabilities of three-component (3-C) and array stations for estimating azimuth and slowness are compared in this preliminary study. In a theoretical investigation by Harris (1982), upper bounds on the uncertainty of the direction estimates of a plane incident P wave in the presence of noise were derived for various sensor configurations. Arrays were found to perform better than 3-C stations. Experiments by Kvaerna and Doornbos (1986) indicated that measurements of the slowness vector at the individual 3-C NORESS stations are site-dependent and have a larger standard deviation than measurements using the array of vertical sensors.

In this empirical study, azimuth and slowness estimates from broadband frequency-wavenumber (F-K) analysis, using Kvaerna's algorithm (Kvaerna and Ringdal, 1986), and polarization analysis, using the technique developed by Jurkevics (Jurkevics, 1988) are compared for P-type phases recorded at the NORESS array in the short-period band. 145 events were analyzed: 74 teleseismic and 71 regional events. They were selected from a variety of distances and azimuths, and cover a wide range of signal-to-noise ratios. Independent determinations of azimuth and/or slowness were obtained from locations in the NEIS bulletin for teleseismic events, and in regional network and PDE bulletins for regional events.

The F-K method is found to be more robust, over a wide range of signal-to-noise ratios. However, for sufficient SNR, the two methods are comparable. These results confirm those from theoretical studies. Also, the results from 3-C processing are in good agreement with those from other studies using NORESS and RSTN short-period data and NORESS high-frequency data (Jurkevics, 1988; US/GSE/49, 1987; Walck and Chael, 1989).

### 2.3.2 Review of Theoretical Investigation

Harris (1982) compared the performance of small arrays and three-component stations in estimating the wavefield direction. His study is a theoretical investigation into the uncertainty of direction estimates in the presence of noise. A lower bound on this uncertainty is obtained using the Cramer-Rao bound.

For simplicity, Harris assumed additive, spatially uncorrelated noise, and a simple signal model, free of refraction and scattering effects. This study is limited to the case of a plane incident P wave, for which there is a simple model of particle motion that can be used to derive the slowness vector using 3-C stations. The particle motion measured at the free surface is linearly polarized, and oriented along

the azimuth. The apparent incidence angle, $inc_a$, is easily derived from the true incidence angle, *inc*, for given compressional and shear velocities. For most regional and teleseismic P waves, the incidence angle is between 0 and 60°, in which case $inc_a$ is very close to *inc*.

The main conclusions of Harris' investigation were:

- The bounds for arrays are smaller than the bounds for 3-C stations. Therefore, arrays perform better in estimating direction parameters.
- Since arrays provide better estimates of incidence angles than 3-C stations, they perform better in identifying P waves.
- The difference in performance between arrays and 3-C stations significantly increases as the signal-to-noise ratio decreases.

### 2.3.3. Methods

In this study the capabilities of arrays and 3-C single stations in estimating direction parameters are compared for two sizeable data sets of events (regional and teleseismic) detected by the NORESS array, and recorded at both the vertical and 3-C elements of the array. Azimuth and slowness estimates are obtained using frequency-wavenumber analysis ("F-K") for the array of vertical sensors, and polarization ("3-C") analysis for a 3-C single station. While a measurement of slowness can be directly obtained from F-K analysis, it has to be derived from a measurement of incidence angle when 3-C processing is used.

We applied the broadband F-K analysis technique developed by Kvaerna (Kvaerna and Ringdal, 1986; Kvaerna, 1987). It provides better estimates than the monochromatic F-K method. The processing procedure is the same as that currently used in the "Intelligent Array System" (IAS) at the Center for Seismic Studies. For each phase the arrival time — used to select the analysis window — and the center frequency were the arrival time and dominant frequency, respectively, from the NORESS bulletin.

The polarization method used to analyze the three-component data is based on that developed by Jurkevics (1988). It is a principal component estimator, based on an eigensystem decomposition of the wavefield. Although it is a time-domain technique, a frequency decomposition is also performed through bandpass filtering. For each seismic phase the assumption is made that the particle motion in a given frequency band is purely polarized over the duration of the selected time window. The polarization ellipsoid is computed, using an eigensystem decomposition. Then, "polarization attributes" can be estimated, in particular, P-wave azimuth and incidence angle.

In practice a set of frequency bands covering the range of interest is selected. The data are bandpass filtered in each band. For each one the 3-C SNR (ratio of maximum signal 3-C amplitude to average noise 3-C amplitude) is estimated. Then, the frequency band for which to measure the attributes is selected. We have experimented with two methods of frequency band selection, hereafter referred to as "broadband" and "narrowband", respectively. With the broadband method a subset of frequency bands, for which the SNR is above a given threshold, is selected (if no band is above the threshold, that with the largest SNR is chosen instead). For overlapping windows in a time segment around the arrival the covariance matrices are computed in each of the selected bands and averaged over the bands. The resulting wide-band covariance matrix is used to measure polarization attributes. With the narrowband method only the band with the largest SNR is selected. The most stable estimates are obtained using wide frequency bands.

Some criteria must be used to select the time window in which to extract polarization attributes for each type of seismic phase. The time of largest rectilinearity is selected for P-type phases. As for the F-K analysis, the processing procedure used in this study is the same as that in the IAS, and the arrival times used to select the data segment for analysis were obtained from the NORESS bulletin.

### 2.3.4 Results

Two data sets are used to compare the capabilities of the array of vertical elements with 3-C single stations at NORESS for azimuth and slowness estimation. The first includes teleseismic P arrivals, and the second consists of regional P-type phases. First P arrivals detected at NORESS were analyzed for events carefully selected from bulletins. Although slowness was also measured for the regional events, the results are not discussed here, since slowness estimates are not used to locate such events. For each set azimuth and slowness differences are obtained by comparing the estimates from both F-K and 3-C processing to reference estimates derived from the bulletin locations. In this preliminary study we do not evaluate the accuracy of the bulletin estimates. The effect of noise is studied, using an estimate of the SNR measured for the three-component single station in the frequency band used for signal analysis (i.e., ratio of maximum signal 3-C amplitude to average pre-event noise 3-C amplitude). For this study the broadband method of frequency selection is used for 3-C processing, although the effect of using the narrowband method instead is also investigated. Clearly, the 3-C SNR estimate is smaller than the SNR for the array beam. However, we use it for both methods to insure consistency, and because it helps evaluate the robustness of the 3-C method in the presence of noise.

*2.3.4.1 Results from Teleseismic P-Wave Analysis*

74 teleseismic events were selected, covering a wide range of epicentral distance (from about 20 to 90°), azimuth, and SNR. Independent locations were obtained from the NEIS Bulletin. The event information is given in *Table A1* in the Appendix. Polarization analysis was performed at station NRA0. The set of frequency bands used is 0.5-1, 1-2, 2-4, and 4-8 Hz, and a moving window of 3.5 second length was used to select the best time for measurement within a 14 second data segment centered on the detection time.

Comparison of F-K and 3-C Results

*Figure 1a* shows histograms of the azimuth differences (observed azimuth minus azimuth to NEIS location) obtained for each method. The means, standard deviations and medians are given in *Table I* (one outlier was excluded from the F-K set of measurements). The 3-C method has a significantly larger standard deviation, which is similar to those obtained earlier for teleseismic P waves recorded at RSTN stations, using a similar technique (US/GSE/49, 1987). Next, we study the effect of low SNR events on the standard deviations of the distributions. In *Figure 1b*, the azimuth differences are plotted as a function of 3-C SNR for each method. Low SNR phases, below a threshold of ~ 2 (indicated by the dashed vertical line),do not show more scatter for the F-K estimates, but a large and abrupt increase in scatter for the 3-C estimates. In *Figure 1c* histograms of the azimuth differences are plotted for the 40 phases with 3-C SNR above 2. For this population the difference between the standard deviations of the two methods is not significant (*Table I*).

**Table I. Azimuth Differences of Teleseismic P Phases**

| | Mean (°) | Standard Deviation (°) | Median (°) |
|---|---|---|---|
| F-K | -1. | 11. | -1. |
| F-K (SNR > 2) | -2. | 12. | 0. |
| 3-C | 5. | 39. | 5. |
| 3-C (SNR > 2) | 3. | 13. | 4. |

A similar comparison was performed for the slowness differences (observed minus reference slowness). The 3-C slowness was obtained by converting the measured incidence angle, using a surface P-wave velocity of 6.0 km/s. The reference slowness was derived from J-B tables as a function of epicentral distance. *Figure 2a*

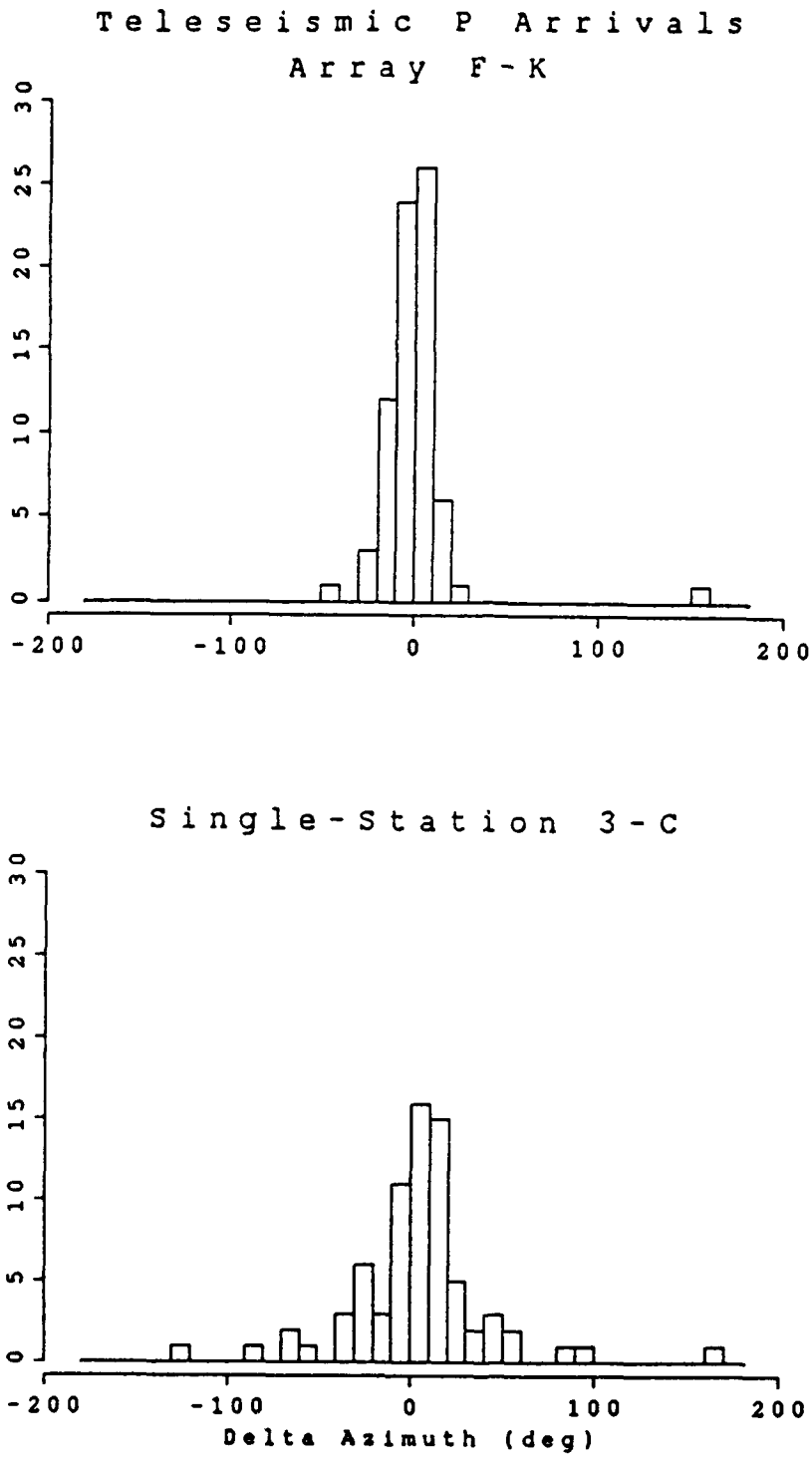


*Figure 1a.* Histograms of azimuth differences for a data set of 74 teleseismic P arrivals described in Table A1.

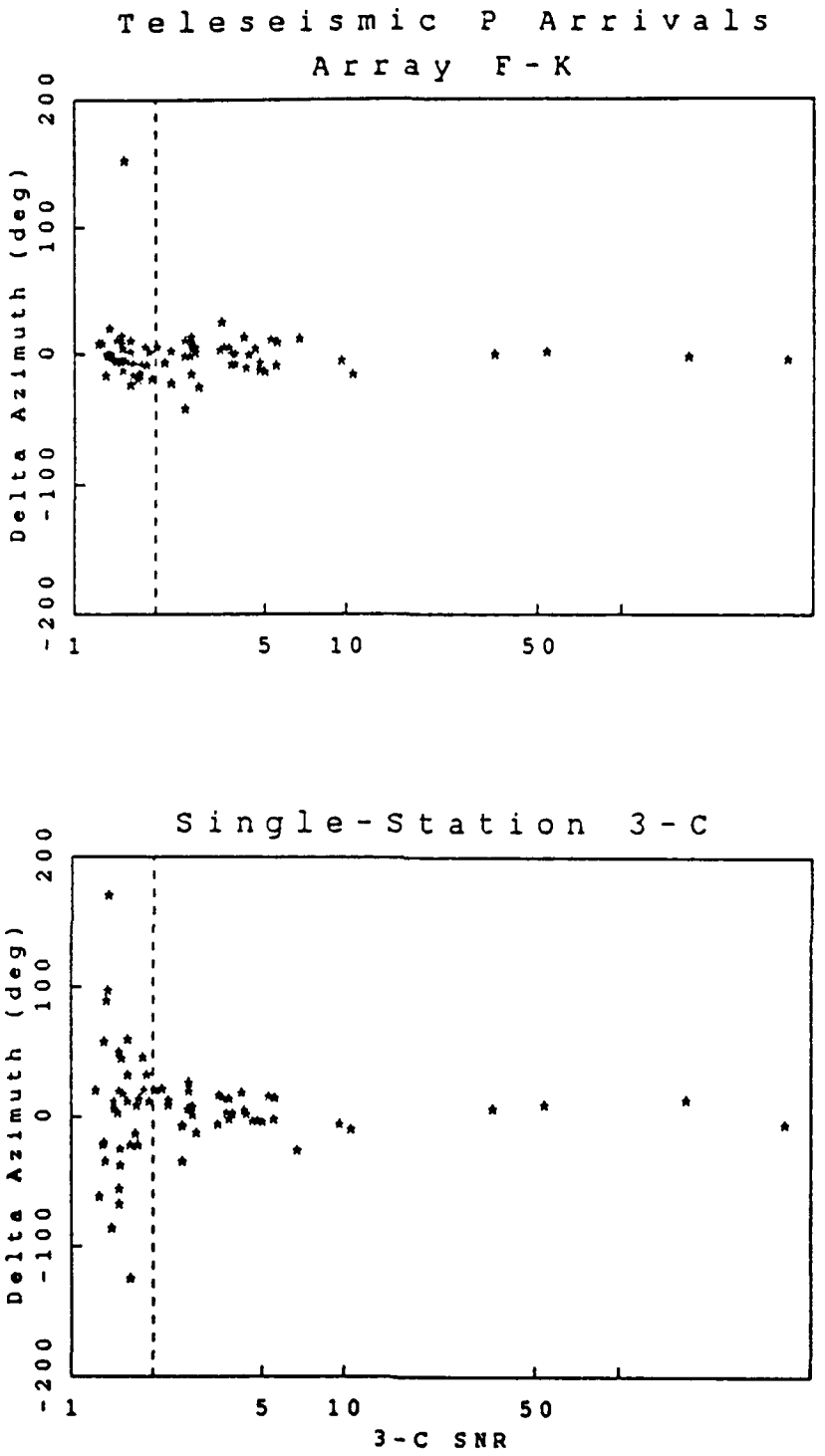


*Figure 1b.* Azimuth differences versus 3-C SNR for a data set of 74 teleseismic P arrivals (the dashed line indicates an SNR of 2).

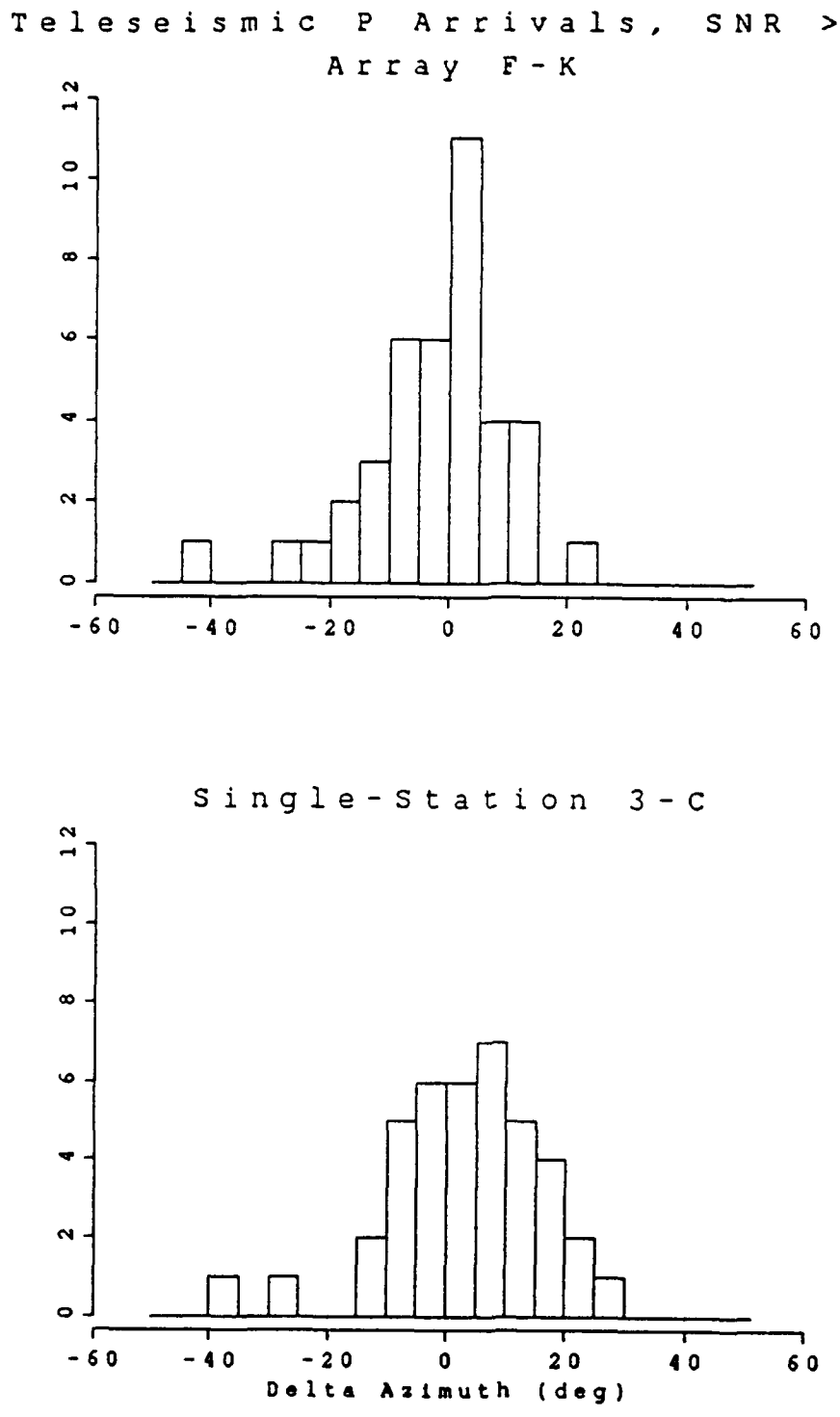


*Figure 1c.* Histograms of azimuth differences for a data set of 40 teleseismic P arrivals with 3-C SNR greater than 2. Note the scale difference between this and Figure 1a.

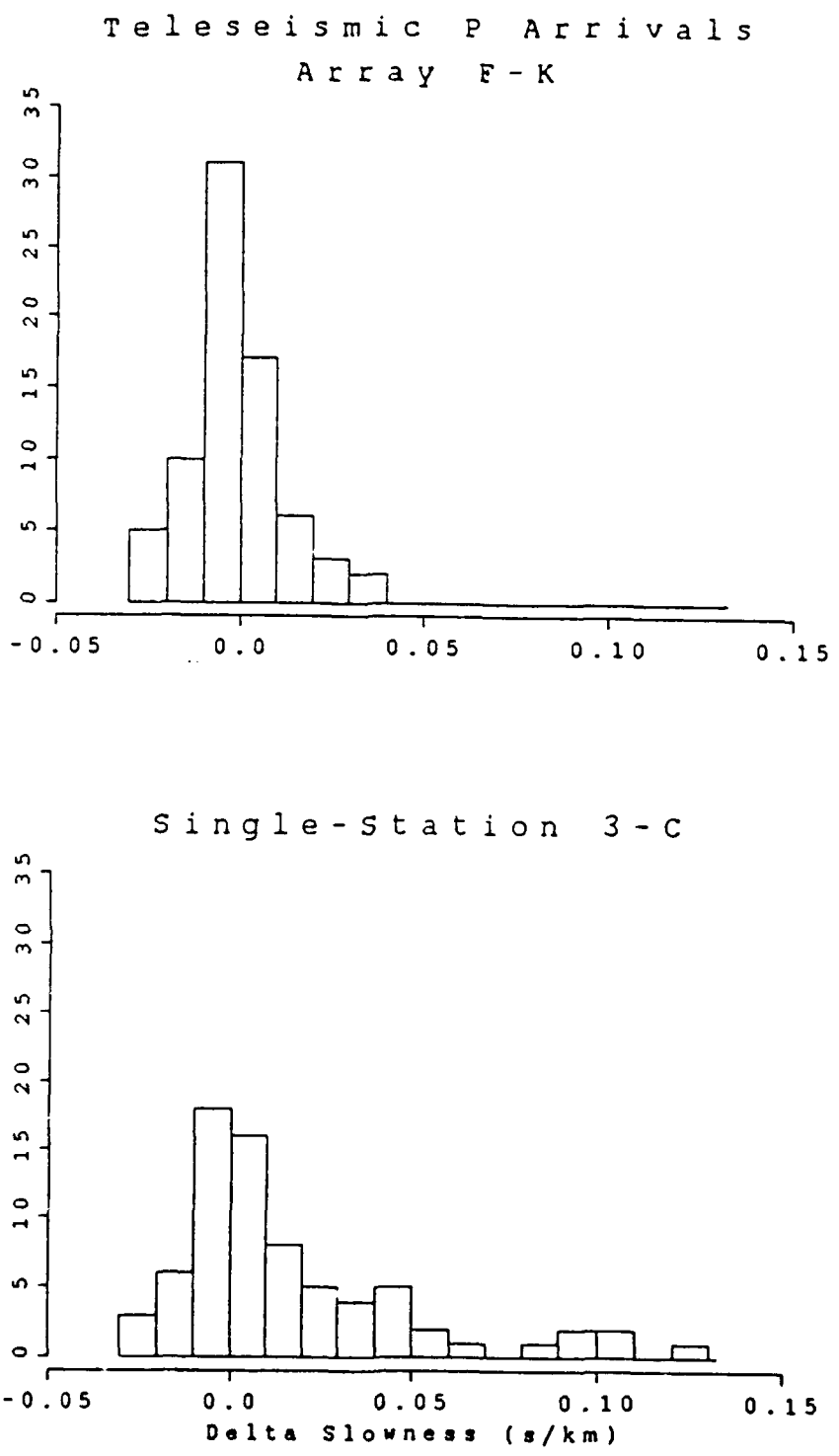


*Figure 2a.* Histograms of slowness differences for a data set of 74 teleseismic P arrivals.

compares the histograms for the two methods, and the corresponding statistical measurements are given in *Table II.* A skewness is observed in the distribution of the 3-C differences, with a large number of positive anomalies. In *Figure 2b* the slowness differences are plotted as a function of 3-C SNR for each method. It shows that the anomalously large 3-C slownesses are mostly for low SNR events (below a threshold of ~ 2, as indicated by the dashed vertical line). This is probably due to the increase in incidence angle produced by the increase in noise level on the horizontal channels, which have small signal amplitudes for the large apparent velocities of teleseismic P arrivals. When only phases with SNR above 2 are included in the statistical analysis, the difference between the standard deviations for the two methods, as well as the skewness of the 3-C distribution toward positive anomalies, almost disappear (*Figure 2c* and *Table II*).

**Table II. Slowness Differences of Teleseismic P Phases**

| | Mean (s/km) | Standard Deviation (s/km) | Median (s/km) |
|---|---|---|---|
| F-K | -0.001 | 0.012 | -0.003 |
| F-K (SNR > 2) | -0.003 | 0.010 | -0.003 |
| 3-C | 0.017 | 0.032 | 0.006 |
| 3-C (SNR > 2) | 0.004 | 0.014 | 0.002 |

Our 3-C slowness estimates can be refined by deriving them from estimates of "true" instead of "apparent" incidence angle, using standard formulas (Bullen, 1959). Assuming a P-wave velocity of 5.8 km/s and a Poisson's ratio of 0.25, we obtained new estimates of 3-C slowness differences. Their distributions do not differ significantly from those previously obtained. The main change is a reduction of the mean of the slowness difference for the entire population (from 0.017 to 0.013 s/km). This is probably due to the fact that for incidence angles between 0° and 60° (which is the range observed for most teleseismic P arrivals), the "true" incidence angle is slightly smaller than the "apparent" one. However, the bias towards positive slowness anomalies remains, and our conclusions still hold.

Comparison of 3-C and Beam SNR

*Figure 3* summarizes the observed measured differences in the 3-C and beam SNR for the teleseismic events considered in this study. It is seen from this plot that the SNR advantage for the array over the single 3-C station is approximately a factor of 7. The mean logarithm of the ratios is measured to be 0.86.

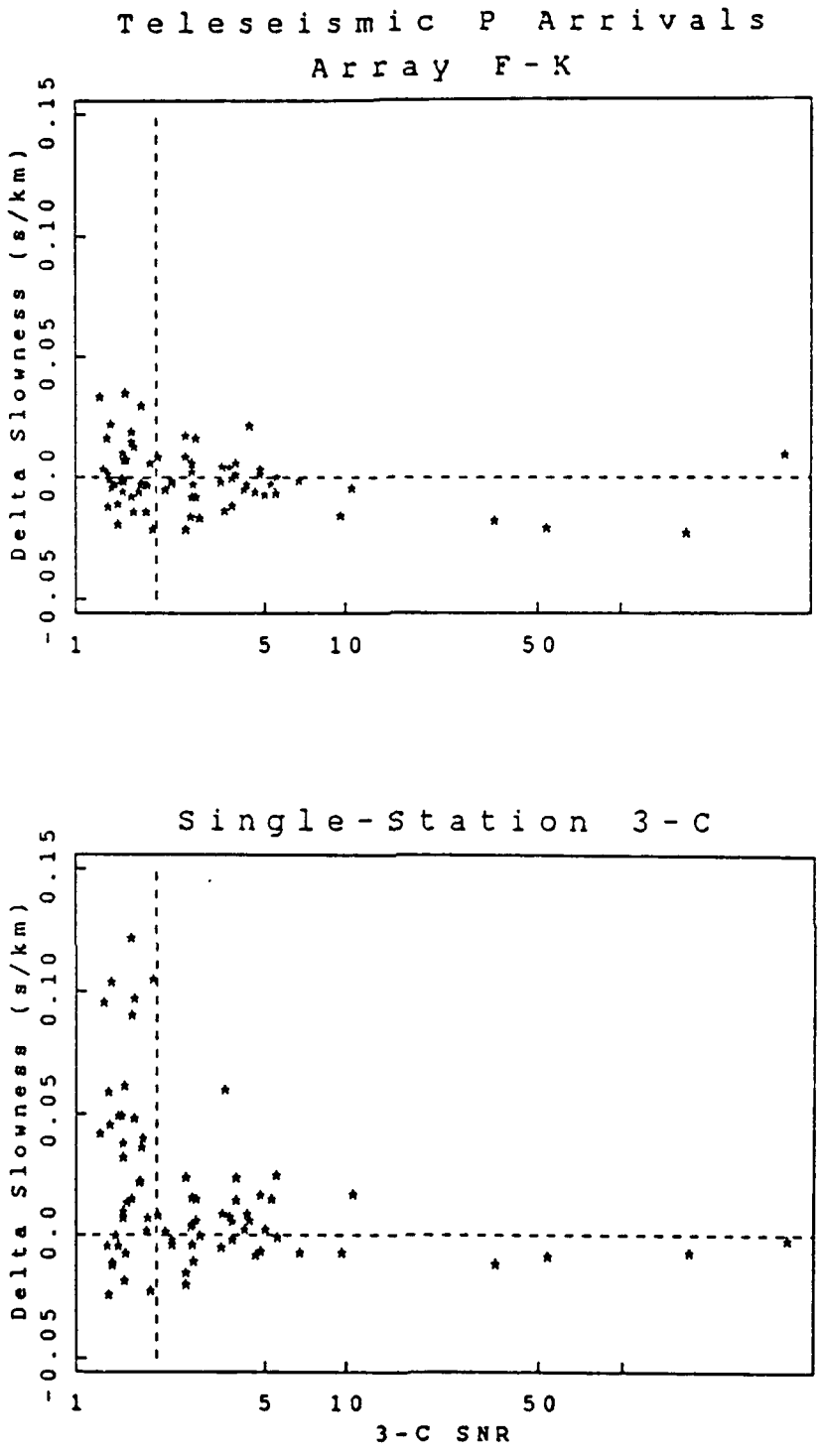


*Figure 2b.* Slowness differences versus 3-C SNR for a data set of 74 teleseismic P arrivals (the dashed vertical line indicates an SNR of 2).

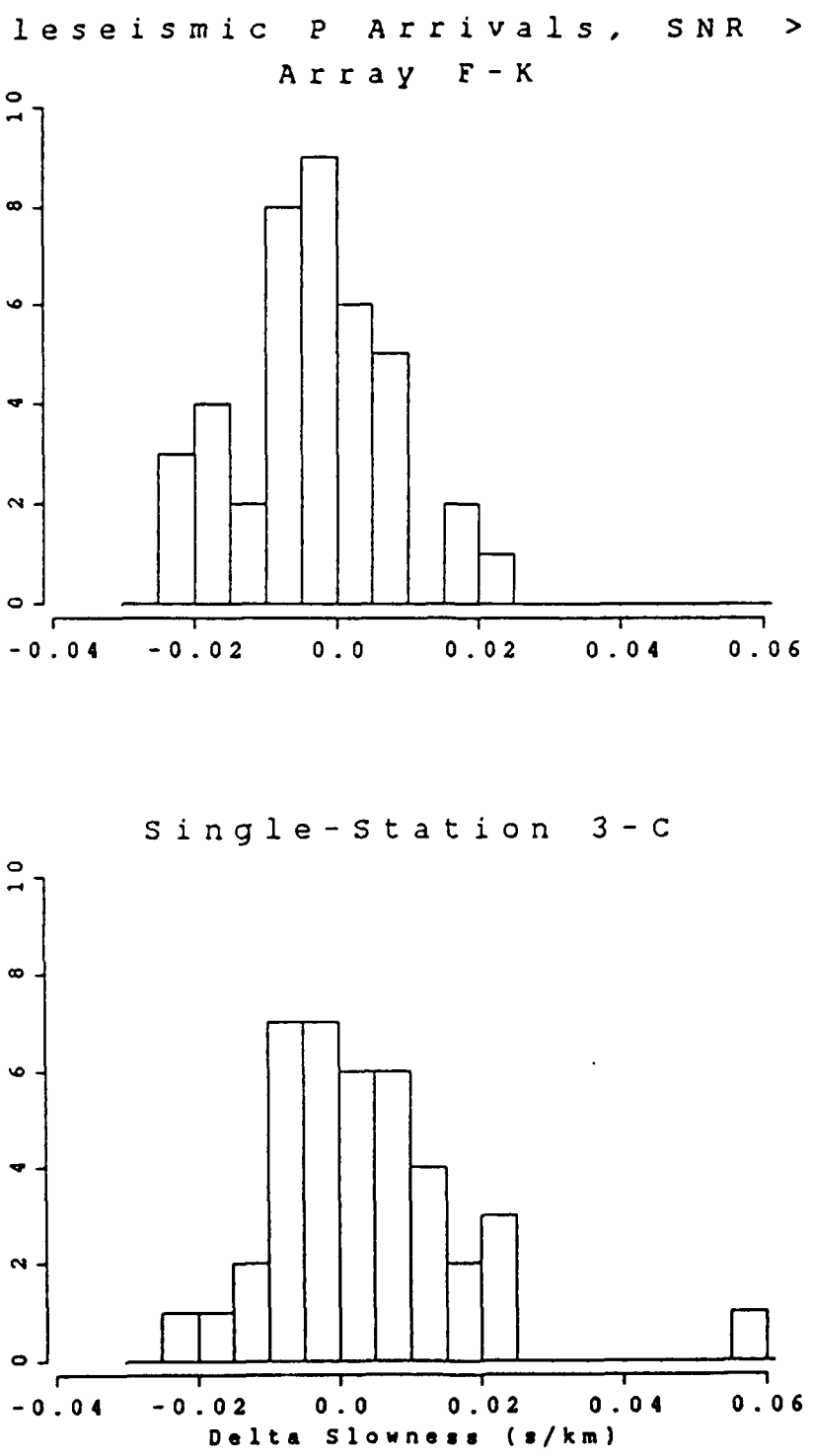


*Figure 2c.* Histograms of slowness differences for a data set of 40 teleseismic P arrivals with 3-C SNR greater than 2. Note the scale difference between this and Figure 2a.

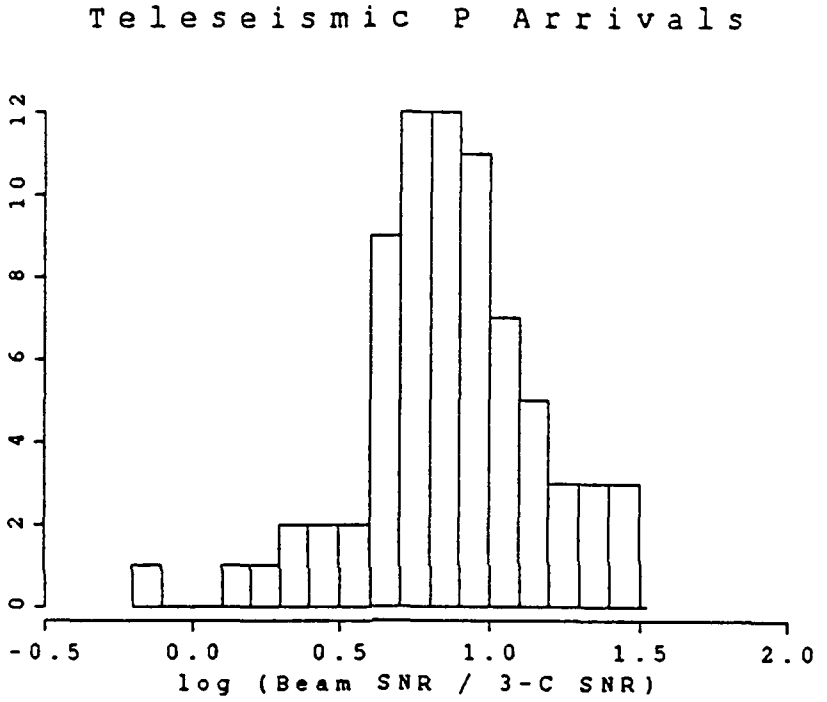


*Figure 3.* Histogram of the differences in the SNRs measured at the single 3-C station NRA0 and the array for a data set of 74 teleseismic P arrivals. The mean difference is 7 (the logarithm is 0.86).

Effect of Frequency Band Selection on 3-C Results

The polarization method is sensitive to parameter settings, such as the length and position of the time window and the frequency band selected for attribute measurement (see, for example, Jurkevics, 1988). In this section we investigate the effect of the selection of frequency band on the azimuth and slowness differences when using polarization analysis for direction parameter estimation. The 74 teleseismic events were reprocessed through single station 3-C processing, using narrow frequency bands for extracting polarization attributes. The difference between this and the previous processing is that the band with the highest SNR is selected. A new narrowband 3-C SNR is defined as the 3-C SNR for data prefiltered in this selected band, as opposed to our previous estimate, which was a wide-band average for bands with SNR above 2. The distribution of the new azimuth and slowness differences as a function of this narrowband SNR shows the same abrupt threshold for SNR of ~ 2. For our data set the population of events with SNR larger than 2 is the same, regardless of which estimate of 3-C SNR is used to define it. Therefore, we can compare the statistical results using broadband and narrowband polarization for the entire population and the population of arrivals with SNR above 2. *Figure 4* shows the azimuth and slowness differences as a function of 3-C SNR for the two methods. The standard deviations of the estimates are given in *Table III.*

**Table III. Standard Deviations for Teleseismic P Phases from 3-C Processing in Broad and Narrow Frequency Bands**

| | Azimuth (°) | Slowness (s/km) |
|---|---|---|
| Broad-Band | 39. | 0.032 |
| Narrow-Band | 39. | 0.033 |
| Broad-Band (SNR > 2) | 13. | 0.014 |
| Narrow Band (SNR > 2) | 15. | 0.017 |

For events with SNR above 2 the standard deviation of the azimuth differences is increased from 13 to 15°, and that of the slowness differences is increased from .014 to .017 s/km, when the narrowband method is used. This indicates that the broadband estimates are slightly better.

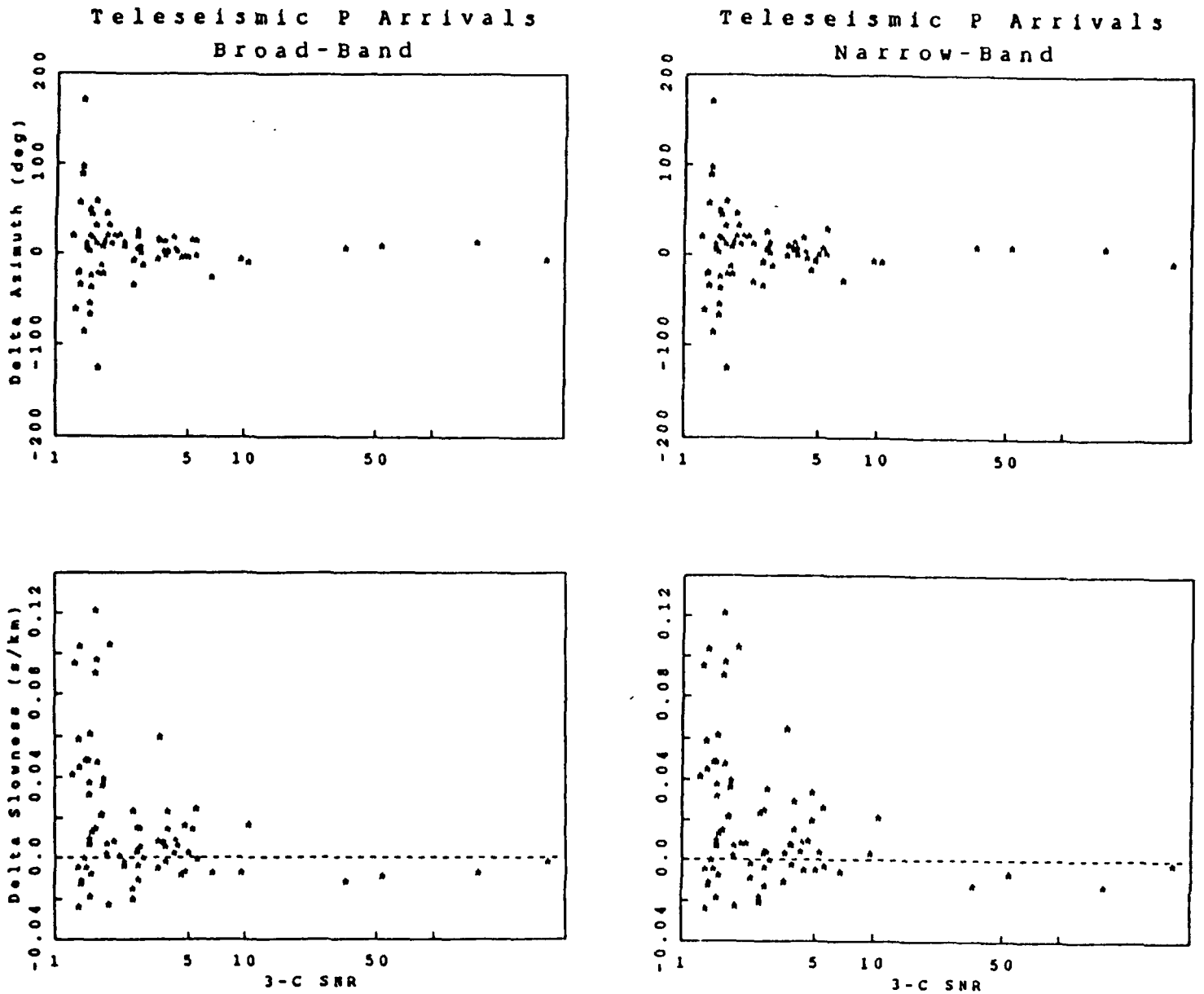


*Figure 4.* Azimuth (top) and slowness (bottom) differences versus 3-C SNR for a data set of 74 teleseismic P arrivals. 3-C processing was performed using two different methods for frequency band selection: broadband (left) and narrowband (right).

Dependence of 3-C Results on Polarization Attributes

In the previous sections we showed the effect of SNR on azimuth and slowness differences obtained from 3-C processing. We now investigate their dependence on various polarization attributes which are measured as part of the automated processing (see Jurkevics, 1988, for a description of those attributes). This will help us assess how they can help predict the errors on the azimuth and slowness estimates. We are mostly interested in the magnitude of the error in the measurements; therefore, the absolute value of the azimuth and slowness difference (hereafter referred to as $\delta az$ and $\delta slow$, respectively) is plotted in the following figures.

*Figure 5a* shows $\delta az$ and $\delta slow$ as a function of the center of the frequency band selected for polarization analysis. As in all following figures, the data points with 3-C SNR > 2 are circled. There is no obvious frequency dependence of the azimuth and slowness differences.

*Figure 5b* shows $\delta az$ and $\delta slow$ as a function of rectilinearity. There is a high correlation between rectilinearity and SNR. All phases with SNR above 2 have rectilinearity above 0.7, and most phases with rectilinearity above 0.87 have SNR above 2 and small azimuth and slowness differences. This suggests that low SNR is a major contributing factor to decrease in rectilinearity, which in turn causes an increase in the scatter of the estimates.

*Figure 5c* shows $\delta az$ and $\delta slow$ as a function of "H/V" (ratio of horizontal to vertical amplitude). The azimuth and slowness differences are highly correlated with H/V and SNR. Phases with H/V less than 0.3 have small azimuth differences and most have SNR above 2. The slowness differences are small for values of H/V up to 0.4. The lower H/V threshold for the azimuth differences may reflect the fact that increase in vertical motion, as well as low SNR, contributes to the scatter in the estimates.

*Figure 5d* shows $\delta az$ and $\delta slow$ as a function of planarity. A large value of this attribute indicates mostly planar motion, and is characteristic of regional S-type phases (Jurkevics, 1988). Well polarized P-type phases are rectilinear, and therefore have low planarity. This is what we observe, although the correlation between the azimuth and slowness differences, SNR and planarity is not very good.

*Figure 5e* shows $\delta az$ and $\delta slow$ as a function of $inc3$ (incidence angle of the normal to the plane of principal motion). As expected, teleseismic P phases with SNR above 2 have large values of $inc3$ (above 50°, with a cluster above 70°), corresponding to mostly vertical motion. However, large values of $inc3$ do not correlate well with small azimuth and slowness differences. Actually, in the presence of noise, the azimuth difference increases as the motion becomes more vertical, due to low signal-to-noise ratio on the horizontal components.

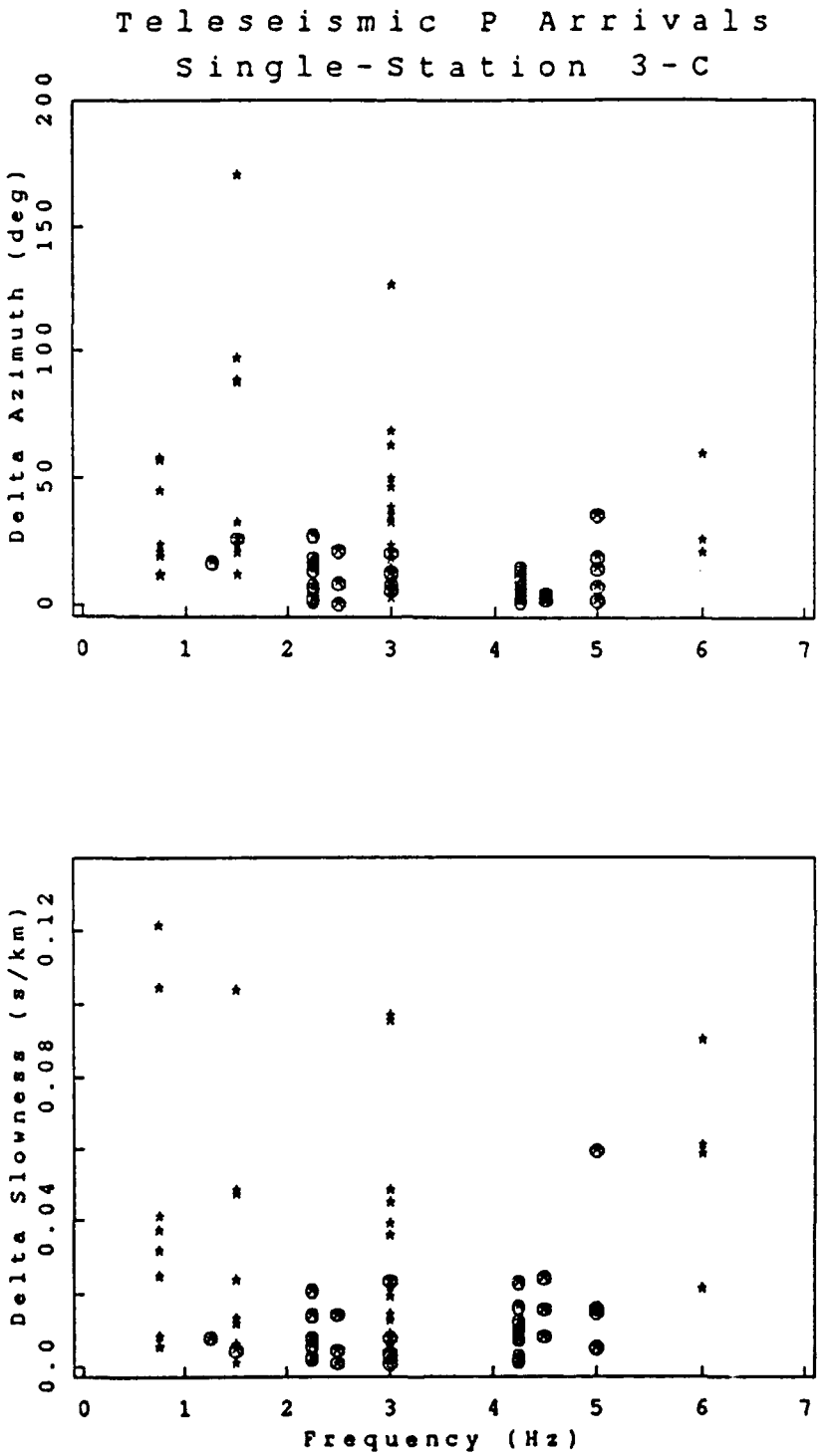


*Figure 5a.* Azimuth (top) and slowness (bottom) differences (in absolute value) versus center frequency for a data set of 74 teleseismic P arrivals. Data points for which 3-C SNR is greater than 2 are circled.

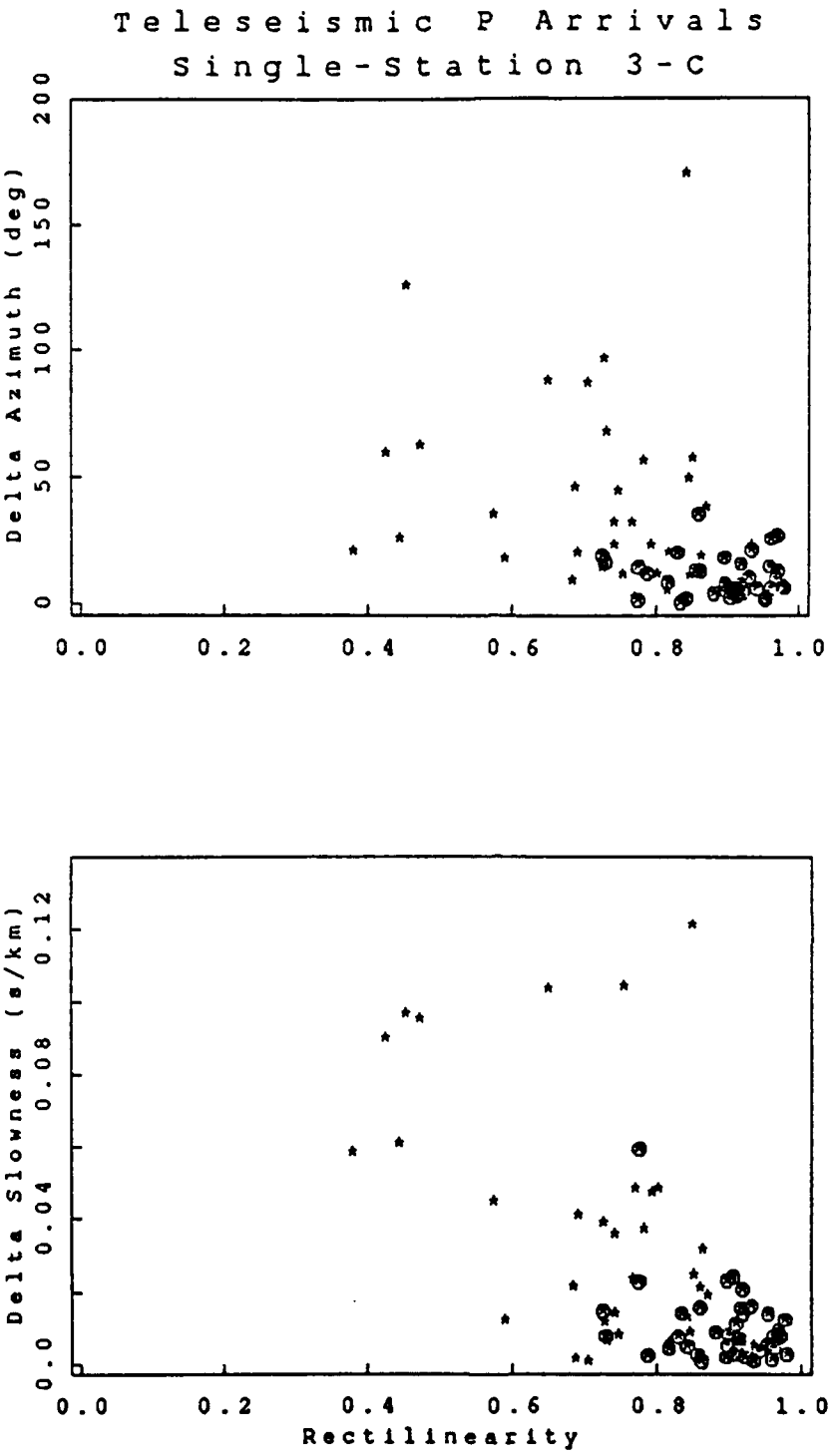


*Figure 5b.* Azimuth (top) and slowness (bottom) differences (in absolute value) versus rectilinearity for a data set of 74 teleseismic P arrivals. Data points for which 3-C SNR is greater than 2 are circled.

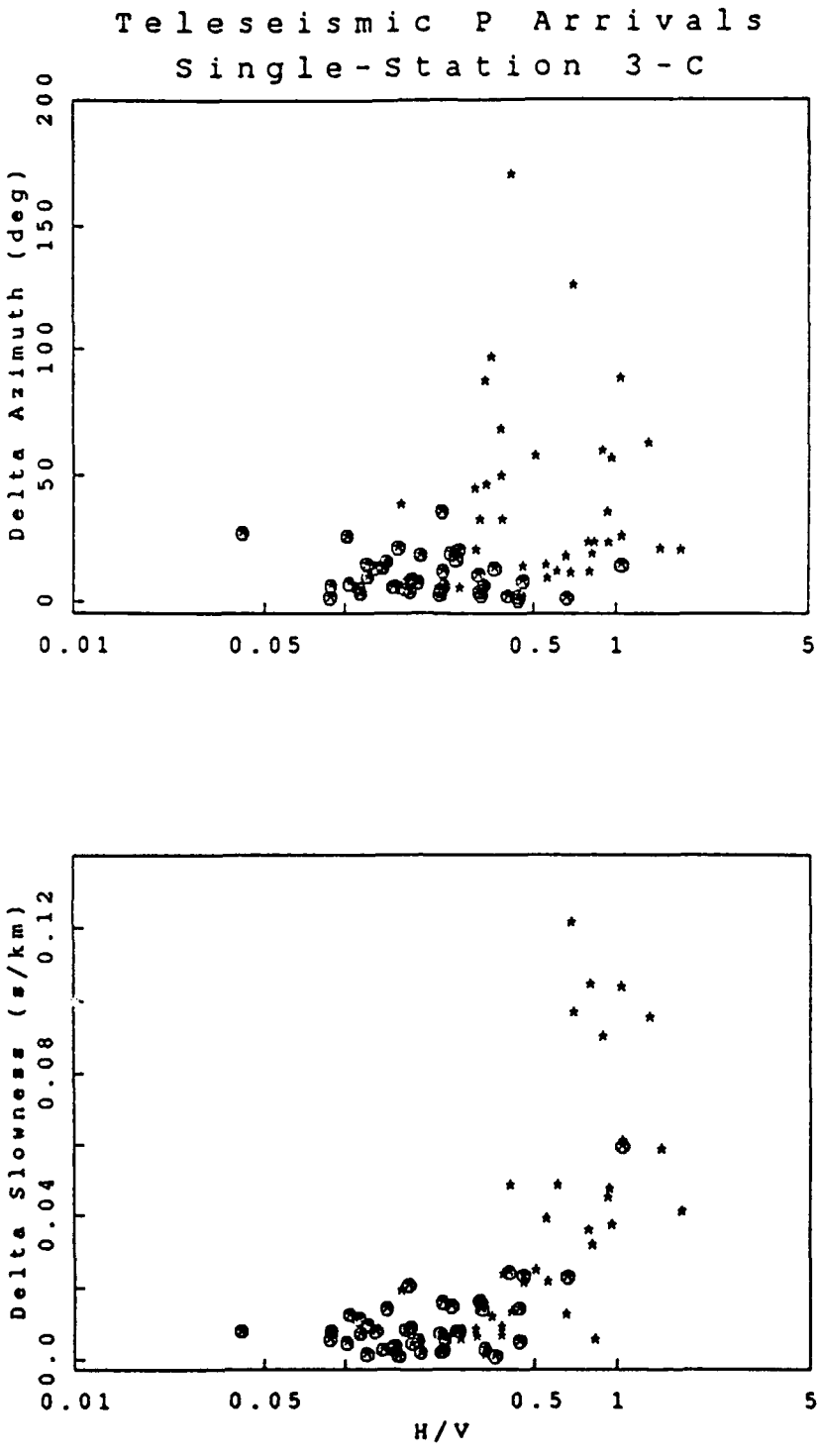


*Figure 5c.* Azimuth (top) and slowness (bottom) differences (in absolute value) versus ratio of horizontal to vertical amplitude for a data set of 74 teleseismic P arrivals. Data points for which 3-C SNR is greater than 2 are circled.

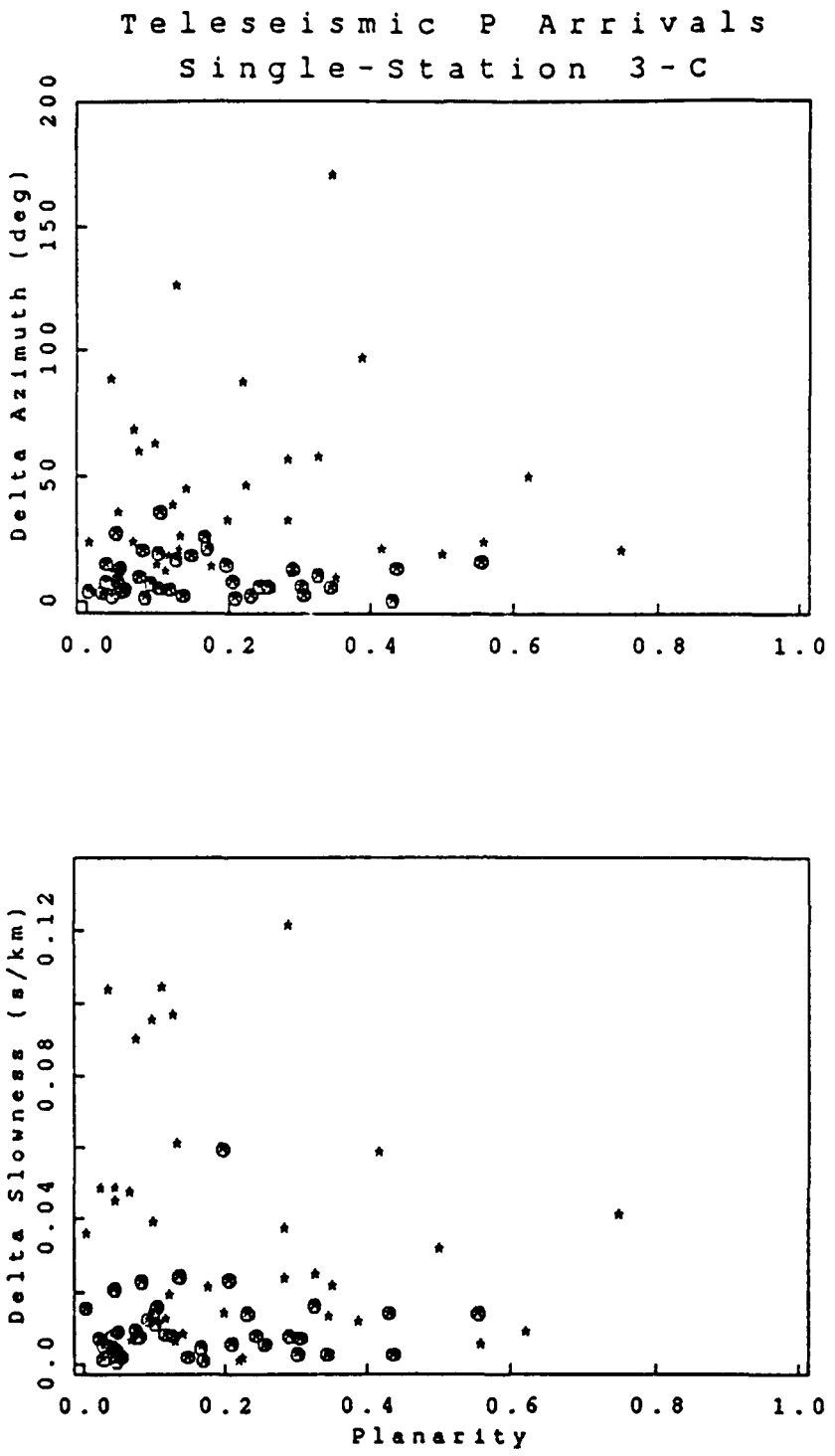


*Figure 5d.* Azimuth (top) and slowness (bottom) differences (in absolute value) versus planarity for a data set of 74 teleseismic P arrivals. Data points for which 3-C SNR is greater than 2 are circled.

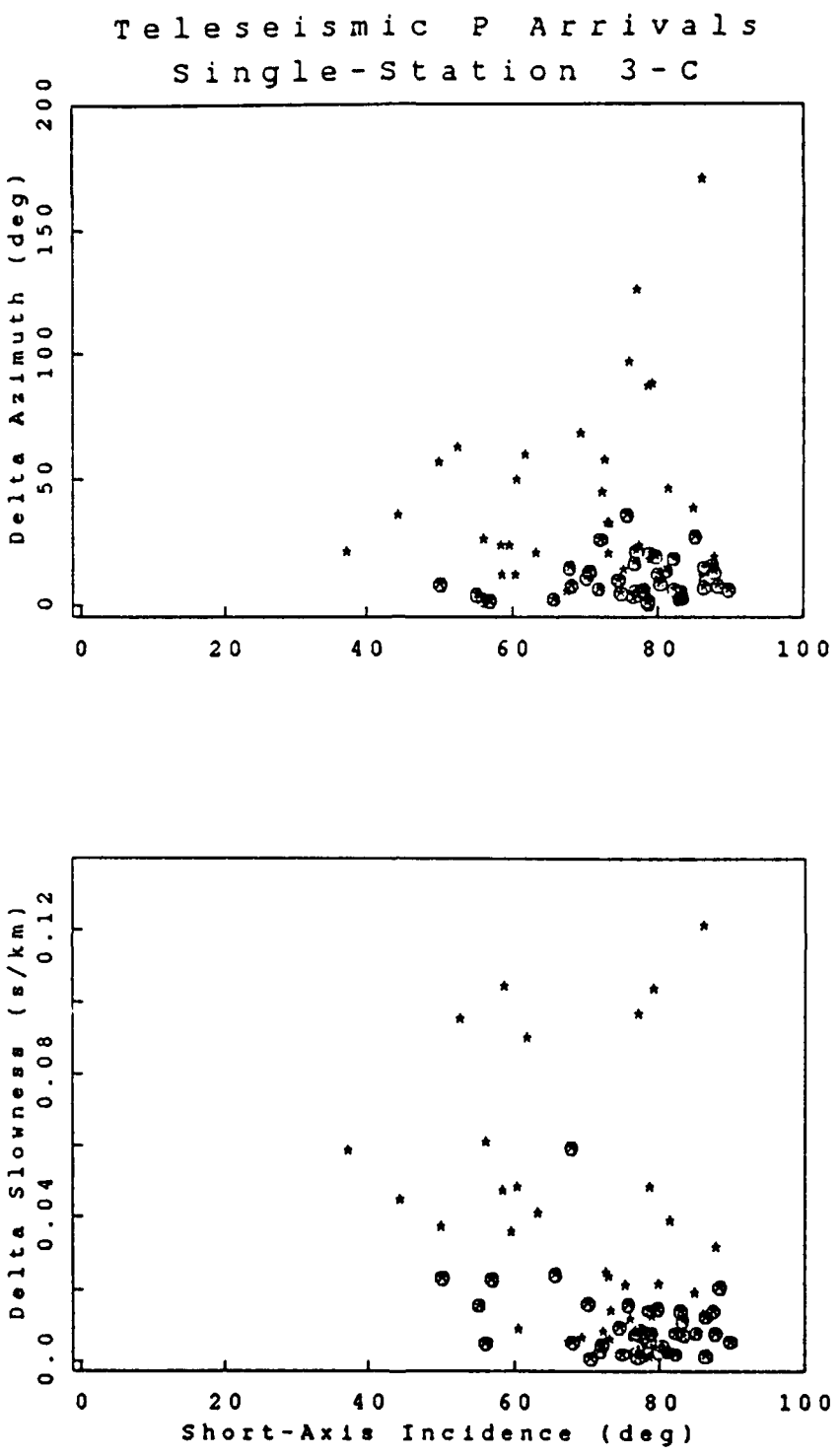


*Figure 5e.* Azimuth (top) and slowness (bottom) differences (in absolute value) versus short-axis incidence angle for a data set of 74 teleseismic P arrivals. Data points for which 3-C SNR is greater than 2 are circled.

Finally, *Figure 5f* shows $\delta az$ and $\delta slow$ as a function of the slowness obtained from 3-C processing. Most phases with SNR above 2 have slowness between 0.04 and 0.12 s/km, which is the range of theoretical slowness for this data set. As expected, values outside that range are mostly associated with low SNR phases, with large scatter in the azimuth and slowness differences. There is a correlation between the measured slowness and its difference. Slowness values between 0.04 and 0.08 s/km correspond mostly to phases with SNR above 2 and have small differences, while these tend to increase with increasing slowness above 0.08 s/km.

In conclusion, for this data set of teleseismic P arrivals, the azimuth and slowness differences are not only well correlated with 3-C SNR, but also with rectilinearity, and ratio of horizontal to vertical amplitude. The slowness differences are also well correlated with the measured slowness. This is due to the fact that loss in rectilinearity (because of complex near-receiver effects), and low SNR on the horizontal components (because of small incidence angle) contribute to increasing the scatter in the estimates. Therefore, along with 3-C SNR, those polarization attributes can help predict the magnitude of the error on the azimuth and slowness measurements from 3-C processing.

*2.3.4.2 Results from Regional P-Wave Analysis*

A similar comparison was performed for a set of 68 regional P-type phases detected at NORESS. It was extracted from a larger research data set compiled at the Center for Seismic Studies. They cover a large range of distances (from local to far-regional), azimuths and SNR. For all events, independent azimuth estimates were obtained from network locations published in the bulletins of Helsinki and Bergen Universities, or from the PDE bulletin. These events are described in *Table A2* in Appendix I. Polarization analysis was performed at station NRA0, except for 20 events, for which NRC4 was used instead because NRA0 data were missing. The set of frequency bands was 1-2, 2-4, 4-8, and 8-16 Hz. A 2-second moving window was used to select the optimal measurement time within an 8-second data segment centered on the detection time.

Comparison of F-K and 3-C Results

The azimuth differences obtained with each method for all 68 regional events are plotted as a function of 3-C SNR in *Figure 6a*. It shows that only a few phases have SNR below 2 (left of the dashed vertical line). The 60 phases with SNR above 2 were further analyzed (one outlier with anomalously large 3-C azimuth difference was excluded), and the results are shown in *Figure 6b* and *Table IV*. The F-K method provides somewhat better estimates.

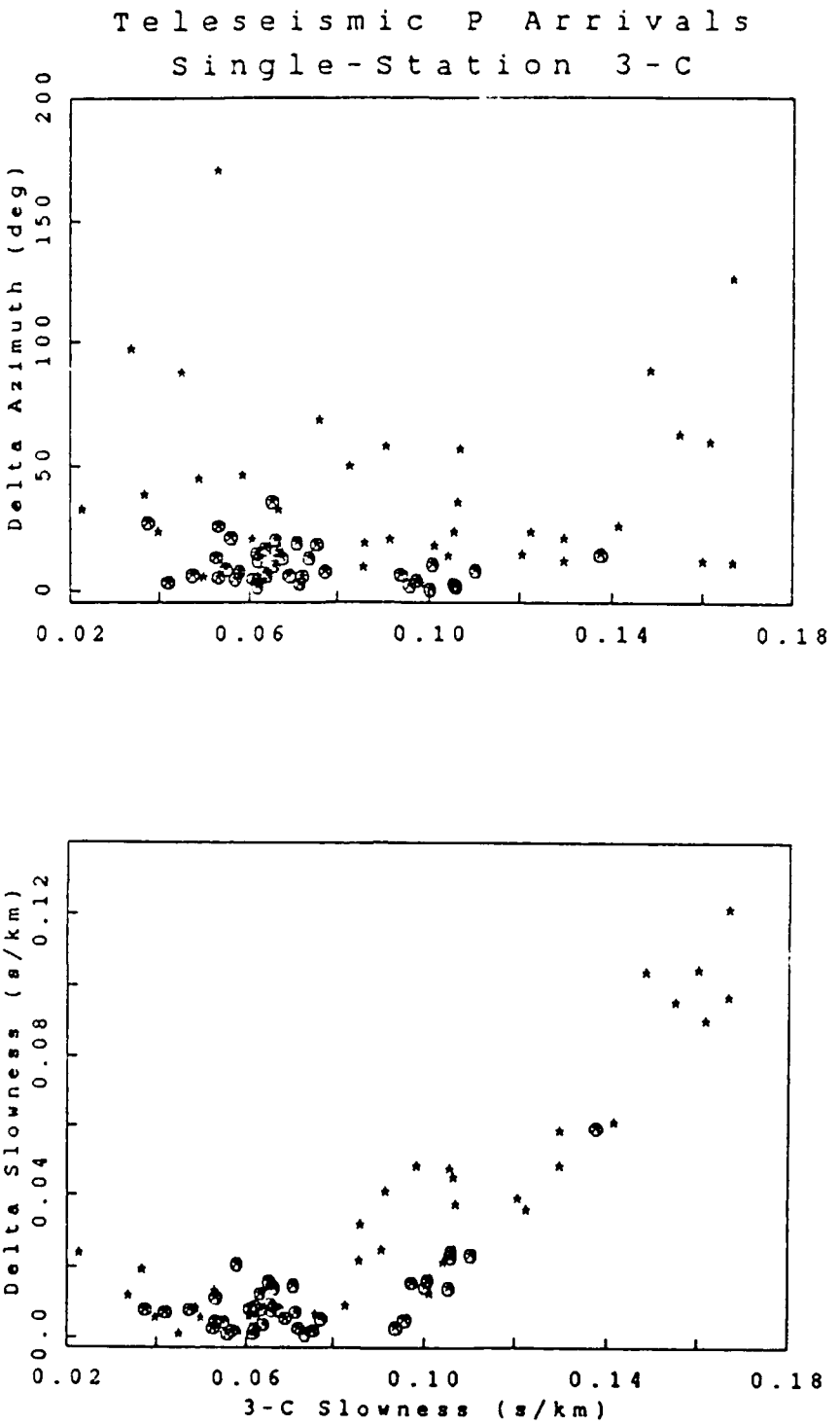


*Figure 5f.* Azimuth (top) and slowness (bottom) differences (in absolute value) versus slowness from 3-C processing for a data set of 74 teleseismic P arrivals. Data points for which 3-C SNR is greater than 2 are circled.

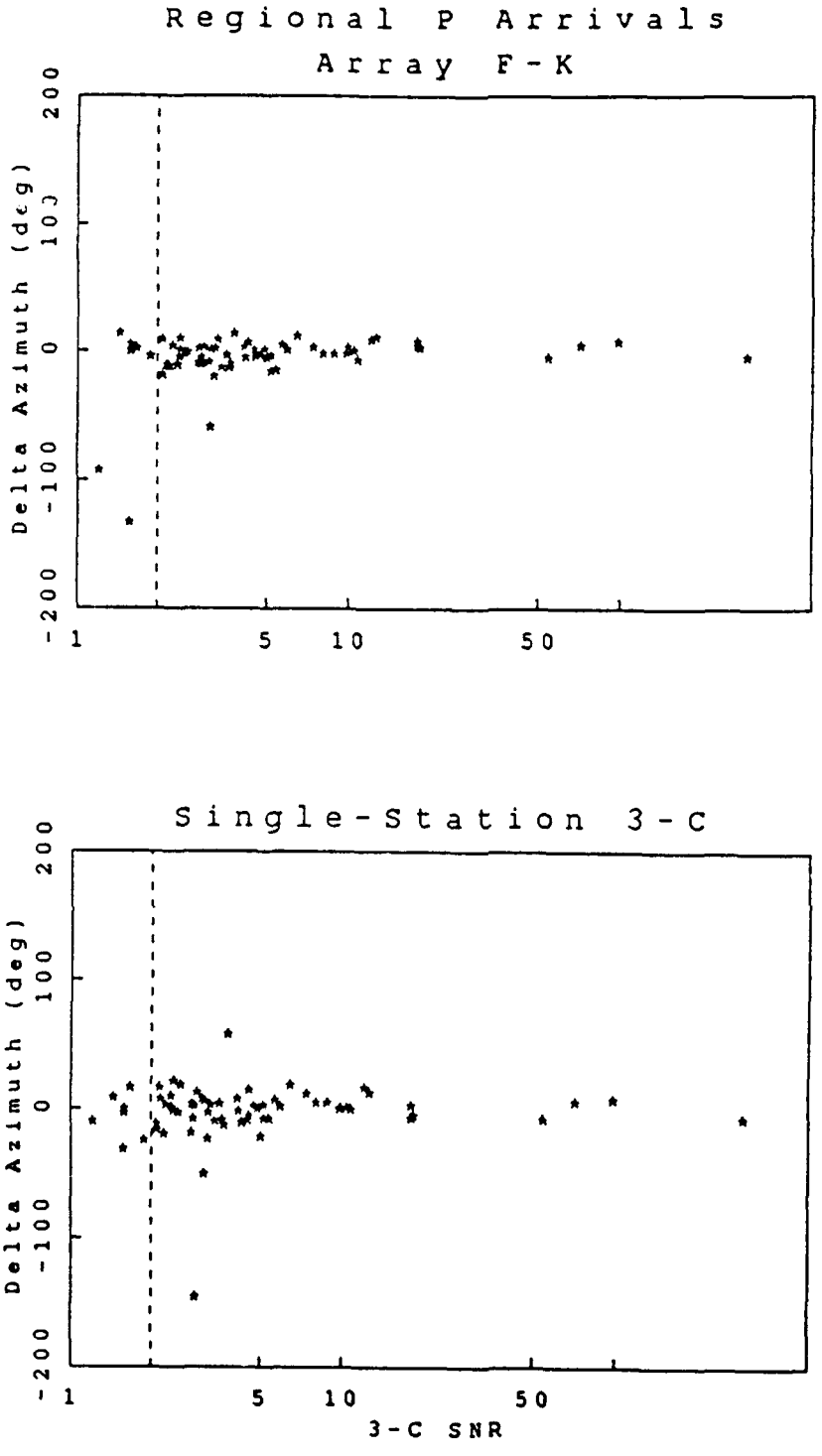


*Figure 6a.* Azimuth differences versus 3-C SNR for a data set of 68 regional P arrivals described in Table A2 (the dashed vertical line indicates an SNR of 2).

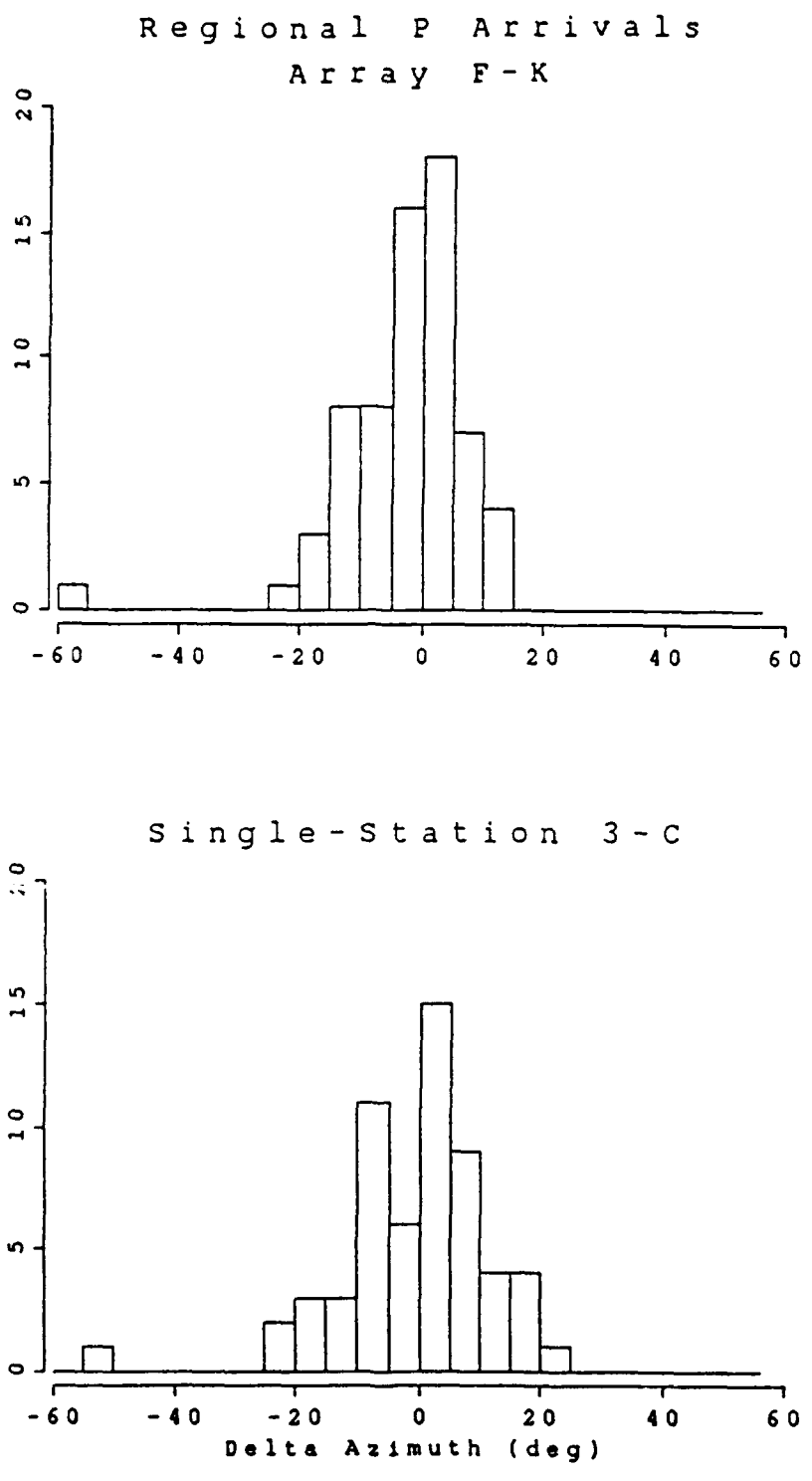


*Figure 6b.* Histograms of azimuth differences for a data set of 60 regional P arrivals with 3-C SNR greater than 2.

**Table IV. Azimuth Differences of Regional P-type Phases**

| | Mean (°) | Standard Deviation (°) | Median (°) |
|---|---|---|---|
| F-K (SNR > 2) | -3. | 11. | -2. |
| 3-C (SNR > 2) | 0. | 14. | 1. |

Comparison of 3-C and Beam SNR

The relevant SNR for the array method is the "beam SNR", which is the ratio of STA to LTA for the best detecting beam. For the single station method we use the "3-C SNR", or ratio of maximum signal 3-C amplitude to average pre-event noise 3-C amplitude in the frequency band used for measuring the azimuth.

We compared these two measures of SNR. *Figure 7 (top)* shows a plot of 3-C SNR as a function of beam SNR, as well as a fit to the data using the L1 norm, on a log-log scale. It is seen that there is a good correlation between the two. The histogram of the logarithm of the beam SNR to 3-C SNR ratio is plotted at the bottom of *Figure 7*. The mean for the ratio is 3.7 and the standard deviation 2.2.

So, for this data set of 68 regional P arrivals, the ratio of array beam SNR to 3-C SNR varies from 2 to 6 on average. A ratio of 3 to 5 is expected from theoretical considerations on noise reduction through beamforming. Therefore, our results are in agreement with theoretical predictions, although there is a significant scatter in the observations.

Effect of Frequency Band Selection on 3-C Results

As for the teleseismic data set we studied the effect of frequency band selection on the results from polarization analysis. For the data set of 48 regional P arrivals at NRA0, four different methods were used to select the frequency band for azimuth estimation:

- Broadband from 1 to 16 Hz: all four bands (1-2, 2-4, 4-8, 8-16 Hz) included.
- Broadband from 1 to 8 Hz: only first three bands included.
- Narrowband from 1 to 16 Hz: all four bands included.
- Narrowband from 1 to 8 Hz: only first three bands included.

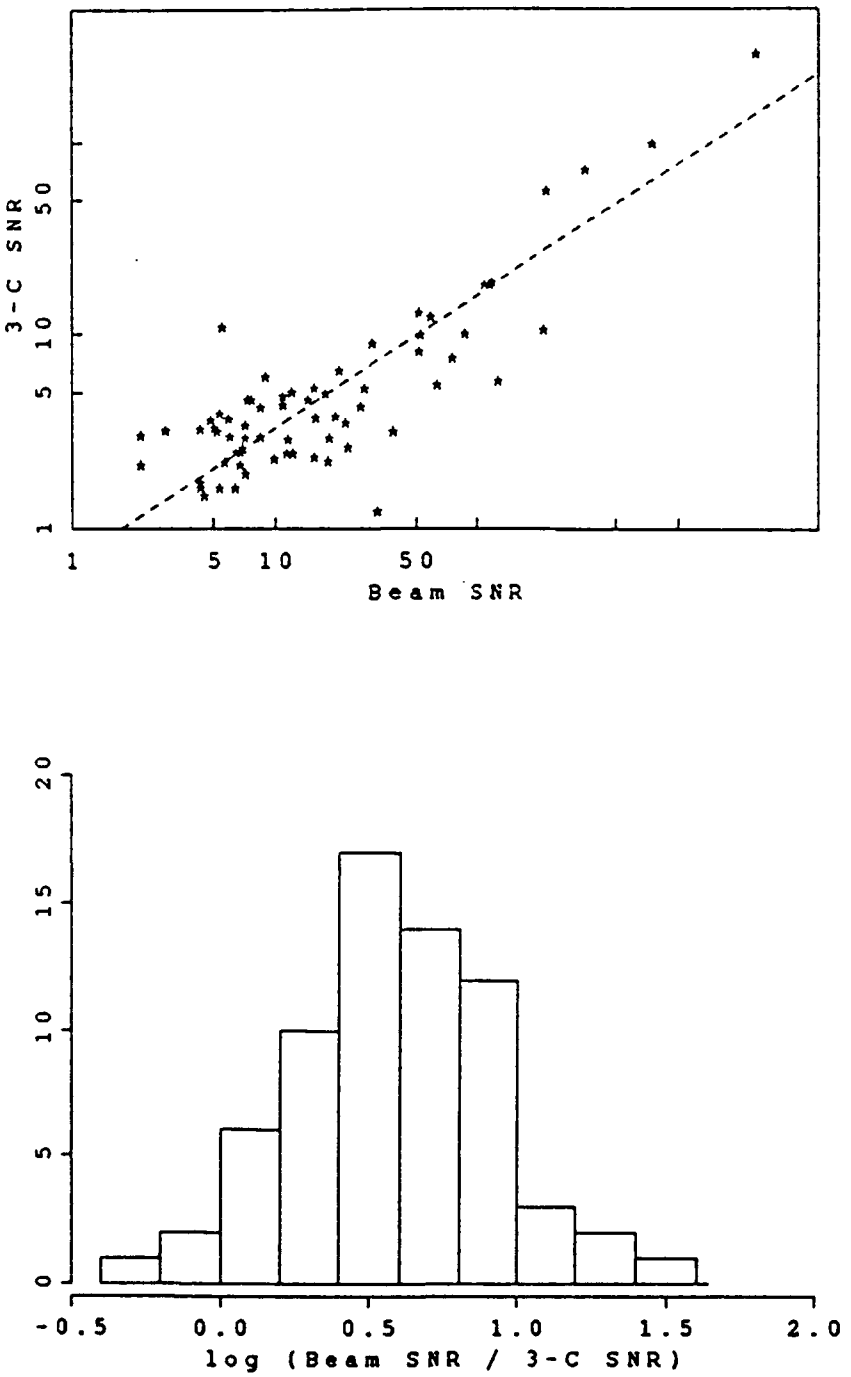


*Figure 7.* Top: 3-C SNR versus beam SNR for a data set of 68 regional P arrivals. The dashed line represents an L1 fit to the data. Bottom: histogram of logarithm of beam SNR to 3-C SNR ratio. The mean ratio is ~ 4 (the logarithm is 0.57).

The azimuth differences were estimated for each method and are plotted in *Figure 8* as a function of 3-C SNR. The main effect of excluding the high-frequency band (8-16 Hz) is to increase the number of outliers. Therefore, for our data set of regional P arrivals at NRA0, automated azimuth estimation from polarization is more stable when all bands from 1 to 16 Hz are included in the analysis. *Table V* compares the standard deviations for the four methods when outliers are excluded. For the narrowband estimates they are slightly lower (by about 1.5°). This may reflect the fact that broadband estimates can be contaminated by the inclusion of frequency bands with relatively low SNR (close to 2). This suggests using SNR to weight the contribution of individual bands as a possible improvement to the broadband method.

**Table V. Standard Deviations of Azimuth Differences for Regional P-Type Phases from 3-C Processing in Various Frequency Bands**

| Broadband 1-16 Hz | Broadband 1-8 Hz | Narrowband 1-16 Hz | Narrowband 1-8 Hz |
|---|---|---|---|
| 16.0° | 15.4° | 14.5° | 14.0° |

Comparison of 3-C Results at Various Stations

Previous studies have indicated that azimuth estimates from single-station 3-C processing and/or their variances are site-dependent (Kvaerna and Doornbos, 1986, US/GSE/49, 1987). In order to assess this effect for our data set of regional events, we performed the same analysis at all four NORESS 3-C stations and compared the results. For most of the events analyzed, not all four stations were recording. Since we processed all available 3-C data, each station has a different event population. Arrivals covering the entire range of SNR were analyzed, but most have SNR larger than 2.

For each station *Figure 9a* shows histograms of the azimuth differences and *Table VI* gives the total number of events analyzed and their standard deviation (excluding outliers).

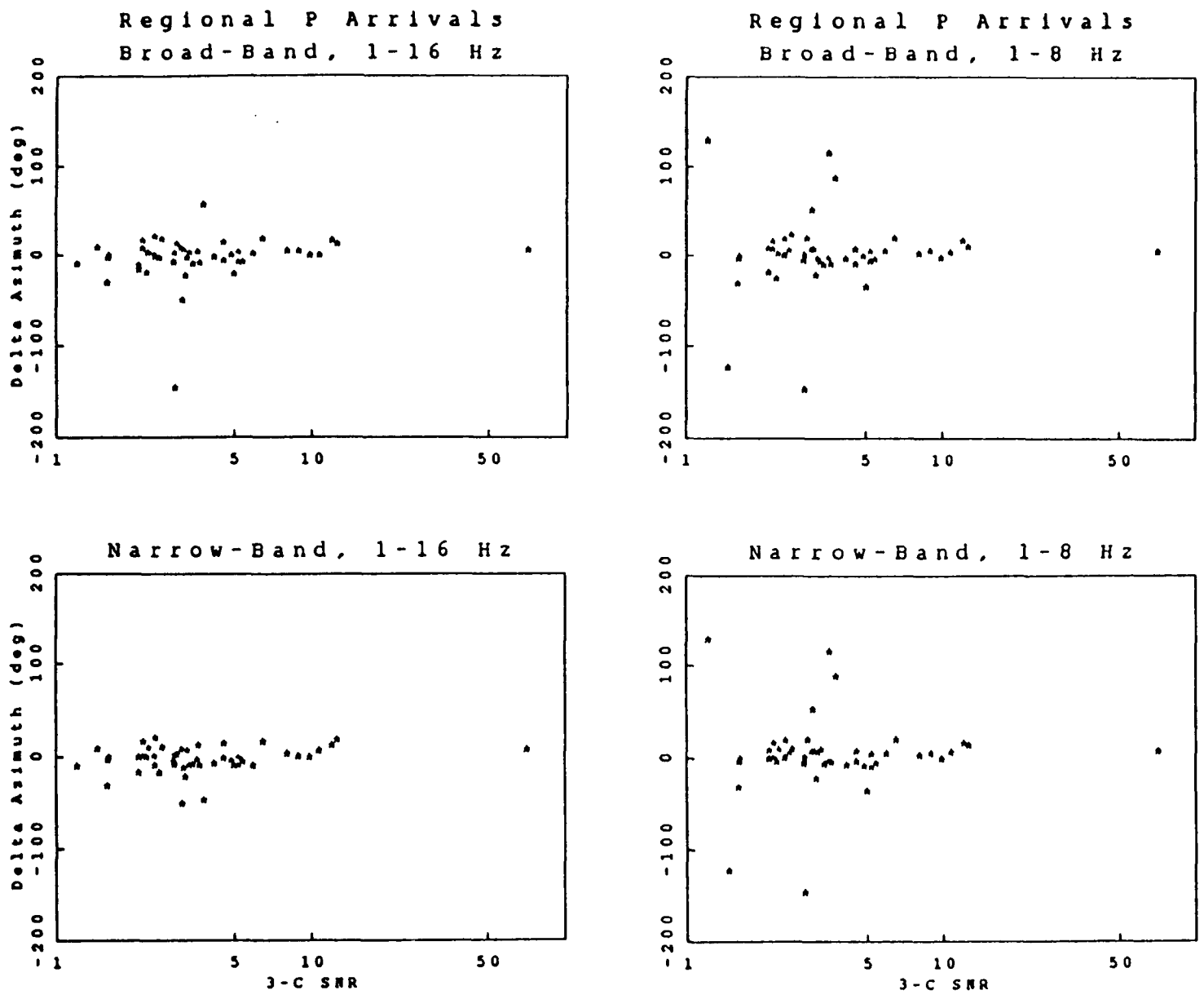


*Figure 8.* Azimuth differences versus 3-C SNR for a set of 48 regional P arrivals at NRAO. 3-C processing was performed using four different methods for frequency band selection (see text for explanation of the methods). In each case 3-C SNR is the estimate obtained with the broad-band, 1-16 Hz, method.

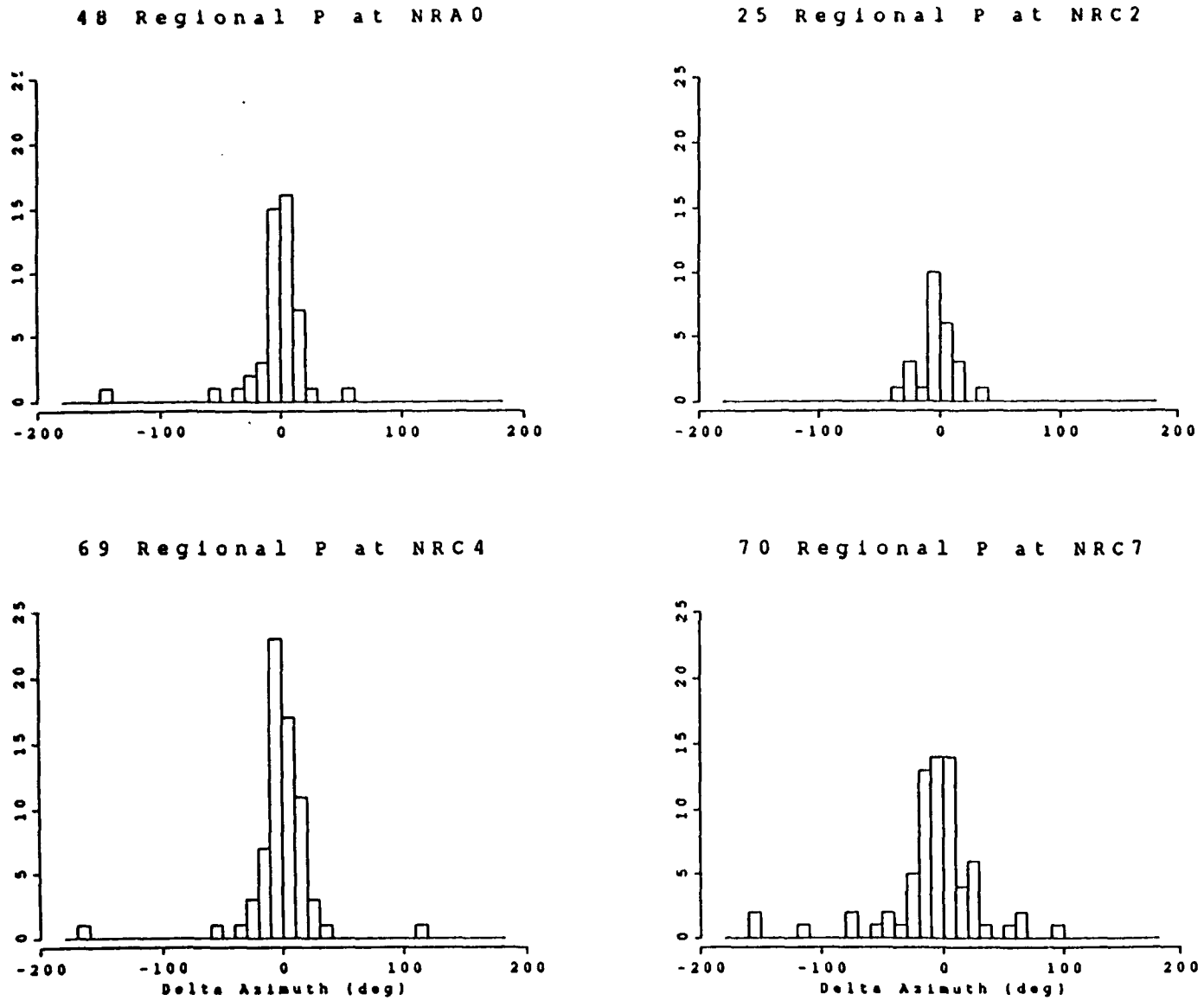


*Figure 9a.* Histograms of azimuth differences for regional P arrivals at the four NORESS 3-C stations.

**Table VI. Comparison of Azimuth Differences at Four NORESS 3-C Stations**

| Station | NRA0 | NRC2 | NRC4 | NRC7 |
|---|---|---|---|---|
| No. of Events | 48 | 25 | 69 | 70 |
| S.D. (°) | 16. | 16. | 15. | 25. |

In spite of different populations, NRA0, NRC2 and NRC4 have similar distributions, with standard deviations of 15° to 16°. This compares well with our previous result of a standard deviation of 14° for a population of 48 NRA0 and 20 NRC4 regional P arrivals with SNR > 2. The similarity of the distributions for NRA0 and NRC4 justifies our use of a mixed population from both stations.

Although NRC4 and NRC7 have almost identical populations, their distributions are very different. NRC7 has a standard deviation of 25°, much larger than that of NRC4 (and the other two stations), and more outliers. This illustrates the site-dependence of the single-station 3-C method for azimuth estimation. Since the paths to NRC4 and NRC7 are very close, the differences must be due to near-receiver structure. Similar results were obtained at RSTN stations (US/GSE/49, 1987): RSSD showed much more scatter than RSNY and RSON, and this was attributed to differences in local geology near the receivers.

To investigate a possible correlation between the large scatter at NRC7 and specific azimuth ranges, the azimuth differences are plotted as a function of theoretical azimuth in *Figure 9b*. Similar plots for the other stations are also given for comparison. Two azimuth ranges show systematic biases, large scatter and outliers. For 17 events in the 90° -100° range the bias is negative, with a median of -18°. For 14 events in the 280° -310° range the bias is positive, with a median of 14°. No such biases and scatter are observed at NRC4 and NRC2, but a similar bias is apparent at NRA0, although less pronounced. These results suggest that better estimates could be obtained at NRC7 by applying azimuth-dependent corrections for those two azimuth ranges. Further investigations are required to determine what causes the observed anomalies at NRC7.

Study of Outliers from 3-C Processing

In the previous section we compared the results of 3-C processing at the four NORESS 3-C stations. Outliers were present for sites NRA0, NRC4 and NRC7. We now attempt to determine in each case the cause of the problem in the azimuth measurement, and a possible remedy.

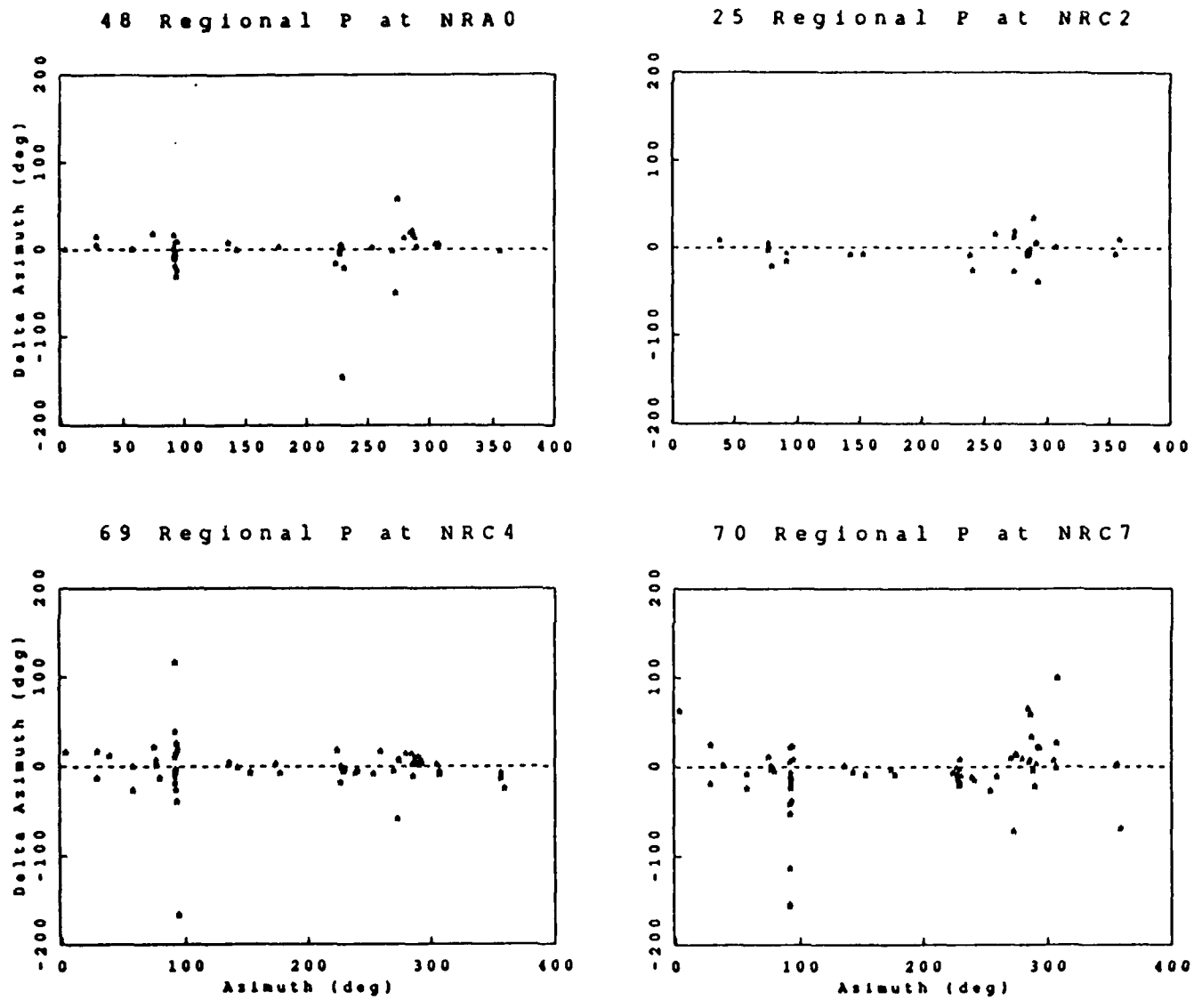


*Figure 9b.* Azimuth differences versus theoretical azimuth for regional P arrivals at the four NORESS 3-C stations.

In three cases, the time at which the measurement was made is 3 seconds ahead of the detection time from the NORESS bulletin. Clearly, this corresponds to a noise measurement. This time was selected because of slightly higher rectilinearity than at the signal arrival. There are two ways this problem might be avoided:

- start searching for the measurement time less than 3 seconds before the detection time,
- use maximum 3-C amplitude in combination with maximum rectilinearity as a criterion for selecting the measurement time.

One event with very low 3-C SNR produced outliers at NRC4 and NRC7. Outliers due to very low SNR may be an intrinsic problem of automated processing.

Two other events produced outliers at NRC7. These measurements are characterized by unusually high incidence angles and occur in the azimuth ranges with large anomalies (see previous section). It is not clear what caused the measurement errors, but it may be related to the source of the observed bias and scatter at those azimuths.

In conclusion, this study of outliers shows that they are due to different causes. Some might be remedied by improvements in the method for selecting the measurement time. Others are due to very low SNR, and appear to be an intrinsic limitation of automated processing. Finally, some may be due to signal complexities at the NRC7 site for some azimuths.

### 2.3.5 Conclusions

The capability of three-component stations for azimuth and slowness estimation critically depends on signal-to-noise ratio. For SNR below a threshold of ~ 2 the scatter in the estimates is very large for both parameters, and the slowness tends to be overestimated. The array measurements obtained with the broadband F-K method are not significantly affected by noise in the range of SNR considered. For events with sufficient SNR, both methods compare well, with only a slightly better performance for the F-K method. The results from this study agree with those from a theoretical investigation by Harris (1982). Also, the effects of SNR on the uncertainty of direction estimates from 3-C processing are similar to those reported in other studies (Jurkevics, 1988; US/GSE/49, 1987; Walck and Chael, 1989).

For regional arrivals the ratio of beam (or array) SNR to 3-C SNR varies from 2 to 6 on average, which is in agreement with theoretical expectations of a ratio of 3 to 5. It is larger for teleseismic P phases, with an average of 7.

The performance of the 3-C method for teleseismic arrivals is slightly improved when using broadband instead of narrowband estimates for SNR > 2. The

opposite is true for regional arrivals, possibly due to noise contamination in frequency bands with SNR close to 2, when using the broadband method. The inclusion of a high frequency band (8-16 Hz) in the 3-C analysis of regional P arrivals reduces the number of outliers, therefore increasing the stability of the method.

As shown by a detailed analysis of the results from 3-C processing of teleseismic P arrivals, the azimuth and slowness differences are not only correlated with 3-C SNR, but also with other "polarization attributes", especially rectilinearity and ratio of horizontal to vertical amplitude. Therefore, these are good candidates for predicting estimated errors of azimuth and slowness measurements from 3-C processing. This study will be extended to regional events in future work.

A comparison of 3-C processing of regional arrivals at the four NORESS 3-C stations showed the results are site-dependent. In particular, the distribution of azimuth differences at NRC7 differs significantly from those at the other stations (larger standard deviation and more outliers). These anomalies seem mostly confined to two azimuth ranges, with biases in their estimates, suggesting that azimuth-dependent corrections could improve the performance at this station. A similar comparison for teleseismic arrivals would provide us with more insight.

A study of outliers observed in the automated 3-C processing of regional data shows they are due to various causes. Although some might be remedied through improvements in the automated processing procedure, very low SNR appears to be an intrinsic limitation for such a method. Other outliers may be due to signal complexities at specific sites and azimuths. The study of outliers in the teleseismic data set will be the object of future work.

Anne Suteau-Henson

## References


Bullen, K. E., 1959. "An Introduction to the Theory of Seismology", Cambridge University Press, London, England, 296 pp.

Harris, D. B., 1982. "Uncertainty In Direction Estimation: A Comparison Of Small Arrays And Three-Component Stations", *Technical Report UCID-19589-82*, Lawrence Livermore National Laboratory, October 8, 1982, 31pp.

Jurkevics, A., 1988. "Polarization Analysis Of Three-Component Array Data", *Bull. seism. Soc. Am.*, Vol. 78, p. 1725-1743.

Kvaerna, T., 1987. "Wide-Band Slowness Estimation Using a Small Aperture Seismic Array", *NORSAR Semiannual Technical Summary, 2-86/87*, 38-45.

Kvaerna, T. and D.J. Doornbos, 1986. "An Integrated Approach to Slowness Analysis with Arrays and Three-Component Stations", *NORSAR Semiannual Technical Summary, 2-85/86*, p. 60-69.

Kvaerna, T. and F. Ringdal, 1986. "Stability of Various F-K Estimation Techniques", *NORSAR Semiannual Technical Summary, 1-86/87*, p. 29-40.

US/GSE/49, 1987. "A Recommendation For Inclusion Of Azimuth As A Reportable Parameter For Three-Component Stations", United States Delegation to the Conference on Disarmament, Geneva, Switzerland, 37 pp.

Walck, M.C. and E.P Chael, 1989. "Optimal Back-Azimuth Estimation for Three-Component Recordings of Regional Events (abstract)", *Trans. Am Geophys. Union*, Vol. 70, p. 1197.

## APPENDIX I

### TABLE A1. INFORMATION ON TELESEISMIC EVENTS

| MoDy 1988 | Time, GMT | Lat. deg.N | Long. deg.E | Dist. deg. | Az. deg. | Depth km. | Mag. | Area |
|---|---|---|---|---|---|---|---|---|
| 1005 | 0:42:11.0 | 35.51 | -3.86 | 27.11 | 208.39 | 32 | 3.80 | STRAITS OF GIBRALTAR |
| 1011 | 4:20:00.7 | 37.36 | 20.86 | 24.13 | 161.60 | 48 | 4.50 | IONIAN SEA |
| 1013 | 0:32:12.7 | 61.88 | 169.63 | 56.56 | 12.23 | 33 | 5.50 | EASTERN SIBERIA |
| 1013 | 14:00:00.0 | 37.09 | -116.05 | 73.54 | 318.65 | 0 | 4.40 | SOUTHERN NEVADA |
| 1015 | 1:22:01.4 | 15.97 | -93.75 | 83.48 | 290.95 | 33 | 4.30 | NEAR COAST OF CHIAPAS, MEXICO |
| 1015 | 8:02:56.9 | 14.63 | -90.83 | 83.30 | 287.82 | 42 | 4.60 | GUATEMALA |
| 1015 | 15:38:04.6 | 44.64 | 11.00 | 16.13 | 181.39 | 10 | | NORTHERN ITALY |
| 1016 | 6:15:29.3 | 37.52 | -25.36 | 32.79 | 241.82 | 10 | 5.10 | AZORES ISLANDS |
| 1018 | 2:26:01.7 | 7.32 | -35.89 | 63.90 | 234.44 | 10 | 5.20 | CENTRAL MID-ATLANTIC RIDGE |
| 1023 | 13:48:35.6 | 44.42 | -129.46 | 70.50 | 331.42 | 10 | 5.30 | OFF COAST OF OREGON |
| 1026 | 6:31:50.3 | 44.51 | -129.81 | 70.49 | 331.70 | 10 | 4.50 | OFF COAST OF OREGON |
| 1027 | 0:31:08.7 | 35.11 | -35.20 | 39.22 | 250.79 | 10 | 5.20 | NORTH ATLANTIC RIDGE |
| 1027 | 17:24:38.8 | 11.94 | -87.95 | 84.28 | 284.05 | 33 | 4.70 | NEAR COAST OF NICARAGUA |
| 1101 | 19:19:47.1 | 16.54 | 41.00 | 48.95 | 141.28 | 10 | 4.70 | RED SEA |
| 1102 | 21:02:29.0 | 37.44 | 20.43 | 23.99 | 162.39 | 42 | 4.50 | IONIAN SEA |
| 1103 | 7:55:09.4 | 16.49 | 41.02 | 49.00 | 141.28 | 10 | 4.70 | RED SEA |
| 1103 | 14:47:10.7 | 13.88 | -90.45 | 83.77 | 287.13 | 69 | 5.60 | NEAR COAST OF GUATEMALA |
| 1103 | 19:42:18.1 | 19.08 | -67.26 | 68.08 | 269.98 | 33 | 5.40 | MONA PASSAGE |
| 1104 | 18:31:22.4 | 44.33 | 148.76 | 69.65 | 31.32 | 44 | 5.10 | KURILE ISLANDS |
| 1105 | 2:14:30.3 | 34.35 | 91.88 | 56.12 | 79.24 | 8 | 5.90 | TSINGHAI PROVINCE, CHINA |
| 1105 | 2:51:36.8 | 37.12 | 135.86 | 72.43 | 43.83 | 339 | 5.20 | SEA OF JAPAN |
| 1106 | 2:17:59.9 | 32.06 | 137.04 | 77.42 | 45.10 | 51 | 4.90 | SOUTH OF HONSHU, JAPAN |
| 1106 | 13:15:43.3 | 23.18 | 99.44 | 69.06 | 79.95 | 10 | 6.40 | BURMA-CHINA BORDER REGION |
| 1106 | 20:35:28.2 | 23.39 | 99.31 | 68.82 | 79.94 | 10 | 4.90 | BURMA-CHINA BORDER REGION |
| 1107 | 3:24:28.9 | 26.53 | 126.42 | 78.36 | 56.08 | 105 | 5.70 | RYUKYU ISLANDS |
| 1107 | 14:26:54.4 | 38.14 | 15.89 | 22.79 | 171.13 | 20 | 3.70 | SICILY |
| 1108 | 8:17:54.4 | 36.58 | 22.66 | 25.19 | 158.61 | 54 | 3.60 | SOUTHERN GREECE |
| 1109 | 23:29:55.1 | 44.33 | 148.29 | 69.53 | 31.66 | 36 | 5.70 | KURILE ISLANDS |
| 1111 | 4:02:49.2 | 35.28 | 22.96 | 26.51 | 158.72 | 48 | 3.90 | MEDITERRANEAN SEA |
| 1111 | 18:50:26.7 | 37.73 | 21.60 | 23.89 | 160.00 | 63 | 3.60 | SOUTHERN GREECE |
| 1112 | 3:30:03.7 | 50.08 | 78.99 | 38.05 | 74.90 | 0 | 5.30 | EASTERN KAZAKH SSR |
| 1112 | 20:05:14.8 | 17.64 | -94.34 | 82.29 | 292.25 | 140 | 4.70 | CHIAPAS, MEXICO |
| 1113 | 6:26:57.3 | 51.38 | -178.34 | 67.96 | 6.66 | 52 | 5.10 | ANDREANOF ISLANDS, ALEUTIAN IS. |
| 1115 | 5:04:01.7 | 27.02 | 60.84 | 47.20 | 112.83 | 33 | 4.30 | SOUTHERN IRAN |
| 1115 | 8:41:42.3 | 52.11 | -171.10 | 67.49 | 1.76 | 23 | 5.90 | FOX ISLANDS, ALEUTIAN ISLANDS |
| 1117 | 1:06:59.2 | 55.58 | 161.71 | 61.65 | 18.72 | 33 | 4.90 | NEAR EAST COAST OF KAMCHATKA |
| 1120 | 1:35:33.6 | 23.46 | 99.39 | 68.79 | 79.84 | 33 | 4.70 | BURMA-CHINA BORDER REGION |
| 1120 | 21:01:05.9 | 35.28 | 28.68 | 27.76 | 148.82 | 10 | 5.20 | EASTERN MEDITERRANEAN SEA |
| 1121 | 10:19:05.4 | 31.47 | -9.54 | 32.42 | 214.99 | 10 | 4.40 | MOROCCO |
| 1121 | 20:22:22.9 | 52.68 | 153.04 | 62.82 | 25.22 | 483 | 4.50 | NORTHWEST OF KURILE ISLANDS |
| 1122 | 15:20:44.3 | 41.78 | 75.10 | 42.12 | 86.92 | 33 | 4.90 | KIRGIZ SSR |
| 1123 | 3:57:06.7 | 49.82 | 78.07 | 37.78 | 75.86 | 0 | 5.30 | EASTERN KAZAKH SSR |
| 1124 | 14:54:37.3 | 36.57 | 71.61 | 44.44 | 94.78 | 128 | 4.20 | AFGHANISTAN-USSR BORDER REGION |
| 1125 | 22:29:40.1 | 34.33 | 91.93 | 56.16 | 79.21 | 25 | 5.10 | TSINGHAI PROVINCE, CHINA |
| 1125 | 23:46:04.5 | 48.12 | -71.18 | 46.51 | 293.63 | 29 | 5.80 | SOUTHERN QUEBEC |
| 1127 | 1:16:21.3 | 35.93 | 70.51 | 44.41 | 96.35 | 92 | 4.80 | HINDU KUSH REGION |
| 1128 | 3:38:11.2 | 23.04 | 99.72 | 69.31 | 79.80 | 27 | 4.90 | BURMA-CHINA BORDER REGION |
| 1130 | 8:13:29.7 | 22.77 | 99.84 | 69.60 | 79.85 | 15 | 5.60 | BURMA-CHINA BORDER REGION |
| 1130 | 8:55:30.6 | 61.35 | -152.27 | 57.61 | 350.84 | 144 | 5.50 | SOUTHERN ALASKA |
| 1201 | 21:52:05.8 | 34.49 | 24.08 | 27.49 | 157.14 | 33 | 4.40 | CRETE |
| 1202 | 6:21:44.0 | 56.56 | -152.27 | 62.35 | 349.96 | 33 | 4.60 | KODIAK ISLAND REGION |

| MoDy 1988 | Time, GMT | Lat. deg.N | Long. deg.E | Dist. deg. | Az. deg. | Depth km. | Mag. | Area |
|---|---|---|---|---|---|---|---|---|
| 1202 | 16:59:13.3 | 29.55 | 81.16 | 54.80 | 91.63 | 33 | 4.50 | NEPAL |
| 1202 | 17:43:04.6 | 40.47 | 22.64 | 21.42 | 156.29 | 10 | 3.50 | GREECE |
| 1202 | 18:15:09.3 | 30.28 | 101.53 | 64.08 | 74.10 | 31 | 4.60 | SZECHWAN PROVINCE, CHINA |
| 1203 | 6:04:48.0 | 36.23 | 72.65 | 45.21 | 94.13 | 33 | 4.80 | AFGHANISTAN-USSR BORDER REGION |
| 1204 | 2:58:14.9 | 38.45 | 99.60 | 56.47 | 70.29 | 10 | 4.30 | TSINGHAI PROVINCE, CHINA |
| 1204 | 5:19:53.0 | 73.39 | 55.00 | 20.49 | 34.42 | 0 | 5.90 | NOVAYA ZEMLYA |
| 1206 | 13:20:41.0 | 29.95 | 51.65 | 40.64 | 120.86 | 10 | 5.50 | SOUTHERN IRAN |
| 1206 | 16:11:36.7 | 59.54 | -152.91 | 59.45 | 350.88 | 94 | 4.90 | SOUTHERN ALASKA |
| 1206 | 22:37:44.8 | 34.39 | 28.31 | 28.51 | 150.01 | 66 | 4.30 | EASTERN MEDITERRANEAN SEA |
| 1208 | 4:09:36.0 | 40.88 | 44.41 | 28.27 | 119.66 | 10 | 4.70 | TURKEY-USSR BORDER REGION |
| 1208 | 20:32:06.4 | 41.15 | 44.21 | 27.96 | 119.60 | 10 | 4.80 | WESTERN CAUCASUS |
| 1209 | 9:31:04.1 | 14.46 | -92.53 | 84.24 | 289.19 | 59 | 5.00 | NEAR COAST OF CHIAPAS, MEXICO |
| 1210 | 13:09:10.4 | 53.18 | -167.55 | 66.43 | 359.40 | 33 | 4.60 | FOX ISLANDS, ALEUTIAN ISLANDS |
| 1210 | 20:30:00.0 | 37.20 | -116.21 | 73.49 | 318.82 | 0 | 5.00 | SOUTHERN NEVADA |
| 1211 | 5:18:24.5 | 53.32 | -166.96 | 66.29 | 359.02 | 67 | 5.00 | FOX ISLANDS, ALEUTIAN ISLANDS |
| 1211 | 14:39:31.2 | 45.01 | 36.63 | 21.63 | 125.33 | 33 | 3.90 | CRIMEA REGION |
| 1212 | 10:36:41.0 | 12.52 | -87.54 | 83.58 | 283.98 | 97 | 4.60 | NEAR COAST OF NICARAGUA |
| 1214 | 11:46:02.8 | 39.18 | 71.79 | 42.48 | 92.27 | 59 | 5.30 | TADZHIK SSR |
| 1215 | 6:40:51.7 | 46.50 | 95.57 | 48.31 | 66.93 | 24 | 5.30 | MONGOLIA |
| 1215 | 9:21:18.3 | 51.14 | 158.02 | 65.27 | 22.52 | 39 | 5.30 | NEAR EAST COAST OF KAMCHATKA |
| 1216 | 5:53:04.9 | 33.98 | -116.68 | 76.59 | 317.85 | 8 | 4.80 | SOUTHERN CALIFORNIA |
| 1217 | 4:18:06.9 | 49.89 | 78.93 | 38.15 | 75.16 | 0 | 5.90 | EASTERN KAZAKH SSR |
| 1217 | 18:24:03.2 | 34.98 | 24.02 | 27.00 | 156.99 | 28 | 4.50 | CRETE |

## TABLE A2. INFORMATION ON REGIONAL EVENTS

| YrMoDy | Time, GMT | Lat. deg.N | Long. deg.E | Dist. km. | Az. deg. | Mag. | Area |
|---|---|---|---|---|---|---|---|
| 850801 | 11:17:35.7 | 45.77 | 26.66 | 1939.08 | 142.47 | 4.7 | RUMANIA |
| 851025 | 12:03:47.0 | 59.30 | 28.10 | 935.93 | 92.58 | 2.3 | EUROPEAN USSR |
| 851027 | 4:36:24.4 | 61.12 | 4.92 | 362.01 | 279.71 | 2.8 | SOUTHERN NORWAY |
| 851108† | 14:18:54.6 | 58.34 | 6.43 | 393.65 | 229.52 | 2.4 | SOUTHERN NORWAY |
| 851113 | 12:07:48. | 59.30 | 28.10 | 935.93 | 92.58 | 2.3 | EUROPEAN USSR |
| 851120 | 22:10:44.2 | 57.61 | 5.67 | 484.00 | 226.51 | 2.3 | NORTH SEA |
| 851120 | 22:24:38.1 | 57.66 | 5.72 | 477.85 | 226.68 | 2.2 | NORTH SEA |
| 851120 | 22:57:10.8 | 57.63 | 6.27 | 459.14 | 223.35 | 2.2 | NORTH SEA |
| 851120 | 23:10:47.5 | 57.66 | 5.35 | 492.79 | 228.61 | 2.3 | NORTH SEA |
| 851120 | 23:17:28.9 | 57.69 | 5.45 | 486.26 | 228.37 | 2.3 | NORTH SEA |
| 851120 | 23:23:10.0 | 57.64 | 5.62 | 483.50 | 227.04 | 2.2 | NORTH SEA |
| 851120 | 23:28:23.1 | 57.58 | 5.49 | 493.68 | 227.19 | 2.2 | NORTH SEA |
| 851123 | 13:06:18. | 59.50 | 25.00 | 760.54 | 94.54 | 2.1 | EUROPEAN USSR |
| 851127 | 4:53:32.8 | 59.73 | 5.71 | 342.32 | 253.42 | 2.8 | SOUTHERN NORWAY |
| 851210 | 12:05:39. | 59.40 | 28.50 | 954.59 | 91.54 | 2.2 | EUROPEAN USSR |
| 851223 | 2:35:08.3 | 60.38 | 1.90 | 530.68 | 269.92 | 2.3 | NORTH SEA |
| 851225 | 13:18:49. | 59.30 | 27.60 | 908.65 | 93.10 |  | EUROPEAN USSR |
| 851227 | 12:16:08. | 59.40 | 28.50 | 954.59 | 91.54 | 2.4 | EUROPEAN USSR |
| 851231 | 6:57:21.0 | 73.43 | 7.93 | 1426.22 | 355.33 | 4.8 | GREENLAND SEA |
| 860103 | 14:58:41.0 | 61.90 | 30.60 | 1026.85 | 74.46 | 2.5 | FINLAND-USSR BORDER REGION |
| 860107 | 14:14:28.9 | 58.29 | 6.40 | 399.03 | 229.13 | 2.2 | SOUTHERN NORWAY |
| 860117† | 14:11:01. | 58.34 | 6.43 | 393.65 | 229.52 | 2.3 | SOUTHERN NORWAY |
| 860119 | 4:59:22.2 | 64.95 | 12.13 | 471.87 | 3.36 | 3.0 | NORTHERN NORWAY |
| 860120 | 23:38:28.3 | 50.18 | 12.31 | 1177.81 | 177.31 | 5.0 | GERMANY |
| 860131 | 12:10:14.0 | 59.30 | 28.10 | 935.93 | 92.58 | 2.3 | EUROPEAN USSR |
| 860205 | 17:53:35.2 | 62.62 | 5.08 | 401.63 | 304.31 | 4.3 | SOUTHERN NORWAY |
| 860206 | 12:22:04.0 | 59.30 | 28.10 | 935.93 | 92.58 | 2.7 | EUROPEAN USSR |
| 860206 | 16:29:55.0 | 67.10 | 20.60 | 836.77 | 28.07 | 2.7 | SWEDEN |
| 860207 | 11:00:01.0 | 64.70 | 30.70 | 1071.37 | 57.41 | 3.1 | FINLAND-USSR BORDER REGION |
| 860210 | 12:41:46.0 | 59.40 | 28.50 | 954.59 | 91.54 | 2.5 | EUROPEAN USSR |
| 860214 | 12:10:21.0 | 59.40 | 28.50 | 954.59 | 91.54 | 2.7 | EUROPEAN USSR |
| 860214 | 14:13:24.9 | 58.31 | 6.16 | 407.50 | 230.77 | 2.7 | SOUTHERN NORWAY |
| 860214 | 16:44:08.0 | 67.10 | 20.60 | 836.77 | 28.07 | 2.6 | SWEDEN |
| 860214 | 17:54:10.6 | 58.30 | 6.40 | 398.24 | 229.25 | 2.3 | SOUTHERN NORWAY |
| 860218 | 10:46:16.0 | 59.30 | 27.20 | 886.83 | 93.53 | 2.6 | EUROPEAN USSR |
| 860218 | 12:45:50.0 | 64.70 | 30.70 | 1071.37 | 57.41 | 2.6 | FINLAND-USSR BORDER REGION |
| 860226 | 2:11:44.6 | 62.76 | 5.29 | 400.32 | 307.06 | 2.5 | SOUTHERN NORWAY |
| 860303 | 7:26:06.2 | 43.70 | 31.40 | 2313.19 | 136.07 | 4.4 | BLACK SEA |
| 860305 | 12:13:19.0 | 59.50 | 26.50 | 842.32 | 92.86 | 2.6 | EUROPEAN USSR |
| 860305 | 13:02:05.0 | 60.63 | 2.58 | 490.18 | 272.53 | 2.1 | NORTH SEA |
| 860308 | 16:21:17.0 | 61.67 | 2.58 | 493.22 | 286.10 | 2.4 | NORWEGIAN SEA |
| 860310 | 4:20:04.0 | 62.81 | 4.91 | 419.85 | 306.33 | 2.5 | NORWEGIAN SEA |
| 860310 | 12:02:09.0 | 59.30 | 28.10 | 935.93 | 92.58 | 2.6 | EUROPEAN USSR |
| 860311 | 12:02:28.0 | 59.30 | 28.10 | 935.93 | 92.58 | 2.6 | EUROPEAN USSR |
| 860312 | 12:01:38.0 | 59.40 | 28.50 | 954.59 | 91.54 | 2.5 | EUROPEAN USSR |
| 860319 | 12:06:40.0 | 59.40 | 28.50 | 954.59 | 91.54 | 2.6 | EUROPEAN USSR |
| 860330 | 3:22:37.7 | 61.66 | 4.53 | 391.20 | 288.34 | 2.2 | SOUTHERN NORWAY |
| 860401 | 9:56:55.8 | 56.67 | 12.28 | 455.37 | 174.25 | 3.6 | SWEDEN |
| 860404 | 22:42:33.8 | 70.98 | 8.97 | 1150.24 | 355.30 | 3.4 | NORWEGIAN SEA |
| 860407 | 0:34:37.3 | 61.84 | 4.88 | 378.14 | 291.91 | 2.3 | SOUTHERN NORWAY |
| 860603 | 14:30:01 8 | 61.54 | 4.10 | 411.02 | 285.82 | 3.0 | SOUTHERN NORWAY |
| 860604 | 9:06:31.0 | 61.50 | 30.40 | 1018.09 | 76.99 | 3.3 | FINLAND-USSR BORDER REGION |

| YrMoDy | Time, GMT | Lat. deg.N | Long. deg.E | Dist. km. | Az. deg. | Mag. | Area |
|---|---|---|---|---|---|---|---|
| 860612 | 9:30:54.0 | 61.50 | 30.40 | 1018.09 | 76.99 | 3.1 | FINLAND-USSR BORDER REGION |
| 860615 | 15:01:04.6 | 61.84 | 4.37 | 404.31 | 290.93 | 3.0 | SOUTHERN NORWAY |
| 860617 | 12:12:07.0 | 59.40 | 28.50 | 954.59 | 91.54 | 2.6 | EUROPEAN USSR |
| 860618 | 11:05:08.0 | 59.40 | 28.50 | 954.59 | 91.54 | 2.5 | EUROPEAN USSR |
| 860619 | 3:55:08.7 | 59.20 | 6.90 | 310.92 | 238.60 | 2.4 | SOUTHERN NORWAY |
| 860620 | 22:07:53.5 | 61.47 | 3.92 | 419.48 | 284.58 | 2.0 | NORWEGIAN SEA |
| 860626 | 4:06:21.3 | 61.88 | 5.10 | 368.33 | 293.08 | 2.4 | SOUTHERN NORWAY |
| 860627 | 3:49:46.2 | 59.28 | 6.76 | 312.49 | 240.79 | 2.5 | SOUTHERN NORWAY |
| 860714 | 13:50:32.3 | 58.25 | 13.88 | 307.64 | 153.43 | 4.1 | SWEDEN |
| 860714 | 14:30:27.0 | 61.10 | 29.90 | 994.92 | 79.66 | 2.9 | FINLAND-USSR BORDER REGION |
| 860714 | 15:02:19.0 | 69.30 | 34.40 | 1426.68 | 38.46 | 2.9 | EUROPEAN USSR |
| 860810 | 5:01:03.9 | 59.99 | 5.34 | 352.54 | 259.07 | 1.7 | SOUTHERN NORWAY |
| 860816 | 4:24:36.2 | 62.82 | 4.98 | 417.34 | 306.71 | 2.5 | NORWEGIAN SEA |
| 860901 | 22:11:25.3 | 60.74 | 3.15 | 458.20 | 273.69 | 3.9 | NORTH SEA |
| 860930 | 20:02:46.8 | 60.79 | 4.23 | 398.97 | 274.06 | 2.4 | SOUTHERN NORWAY |
| 861010 | 19:56:30.8 | 61.97 | 2.33 | 511.98 | 289.60 | 2.3 | NORWEGIAN SEA |
| 861026 | 11:34:41.7 | 61.78 | 3.97 | 423.04 | 289.31 | 4.4 | NORWEGIAN SEA |
| 861026 | 11:57:00.5 | 61.70 | 3.03 | 469.90 | 286.89 | 3.0 | NORWEGIAN SEA |
| 861029† | 21:05:01. | 60.81 | 3.04 | 463.70 | 274.73 | 2.4 | NORTH SEA |
| 861123 | 3:30:44.4 | 73.32 | 10.33 | 1407.23 | 358.41 | 3.0 | NORWEGIAN SEA |

†: Events not included in data set of 68 regional events.

## 2.4 SOME ASPECTS OF DESIGNING A SEISMIC NETWORK FOR GLOBAL MONITORING


### ABSTRACT

A variety of networks based on either existing or hypothetical stations have been proposed for monitoring underground nuclear explosions. These networks are usually not selected on the basis of achieving a specified performance, and therefore, often have undesirable features. In this paper we define three general technical characteristics, based on symmetry, that would be desirable for the station network of a global cooperative system: *geographical uniformity, balance between seismological functions,* and *monitoring capabilities superior to other existing networks.* From these characteristics major seismological functions are specified, station selection procedures broadly described, and the capabilities of various seismological functions outlined as a function of number and types of stations and their geometries. It is concluded that the following factors would be particularly important to satisfy the general characteristics defined above in the design of a global station network for nuclear explosion monitoring: *Extensive use of array stations* to obtain sufficient sensitivity and minimize problems related to unassociated station detections, *epicenter determination with a global set of master events* for precise event locations as proposed by Bolt (1973), *a large enough number of stations* to maintain sufficient depth estimation capability, and *high-sensitivity long-period station network* for $M_s$ determinations.


### 2.4.1 Introduction

A variety of seismic networks consisting of both hypothetical and existing stations have been proposed and assessed for monitoring underground nuclear explosions (for a list of references see compilation by Harjes, 1985). For all of these networks, the event detection capability varies considerably with region, and a significant number of detected events are not expected to be identified. These assessments estimate the performance from *given station characteristics* like noise amplitudes, geographical coordinates, etc. The reverse problem, of designing a network to achieve a *specified desirable performance* is seldom addressed, partly because of its complexity but also because of the fact that there are no widely accepted performance criteria.

In this paper we attempt to get some insight into this direct network design problem by presenting results of calculations for various hypothetical networks with regard to detection, location, depth estimation and measuring identification parameters. The presentation is limited to *global* networks, even if *regional* detection with internal station networks has been in the focus of seismological verification research

and development related to bilateral test bans between the Soviet Union and the U.S. Global monitoring is of practical interest for the cooperative system of the Group of Scientific Experts (GSE), at the UN Disarmament Conference in Geneva (CCD/558, 1977; CD/43, 1979; CD/448, 1984). For the bilateral case it has perhaps also some remote interest for the situation in which a country might test outside its own territory, which is not unusual in nuclear explosion testing. France, for example, has conducted significant nuclear explosion testing programs in both Northern Africa and the South Pacific.

### 2.4.2 Objectives, Monitoring Functions, and Performance Criteria

The objectives of a seismic monitoring network, which ultimately have to be established from political, military, and other non-technical considerations, have been discussed to some extent by the GSE, but usually only in rather general terms. For example, it has been suggested that the purposes of an international cooperative network would be: *(a)* to deter from clandestine testing, *(b)* to provide confidence that treaty obligations are observed, and *(c)* to counteract suspicions about natural seismic events (GSE/Canada-Sweden/1/1987). Since there are no precise network or seismic station specifications that have widespread acceptance, we use here theoretical concepts for the definition of seismological monitoring functions and performance criteria. This approach attempts to maximize the capability to detect underground explosions and to minimize the risk of mistaking detected earthquakes for explosions (Ericsson, 1970). As an additional condition unexplained or unassociated data collected by the station network should be minimized. This would satisfy the three purposes listed above for an international cooperative system. More specifically, the stations should be selected so that the following *six seismological monitoring functions* are optimized:

*1. Detection of explosions;* For simplicity it is assumed that explosions are fully decoupled and carried out in hard rock. Evasion schemes based on decoupling appear to have been the most important factor in determining number and types of stations of "internal" networks (Hannon, 1983). Counter-evasion capabilities for this and other evasion schemes can be included if the number and types of stations and their geographical distribution are tailored to each specific case.

*2. Location of explosions;* It is important to minimize the area that has to be analyzed with non-seismological "national technical means (NTM)". Precise locations are also important for events that are located close to national borders.

*3. Depth estimation of explosions;* It is sufficient to establish that the depth is shallower than a certain value, say 20 km. The network should be designed so that it can be established with high probability that detected and located

explosions have shallow depths. However, the point estimate of the depth is less important. The depth estimate has to be based on first arrival times.

4. *Association of station detections;* This function is usually not considered in network assessments. A large percentage (50% or more) of signal detections at stations of existing global networks is often not associated to any seismic event.

5. *Depth estimation of deep earthquakes;* The depth has to be established so that a possible explosion can be ruled out with confidence. Depth estimates can be based on first arrival times or on surface reflected phases, pP and sP.

6. *Detection of surface waves of shallow earthquakes;* Surface wave data are used to identify shallow earthquakes by the $m_b(M_s)$ method.

The seismological functions that identify earthquakes (5 and 6 above) and that associate station detections (4 above), serve to counteract suspicions about national seismic events (c above), whereas the detection and location of explosions (1 and 2 above), and the establishing of shallow depth of explosions (3 above), serve to deter from clandestine testing (a, above). And, all functions (1-6 above) serve together to provide confidence that treaty obligations are observed (b, above).

It is difficult to anticipate exactly which evasion technique a potential violator would use, and the list above does not explicitly include any function that positively identifies explosions. They could be identified *directly* with the $m_b(M_s)$ method provided surface waves are recorded or *indirectly* by negative evidence on the basis of absence of surface waves (Elvers, 1974). It should be noted that according to the list above it is in principle not necessary to optimize the capabilities to detect, locate, and estimate depth of *shallow* earthquakes since we assume that they can largely be ruled out as being explosions from the $m_b(M_s)$ data.

The functions above require different kinds of information from the seismic recordings. A network designed to optimize only one function may therefore not necessarily perform in an optimum manner for another. Because of this tradeoff, one may have to strike a *balance* among the functions, and aim at a minimum gap between the detection threshold and other functions. If an event is detected it should also be located with sufficient accuracy and data should be available to identify the event with sufficient confidence. One of the functions above, detection of surface waves, can however be optimized independently of the others, provided long-period stations are not necessarily co-located with the short-period stations.

For an international cooperative system it seems natural to require that the capabilities be *uniform* geographically, with little variation between regions. Since nuclear weapons testing has been conducted on remote islands in the oceans, the whole world should be included in the "target" area for the monitoring system. The

overall level of a station network is difficult to specify, since different countries may have different monitoring requirements. It can be noted that the GSE has been discussing a global system, with no explicit assumption or agreement on performance level. It has been implicitly assumed that the system should consist of existing and planned seismological facilities. In the early years of detection seismology it was suggested that a seismic monitoring system should not be too sensitive, since it would give rise to many false alarm reactions to earthquakes (Dyson, 1984). It is obvious that an international system of the GSE type must, in a treaty situation, be *superior to other public systems* with regard to detection, location and identification, otherwise confusion or unnecessary suspicion could make the system counterproductive to its purposes and it would become politically unworkable. It is therefore important to take full advantage of the technology developed in recent decades, specifically for explosion detection. For the purpose of this study we consider monitoring of events with magnitude greater than $m_b$=4.0, based on observations primarily in the *teleseismic* distance range. This is a level of sensitivity that has been widely used for research purposes, but it is not necessarily the lowest limit that can be achieved by a global network. At least theoretically, significantly lower *detection* levels can be obtained by deploying a sufficient number of stations. Neither is the $m_b$=4.0 range the lowest limit that has been considered for monitoring by seismological means. Much lower thresholds have been discussed for internal station networks in the Soviet Union or the U.S. Just as for event detection, there are no widely agreed numbers on desirable location accuracies or capabilities of depth determination, let alone on identification capabilities.

### 2.4.3 Procedures and Algorithms for Station Selection

For simplicity the explosion detection capability of a station network is usually described in terms of the magnitude thresholds ($m_{bT}$) at a certain probability, $p$, which is often chosen to be 90%. The magnitude values can be converted into equivalent explosions yields, including yields under assumptions of specific decoupling conditions. It is required that signals be detected at a minimum number of stations (usually four single stations or two arrays) for the explosion to be located. For a given station network, the detection threshold becomes a function of the geographical coordinates ($\Phi$,$\Lambda$) of the target area $A_t$, *i.e.*, $m_{bT}=m_{bT}(\Phi,\Lambda\,|p)$. The station selection could then aim at achieving a minimum average threshold, $m_{b0}$, i.e.:

$$\overline{m}_{bT}=\int_{A_t} m_{bT}(\Phi,\Lambda)\,d\Phi\,d\Lambda \Big/ \int_{A_t} d\Phi\,d\Lambda \leq m_{b0}$$

with a uniform capability, as described for example by a maximum variance of the threshold, $\sigma_0^2$:

$$\sigma^2(m_{bT}) = \int_{A_t} (m_{bT}(\Phi,\Lambda) - \bar{m}_{bT})^2 d\Phi d\Lambda \Big/ \int_{A_t} d\Phi d\Lambda \leq \sigma_0^2$$

Station selection could, however, also be based on obtaining at least a certain minimum threshold, $m_{b0}$, throughout the target area, $A_t$, *i.e.*:

$$\max_{\Phi,\Lambda} \left\{ m_{bT}(\Phi,\Lambda); (\Phi,\Lambda) \in A_t \right\} \leq m_{b0}$$

This means that in some parts of $A_t$ the threshold could be significantly below $m_{b0}$, whereas in other parts it could be significantly higher but still not greater than $m_{b0}$. Measures like $\bar{m}_{bT}$ and $\sigma(m_{bT})$ can also be specified for the other monitoring functions: association of station detections, epicenter location, depth determination, and surface wave detection (Israelsson, 1987). The criteria for each such function with its measure $\mu_i$, can be formulated as an inequality:

$$\mu_i \leq c_i$$

where the parameter value $c_i$ represents an upper limit of desirable performance for function $i$.

The problem of designing a network then consists of determining sites and types (e.g., single station or array) for seismic stations (preferably with a minimum number) in a given siting area, so that these inequalities are satisfied. A variant of this problem is to select the sites for a *given number* of stations so that optimum capabililties are obtained (i.e., minimize the $\mu_i$). In this case, a certain desired performance may, of course, not be achieved. This way of looking at the network design problem is, however, not uncommon. For example, in the discussions of internal station networks in the Soviet Union and the U.S., the number of stations and their *negotiability* are both important parameters (Hannon, 1983). And the GSE is considering a network of "50 stations or more" for its cooperative system.

Intuitively, it appears that there *may in most instances* not exist any practicable network that would satisfy given values for the measures $\mu_i$, i.e., if we required strict equalities $\mu_i = c_i$. It is at least theoretically possible to satisfy the inequalities (i.e., $\mu_i \leq c_i$) with a sufficient number of stations, except perhaps for the association of station detections (we would like to minimize the number of unassociated station detections). In other words, for a given set of $c_i$ values we can at least in principle always find one network by, for example, siting a sufficiently large number of stations with equal spacing across the siting area and verify by calculations that the inequalities are satisfied. This means that the station selection problem is essentially reduced to finding the dependence of the measures $\mu_i$ on the number of stations and their detection characteristics, and on the network geometry. The presentation in

the following sections will mainly deal with such dependences.

In practice there will of course be limitations on the number of stations and/or the number of sites where stations can be deployed. With a finite number of specified sites that can be selected for stations, say $N$, and with $n$ stations to be sited, one can calculate the measures $\mu_i$ for each possible station siting and systematically go through all combinations of stations and sites. Although the computational time for this approach is in principle polynomial in the number of sites ($\binom{N}{n}$ combinations, which is less than $N^n$) the computer time becomes intractable for large numbers of sites and stations (like $N=1000$ and $n=100$). However, if we look at a situation where we want to add a small number of stations (one or two) to a given network, the computer times become more tractable.

There are also techniques of partial searches that can be used in finding the coordinates for all the stations of a network. For example, the method of detection by optimization has been used to select optimum station distributions for epicenter determinations (Savarenskiy *et al*, 1979). The station coordinates are obtained by successive selections, starting with two stations, among a limited set of possible sites ($N$). Initially, the coordinates of these two stations are chosen arbitrarily and the coordinates of a third station are chosen so that the measure $\mu_i$ (e.g., estimated area of location error) is minimized. As the next step of this procedure the coordinates of the first and the second station are chosen again in a similar way for one station at a time so that measure $\mu_i$ is minimized. Finally, the coordinates of the third station are chosen again with the coordinates for the two other stations fixed. When the coordinates for the three stations have been selected, a fourth station is added and the coordinates for all stations are revised in a way similar to that for the first three stations. When the iteration is completed for four stations, one station is added at a time until $n$ stations have been included. The measure $\mu_i$ has to be calculated for $(k+1)\cdot N$ networks in the step of adding station $k$, and the total number of calculations of $\mu_i$ becomes: $N\cdot(n\cdot\frac{(n+1)}{2}-7)$. Finally, simple symmetry considerations can be used as a method to find the coordinates for stations of networks for uniform capabilities. If the stations are uniformly distributed geographically the network will also have capabilities with uniform geographical coordinates.

### 2.4.4 Detection

As mentioned above, it is theoretically possible to obtain any desirable detection capability by deploying a large enough number of stations. In order to outline the detection capability as a function of number of stations we look at hypothetical networks with equal spacing on a sphere. Although the problem of finding the coordinates for the stations so that they become equally distributed on a sphere has so far no general *analytical* solution, there are many analogies to this problem in the

mathematical literature (e.g., finding the locations of a given number of equal electrical point charges free to move over the surface of a sphere). Short of analytical solutions, the problem can at least in principle be solved by straightforward (although sometimes extensive) numerical and combinatorial computations. We will use either analytical or numerical solutions for small values ( $n \leq 20$ ) available in the literature in the computational examples here. For $n>20$, networks with only approximately uniform station distributions will be used. These approximate networks have stations with equal spacing in latitude and longitude together with stations on the poles. For spacings 30°, 36°, and 45°, they consist of 62, 52, and 26 stations, respectively. Although the station spacing for these approximate networks is variable with latitude, this turns out to have a small effect on the overall detection thresholds.

The calculations here assume that P-wave (or PKP) detections (with signal-to-noise ratio >1.5) at four or more stations are required for event detection by the network. It is also required that at least one of the detecting stations be at an epicentral distance less than 100°. The stations are assumed to have equal noise amplitudes (10 nm/s, which is the median value for the stations of the GSETT, i.e., the GSE technical test in 1984). Magnitude thresholds have been computed for a fifteen-degree grid of latitude and longitude (266 coordinates). The map in *Figure 1* shows contours of the 90% detection thresholds for the network with 20 stations. Because of the symmetry of the networks, the stations often have coordinates at or close to the grid points for which thresholds are calculated. *Figure 1* also shows calculated average thresholds, $\overline{m}_{bT}$, with associated error bars (corresponding to one standard deviation, $\sigma_{bT}$) for the networks as a function of number of stations. For $n \geq 20$, the average values have been obtained as weighted means with the cosine of the latitude as a weighting factor. Elimination of coordinates close to stations (i.e., 7-10° ) does not significantly affect the means and standard deviations.

For networks with more than ten stations the average threshold, $\overline{m}_{bT}$, drops as a function of number of stations, $n$, with the derivative $d\overline{m}_{bT}/d\log_{10}(n)$ somewhat faster than -0.5 and for large values of $n$ the data appear to asymptotically approach the -0.5 slope, i.e, $\overline{m}_{bT}=const-½\cdot\log_{10}(n)+\nu$, where $\nu$ denotes the station noise (on a logarithmic scale) which is assumed to be equal among the stations. If we assume that each station is upgraded to an array with $k$ elements, all of which have the same noise value $\nu$, and that array processing gives a noise reduction proportional to the square root of number of elements, (i.e., $\nu=\nu(1)-½\cdot\log_{10}(k)$), we get the average network threshold :

$$\overline{m}_{bT}=const-½\cdot\log_{10}(n\cdot k)+\nu$$

Here the product $n.k$ is the total number of seismometers of array network of $n$ arrays with $k$ elements. This means when this product is large the individual seismometers are distributed on arrays. For example, 25 arrays with 20 elements

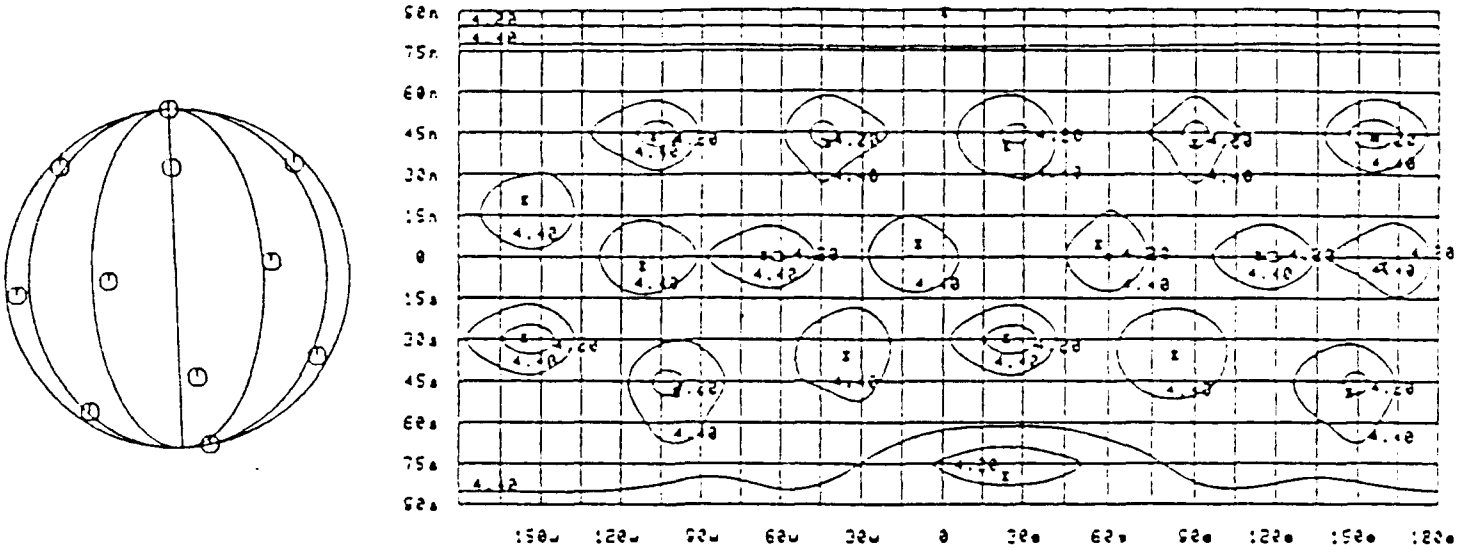

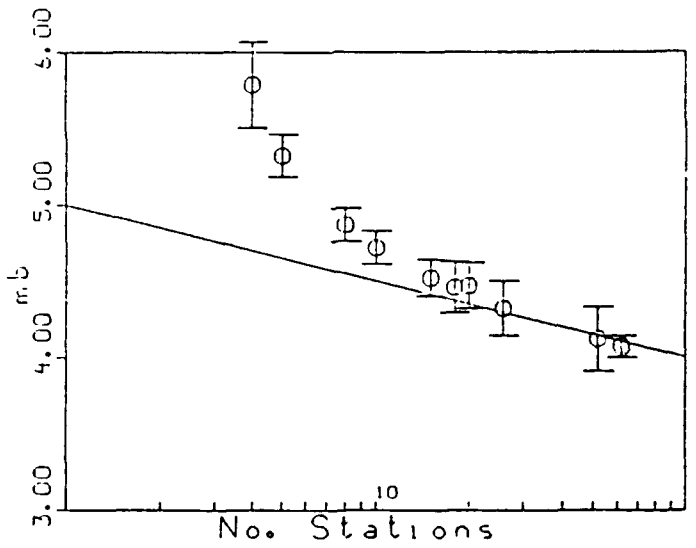


*Figure 1.* The sphere shows the locations of a network with 20 equally spaced stations. The map shows the contours of the magnitude ( $m_b$) detection threshold (90%) for the 20 station network. The station locations are marked by asterisks. The diagram shows the average magnitude threshold as a function of number of stations for networks with equal spacing on a sphere. The error bars represent the standard deviation of the thresholds calculated every 15° latitude and longitude. The line has a slope of -0.5 corresponding to a reduction of the threshold inversely proportional to the square root of the number of stations.

each (total of 500 elements) would perform the same as a network of 500 single stations. However, with a smaller number of total stations/elements (on the order of 50) it is possible to find array sensor combinations that provide a minimum detection threshold (Israelsson, 1986a). It should also be pointed out that these comparisons of single station vs. array station networks are based on the $\sqrt{k}$ gain, which often cannot be achieved, for example, for regional arrays.

According to the data in *Figure 1* the sharpest reduction in detection threshold occurs for $n<10$. If we want to significantly improve a station network that consists of about 10 stations, a fairly large number of additional stations (with similar detection characteristics) are required. For example, a reduction by half a magnitude unit would require approximately 90 additional stations. It may be easier to reduce the network threshold by improving the *available* stations, rather than adding new stations. If the noise can be reduced at all available stations by a factor of three (e.g., by an improved installation in a borehole) the threshold would also go down approximately half a magnitude unit for a ten-station network.

In the examples above it was assumed that all stations had the same noise amplitudes. However, the detection threshold of seismic stations varies considerably and is determined by several factors including local seismic noise, type of station, local geology, as well as tectonic structure. *Table 1* summarizes mean values of short-period noise amplitudes by tectonic region for three global networks consisting of 60 (GSETT), 115 (Ringdal, 1986), and 500 (Ringdal *et al.*, 1977) stations, respectively. The mean values are consistently lowest for shield and platform stations. Since the noise amplitudes have been obtained in somewhat different manners for the three networks, direct comparisons between station averages of regions that belong to *different* studies have to made with some care, whereas comparisons between regional averages *within* a study can be made more easily. It should be noted that the detection threshold can be very sensisitve to the local geology at the station site. In a study of about 30 stations in North America, Evernden and Clark (1970) found the effect of local geology to be more pronounced than that of tectonic regions. Here we assume that the large number of stations (at least for the Ringdal *et al*, 1977, study) sample a variety of local geology and effects other than tectonic region so that the average values are representative of tectonic region. Seismic stations located on shields and platforms may not only have lower event detection thresholds than those for stations located in tectonic regions. The simplicity of shield and platform structures also frequently results in comparatively simple recorded seismic signals. This facilitates, for example, identification of depth phases and waveform analysis, which has become an important new element of the upgraded GSE-system. Shield and platform areas where seismic stations have been or are located are marked in *Figure 2*, which is based on a station list including about 4000 stations compiled at the Center for Seismic Studies (This list is primarily based on compilations by the USGS (USGS, 1985)). There are 58 and 75 segments (five by

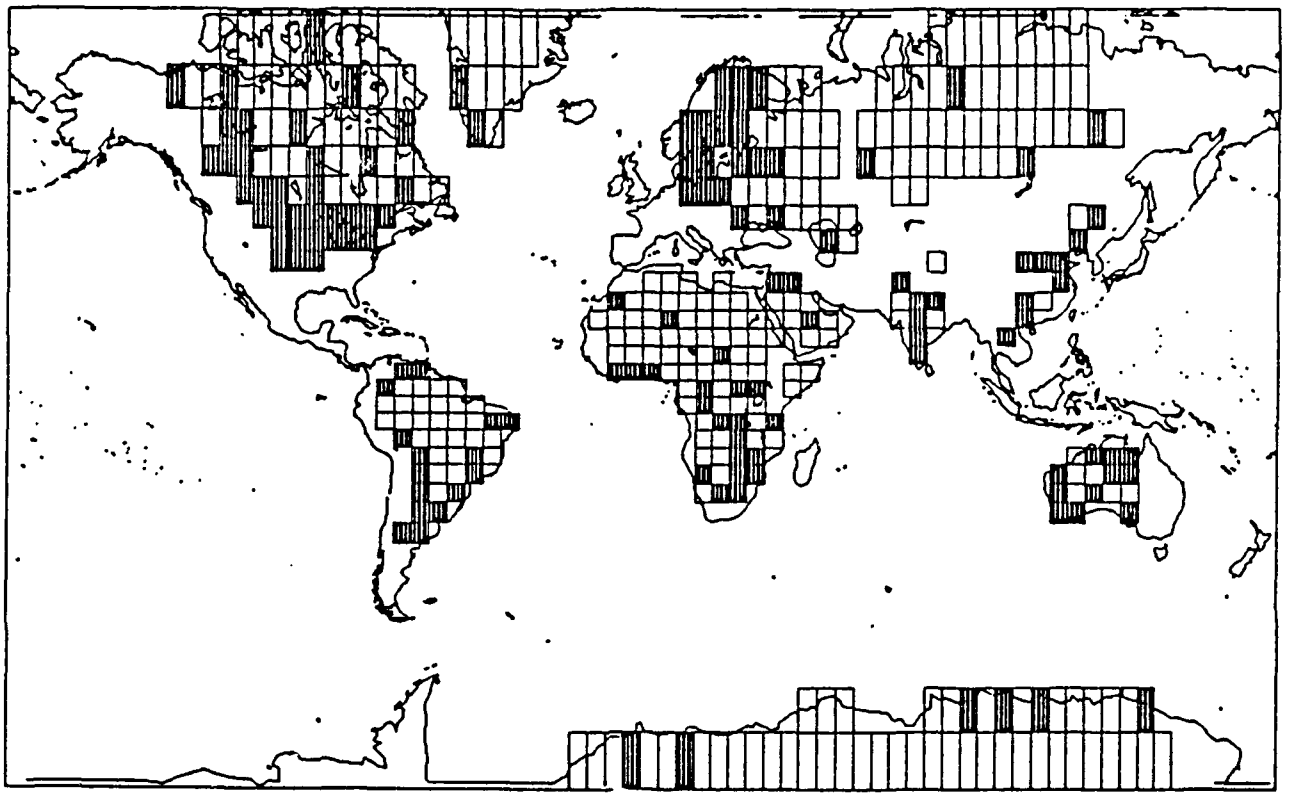

*Figure 2.* The map shows the shield and platform segments on which one or more stations are or have been operating (indicated as filled rectangles; unfilled rectangles are on shield platform but have no stations). The shield and platform segments are in accordance with the tectonic regionalization by Jordan (1980).

**TABLE I.**

| Tectonic Region | Ringdal (1977) No | Mean (nm) | SD (log) | Ringdal (1986) No | Mean (nm) | SD (log) | GSETT No | Mean (nm) | SD (log) |
|---|---|---|---|---|---|---|---|---|---|
| Young Ocean | 3 | 69.7 | 0.25 | | | | | | |
| Intermediate Ocean | 49 | 46.6 | 0.40 | 4 | 23.7 | 0.25 | 3 | 21.5 | 0.46 |
| Old Ocean | 10 | 46.6 | 0.42 | 2 | 23.7 | | | | |
| Orogenic | 345 | 32.6 | 0.39 | 66 | 12.7 | 0.23 | 37 | 10.4 | 0.43 |
| Platform | 49 | 15.0 | 0.42 | 19 | 7.7 | 0.19 | 5 | 9.6 | 0.29 |
| Shield | 45 | 10.5 | 0.58 | 24 | 10.1 | 0.23 | 15 | 6.6 | 0.48 |

five degrees in latitude and logitude according to regionalization by Jordan, 1980) with one or more stations for shield and platform regions, respectively. In all, this gives 133 segments with one or more stations out of a total of 510 possible segments. This number can be compared with the number (20) of shield and platform stations that participated in the GSETT.

Calculations of event detection capabilities were made for several hypothetical networks including one consisting of 133 stations located at the segments where seismic stations are or have been in operation. For the sake of comparison, calculations were also made for networks with 25 - 175 stations more uniformly distributed over the shield and platform areas, and for a hypothetical version (equal station noise) of the GSETT network (total of 69 stations) and the GSE concept network (GSE/US/44, 1987). The latter consists of 50 stations, eight of which have arrays. The same station parameters were used for all networks (the only exceptions were the eight array stations of the concept network, which were given a short-period noise amplitude of 2 nm instead of 10 nm). The calculations assumed only teleseismic observations within 100° , i.e., secondary regional phases ($S_n$, $L_g$, etc.), which are particularly important for depth estimation, or PKP phases were not included.

Examples of calculated detection thresholds ($m_{bT}$ for the whole world) for these networks are summarized in *Figure 3*. The figure suggests that there is a fairly large geographical variation of the threshold, and there is no significant lowering of the world average threshold by increasing the number of stations beyond ≈75 for shield/platform networks. The GSE concept network has a fairly small range of variation ($m_b$ 4.4-4.6), as would be expected from its uniform station distribution. The GSETT network has a much larger range of variation, primarily because of the concentration of stations in Europe. The GSETT network also has lower maximum threshold than that of 75 shield/platform stations, owing to some oceanic stations. Even if the shield and platform networks have non-uniform detection capabilities on a global scale, reasonably uniform capabilities can be obtained on the continents, provided a sufficient number of stations are available.

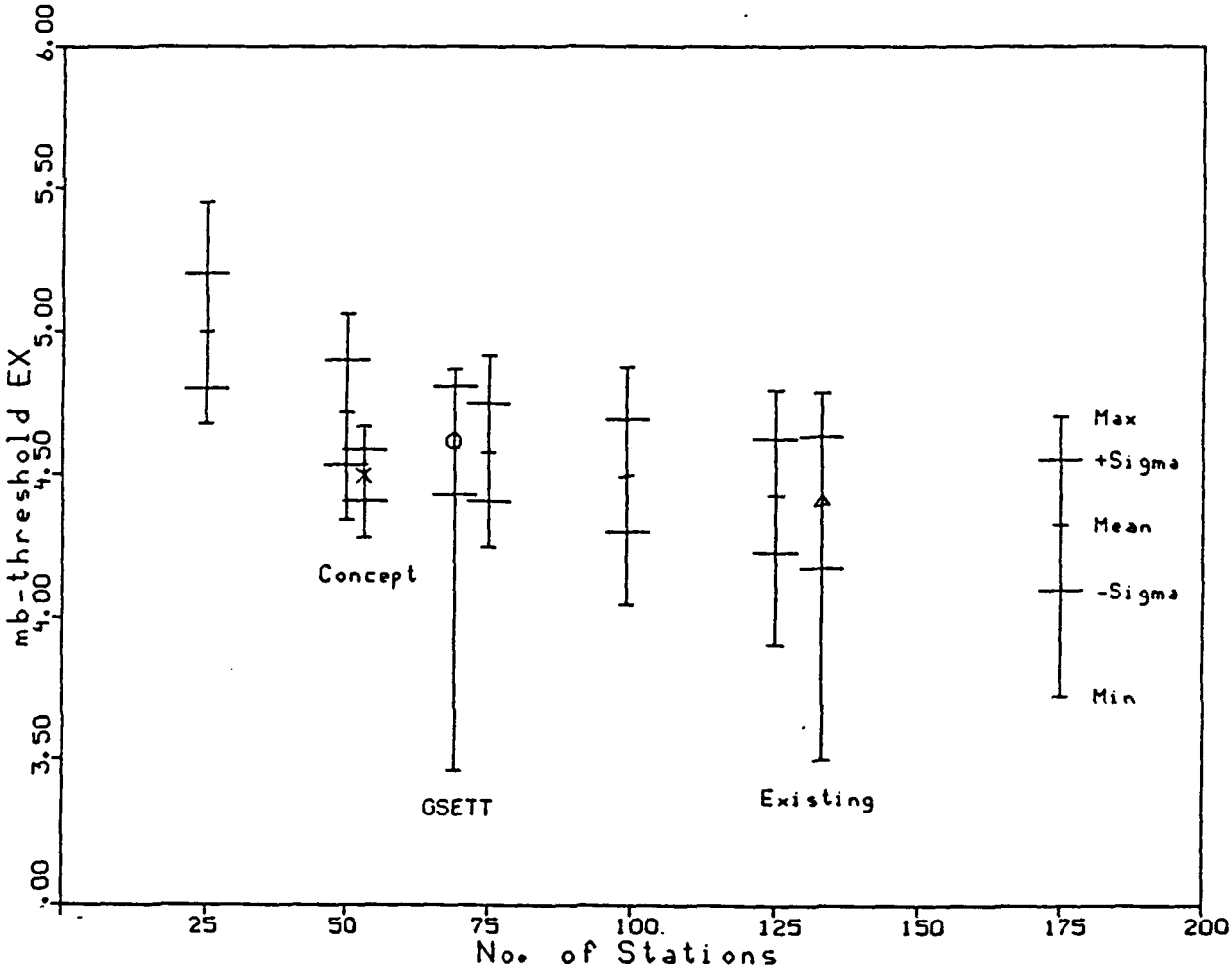


*Figure 3.* Detection threshold, $m_{bT}$, as a function of number of stations for shield/platform networks. Detection of P signals at four or more stations within 100° is used as event detection criterion. The diagram shows the mean, range of variation (minimum and maximum) and standard deviations for each network, as indicated for the 175-station network to the far right of the diagram. Results are also included for the GSE concept, the GSETT networks and a hypothetical 133-station network of existing stations as marked in the figure. The GSE concept network, which includes 50 stations, has been displayed slightly to the right for the sake of clarity.

### 2.4.5 Association of Station Detections

Because of the large variation in station sensitivity and non-uniform geographical station distribution of existing global networks, a large number of recorded signal detections cannot be associated with any seismic event that is detected and located by the networks. Many of these unassociated station detections are local or regional signals, or weak teleseismic signals at isolated sensitive stations. There can, of course, also be false alarm detections at the stations caused by noise triggering. It seems to be difficult to eliminate this problem completely, since there is always the possibility that a small event occurs so close to a station that it cannot be detected at other stations. A likely area for the epicenter of such an event may of course in some instances be mapped. Let us assume, for example, that we have an unassociated detection at station $i$, and that the signals originate from an event with magnitude $m_b$ at coordinates $\Phi,\Lambda$. We can then calculate the maximum likelihood value of the magnitude $\hat{m}_b$, in the usual manner and the likelihood value $L$ that the signals of an event with magnitude $\hat{m}_b$ at coordinates $\Phi,\Lambda$ are detected only at station $i$. Both the likelihood function $L=L(\Phi,\Lambda)$ and magnitude $\hat{m}_b=\hat{m}_b(\Phi,\Lambda)$ can be mapped. Even if such maps to some extent provide information on the origin of the unassociated signals and in a way are confidence areas and intervals for location and magnitude of the event, it is important in the network design process to minimize the number of such unassociated station detections for $m_b$ larger than some design threshold.

A similar approach can also be used to check that a network which, for example, maximizes the detection capability is also balanced geographically with regard to *association* of station detections. If we make assumptions about the magnitude recurrence relationship, we can for a given station calculate the percentages of unassociated detections as a function of geographical coordinates (Israelsson, 1986b). This is illustrated in *Figure 4* for the stations ASPA and SUF of the GSETT network. ASPA with a high detection capability in the southern hemisphere is likely to have most of its unassociated detections caused by earthquakes in the southern hemisphere, since the GSETT network as a whole has a low detection capability there compared to the northern hemisphere. The situation is reversed for the station SUF in the northern hemisphere, which also has a significantly lower percentage of unassocited detections, in general.

The simplest and most effective way to minimize the difficulty with unassociated arrivals of a network is to deploy array stations to the maximum extent possible. Usually detections (slowness and azimuth) at only two arrays are considered sufficient to locate an event, whereas detections at four stations are required for a network of single stations. For a single station network, the detections at only two or three stations will thus contribute to the unassociated data. Furthermore, the rough estimate of event epicenters provided by unassociated detections at one array may in many cases be sufficient from the point of view of monitoring.

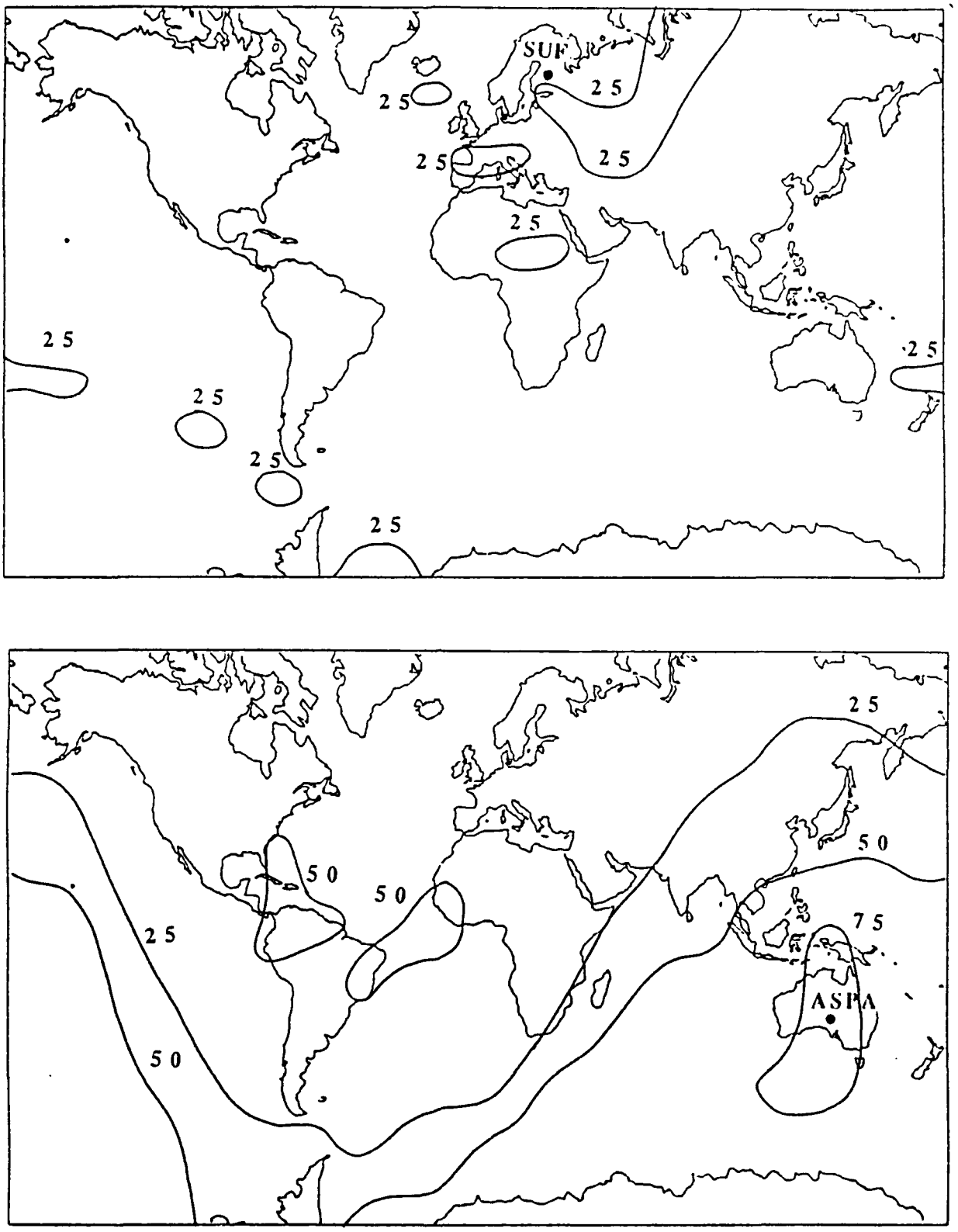


*Figure 4.* Calculated percentages of unassociated detections at station SUF (top) and ASPA (bottom) of the GSETT network as a function of geographical location of the events. An exponential distribution of the magnitudes with *b* - value of 0.9 is assumed. The results are presented as contour lines of 25, 50, and 75%.

### 2.4.6 Location Of Explosions

The quality of an epicenter estimate depends on several factors, one of which is the geometry of the detecting stations in relation to the epicenter. A symmetrical distribution of the stations around the azimuth from the event is always desirable, but this is often not possible to achieve in practice. Estimation of the epicenter (latitude and longitude) of an event is part of a procedure which also gives estimates of origin time and focal depth. Since we are mainly concerned with the location capability for explosions, i.e., events with surface focus, we limit ourselves to analyzing the joint marginal confidence region for the estimated epicenter (Flinn, 1965).

We introduce a Cartesian coordinate system, $\mathbf{X}=(x_1,x_2)$, with origin at the true epicenter. The epicenter determination is assumed to be based on first-arrival-time readings at $n$ stations, which are located at distances $\Delta_k$ and azimuths $\phi_k$ from the epicenter. The arrival-time residuals or data errors are assumed to be normally distributed and are characterized by an *a priori* standard deviation, $\sigma$. These data errors include reading errors at the stations as well as uncertainties of the traveltime model. Standard error is usually dominated by uncertainties in the traveltime model, and it is assumed here that all observations have the same $\sigma$. The joint marginal confidence region for the estimated epicenter is given by

$$\sigma^{-2}\cdot\mathbf{X}^T\cdot\mathbf{S}\cdot\mathbf{X}\leq\chi_2^p(2)$$

Here $\chi_2^p(2)$ denotes the $p$ - percentile of a Chi-square distribution with two degrees of freedom. The elements of the symmetrical covariance matrix $\mathbf{S}$ are determined by the relative locations of the $n$ detecting stations as described by their azimuths from the source ( $\phi_k;k=1,2,...,n$ ) and their slowness values ( $p(\Delta_k)$):

$$S_{11}=\sum p(\Delta_k)^2\cdot\cos^2(\phi_k)$$

$$S_{22}=\sum p(\Delta_k)^2\cdot\sin^2(\phi_k)$$

$$S_{12}=\sum p(\Delta_k)^2\cdot\cos(\phi_k)\cdot\sin(\phi_k)$$

In order to simplify the expressions above for the elements of the matrix $\mathbf{S}$ it is assumed that the epicenter is at the north pole and station coordinates are transformed accordingly. The confidence region is an ellipse, and the orientation and the lengths of its axes are thus determined by the elements of the matrix $\mathbf{S}$. It can be shown that the area of the confidence ellipse (i.e., $\pi$ times the lengths of the major and minor axes) is inversely proportional to the determinant of the matrix $\mathbf{S}$:

$$\pi \cdot \chi^2_2(2) \cdot \sigma^2 / (S_{11} \cdot S_{22} - S_{12}^2)$$

This formula is 180° symmetric with regard to the azimuthal station distribution: if a station is moved 180° around the source azimuth the location error will still be the same. This means that a 360° coverage of stations around the source azimuth will not give a smaller location error than a coverage of 180°. This conclusion is based on the particular assumptions about the model used here; in practice, due to lateral variation of the velocity in the source region *systematic* azimuthal bias may be introduced with stations in only a 180° sector around the source.

In order to study the effect of distance and azimuth coverage on location errors the location errors have been calculated for some hypothetical networks (Israelsson, 1986a), which are distributed along one or more circular arcs around the epicenter at various epicentral distances, i.e., $P(\Delta_k)=P$ for stations on a given arc at distance $\Delta_k$. For networks with stations on only one arc the area of the error ellipse simplifies to the formula:

$$\pi \cdot \chi^2_2(2) \cdot \sigma^2 \, |\mathbf{S}'| / P^2$$

here the elements of the matrix $\mathbf{S}'$ do not contain the slowness values. We note that the area of the confidence ellipse is inversely proportional to the slowness value and directly proportional to the *a priori* standard deviation. In *Figure 5* the relative location error is shown as a function of azimuthal coverage for a stochastic model with "uniform" distribution of the stations around the azimuth. The details of this model are included in the Appendix. The curve indicates that the error decreases rapidly with increasing coverage and a coverage of about 90° gives an error only ≈20% larger than that with a complete coverage of 180°.

Because of the sensitivity to bias effects of the traveltime model as described by the direct proportionality of the location error (square root of area) on the data error, $\sigma$, location errors are often quite large. If corrections for bias can be made (i.e., reducing $\sigma$) the location errors will be reduced by as much as a factor of ten or so. This has been demonstrated by the "joint hypocenter" ("master event") technique in a number of studies. This technique has, however, not been employed in a routine and systematic manner by agencies and services that are processing global teleseismic data. It has been proposed by Bolt (1973) that a suitable set of globally distributed master events with well-known locations be identified so that such techniques can be utilized in a systematic manner on a broad global scale. The definition of such a set of master events appears to be one important task as part of the selection of stations for a global monitoring network.

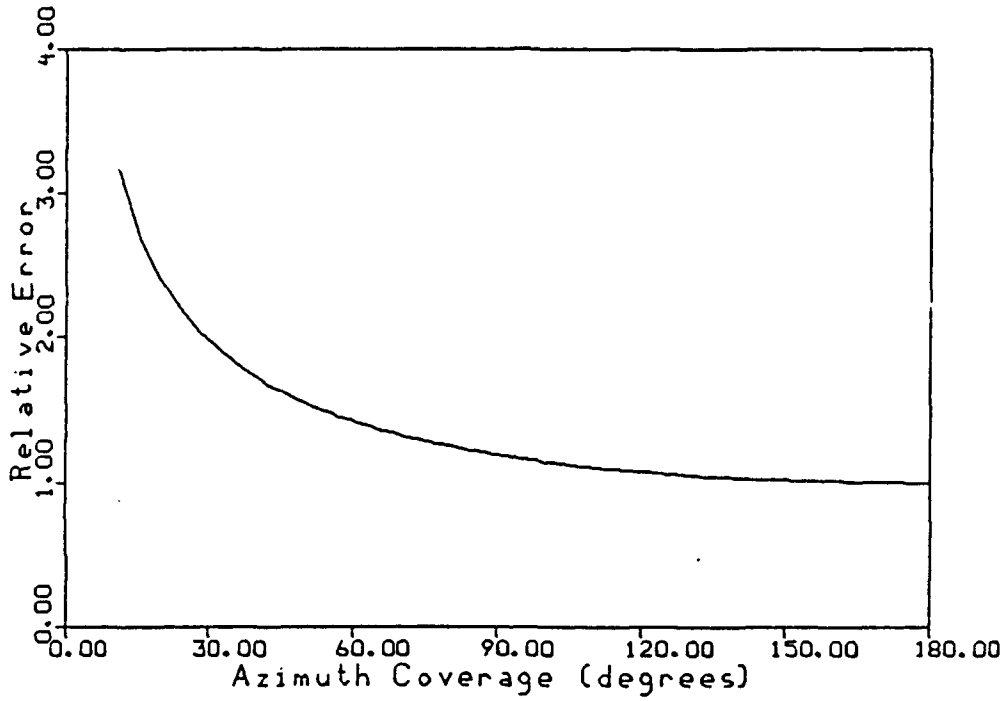


*Figure 5.* The curve shows the relative location error (square root of area) as a function of azimuth for a uniform station distribution represented by a stochastic model described in the Appendix.

### 2.4.7 Depth Estimation

Estimates of the depth of explosion sources have to be based on first arrival times, which is also the most commonly used type of data for depth determinations of deep earthquakes. We use a simplified approach to study the accuracy of depth estimates as a function of geographical distribution of stations (Lomnitz, 1977). It is assumed that the epicenter of the event is known and that $n$ stations have observed arrival times, $t_{oi}$, which all have an error with the same standard deviation $\sigma$. Forming the residual, $r_i = t_{oi} - t_{ci}$, between the observed and the calculated arrival times, we get the following relations between the residuals and the adjustments in depth , $dh$, and in origin time, $d\tau$:

$$r_i = d\tau + dh \cdot \left\{ \frac{dt}{dh} \right\}_i$$

This can be regarded as a straightforward linear regression relation and the variance of the estimated $dh$ can be written as:

$$V(dh) = \frac{\sigma^2}{\sum \left( \left\{ \frac{dt}{dh} \right\}_i - \overline{\frac{dt}{dh}} \right)^2}$$

For standard traveltime models the derivative $\frac{dt}{dh}$ is given as a function of epicentral distance $\Delta$ only for a given depth $h$. Examples of this derivative as a function of distance for the Jeffreys-Bullen traveltime model for focal depths at 10, 30, 50, 100, 200 km are shown in *Figure 6*. The curves for depths at 30 km and more are monotonically decreasing with distance with most of the decrease occurring at distances less than 20°. Since the range of variation of $\frac{dt}{dh}$ is limited, the minimum variance of $dh$ is obtained if all the stations are located at the boundaries of the distance interval over which they are distributed. In other words, if there are $n$ stations (assuming $n$ even) that can be located anywhere within the distance interval $\Delta_{min}$ to $\Delta_{max}$, the minimum variance is obtained if half of the stations are located at $\Delta_{min}$ and the other half at $\Delta_{max}$, and the standard deviation of $dh$ becomes:

$$\sigma(dh) = 2 \cdot \frac{\sigma}{\sqrt{n} \cdot (dt/dh(\Delta_{min}) - dt/dh(\Delta_{max}))}$$

This formula is used in the case of networks of four stations, two at each end of the distance interval covered (*Figure 7*). Two of the stations are assumed to be at 80° distance, and the standard deviation is shown as a function of the epicentral distance of the two other stations (minimum distance), for events at 30 and 200 km

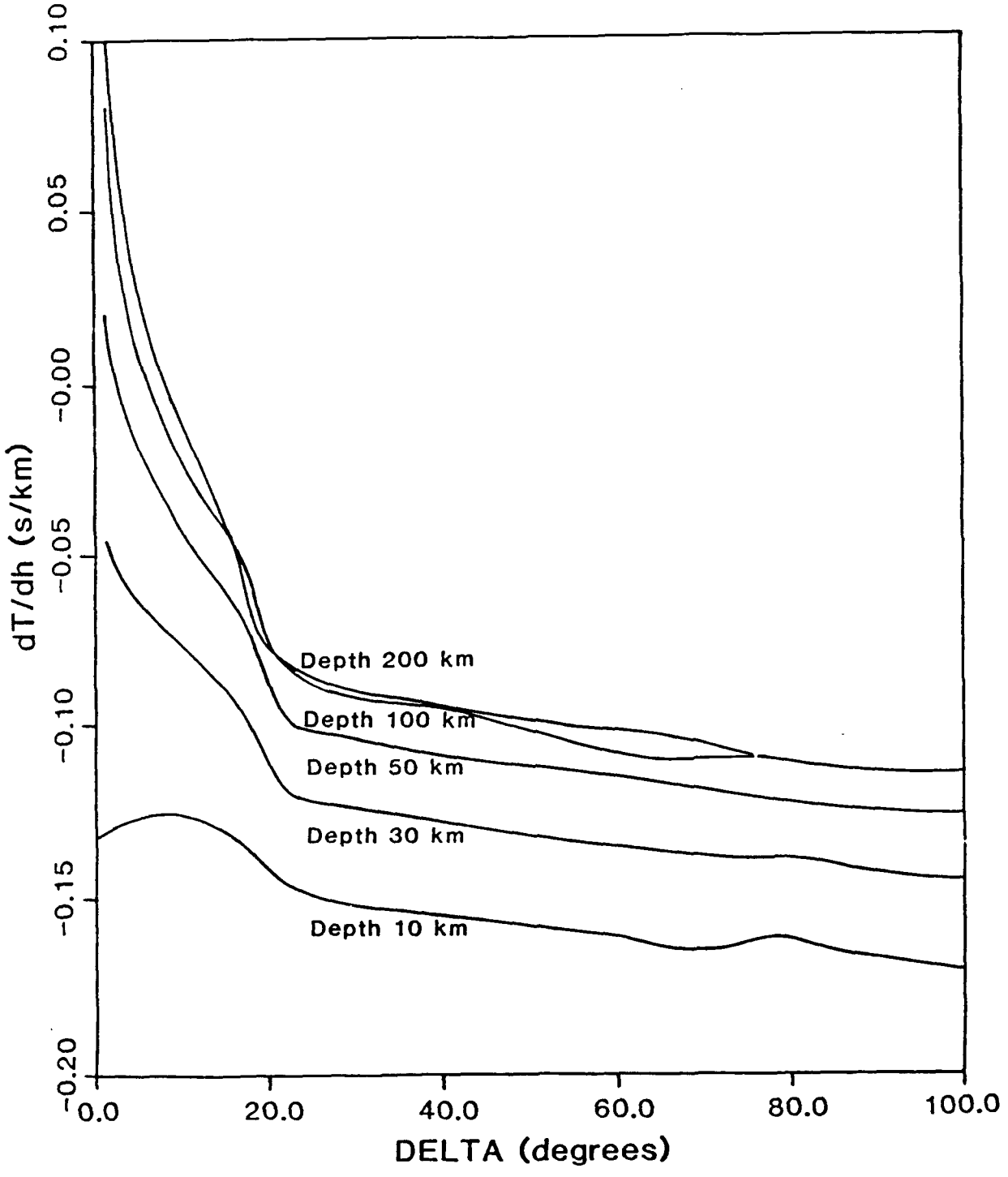


*Figure 6.* Traveltime depth derivative, $dt/dh$, as a function of epicentral distance, derived from the Jeffreys-Bullen *P*-traveltime tables. The curves were obtained through a bicubic two-dimensional spline approximation of the traveltime data and smoothed by hand.

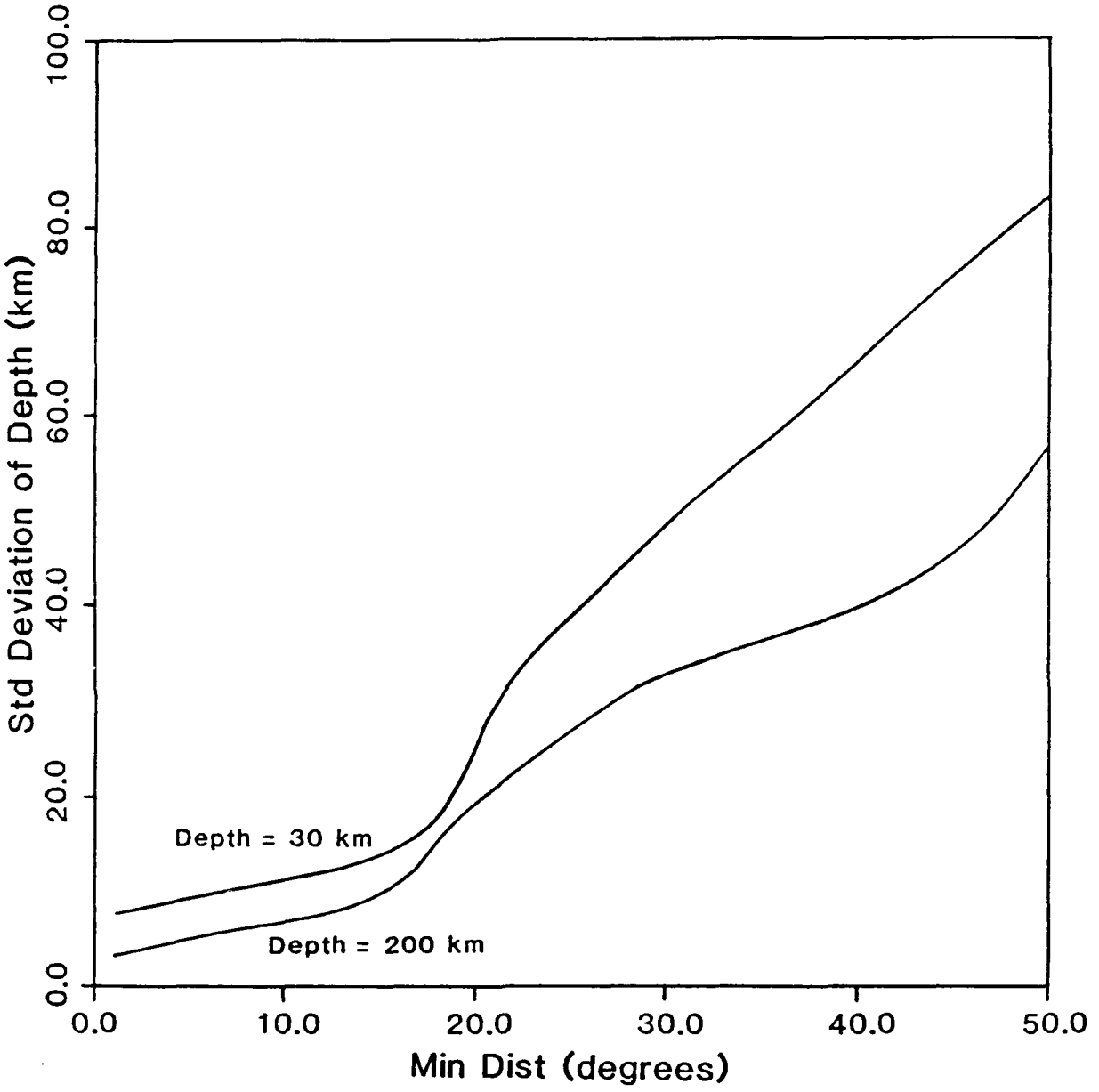


*Figure 7.* Standard deviation of focal depth for events detected by four stations. Two stations are at 80° distance from the epicenter, and the other two are at various distances, as indicated by the horizontal axis of the figure. Note that the standard deviation increases rapidly as this minimum distance increases from 10° to 25°. The curves have been smoothed by hand.

depths. The standard deviation increases significantly as the minimum distance becomes larger than ≈ 15° (factor of four increase from 10° to 30°). degrees. This illustrates the importance of having stations at local or regional distances in a network based primarily on teleseismic detection.

We can ask: What is the probability that stations within, say, 15° do not detect an event and four or more stations at distances beyond 15° do detect the event for any given location. In this case, the standard deviation of the estimated depth will be fairly large. The probability for this to happen is thus denoted $P(\sigma_{large})$ and a low probability is desirable. As an example we look at a network of $n$ stations with fairly equal spacing on a sphere so that the number of stations within $\Delta°$ of the event is: $n(\Delta)=(1-\cos(\Delta))/2\cdot n$. The probability for $\sigma_{large}$ as defined above can be written as:

$$P(\sigma_{large})=P(\xi\geq 4)\cdot P(\eta=0)$$

where $\xi$ and $\eta$ are binomial stochastic variables for the number of detecting stations between 15° and 80° and less than 15°, respectively. The probability curves of *Figure 8* are shown as a function of magnitude, $m_b$, for example networks with $n=75$ to 1000 stations. The curves suggest that a significant reduction of $P(\sigma_{large})$ is only obtained with increasingly large number of stations, several hundred or more for a complete coverage of the globe. If the network is designed with coverage limited to the continents these numbers would, however, be reduced accordingly.

The value of depth phases for reliable estimates of earthquake focal depth is well known. One difficulty with using depth phases is the positive identification of pP or sP. Is has been estimated that the probability that all three phases P, pP, and sP will be prominent is less than 12% for a station in the teleseismic range (Pearce, 1980). Other phases, like PcP (for $\Delta=62-78°$), can also be mistaken for depth phases. A network approach with observations at many stations improves the prospects for correct phase identification. The increased delay of the depth phases after the first arrival with increasing epicentral distance ("stepout") is one criterion for network identification of depth phases. The curves for delay and stepout of pP and sP are approximately linear between 30° and 90°. The total stepouts, i.e., change in delays for pP and sP over the interval 27° - 86°, are 4.5 and 3.2 seconds, respectively, for a depth of 100 km. The problem of positively identifying depth phases is here viewed as the problem of estimating the derivative of the delay ( $\tau$) with epicentral distance ($\Delta$). Epicentral distances to the detecting stations are assumed to be known sufficiently well that estimation of the stepout can be considered as a straightforward linear regression, i.e., estimation of $d\tau/d\Delta$ and test of the compatibility of the estimate with one of the depth phases. Here we discuss the distribution of stations relative to a given epicenter in order to estimate the minimum variance of the stepout from teleseismic observations. Assuming $n$ detecting stations at epicentral

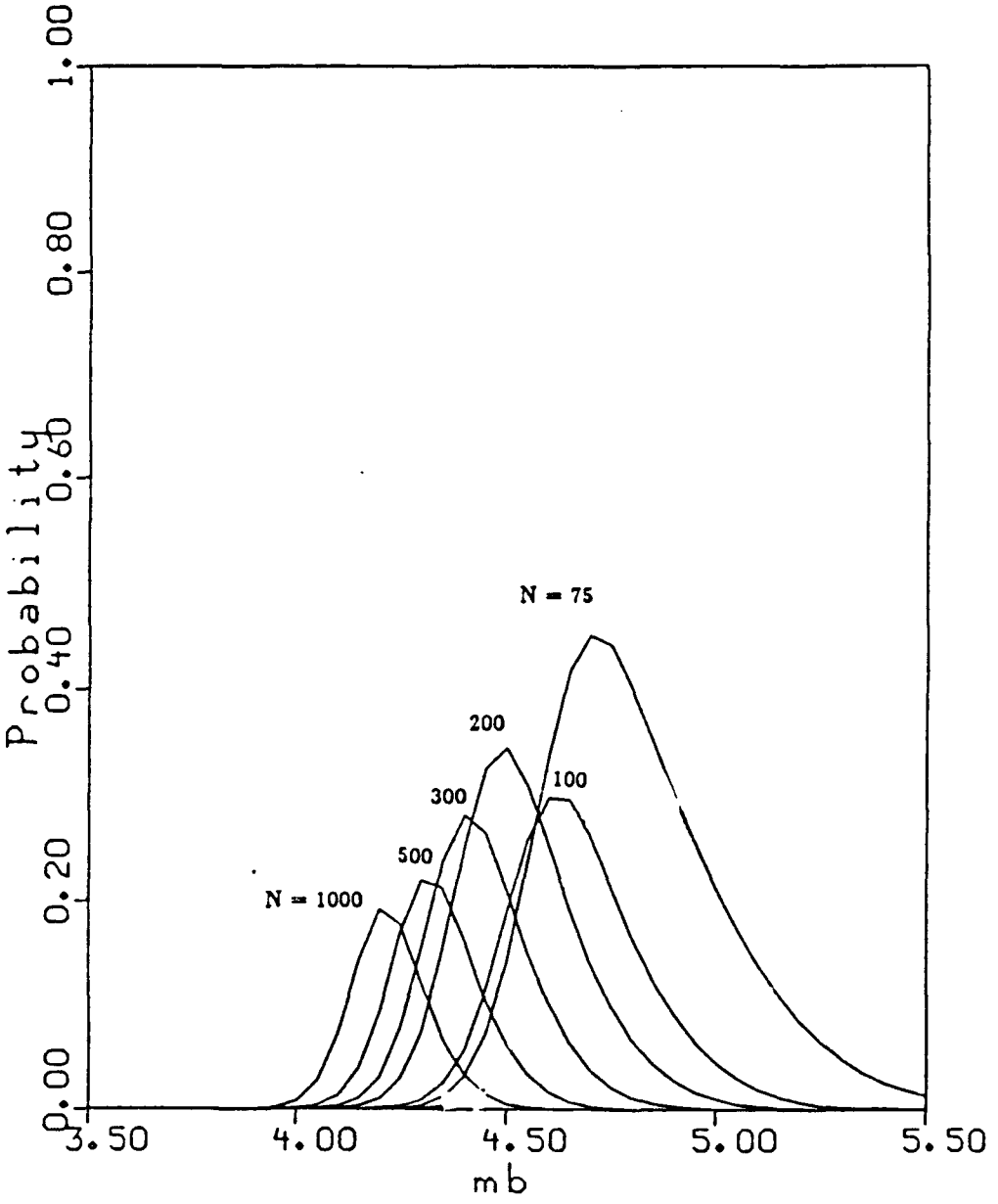


*Figure 8.* The diagram shows the probability that no station within 15° from the event epicenter detects an event, and four or more stations between 15° and 80° detect the event. The probability is shown as a function of event magnitude and for ideal networks with equal spacing, as defined in the text. It is assumed that the station detection thresholds are 4.72 and 5.0 (at 50%) for stations at distances less than 15° and between 15° and 80°, respectively. The standard deviation of the stations thresholds were given the value of 0.4.

distances $\Delta_i$ with independently measured delays (with standard error $\sigma$), the variance of the estimated derivative becomes:

$$V(d\tau/d\Delta)=\frac{\sigma^2}{\sum_{i=1}^{n}(\Delta_i-\bar{\Delta})^2}$$

where $\Delta_i$ belong to the admissible distance interval for pP.

The larger the variance of the epicentral distribution of the stations, the smaller the variance of the estimated stepout. The above formula for maximizing the variance of the station distribution assumes that detection probabilities are similar among the stations, but it can be generalized to account for variations. The task of selecting a network of $n$ stations with optimum capability of measuring depth phases can be reduced to the problem of choosing the coordinates of the stations so that the variance of the stepout of events in a given region is minimized. The detection by optimization algorithm outlined above has been applied to a hypothetical case for the sake of illustration, the results of which are shown in *Figure 9*. Ten U.S. station sites are required to be selected so that the capability to measure depth phases is optimized (i.e., minimum variance of stepout) with regard to events in the Kamchatka region. The sites could be chosen among 52 possible locations shown on the map in *Figure 9*. The selected sites are indicated by asterisks.

Regular reporting and analysis of waveform data will be one of the most important new features of the global seismic system being developed by the GSE. Although global network waveform data have been used for some time for depth determination there is comparatively little experience reported in the literature on its use for analysis of small magnitude events ($m_b$<5.0). Promising results with analysis of multi-station waveforms were obtained in an early data exchange experiment carried out in 1980 within the framework of the GSE. This experiment, referred to as the Common Data Base Experiment (CDBE), resulted in the compilation of digital recordings from some 30 globally distributed stations. The data for the CDBE cover a time period of two weeks. In one of the studies on waveform analysis carried out on this data base, a procedure for depth determination was defined and applied with encouraging results (Roy, 1984). This procedure involves several waveform processing steps, including identification of depth phases, stacking of multi-station records, and deconvolution. The calculated magnitude detection threshold is compared in *Figure 10* with the percentage of events for which depth could be determined from waveform data. *Figure 10* shows that the *applicability* of the depth estimation procedure is quite high. Depths could be determined for almost 90% of the events at the calculated 90% $m_b$- detection threshold. The applicability of the procedure narrows the gap between detection and depth estimation and is high compared with results based on routinely reported depth phases. For example, about 10% and 22% of the depth determinations by NEIS of the USGS for events

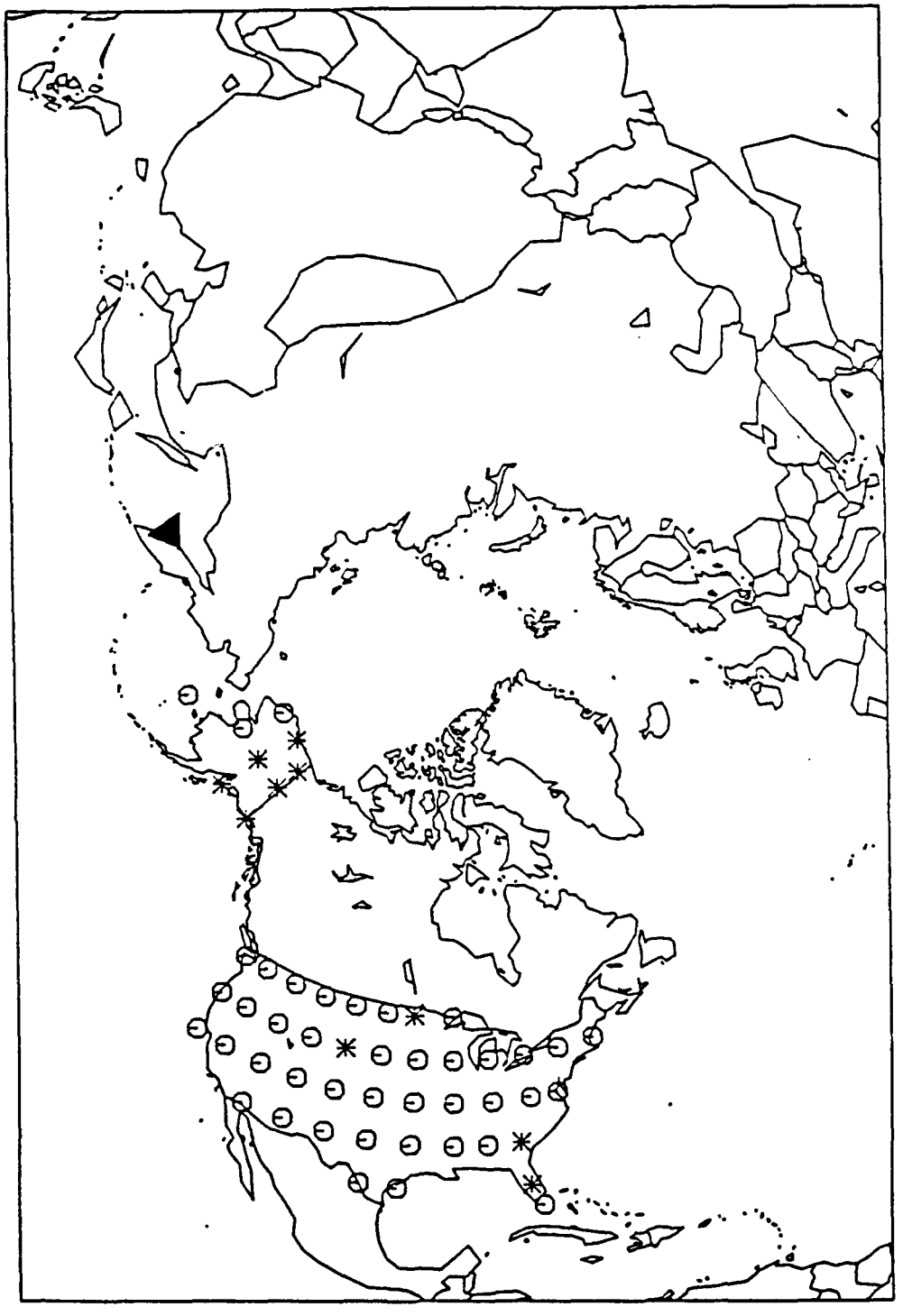

*Figure 9.* Example of selection of station locations for measurements of depth phases from events in the Kamchatka region. The open circles and asterisks represent 52 possible sites from which ten sites can be selected. The selected sites are indicated with asterisks.

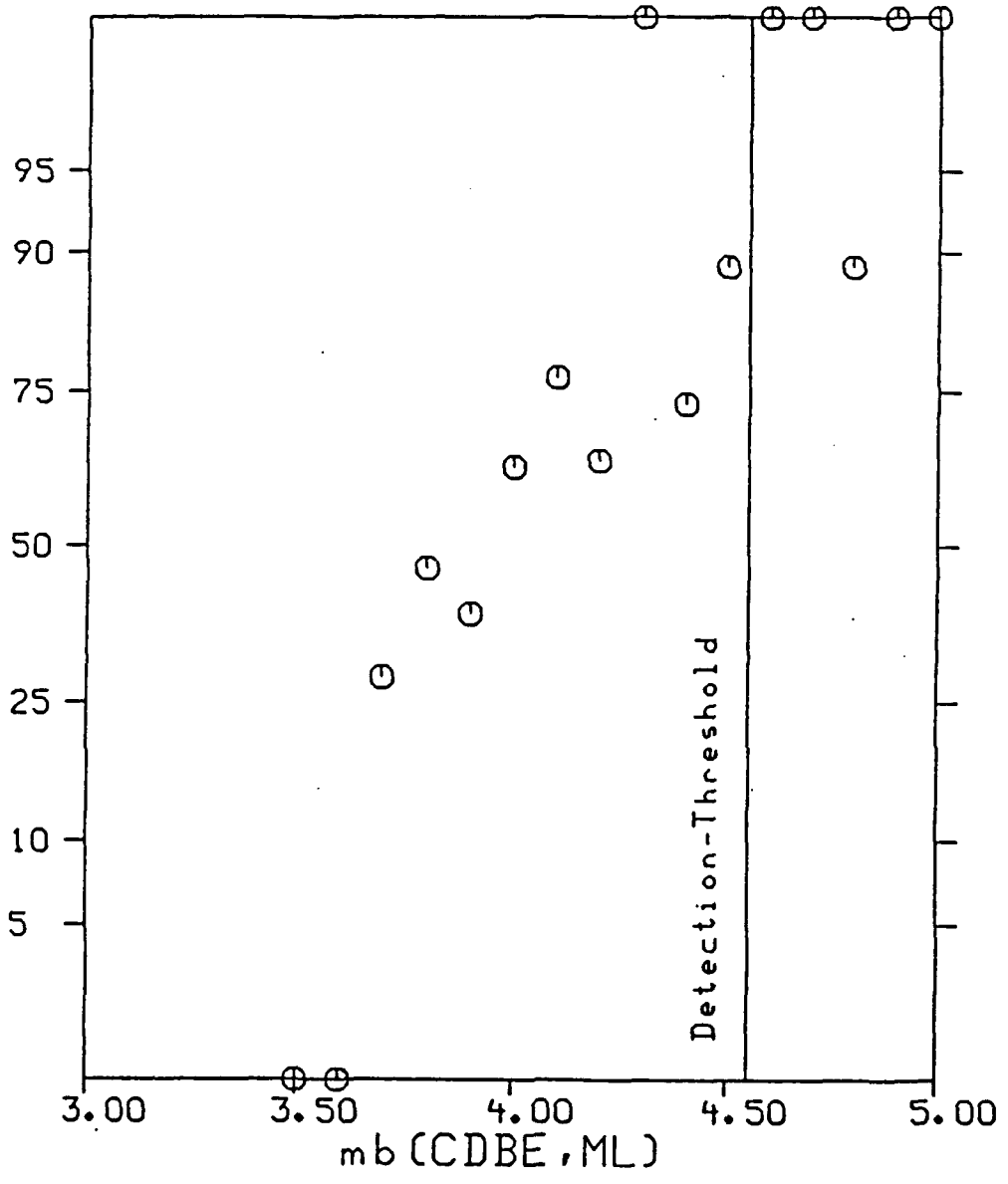


*Figure 10.* The diagram shows the percentages of CDBE events for which depth could be determined from analysis of waveform data, according to the procedure by Roy (1984), as a function of magnitude, $m_b$ (open circles). The vertical scaling is transformed so that data following a normal distribution would be on a straight line. The calculated average 90% $m_b$ detection threshold is included in the diagram for comparison.

during the GSETT were obtained from surface reflections and other geophysical evidence (i.e., not first arrival times), respectively. It should be noted, however, that the high applicability of the waveform procedure for depth calculation does not necessarily mean small error estimates are associated with the results.

### 2.4.8 Surface Wave Magnitudes for Shallow Earthquakes

Compilation of event identification data is an important function for the GSE cooperative system, but the system is not required to identify seismic events since event identification is looked upon as a national matter. Apart from depth estimates, which can be used to identify deep earthquakes as non-explosions, we consider detection of surface waves and compilation of $m_b(M_s)$ data as the most important function for identification of shallow earthquakes. Design of the network would then aim at determining surface wave magnitudes for all shallow earthquakes that are detected and located. The capability of determining $M_s$ for shallow earthquakes with a depth less than a certain value, say 30 km, can be described by the $M_s$ detection threshold in a similar way as the $m_b$ detection threshold is used. Usually the coefficients $a$ and $b$ of the linear relation between $m_b$ and $M_s$ ( $m_b = a(\Phi,\Lambda) + b(\Phi,\Lambda)\cdot M_s$) can be estimated for each sub region (described by coordinates $\Phi,\Lambda$) of the target area. The difference between the $m_b$ threshold (denoted $m_{bT}$) and the "equivalent" $m_b$ threshold for surface waves from shallow earthquakes, derived from the actual $M_s$ threshold (denoted $M_{sT}$), can be written as:

$$\Delta m_{bT}(\Phi,\Lambda)=m_{bT}-(a+b\cdot M_{sT})$$

and is a function of the coordinates $\Phi,\Lambda$.

It is also desirable that

$$\underset{(\Phi,\Lambda)}{Min}\left\{\Delta m_{bT}(\Phi,\Lambda);(\Phi,\Lambda)\in A_t\right\}>0$$

This means that the detection capability of surface waves should be at least as high as that of body waves for shallow earthquakes. For $m_b$=4.0 this corresponds to $M_s$=3.0 or less (e.g., using the relation $m_b$=0.63·$M_s$+2.03, obtained by Weichert and Basham (1973) for a large sample of shallow earthquakes). This would require, however, that the $M_s$ detection threshold of existing networks would have to be lowered significantly. For example, the differences in detection threshold between surface and body waves for the GSETT network were, for the whole world, ≈ 0.5. It has also been estimated that even given numerous high-quality long-period stations, including arrays, the $M_s$ threshold can be lowered only to $M_s$≈3.5 (Marshall and Douglas, 1985). On the other hand, there are instances in which this threshold has been obtained for more modest networks. For example, a global network of only 23 long period stations is observed to have an estimated 90% cumulative threshold for $M_s$ determination of 3.4 (Johansson, 1982). Moreover, the equivalent $M_s$ thresholds for the large

arrays ALPA, LASA, and NORSAR were estimated to be around $m_b$=3.5 (CCD/338). With regional data the $m_b(M_s)$ criterion has been applied to low-magnitude events, i.e., down to $m_b$=3.0 ( $M_s$=2.0). In this case we are, however, no longer talking about a teleseimic network. There has also been discussion on the separation between explosions and shallow earthquakes provided by the $m_b(M_s)$ method for events below $m_b$=4.0 (e.g., Patton, 1989).

The $m_b$ and $M_s$ estimates are assumed to be obtained with the maximum likelihood (ML) technique (Ringdal, 1976). The maximum likelihood method is based on information on detecting and non-detecting stations and not necessarily on the amplitude/period measurements themselves. Information on station noise and detection characteristics is necessary, but this information can in principle always be obtained. This method has several advantages. The ML estimates are not biased at magnitudes close to the detection thresholds of the network and can be estimated for every detected and located event. The most important advantage to be accrued from the maximum likelihood method is that in this context it theoretically closes the gap between the event detection threshold and the threshold for obtaining identification parameters ($m_b(M_s)$ - data) for shallow earhquakes (provided $\Delta m_{bT}>0$). This is because it does not require that amplitudes be measured for small events. The fact that the amplitudes are above the station thresholds at detecting stations and below at non-detecting stations is sufficient.

The above discussion is focused on detection of surface waves from earthquakes. Detection of surface waves from explosions would require even higher sensitivity of the long-period stations. It is sometimes assumed that to be able to use the $m_b(M_s)$, method values of both $m_b$ and $M_s$ are required (OTA, 1988). However, small explosions may be identified by negative evidence (Elvers, 1974), using statistical methods that formally handle absence of surface waves.

### 2.4.9 Concluding Discussion

Networks proposed for nuclear explosion monitoring are often found to have undesirable features. These networks are usually based either on existing facilities or on hypothetical stations that are planned to be installed in the future. Network assessments estimate capabilities of various seismological functions based on assumed station characteristics but do not attempt to define a network in terms of achieving a specified desirable performance.

It is widely recognized that the perceived requirements of a seismic station network for test ban treaty monitoring may differ significantly among countries, as well as among interest groups within a country, and specific criteria for selecting stations for a monitoring network have not been generally agreed upon. In this paper we therefore define three *general technical* characteristics, based on symmetry, that would be desirable for the station network of a global cooperative system.

*Geographical uniformity.*

For an international system, it appears natural to require that the capabilities of the system should not vary strongly with region. The GSE has also consistently pointed out the large differences in capability between the southern and northern hemispheres. The GSETT also showed that there may even be significant variations from region to region within the hemispheres. In addition, since nuclear testing has been carried out on remote islands it may be desirable to designate the whole world, including the oceans, as the "target area" for monitoring.

*Balance between seismological functions.*

A monitoring system should provide sufficient data so that detected and located events can be confidently identified. In other words, there should be a minimum gap between the thresholds for detection, location and identification. A large number of station detections that never become associated with detected and located events is another undesirable feature that is often neglected in network assessments. It is, of course, important to minimize such "unexplained" data collected by a network.

*Superior to other existing systems.*

It may be difficult to obtain agreement on the overall level of monitoring capability, i.e., whether it should be in the $m_b$=4.0 range or something else. In order to be workable a monitoring system should *as a minimum* have capabilities superior to those of existing cooperative global station networks.

From these characteristics major seismological monitoring functions are identified, station selection procedures are described in general terms, and the capabilities of various seismological functions are outlined as a function of number and types of stations and their geometries. These discussions indicate that the following factors have special potential to help satisfy the general characterisctics defined above in the design of a global station network for nuclear explosion monitoring.

*Array stations.*

Array stations that were introduced in seismology as a tool specifically designed for detecting nuclear explosions have detection capabilities that can be far superior to single stations. Use of array stations would also help to alleviate the problem of unassociated station detections. Each array detection provides a rough epicenter estimate of the associated event. Moreover network event detection criteria usually only require two detections at each of two arrays (as opposed to four stations of a single station network). Finally, array processing can be automated, so that the influence of the subjectivity of an analyst in the station detection process is minimized.

*Master event location.*

Location capabilities for global networks are primarily limited by accuracy of the traveltime models. Master event locations have in many case studies demonstrated significant improvements in consistency and accuracy. Bolt (1973) proposed that a set of earthquakes with global distribution be identified as master events to be used at international seismological agencies that routinely locate earthquakes on the basis of primarily teleseismic data. Such a set of master events could also significantly improve the location capabilities of a seismic station network for test ban monitoring.

*Increased number of stations.*

The depth estimation capability based on first arrival times is to a large extent dependent on the distance coverage of the detecting stations. It is particularly important to have data from stations closer than about 15°, as well as in the teleseismic distance window. For a network with the world as a target area this would require more than the 50 stations that have been considered by the GSE.

*Long-period station network.*

The purpose of a network of long-period stations would primarily be to detect surface waves from shallow earthquakes. If sufficiently low detection thresholds can be obtained for surface waves, the gap between detection and identification will be virtually closed, using the maximum likelihood method for the magnitude calculations. The long-period station network, in principle, can be designed independently of the network of short-period stations.

Hans Israelsson

## ACKNOWLEDGEMENTS

I would like to thank Dr. Alan Ryall for his encouragement to prepare this report and for reviewing the original manuscript with several thoughtful and valuable suggestions.

## REFERENCES


Berezin, A., 1986. "Simple Electrostatic Model of the Structural Phase Transition," *Am. Jour. of Physics*, Vol. 54, pp. 403-405.

Bolt, B. A., 1973. "A Proposal for the Global Calibration of Group Earthquake Locations," *Geophys. J. Roy. astr. Soc.*, Vol. 33, pp. 249-250.

Dyson, F., 1984. "Weapons and Hope," Harper and Row Publishers, New York, 340 pp.

Elvers, E., 1974. "Seismic Event Identification by Negative Evidence," *Bull Seism. Soc. Am.*, Vol. 64, pp. 1671-1684.

Ericsson, U. A., 1970. "Event Identification for Test Ban Control," *Bull Seism. Soc. Am.*, Vol. 60, pp. 1521-1546.

Evernden, J. and D. M. Carter, 1970. "Study of Teleseismic P, II-Amplitude Data," *Phys. Earth Planetary Interiors*, Vol. 4, pp. 24-31.

Flinn, E. A., 1965. "Confidence Regions and Error Determinations for Seismic Event Location," *Reviews of Geophysics*, Vol. 3, pp. 157-185.

GSE/Canada, Sweden/1, 1987. *Working Document Submitted by the Canadian and Swedish Delegations to the Committee on Disarmament.*

GSE/US/44, 1987. "Technical Concepts for a Global System for Seismic Data Exchange," *United States Delegation to the Conference on Disarmament, Geneva, Switzerland.*

Hannon, W. J., 1983. "Seismic Verification of a Comprehensive Test Ban," *Energy and Technology Review*, Lawrence Livermore National Laboratory.

Harjes, H. P., 1985. "Global Seismic Network Assessment for Teleseismic Detection of Underground Nuclear Explosions. 1. Model Calculations for Different Amplitude Attenuation Curves," *Journal of Geophysics*, Vol. 57, pp. 1-13.

Israelsson, H., 1986a. "A Note on Network Design: Equally Spaced Stations on a Sphere." *Center for Seismic Studies, Tech. Rept. C86_07*, 8 pp.

Israelsson, H., 1986b. "Unassociated Signal Detection at the GSETT Network," *Center for Seismic Studies, Tech. Rept. C86_05*, pp. 16-21.

Israelsson, H., 1987. "Network Performance and Station Selection Criteria," *Center for Seismic Studies, Tech. Rept. C87_01*, 17 pp.

Johansson, P., 1983. "Common Data Base Experiment - Long Period Surface Wave Signals," *National Defense Research Institute, Stockholm, Sweden, Report C 20462-T1.*

Jordan, T. H., 1981. "Global Tectonic Regionalization for Seismological Data Analysis," *Bull. Seism. Soc. Am.*, Vol. 71, pp. 1131-1141.

Lomnitz, C., 1977. "A Procedure for Eliminating the Indeterminacy in Focal Depth Estimation," *Bull. Seism. Soc. Am.*, Vol. 67, pp. 533-536.

Marshall, P. D. and A. Douglas, 1985. "Earthquake or Explosion: Teleseismic Monitoring-Where are we now?," In: *The Vela Program-A Twenty-Five Year Review of Basic Research* (A.U. Kerr Editor), Defense Advanced Research Projects Agency, pp. 633-657.

OTA, 1988. *Seismic Verification of Nuclear Testing Treaties*, U.S. Congress, Office of Technology Assessment, OTA-ISC-361, Washington, D.C.; U.S. Government Printing Office, May 1988.

Patton, H. J., 1989. "Seismic Moment Estimation of Underground Nuclear Explosions: A Review of Surface Wave Results and Implications for the Source," *DOE/LLNL Symposium on Explosion-Source Phenomenology*, CONF-890398, pp. 128-134.

Pearce, R. G., 1980. "Fault plane solutions using relative amplitudes of P and surface reflections.: Further Studies," *Geophys. J. Roy. astr. Soc.*, Vol. 60, pp. 459-488

Ringdal, F., E. S. Husebye, and J. Fyen, 1977. "Earthquake Detectability Estimates for 478 Globally Distributed Seismograph Stations," *Phys. Earth. Planet. Interiors*, Vol. 15, pp. 24-32.

Ringdal, F., 1976. "Maximum Likelihood Estimation of Seismic Magnitude," *Bull. Seism. Soc. Am.*, Vol. 66, pp. 789-802.

Ringdal, F., 1986. "Study of Magnitudes, Seismicity, and Earthquake Detectability Using a Global Network," *Bull. Seism. Soc. Am.*, Vol. 76, pp. 1641-1659.

Roy, F., 198[illegible]. "Source Depth Estimation Using Multistation Waveform Data," *Bull. Seism. Soc. Am.*, Vol. 74, pp. 1623-1643.

Savarenskiy, E. F., V. V. Sofronov, A. B. Peshkov, L. B. Verbova, and I. V. Peshkova, 1979. "Optimum Distribution of Seismic Stations for Minimizing Errors in Epicenter Determination," *Izvestiya, Earth Physics, (English Translation)*, Vol. 15, pp. 572-577.

USGS, 1985. "Seismograph Station Codes and Coordinates, National Earthquake Information Center," *USGS Open-File Report, 85-714.*

Weichert, D. H. and P. W. Basham, 1973. "Deterrence and False Alarm in Seismic Discrimination," *Bull. Seism. Soc. Am.*, Vol. 63, pp. 1119-1132.

## APPENDIX

## A STOCHASTIC MODEL FOR THE DETERMINANT OF LOCATION COVARIANCE

If we assume that all stations are at the same distance from the source with equal slowness values (i.e., $dT/d\Delta_k = P$), the determinant of $\mathbf{S}$ can be written as:

$$|\mathbf{S}| = P^2 \left\{\sum \cos^2(\phi_k)\right\}\left\{\sum \sin^2(\phi_k)\right\} - \left\{\sum \sin(\phi_k)\cdot\cos(\phi_k)\right\}^2$$

According to Cauchy's inequality the determinant is always greater than zero except when: $\sin(\phi_k) = c\cdot\cos(\phi_k)$, for all $k$, where $c$ is a constant.

In order to study distributions with a maximum value of the determinant we write $x_k = \sin(\phi_k)$ and this gives the following expression for the determinant:

$$P^2 \left\{\sum x_k^2\right\}\left\{\sum (1-x_k^2)\right\} - \left\{\sum x_k \sqrt{1-x_k^2}\right\}^2$$

Rather than attempting to find the $x_k$ values for a given $n$ that maximize the determinant, we assume that the $x_k$ are realizations of a stochastic variable $\xi$ with the range of variation (-1,1). We also replace the summations with expectation operators, $E$, and get:

$$P^2 E(\xi^2) E(1-\xi^2) - (E(\xi\sqrt{1-\xi^2}))^2$$

We are interested in finding the distribution of $\xi$ that maximizes the expression above. For simplicity we assume that $\xi$ is uniformly distributed over the interval $\alpha, \beta$. In this case the determinant can then be written in a closed form:

$$P^2 \left\{1/9(\beta-\alpha)\right\}^2 \cdot \left\{(\beta^3-\alpha^3)\cdot(3(\beta-\alpha) - (\beta^3-\alpha^3) - \left\{(1-\alpha^2)^{3/2} - (1-\beta^2)^{3/2}\right\}^2\right\}$$

For $\alpha$ and $\beta$ we have:

$$-1 \le \alpha \le \beta \le 1$$

## 2.5 A NOTE ON WAVEFORM PROCESSING: DEPTH ESTIMATION BASED ON PEARCE'S APPROACH

### 2.5.1 Introduction

Promising results of depth estimation from waveform data based on phase fitting and beamforming have been reported by Yamamoto (1974) and Roy (1984). The phase fitting approach essentially determines the focal depth that fits the largest number of depth phases, *pP* or *sP*, from a set of measured secondary phases that are initially unidentified. The beamforming approach attempts to detect depth phases hidden in the waveform coda due to scattering and multipathing. The stacking of records from many stations is expected to make the surface reflections *pP* and *sP* appear as clear peaks after the initial *P* phase.

According to the standard double couple source model for shallow earthquakes, depth phases would mostly be recorded in an irregular fashion by the stations of a widely distributed network (Pearce, 1977, 1980). In some instances neither phase fitting nor beamforming may be of much help for detecting the surface reflected phases. In fact, it has been estimated that the probability that a station will detect all three phases, (*P*, *pP*, and *sP*) is only 12% (Pearce, 1980).

In this note we attempt to account for the effect of the source radiation pattern on the observability of *P*, *pP*, and *sP*. This approach is based on a comparison between calculated amplitude ratios *pP/P* and *sP/P* (according to Pearce (1977, 1980)) with observed ratios, measured automatically on the waveforms. The results presented here are only preliminary, and further evaluation is necessary to determine whether this method can be applied successfully in a systematic and routine manner.

### 2.5.2 Pearce's Algorithm and Focal Depth

Pearce's algorithm attempts to estimate the *focal mechanism* of an earthquake using the amplitude ratios of the surface reflected phases and the direct *P* (Pearce, 1977, 1980). The algorithm assumes that surface reflections and associated polarities have been correctly identified on the waveform traces. The observed ratios (and polarities) are compared with calculated ratios for various values of the focal angles (strike, slip, and dip). Since the angles often are underdetermined, actual estimates may not be obtained, but the set of source angles that are compatible with the observations can be mapped. A maximum likelihood procedure that gives actual point estimates has been formulated by McLaughlin (1985).

Therefore, the purpose of Pearce's algorithm is primarily to estimate the focal parameters of a simple double couple mechanism, and depth is obtained only indirectly from the positively identified depth phases. In fact, the estimation procedure is

entirely independent of the focal depth which never enters the calculations. In this note, however, we are primarily interested in depth estimation, and the focal parameters are only of secondary interest and may not even be well determined. We attempt to determine the most likely depth that fits the recorded waveforms, whereas the focal angles may still be underdetermined.

### 2.5.3 A Least Squares Formulation

We introduce a few notations for source parameters and observations. Let $\sigma$, $\psi$, and $\delta$ denote the angles of the fault plane and slip, respectively (after Pearce, 1977), and $h$ denote source depth. Let $\xi$ denote the amplitude ratio of $pP$ and the initial $P$ phase. Similary, $\eta$ is the amplitude ratio of $sP$ and $P$.

The recorded seismogram at station $i$ is converted to its envelope by a standard Hilbert transform after prefiltering (Butterworth three-pole band-pass: 0.5-5 Hz). Then, it is normalized and shifted so that the first maximum of the first $P$ phase has an amplitude of one and is aligned with the transformed records at all other stations. This transformed envelope trace, as a function of time, $\tau$, from the first $P$, is denoted $e(\tau)$. For a given focal depth $h$, the values of the ratios $\xi$ and $\eta$ can be obtained directly from the waveforms transformed into amplitudes in this manner, i.e., $\xi = e(\tau_{pP-P})$ and $\eta = e(\tau_{sP-P})$. In this note the polarities of the initial $P$ and surface reflections are not utilized in the estimation procedure.

The ratios can also be calculated from Pearce's model. The depth estimation can be formulated as a least-squares problem, which attempts to minimize the differences between observed and calculated amplitude ratios. For a given station, $i$, the least-squares sum for $pP$ and $sP$ can be written as:

$$Q_i(pP) = \frac{\left(\xi_i(h) - r(pP)_i\right)^2}{s_\xi^2}$$

$$Q_i(sP) = \frac{\left(\eta_i(h) - r(sP)_i\right)^2}{s_\eta^2},$$

where $r(pP)$ and $r(sP)$ denote the calculated ratios. The depth dependence of the observed ratios $\xi$ and $\eta$ is indicated by the argument $h$. The calculated ratios do not depend on depth but only on the focal angles. The standard deviations $s_\xi$ and $s_\eta$ are assumed to be 0.25 (McLaughlin, 1985).

In order to account for the low coda amplitudes of time segments where no surface reflections or other secondary phases are observed, we also add the term:

$$Q_i(coda)=\sum_k \frac{\xi_i(k)^2}{s_\xi^2 K_i},$$

where summing is performed over those $k$ corresponding to time intervals with no $P$, $pP$ or $sP$ or other secondary phase (e.g., $PcP$). To incorporate this partial sum in the likelihood function we normalize over the number of samples, $K_i$, which may differ from station to station.

The total least-squares sum to minimize can then be written as:

$$Q_{tot}=\sum_{i=1}^{N}\delta_i(pP).W_i(pP).Q_i(pP)+\delta_i(sP).W_i(sP).Q_i(sP)+W_i(coda).Q_i(coda)$$

Here $\delta_i$ is 0 if the depth phase is at a time that may interfere with another secondary phase (e.g., $PcP$) and 1 otherwise. The weights $W_i$ may have values other than 1. With this formulation the depth estimation is reduced to minimizing $Q_{tot}$ with respect to the four variables (depth, slip, dip, and strike). The focal angles are constrained to intervals limited by their periodicity and the time windows of the recordings. In the calculations below we used the subroutine ZXMWD of the IMSL Library (IMSL, 1975) to search for the values that minimize $Q_{tot}$.

If a station is located in a nodal direction of the radiation pattern the observed amplitude ratio as defined above may be overestimated. Then, the calculated ratio will be less than or equal to the observed value, i.e., :

$$r_i(pP)\leq\xi_i$$

If the observed ratios are assumed to follow normal distributions a maximum likelihood approach can be applied. The probability that the observed values are greater than or equal to the calculated values at station $i$ can be written as:

$$P_i(pP)=1-\Phi\left(\frac{\xi_i-r_i(pP)}{s_\xi}\right)$$

Here, $\Phi$ is the standard normal distriution function. The combined likelihood for a network of stations can then be written as:

$$L = \prod_i P_i(pP).P_i(sP)$$

### 2.5.4 Synthetic Examples

We tested the procedure outlined above on synthetic examples. The first example is based on synthetic data for an event (in Uzbekistan) studied by Pearce (1980), who obtained the following source parameters: depth 9.8 km and focal angles $\psi$=60°, $\delta$=120°,

and $\sigma$=340°. The event was recorded at the UK array stations EKA, GBA, WRA, and YKA. The envelopes obtained from simple body wave synthetics are shown in *Figure 1.* Although all stations show clear depth phases, both *pP* and *sP*, there is a considerable variation in waveforms among the four records. The estimation procedure gave the following results: depth 8.8 km and focal angles $\psi$=55°, $\delta$=125°, and $\sigma$=28°. The strike angle ($\sigma$) has a discrepancy of $\approx$ 50° with the estimate obtained by Pearce (1980). It should be noted that Pearce (1980) uses polarities in addition to amplitude ratios to constrain the focal angles.

The second example is for an event in the Kuriles (December 3, 1984) with focal mechanism determined by NEIS and other Seismological Services (the angles are assumed to be: $\psi$=61°, $\delta$=40°, and $\sigma$=211°, and the depth is set to 15 km). Simple *P*-wave synthetics are shown in *Figure 2.* In this case the waveforms look rather similar among the stations. The estimation procedure gave the following results: depth 13.6 km and focal angles $\psi$=118°, $\delta$=42°, and $\sigma$=91°.

### 2.5.5 Examples With Data

The procedure outlined above was also applied to actual data for a few events. It was modified to account for *PcP* phases, so that 2-second time windows around expected *PcP* arrivals are not included in the least-squares function defined above.

In the first example we use data from the Kuriles event studied above (the estimated focal angles are assumed to be: $\psi$=61°, $\delta$=40°, and $\sigma$=211°, according to ISC, and the depth determined from surface reflected phases is 57 km). The recorded signals used here are shown in *Figure 3* before and after filtering and envelope transformation. The estimation procedure gave the following results: depth 39 km and focal angles $\psi$=73°, $\delta$=42°, and $\sigma$=132°.

The second example is for an earthquake in Peru (December 10, 1984 at 10:22:05). The estimated source depth from depth phases is 53 km (ISC), and the focal angles (from HRVD moment tensor solution) are: $\psi$=254°, $\delta$=9°, and $\sigma$=221°. The recorded signals used here are shown in *Figure 4,* before and after filtering and envelope transformation. The estimation procedure gave the following results: depth 51.0 km and focal angles $\psi$=80°, $\delta$=42°, and $\sigma$=78°.

Hans Israelsson

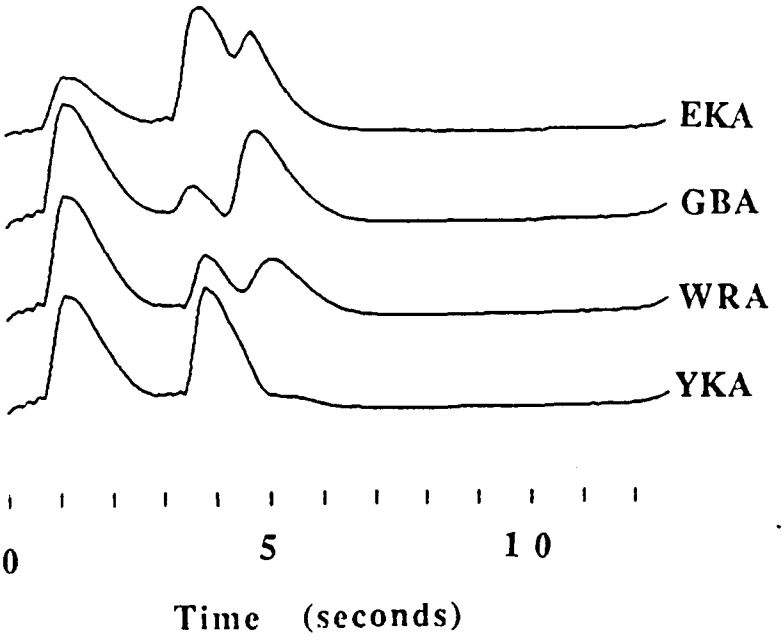


*Figure 1.* Envelopes of synthetic records for an event in Uzbekistan studied by Pearce (1980). The focal depth was 9.8 km. A reflectivity program was used to generate the seismograms.

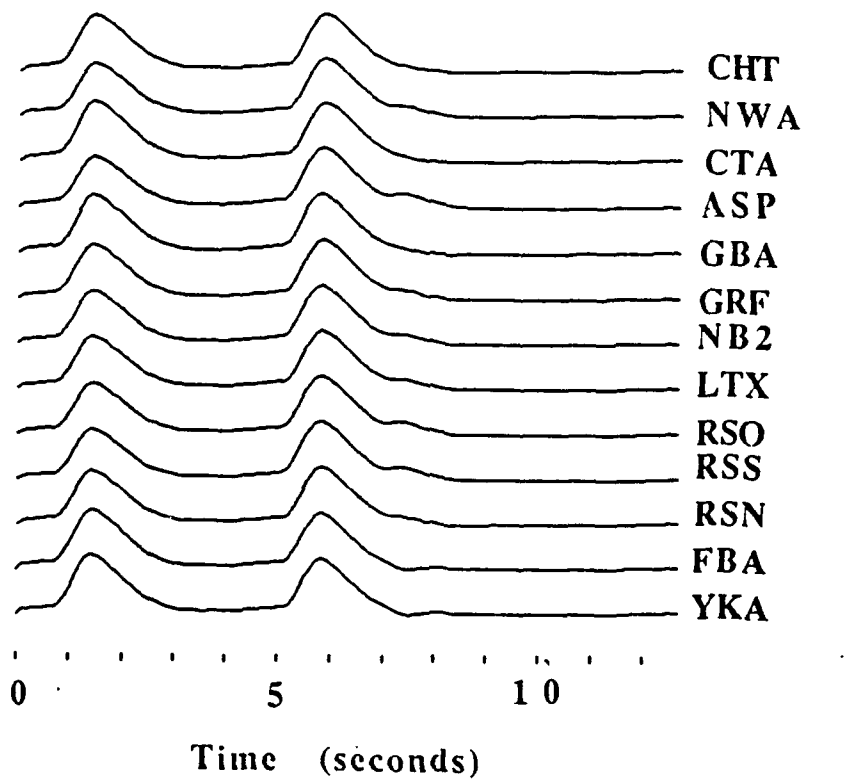


*Figure 2.* Envelopes of synthetic records for an event with the same focal mechanism as an earthquake in the Kuriles (as determined by NEIS) and focal depth 15 km. A reflectivity program was used to generate the seismograms.

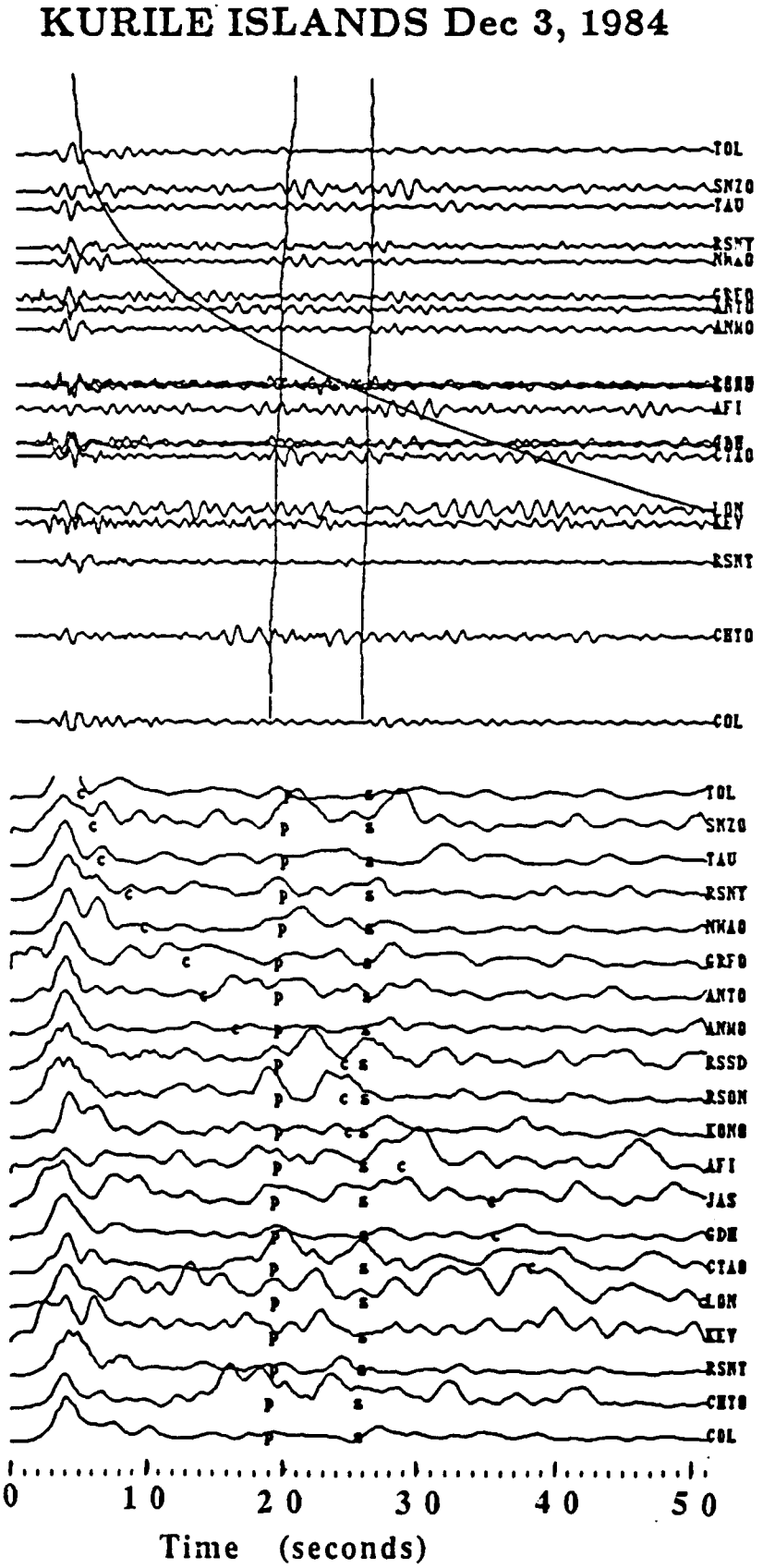


*Figure 3.* Records (top) and envelopes (bottom) for an earthquake in the Kuriles. Expected arrival times of depth phases and *PcP* (denoted by "*p*" for *pP*, "*s*" for *sP* and "*c*" for *PcP*), according to depth estimated by least-squares procedure, are indicated on the traces.

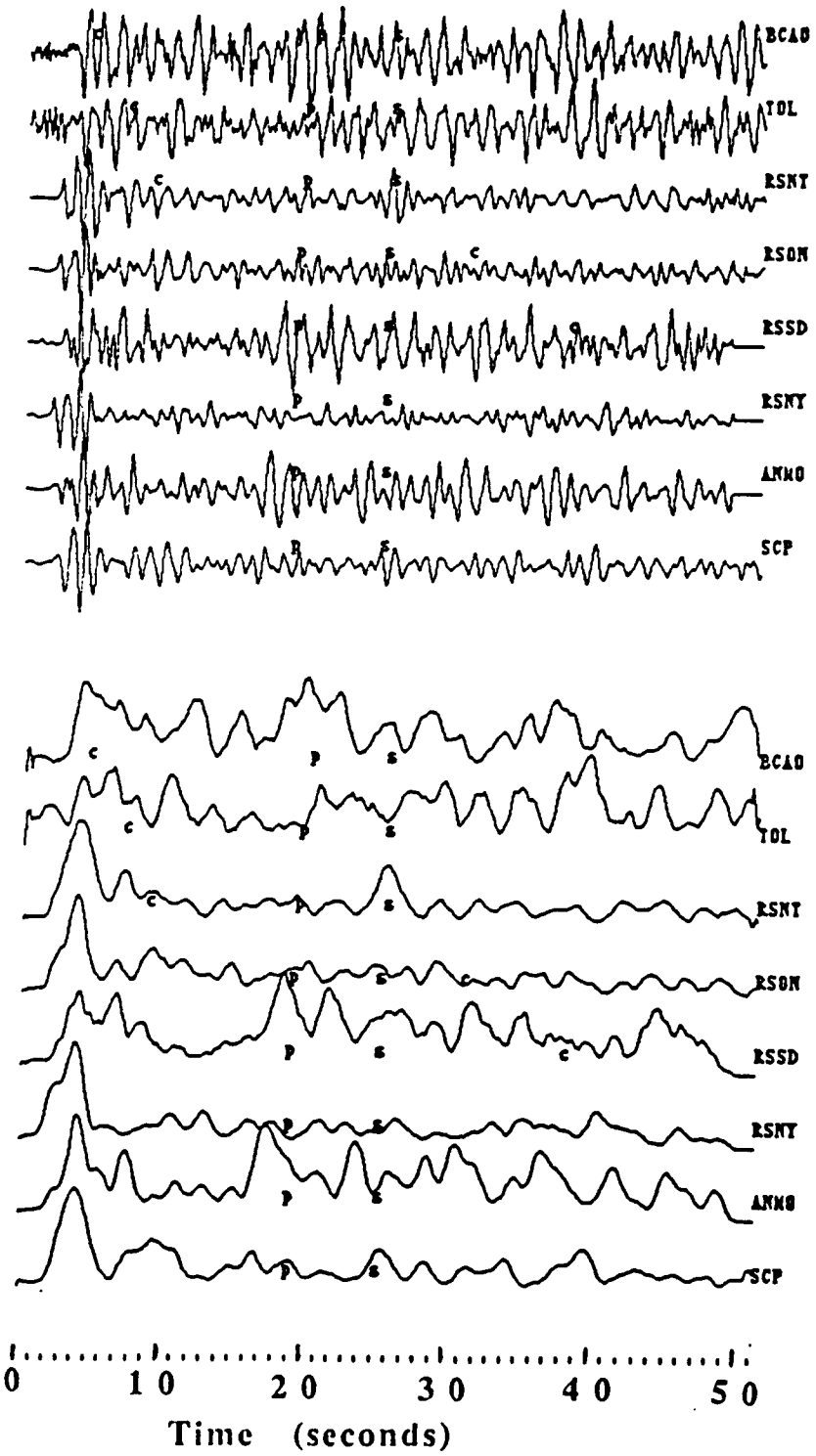


*Figure 4.* Records (top) and envelopes (bottom) for an earthquake in Peru. Expected arrival times of depth phases and *PcP*, according to depth estimated by least-squares procedure, are indicated on the traces, as in *Figure 3.*

## References


Keilis-Borok, V.I., S.S. Mebel, I.I. Pyaatetskii-Shapiro, L. Yu. Varanova, and T.S. Zhelankina, 1972. "Computer Determination of Earthquake Focal Depth", in *Computational Seismology*, Consultants Bureau, New York (English Translation).

McLaughlin, K.L., 1985. "Evaluation of Small Events Using the Pearce Focal Plane Algorithm", *Teledyne Geotech Alexandria Laboratories, Report TGAL-85-11a.*

Pearce, R.G., 1977. "Fault Plane Solutions Using Relative Amplitudes of *P* and *pP*", *Geophys. J. R. astr. Soc.*, Vol. 50, pp. 381-394.

Pearce, R.G., 1980. "Fault Plane Solutions Using Relative Amplitudes of *P* and Surface Reflections: Further Studies", *Geophys. J. R. astr. Soc.*, Vol. 60, pp. 459-487.

Roy, F., 1984. "Source Depth Estimation Using Multi-Station Waveform Data", *Bull. Seism. Soc. Am.*, Vol. 74, pp. 1623-1644.

Yamamoto, M., 1974. "Estimation of Focal Depth of *pP* and *sP* Phases", *National Defense Research Institute, Stockholm, Report C 20027-T1.*

## 3.1 WAVEFORM CORRELATION OF CLOSELY SPACED REGIONAL EVENTS (SUMMARY)

We studied waveforms recorded at the high-frequency element of the NORESS array, from 137 small events in a mining area in Sweden, at distances of about 200 km. None of the events has been reported in local event bulletins ; therefore, their epicenter determinations are limited by the location accuracy of NORESS. Most events are probably "ripple-fired" explosions, but detailed information on source properties is not available. This situation, where precise epicenter locations are not known and source characteristics are uncertain, is similar to that encountered in test ban monitoring, where stations have to be deployed in areas with little or no previous experience of seismological recordings. The case-based approach for event identification assumes that events can be identified on the basis of similarity with waveforms of previously recorded events. However, a visual inspection of the records analyzed indicated that there were few pairs of nearly identical records. In order to quantify comparisons, correlations based on the covariance matrix of three-component recordings (Jurkevics, 1987) were calculated for all event pairs. Correlations defined in this way are insensitive to minor variations in waveforms of individual components due to data smoothing, but are sensitive to backazimuth of three-component recordings. Cut-off values of correlations, used to separate waveforms with poor and good correlation, were defined from the statistical uncertainty of NORESS backazimuths. Using hierarchical clustering (single link) the events could be grouped into one large group of 98 events and four smaller groups. The NORESS epicenters of the large group were scattered over an area of 20 by 75 km. If one assumes that these events had the same location, the 95% confidence region of the epicenter has an aperture of about 10 km. If waveform correlations among close events are reduced as a function of source separation in a known manner, relative epicenters can be determined from the correlation values. This approach was illustrated for a waveform correlation having an exponential decay with source separation obtained from a fit to the data. This constrained the epicenters of the large event group to within 1 km. High correlations were obtained at frequencies above 15 Hz for one small event group, constraining the epicenters of these events to within 0.1 km, based on the "quarter-wavelength argument".

Hans Israelsson

### Reference

Jurkevics, Andy, 1987. "Particle Motion Signatures for Source Identification", *Center for Seismic Studies Tech. Rept. C87-01*, pp. 3.1-3.11.

## 3.2 SUMMARY OF SPECTROGRAM CHARACTERIZATION OF REGIONAL EVENTS

### 3.2.1 Introduction

The use of 3-D spectrogram plots to characterize regional events has been investigated, using NORESS recordings of repeated events at distances of 800-1300 km, as well as local/regional events recorded by the NRDC network. A full report is given elsewhere (Suteau-Henson, 1989). Here, we summarize the part of that study addressing the question of how events can be characterized by comparison with previous events at the same location.

Accurate location and source type identification of small seismic events recorded at local/regional distances depend on our ability to characterize their signals. Regional discriminants have been proposed, including *P*- to *S*-wave spectral ratios, depth phases, and other waveform and spectral characteristics (such as spectral complexity and cepstral peaks). Recent studies using data from the NORESS array include Dysart and Pulli (1988), Baumgardt and Ziegler (1988) and Suteau-Henson and Bache (1988). Although these methods of event characterization have met with some success, there is a need to assess their performance

- as signal-to-noise ratio (SNR) decreases or epicentral distance increases, and
- with data recorded at a single station without the benefits of array-averaging.

In this study we begin to address these questions for events at both far-regional and local distances. Event characterization is performed using spectrograms, built from high-frequency spectra covering the entire event.

### 3.2.2 Analysis Technique

The technique used to characterize regional events combines the advantages of waveform and spectral techniques, by making it possible to view and analyze the entire seismic wavefield throughout the event, in both time and frequency. "Spectrograms" displayed as 3-D perspective plots show the variation of spectral content above noise level, as a function of time, for a data segment containing the event. Spectra are calculated for fixed-length (3 to 5 seconds) time windows, using a technique similar to that of Suteau-Henson and Bache (1988). They are formed for the vertical channel (in the case of single-station recordings such as NRDC data), or for each vertical channel and then averaged over all channels for array data (such as NORESS recordings). Then, they are instrument-corrected, smoothed, and noise-corrected.

### 3.2.3 Results

The dataset includes events recorded at the regional array NORESS and detected by the Helsinki network, and which were located at distances of 800 to 1300 km, in a N-NE direction from the array. The Helsinki bulletin also listed their local magnitude (ranging from 2.0 to 3.6), and indicated that most were explosions from known mines. Of particular interest are a set of earthquakes with magnitudes 2.9 and above from a seismic area in Northern Sweden, and a set of 16 explosions with magnitudes 2.0 to 2.7 from a nearby mine at ≈ 800 km distance from NORESS (designated as "R1" in the Helsinki bulletin). Since these events are located in the same area, spectral differences due to regional path effects are not expected to be dominant, and source effects can easily be observed.

*Figure 1* shows the spectrograms for two R1 explosions, with local magnitudes 2.7 and 2.0, respectively. All R1 events have characteristic spectral modulations that last throughout the entire wavetrain. As expected, they become less visible as the magnitude (and SNR) decreases, although they can still be observed for events with magnitude as low as 2.0. The $S_n$ spectral content is very similar to that of $P_n$ for the entire coda. In contrast, $L_g$ is characterized by much lower frequencies. For larger events, $S_n$ arrives in the $P_n$ coda; therefore some frequencies are contaminated by $P$-type signal. A worse contamination occurs for $L_g$, which arrives in the $P_n$/ $S_n$ coda.

The spectrograms for two nearby earthquakes (with local magnitudes 3.6 and 3.4) are shown in *Figure 2*. As for R1 events, the $S_n$ and $P_n$ spectral contents are very similar for the entire coda, while $L_g$ has much lower frequencies. Also, each secondary phase is contaminated by coda energy from previous arrivals. Apart from this, in spite of nearby locations, the earthquake spectrograms are remarkably different from those for R1 explosions. First, the ratio of $P$ to $S$ energy is much smaller, as expected. Second, the spectrograms do not show any spectral modulations and are generally lacking in character. They are very similar for those two earthquakes, located only 14 km apart by the Helsinki network. Explosions from more distant mines V10 (≈ 1100 km from NORESS) and K1 (≈ 1300 km) were also analyzed. At K1, the available signal bandwidth is so narrow, due to strong attenuation of higher frequencies, that spectral modulations could not be observed.

The evaluation of the use of this technique for events recorded at single stations of the NRDC network (located in Eastern Kazakhstan near the Soviet Test Site) is reported elsewhere (Suteau-Henson, 1989, and Section 1.1 of this report). In particular, the spectrograms of three known H.E. calibration shots are very similar. As expected, no spectral modulations are observed for those single explosions. Also, the scatter in the spectrograms is larger than for NORESS events, since no array-averaging could be performed.

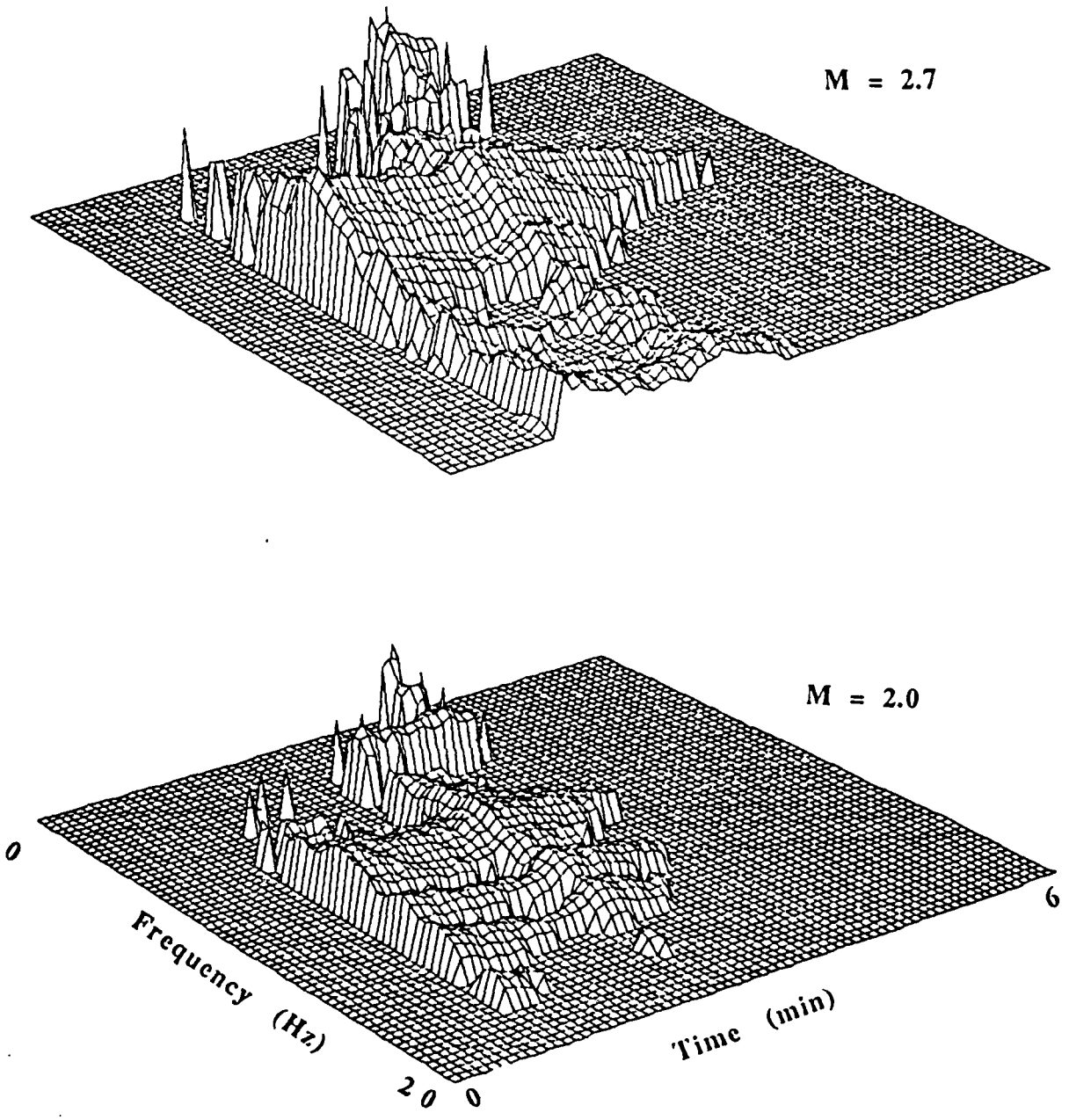


*Figure 1.* Spectrograms of two explosions from mine R1 at NORESS. The frequency scale is linear, from 0 to 20 Hz; the time scale includes one minute before the *P*-wave and five minutes after. A logarithmic scale is used for the spectral values, which represent instrument- and noise-corrected spectral amplitudes. Frequencies below 0.5 Hz are masked to avoid spurious peaks due to noise non-stationarity.

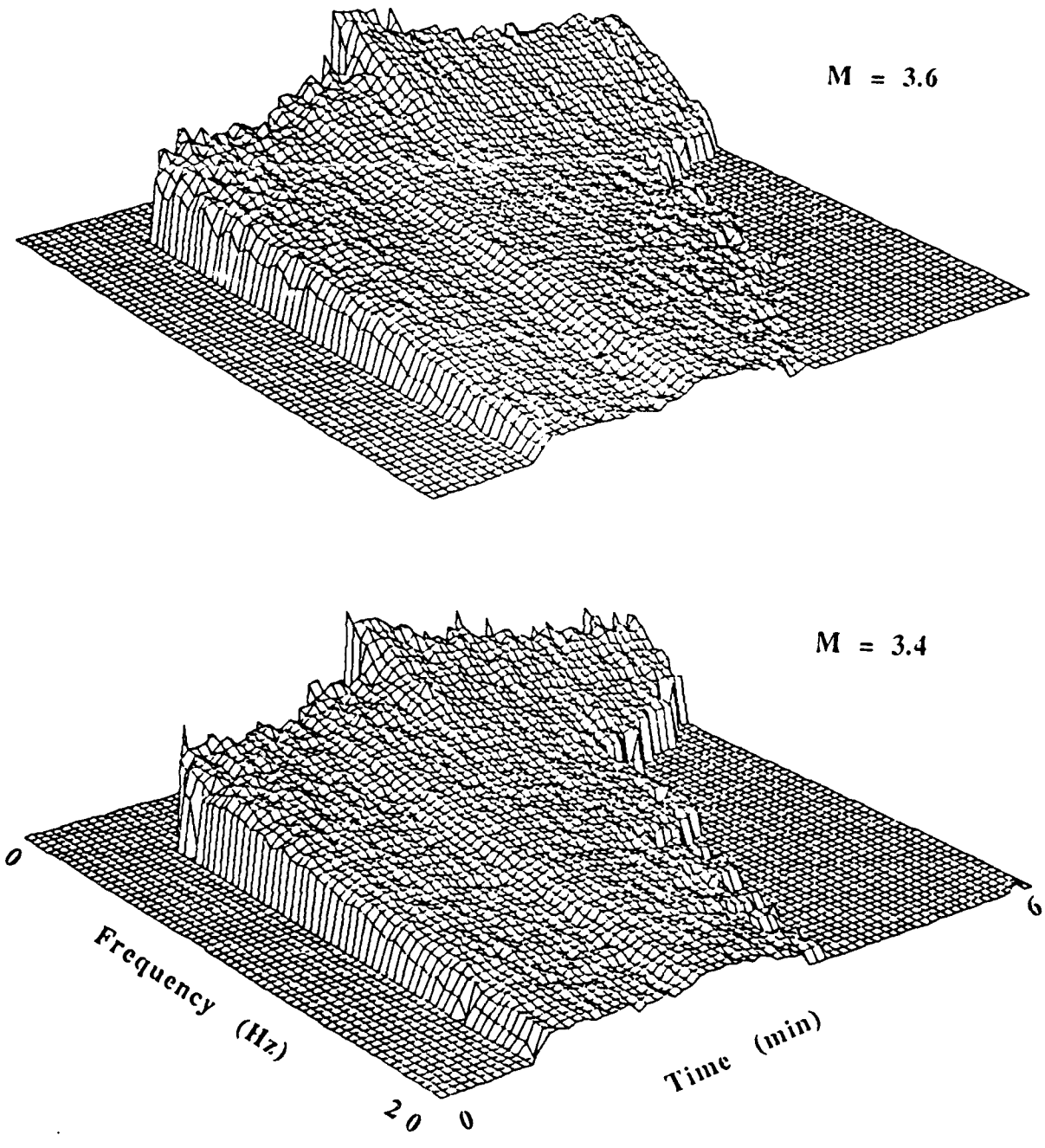


*Figure 2.* Spectrograms of two Northern Sweden earthquakes at NORESS. The scale and other parameters are the same as in *Figure 1.*

### 3.2.4 Conclusions

We have shown how spectrograms can be a useful tool to characterize events, especially during an interactive analyst review, because of the amount of visual information present. For example, small explosions from a mine in northern Sweden show distinctive patterns of modulations for the entire wavetrain. These are attributed to ripple-firing, and can help identify an event as an R1 explosion, down to local magnitudes of 2.0. Earthquakes in the vicinity of this mine have smooth spectrograms that are very similar for nearby events. Modulation patterns were not usually observed for more distant mines (although more data should be analyzed before definite conclusions can be reached). Therefore, at far-regional distances, the usefulness of this method is limited by the narrower bandwidth of the signal due to attenuation of high frequencies.

The scatter in the spectrograms of events recorded at NRDC stations is larger than at NORESS, due to lack of array-averaging, thus increasing the uncertainty attached to this characterization technique. We recommend evaluating the use of interactive analysis graphics to compare spectrograms of unidentified and reference events.

Anne Suteau-Henson

### References

Baumgardt, D. R. and K. A. Ziegler, 1988. "Spectral Evidence for Source Multiplicity in Explosions: Application to Regional Discrimination of Earthquakes and Explosions," *Bull. Seism. Soc. Am.*, Vol. 78, pp. 1773-1795.

Dysart, P. S. and J. J. Pulli, 1988. "Waveform and Spectral Characteristics of Regional Earthquakes and Chemical Explosions Recorded at the NORESS Array," in *Center for Seismic Studies Tech. Rept. C87_03*, 35 pp.

Suteau-Henson, A. and T. C. Bache, 1988. "Spectral Characteristics of Regional Phases Recorded at NORESS," *Bull. Seism. Soc. Am.*, Vol.78, pp. 708-725.

Suteau-Henson, A., 1989. "Characterization of Earthquakes and Explosions Recorded at NORESS and the NRDC Stations," in *Center for Seismic Studies Tech. Rept. C89_01*, 38 pp.

## 3.3 USE OF SURFACE WAVES FOR EVENT IDENTIFICATION (SUMMARY)

In this study we discuss the usefulness of the $m_b(M_s)$ method as the main criterion for discriminating between shallow earthquakes and explosions. We consider worldwide systems like the GSE network, which is not required to actually identify seismic events, but rather must provide sufficient data that can be used for event identification.

Most seismic identification parameters require a greater signal-to-noise ratio than for signal detection alone. For some parameters it has been suggested that a difference of 0.5 to 0.6 magnitude units would be necessary to provide adequate signal-to-noise ratios. However, this would not be the case with the $m_b(M_s)$ method, provided the networks of short-period and long-period stations are balanced in such a way that the system would detect surface waves with a high probability for shallow earthquakes located on the basis of short-period body waves. The maximum likelihood technique can be used to estimate $m_b$ and $M_s$, from the knowledge of detecting and non-detecting stations, together with the noise levels at the stations. Amplitude measurements are actually not required since they would be above and below noise level at detecting and non-detecting stations, respectively. Employing the maximum likelihood technique for the $m_b(M_s)$ method in this way virtually eliminates the gap between detection and identification thresholds. Surface waves may not be detectable for small underground explosions, which, however, could be identified from "negative evidence" or absence of surface waves.

The approach outlined here would require that the $M_s$ detection threshold of routinely reporting networks, as we'l as that of the GSE network, be lowered significantly. It has been suggested that even given numerous high-quality long-period stations the $M_s$ threshold could be lowered to only $M_s \approx 3.5$. On the other hand, there are examples of case studies in which this threshold has been obtained for more modest networks. Therefore, it appears that surface wave detection capability is an area where there still are considerable uncertainties.

Hans Israelsson

## 3.4 SUMMARY OF WORK DONE ON AUTOMATIC ASSOCIATION PROGRAM

The computer program employed during the GSETT for automatic association and location gave a fairly large percentage of spurious events. However, few real events were missed in the processing. If the computational parameters that drive the program are changed so as to reduce the number of spurious events, some real events will be rejected too.

In an attempt to reduce the number of spurious events and maintain the high detectability a scheme was designed that identifies spurious events in the output of the automatic association program. The purpose of the scheme is primarily to point out to the analyst those events that may be spurious. The analyst has to make the final decision whether or not to reject such an event. Once sufficient experience has been acquired, the analyst's decision may be supplanted, at least partially, by an automatic procedure.

The main categories of potentially spurious events include *multiple events* and *split events.* In addition, events based on phases for which there are *inconsistencies between reporting and association* could be potentially spurious. Furthermore, events with *poorly estimated source parameters* (as indicated by large estimated errors) are pointed out.

*Multiple events* are events based on one or more common defining phase. The automatic association program allows a phase to define more than one seismic event. Events with common defining phases are grouped together as hypotheses for one single event. A selection among events in such a group can be made on the basis of the total number of defining stations. If necessary, the event with the largest total event plausibility measure is selected among those with equal number of defining stations. Events not selected in such an event group are then rejected as spurious.

*Split events* mostly refer to events that are spuriously generated from phases actually associated with a large event. Such phases do not have sufficiently small arrival time residuals to be defining for the large event, and, therefore, become "free" to generate new events. A split event often has a location and origin time close to that of the large event. If its defining phases fit the large event fairly well, it is rejected.

A computer program (called *raa*), based on the rules outlined above, was written by Michael A. Tiberio and tested on some of the GSETT data with good results.

Hans Israelsson

## 3.5 INTERNATIONAL DATA CENTER WORKSHOP

### 3.5.1. Introduction

To illustrate the usefulness of waveform data exchange at IDC's, a demonstration of waveform processing was presented to the *US Technical Workshop on the Design and Functions of an International Data Center* (IDC), at the Center for Seismic Studies, on 27 October 1987, and a report titled *Use of Waveform Data for Seismic Processing at International Data Centers* was included in a report distributed to the GSE in the spring of 1988. The purpose of the demonstration was to show that waveform data can greatly improve the quality of seismic processing at IDC's, specifically in the context of verifying events reported in Initial Event Lists (IEL's) and resolving problems in event location, depth determination, etc. Such problems arise as the IDC's check the Level I data received from a global network of seismic stations, prepare Final Event Bulletins (FEB's), and reconcile differences with other IDC's.

The IDC Workshop demonstration was designed to show how supplementary data might have been used to resolve problems that the Stockholm, Moscow and Washington IDC's failed to reconcile during the 1984 GSE Technical Test (GSETT). The events used were those that occurred during the GSETT, and the data set included some, but not all, of the GSE stations. The demonstration showed how waveform data improves the quality of IDC processing as well as the accuracy of the FEB's, and it illustrated several types of problems in analysis and interpretation that could be alleviated through a waveform data exchange. It included examples to show the kinds of difficulties that arise in using data of the type that is currently available to try and resolve problems in analyzing poorly detected events, which underscores the need for standardized stations equipped with modern, high-quality digital seismometers, located at sites with low background noise levels. Finally, it included a description of the types of analysis software tools that will be needed to handle waveform data processing at IDC's.

*3.5.1.1 Selection of Data.*

In designing the demonstration, the Center staff felt that the selection of a few "problem events" from the entire GSETT data set might be criticized as specious. On the other hand, simply demonstrating analysis tools on waveforms exchanged by GSE participants would fail to make a point about resolving analysis problems, since the events selected as the basis for exchanging data were large, well-recorded, and generally well-located. Instead, we constructed a data set that included all the waveforms available at the Center for a typical day of the GSETT reconciliation period, 2 December 1984. To do this, we had to use waveforms that were on hand, specifically those in the Center's *RSTN* and *GDSN* databases. These included some

(13), but not all of the GSE stations reporting during the GSETT. As a result, the demonstration "simulated" the way waveform data would be received from a global network of participating stations, but it was realistic in spite of this departure from the actual 1984 network. NORSAR and NORESS data were also available at the Center for 2 December 1984, and some of this array data was included in the demonstration.

As *Table I* shows, eighteen events were reported in the Washington, Stockholm and Moscow FEB's for 2 December 1984. The "REMARKS" column in the table contains comments about problems with the events. For example, about ten events had large location uncertainties, or were given different locations by the different IDC's. Four or five events had focal depth that was determined inconsistently by the IDC's. Several events had surface wave recordings, but $M_s$ was not determined. In one or more cases surface waves were complicated by interference from other events. Three events were reported by only a single IDC, and were questionable as to whether they represented actual seismic phases or noise. Another three events appear to belong to a single sequence, although one of them was not consistently reported by the IDC's. In some cases, analysis of weak events could have been improved by adding beamed and possibly filtered array data from NORSAR or NORESS. In the Center's experience during the data exchange, the number and variety of problems encountered on 2 December 1984 were probably typical for the type of analysis represented by the GSETT, and provided a useful basis for demonstrating the improvements that would be achieved by a waveform data exchange.

The International Seismological Centre (ISC) reported six events on 2 December 1984 that were not reported by the IDC's, and two events listed by the Washington or Stockholm IDC's were not reported by the ISC. In the demonstration ISC locations were used as a standard for comparison with those determined by the IDC's, even though the ISC solutions were not available at the time of the GSETT. The six events reported by ISC but missed by the IDC's were not considered in the demonstration, as they were most likely missed because of different detection thresholds of the two networks.

*3.5.1.2 The Demonstration.*

In the Workshop demonstration we did not try to show how waveform analysis would eliminate each and every problem for the 2 December 1984 sample. Instead, several events were selected that illustrated different types of problems listed in the "REMARKS" column of *Table I*, and the best analysis software tools available at the Center in 1987 were applied to waveforms for these events to show how the problems might be attacked. In one case, the analysis of a relatively small event in Burma was carried from the IEL stage through the FEB. This event was poorly located during the GSETT, and the use of waveforms from additional stations greatly improved the accuracy of the location and added long-period measurements

**Table I.** Reported events for 2 December 1984.

| IDC | TIME | EPICENTER | | DEPTH | MB/MS | NSTA | REMARKS* |
|---|---|---|---|---|---|---|---|
| wdc | 15352.6 | 37.50N | 72.70E | 1 | 4.3 | 8 | Inconsistent depths |
| m | 15359.4 | 37.60N | 72.40E | 3 | 4.7 | 9 | (ISC depth 168 km) |
| st | 15502.2 | 39.60N | 71.00E | 551 | 4.4 | 11 | |
| wdc | 20157.8 | 4.10S | 105.50E | 1 | 4.5 | 4 | Verify Event (by ISC) |
| wdc | 31905.9 | 50.00N | 79.10E | 1 | 5.7/4.4 | 33 | Explosion |
| st | 31906.1 | 50.00N | 79.10E | 1 | 5.7 | 34 | |
| st | 53324.1 | 13.30N | 114.10W | 8 | 4.1 | 5 | Inconsistent Locations. |
| wdc | 53407.1 | 19.20N | 115.90W | 8 | 4.1 | 4 | Probably close to events |
| m | 53410.1 | 19.47N | 115.88W | 3 | 4.6 | 5 | at 0609 and 0820. No Ms |
| wdc | 60942.2 | 20.40N | 116.20W | 8 | 5.9/6.2 | 34 | |
| st | 60942.1 | 20.10N | 115.90W | 12 | 6.0/6.4 | 36 | |
| m | 60945.6 | 20.18N | 116.05W | 33 | 6.0 | 33 | |
| wdc | 82006.8 | 20.37N | 115.47W | 70 | 4.1 | 5 | Compare depth with |
| st | 82007.2 | 20.40N | 115.20W | 58 | 4.0 | 6 | 0533 and 0609. No Ms |
| wdc | 83541.7 | 63.40N | 150.31E | 6 | 5.0/4.4 | 24 | |
| st | 83541.9 | 63.40N | 150.30E | 7 | 5.0/4.5 | 25 | |
| m | 83542.5 | 63.39N | 150.49E | 7 | 5.3 | 24 | |
| m | 84215.1 | 37.29N | 79.50E | 33 | 4.5 | 7 | Inconsistent Locations. |
| wdc | 84230.2 | 40.70N | 80.20E | 19 | 4.3 | 8 | No Ms, LP interference. |
| st | 84230.2 | 40.70N | 80.10E | 18 | 4.2 | 8 | |
| wdc | 90626.8 | 28.80N | 96.87E | 21 | 4.1 | 4 | Verify Event (by ISC) |
| wdc | 92516.1 | 25.74S | 68.57W | 13 | 4.3 | 4 | Verify Event (by ISC) |
| wdc | 95157.8 | 36.17N | 67.70E | 228 | 4.1 | 6 | Verify Event (not by ISC) |
| wdc | 105813.6 | 50.10N | 43.50E | 69 | 3.9 | 5 | Check Location. |
| st | 105813.0 | 50.10N | 43.60E | 68 | 3.3 | 5 | |
| st | 152035.4 | 24.90N | 94.40E | 24 | 4.1 | 6 | Large estimated location |
| wdc | 152032.8 | 24.90N | 94.20E | 23 | 4.2 | 6 | errors. No Ms. |
| m | 160735.6 | 33.15S | 179.33W | 33 | 5.0 | 8 | Inconsistent Depths. |
| wdc | 160729.8 | 33.10S | 179.00E | 1 | 4.6/4.8 | 7 | |
| st | 160812.5 | 38.30S | 119.70E | 33 | 4.5 | 7 | |
| st | 165031.9 | 51.40N | 15.70E | 22 | 3.9 | 4 | Check Location |
| wdc | 165027.8 | 51.58N | 16.19E | 26 | 3.0 | 5 | |
| wdc | 210924.2 | 3.63S | 152.10E | 21 | 5.0 | 9 | No Ms |
| m | 210927.7 | 4.55S | 153.26E | 3 | 0. | 13 | Inconsistent Depths. |
| st | 211025.8 | 6.20S | 148.50E | 407 | 4.7 | 9 | |
| st | 213650.8 | 43.40N | 15.80E | 329 | 3.0 | 4 | Verify Event (not by ISC) |
| wdc | 234010.3 | 13.77S | 175.86E | 10 | 4.6 | 6 | Inconsistent Depth. |
| m | 234019.1 | 14.26S | 176.26E | 88 | 4.4 | 6 | |
| st | 234025.3 | 13.60S | 175.90E | 123 | 4.5 | 5 | |

* Comments indicate whether or not ISC reported the events

for $M_s$ determination. Other examples were presented, to illustrate the use of reference events, improvement in focal depth estimation using depth phases and long-period secondary arrivals, and use of array data to determine backazimuth and

identify regional phases. The demonstration involved a set of interactive software "tools" that are typical of those that would be needed at IDC's, and the tools were discussed separately at the end of the Workshop paper. The **sunpick** program, which was used as the primary analysis workstation tool, is described in Section 4.1 of this report, as is a program to generate record sections, **rsx**. Other software tools are not described here, nor are the examples described in the Workshop report. Interested parties may refer to the original report, referenced below.

Alan Ryall
Hans Israelsson

**Reference**

Center for Seismic Studies, 1987. "Use of Waveform Data for Seismic Processing at International Data Centers", *Technical Workshop on the Design and Functions of an International Datacenter*, Rept. of U.S. Delegation, Group of Scientific Experts, 36 pp.

## 4.1 SOFTWARE IMPLEMENTATION AT THE CENTER

### 4.1.1 Introduction

Over the last year and a half, a variety of research software has been installed at the Center for Seismic Studies. This includes code written at the Center during the last three years, as well as code contributed by outside sources. These programs cover a wide range of applications — from seismic research programs, to tools for software maintenance, to foreign tape reading. All of the software has been installed under *~css*, with executables available in *~css/bin*.

In addition to the software directories, a new directory *~css/EXAMPLES* has been created on Beno (Sun 4), Maui (Sun 3) and GSE2 (Sun 2). This directory contains examples showing how some of the programs work. In all subdirectories, there is a shell script that can be invoked to run the program using the supplied test data. Each subdirectory also contains a *README* file that explains the input and output of the program, and states whether the program can be run from the present directory. A user cannot run a program in the present directory if output is written, since the user will not have write permission for the *~css* directory. Under these conditions, the user must copy the contents of the directory in question into a directory where the user has write permission, make any changes specified in the *README* file, and invoke the appropriate script.

Some of the programs in *~css/EXAMPLES* can only be run from a graphicstool and/or a shelltool on a Sun workstation running Sunview. If this is the case, it will be so stated in the subdirectory's *README* file.

The purpose behind creating *~css/EXAMPLES* was twofold: (1) to provide an easy way for users to familiarize themselves with software available at the Center, and (2) to provide a way to test that consistent results were obtained on dissimiliar machines. Our intention is to continue to add to *~css/EXAMPLES* as new software is added to *~css*.

In the following subsections we discuss the new Center software by category. Recently installed analysis software is listed in *Table I* and pre-existing additional programs are given in *Table II*. *Appendix I* contains available manual pages.

### 4.1.2 Center Database Version 2.8 Extensions and Utilities

Under the current *Version 2.8 Database Document*, there are ten different supported data types: ASCII single precision, ASCII double precision, ASCII integer, IEEE single precision, IEEE double precision, IEEE integer, VAX single precision, VAX double precision, VAX integer, and NORESS gain-ranged. Recently a decision was made to include formats for IEEE short integers and VAX short integers. Consequently, there

## TABLE I. RECENTLY INSTALLED ANALYSIS SOFTWARE

| *Name* | *Author* | *Function* |
|---|---|---|
| **apiir** | Harris | apply iir filter to a data sequence |
| **assoc_form** | Brennan | correct a bad assoc file format if possible |
| **beamform** | Jurkevics | Prototype beam former |
| **beamprep** | Jurkevics | Beam plotting expediency |
| **butfilt** | Coyne | Butterworth filter |
| **counter_form** | Brennan | correct a bad counter file format if possible |
| **css2ah** | Lamont | convert version 2.8 format data to Lamont ah format |
| **filt** | Coyne | apply a filter to waveforms in a wfdisc |
| **firstloc** | Brennan | make a trial origin from a first arrival record |
| **fk** | Jurkevics and others | compute and display fk spectrum |
| **fseis** | Pulli | filter and display seismic data |
| **geobase** | Lamont | Map plotting program |
| **iirdes** | Harris | design iir digital filters from analog prototypes |
| **mkarrival** | Brennan | make an arrival record from a simple list of signal information |
| **mkcss1** | Brennan | aid for creating manual pages |
| **mkdirs** | Brennan | make missing directory path components |
| **piecer** | Coyne | create waveform segments and change data types |
| **plotxy** | Shure and Parker | a simple plot program |
| **polarcomp** | Jurkevics | 3-component polarization analysis |
| **polarfilt** | Jurkevics | Polarization filtering of 3-component waveform |
| **plotarr** | Coyne | script for making hardcopies of waveforms |
| **rdseed** | O'Neill | read an FDSN SEED format volume |
| **recall** | Jurkevics | display bit-mapped fk output quickly |
| **riffle** | Pulli | display bitmaps of waveforms |
| **rsx** | Lamont | plot record section (time - delta plots) |
| **totype** | Brennan | function to convert between data types |
| **vwave** | Coyne | create a virtual waveform given a wfdisc file and origin information |
| **wdisp_this** | Coyne | create hardcopies of all waveforms in a wfdisc |
| **wfdisc_form** | Brennan | read a wfdisc file and write it with correct format |
| **wpix** | Pulli | create bitmaps of waveforms for quick display by riffle |

**TABLE II. PRE-EXISTING COMPLEMENTARY ANALYSIS SOFTWARE**

| *Name* | *Author* | *Function* |
|---|---|---|
| **arseg** | Science Horizons | produce waveform segments from arrivals |
| **bps** | Anderson | Chebyshev bandpass filter |
| **css2sac** | Tiberio | convert version 2.8 format data to SAC format |
| **lev2** | Tiberio | create GSE level 2 waveform exchange file |
| **r2** | Tiberio | convert GSE Level II data files into version 2.8 |
| **sac2css** | Tiberio | convert from SAC format to version 2.8 |
| **wdisp** | unknown | view .w formatted waveforms on a tektronix 4014 |

are now 144 possible combinations when changing from one data type to another. In the past, before application programs could run, the user had to insure that the waveforms were in the native machine format. This was done with the routine **wfport**. However, due to the rapid growth in volume of incoming data and a simultaneous increase in cpu power, a decision was made to convert to native machine format "on the fly." The new function **totype** accomplishes this task. Given the input and output data types, the number of values to convert, and input and output buffers, **totype** converts the data in the input buffer to the proper data type in the output buffer. The Center staff is currently in the process of installing **totype** in Center software.

Since there are other commonly used formats to store seismic data in the DARPA community, the Center has a series of programs to convert between version 2.8 data and other formats. For SAC format data, there are the programs **css2sac** and **sac2css**. For GSE format, there are the programs **lev2**, which creates GSE level II waveform exchange file given version 2.8 input, and **r2**, which reads a GSE Level II data file and creates version 2.8 output. For the Lamont *ah* format, there is the program **css2ah**, which converts version 2.8 data into *ah* format.

When working with or creating external version 2.8 files, there is sometimes a need to correct the format of the files. There now exist three utilities for correcting the format of *wfdisc*, *counter*, and *assoc* files, **wfdisc_form**, **counter_form**, and **assoc_form**, respectively. Each of these programs reads the file specified on the command line, and attempts to write out a new file with the correct format.

At times it is useful to make an arrival file from a list of arrival information, e.g., when creating *arrival* records from a paper bulletin. **mkarrival** is an interactive program that prompts for the information it needs to create an *arrival* file. Once an *arrival* record exists, it is sometimes necessary to produce a trial origin. This can be accomplished with the **firstloc** program, which outputs files using the time and location of the first record in the arrival file for the origin.

When working with *wfdisc's* that point to very long waveforms (> 1 hour), it is often useful to extract just a segment from that waveform. The version 2.8 database provides for this with a virtual *wfdisc*, where the *foff* and *nsamp* are set to point to the proper segment. A user may want to choose this time window based on arrival or origin information. In the case of arrival information, the program **arseg** (written by Science Horizons) can be run, which produces virtual waveform segments based on arrival information and a *wfdisc*. If the origin is known, the new program **vwave** may be run, which also produces virtual waveform segments based on origin information and a *wfdisc*.

Two other new useful utilities are **mkcss1**, an aid for creating manual pages, and **mkdirs**, a routine for making missing directory path components.

### 4.1.3 Seismological Application Software

The Center has recently received new infinite impulse response (iir) filtering routines from David Harris at Lawrence Livermore National Laboratory. These FORTRAN subroutines (**apiir.f**, **bilin2.f**, **bupoles.f**, **cutoffs.f**, **iirdes.f**, **lpa.f**, **lptbpa.f**, **lptbra.f**, **lpthpa.f**, **secord.f**, **warp.f**) have been installed in *libseis*, and can be used by linking to that library from either C or FORTRAN programs. The two most commonly used routines will probably be **iirdes**, which designs iir digital filters from analog prototypes, and **apiir**, which applies an iir filter to a data sequence.

Once Harris' filtering routines were installed, **butfilt** was written, which acts as a standard UNIX filter, applying a Butterworth filter to a waveform on standard input and writing the resultant waveform to standard output. **butfilt** is analogous to **bps**, which performs the same action using a Chebyshev filter.

After **butfilt** and **bps** were completed, a more general driving routine was written. Named **filt**, this routine reads a *wfdisc*, and applies the specified filter (either butterworth or Chebyshev) to all waveforms in the *wfdisc*. A new *wfdisc* and waveforms are created. When creating the new waveforms, **filt** calls **piecer**, which extracts a waveform segment starting at the byte offset specified by *foff*, and continues for *nsamp* samples. **filt** also calls **totype** (described above), so the input data can be in any data type. All waveforms produced by **filt** will be in native floating point format, since that is the format produced by both filtering routines.

There have been a series of scripts written to produce hardcopies of waveforms on the laser printer. Each script uses the same graphics as **wdisp**. The two basic scripts are **prwave** and **wdisp_this**. The former prints out all waveforms pointed to in a *wfdisc*, while the latter requires the same input as **wdisp**, i.e , the *wfdisc* prefix, the starting point in the *wfdisc* to plot, the number of points to plot, the line number of the first *wfdisc* entry to plot, and the number of lines from the *wfdisc* to plot. The third script is **plotarr**, which produces hardcopies of waveforms given a *wfdisc*, origin or arrival information, and a specified time window.

**plotxy** is a general purpose plotting program which can create either standard UNIX plot files or postscript files. Either output file can be displayed on a Sun terminal or a laser printer.

For a detailed description of each of these programs, see the manual pages in Appendix I.

### 4.1.4 Capabilities of the Sunpick and Locate Programs

The **sunpick**, **locate** and other programs demonstrated in the 1987 IDC Workshop represented the best Sun-3 software available to the Center at that time for

illustrating IDC functions. However, the various software modules were not assembled into an optimally linked system for IDC use, and no additional work has been done on the programs since 1987, since DARPA is supporting the development of more advanced analysis systems using Sun-4 technology. Nevertheless, the programs included in the 1987 demonstration could be optimized for use in an IDC and would, at the very least, provide a great improvement over waveform analysis software that was available to the US during the 1984 GSETT. In this section, the programs involved in the Center demonstration are briefly described below.

#### *4.1.4.1 Display and Analysis Program*

The **sunpick** program (written at Lamont-Doherty Geological Observatory) can be used to resolve problems connected with bad readings of arrival time, amplitude or period, such as mislocated events or incorrect magnitudes. It can also be used to add information, such as depth phases or other diagnostic phases. The program at the Center includes routines written by A. Jurkevics to filter the data, rotate horizontal components, perform polarization analysis, and calculate spectra. It reads and writes files such as *w*, *wfdisc* and *arrival* files in standard Center database format. Features of the program are the following:

Display waveforms.

For a given event, the waveforms can be aligned on specified arrivals, or can be displayed in absolute time. In the data exchange, the start time of a waveform would be an agreed number of seconds before the detected phase. *Figure 1*, showing waveforms for three stations, is an example of the type of display used by the program. The number of traces shown in the figure can be selected by the analyst, and paging is used to see all the traces for a given event. The display includes station and channel designators, amplitude in nm, and phase names selectable from a menu and corresponding to picks in a Center-standard *arrival* file.

Align, scroll, zoom.

Analysis is done in a separate window, which shows all the traces for a single station. *Figure 2* is an example of an analysis window with the traces for a three-component station. This window is used to pick times, amplitudes and periods of the signals. The display can be zoomed to any time scale. Amplitude of the displayed trace can be changed by factors of 2 or 4, and the shaded area on the reference trace can be lengthened, shortened or moved to look at different parts of the trace. Filtering can be done in this window. Results of analysis are written to *arrival* files, which are then input to the location program.

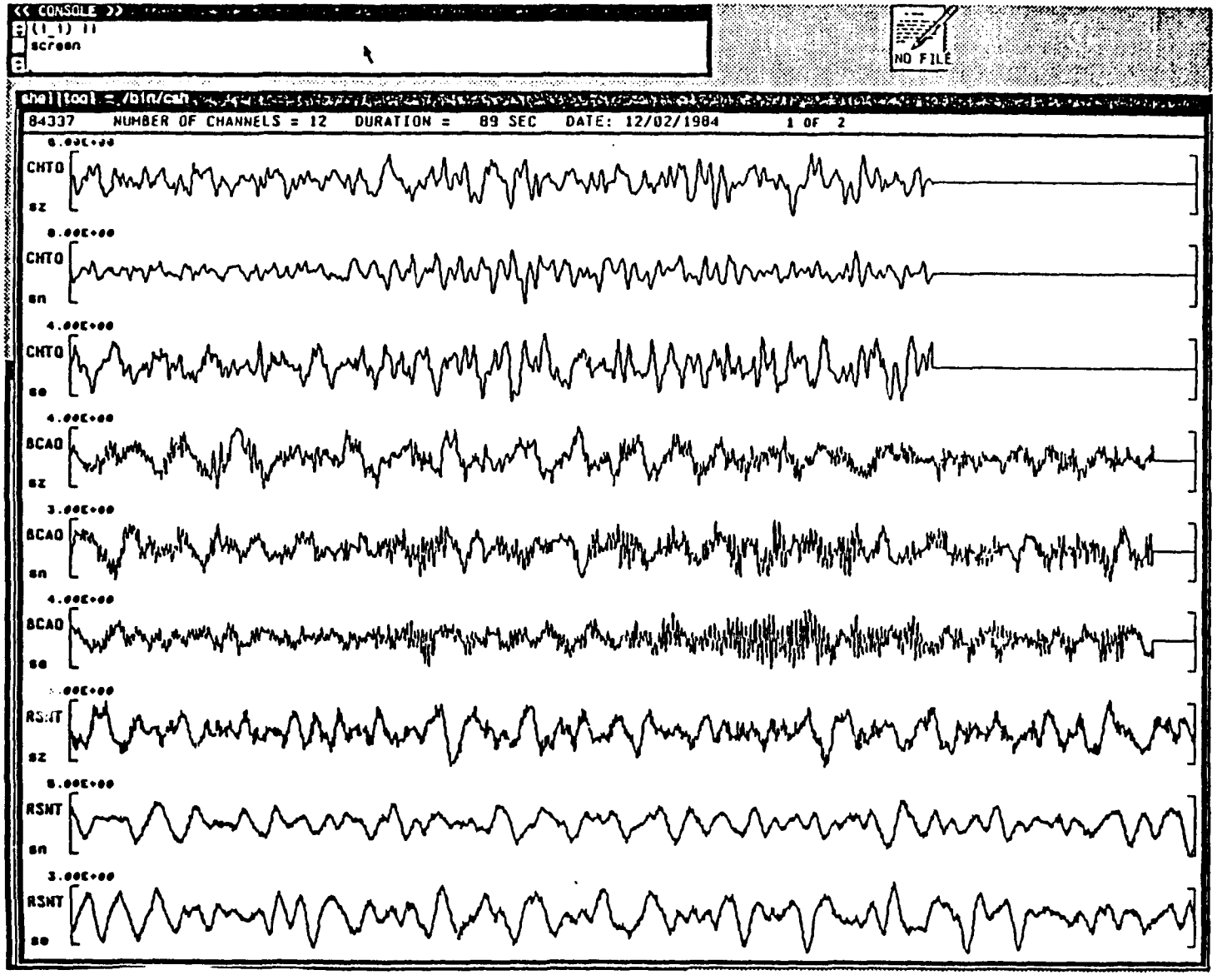


*Figure 1.* Screendump showing 89 seconds of unfiltered short-period waveforms (Z, N and E components) around the expected P-arrival time, for stations CHTO, BCAO and RSNT. Amplitudes, in nm, corresponding to the length of the bar, are shown at the upper left corner of each trace. The amplitudes have been corrected for a nominal gain factor but not for instrument response.

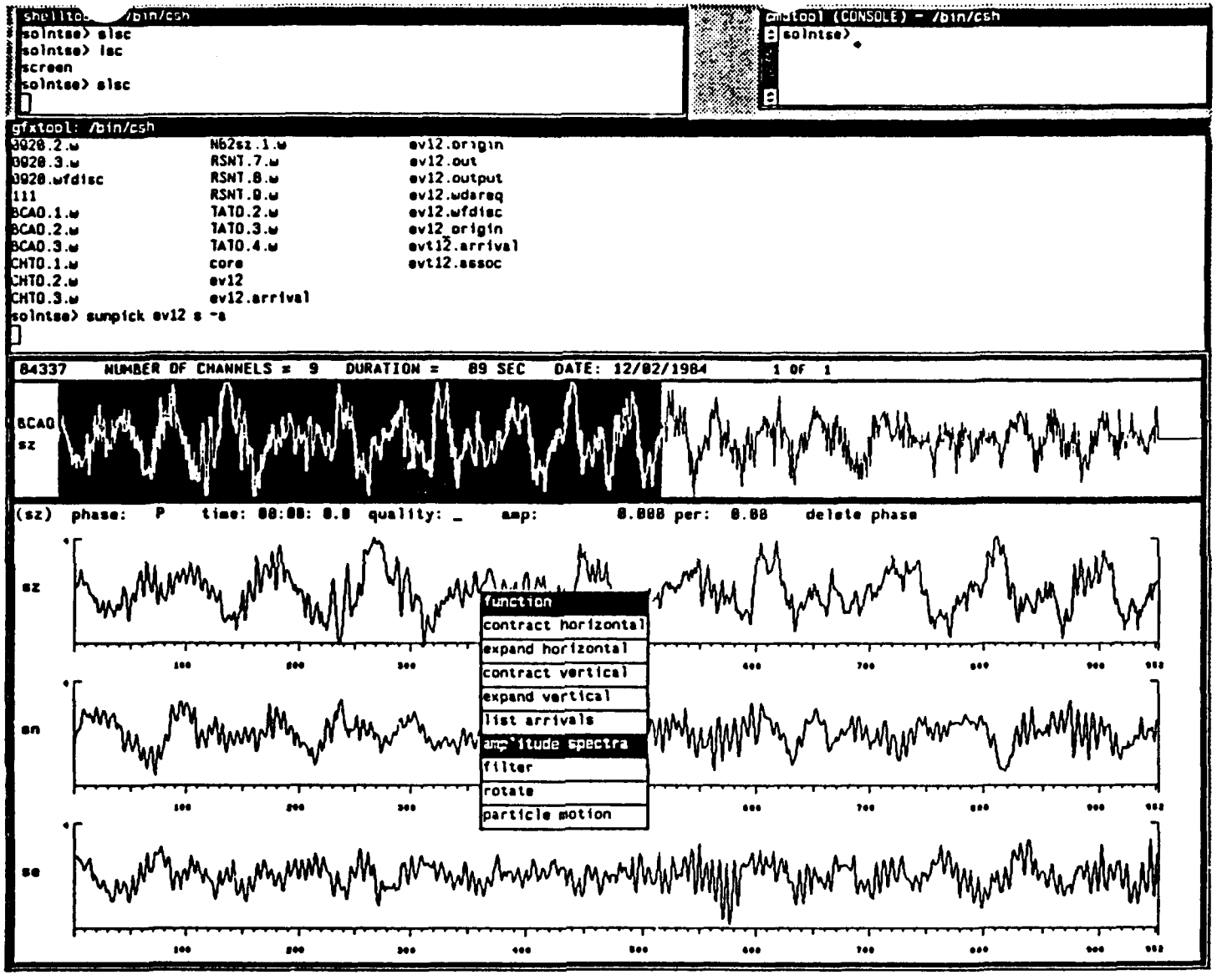


*Figure 2.* Screendump showing analysis window with pull-down menu.

Change, add, delete picks.

The analyst can interactively change, add or delete time picks, amplitude measurements, period measurements, or phase names. The latter are selected from a menu which currently lists 15 diagnostic teleseismic and regional phases.

Delete, add waveforms.

Waveforms that are unsuitable for inclusion in the analysis can be deleted, or new waveforms or beams added.

Rotate.

Given a backazimuth, this program will rotate the EW and NS component traces to produce radial and transverse components.

Calculate spectrum.

A menu-selectable option enables the analyst to display the signal and noise spectra on a single plot, for use in selecting a filter passband to improve the signal-to-noise ratio. The input is mouse-selectable from the reference trace and the output can be smoothed by a specified amount. Frequency can be read off the output spectrum using the mouse, to aid the analyst in selecting a frequency band for filtering.

Polarization analysis.

Three-component analysis can be used to extract the backazimuth, incidence angle and rectilinearity of a portion of the signal in the analysis window, for use in characterizing events and identifying phase types.

Filter.

A bandpass filter can be applied to signals in the pick window. When **filter** is selected a query appears asking for high- and low-pass corner frequencies. These are entered from the keyboard to invoke a third-order Butterworth filter.

#### *4.1.4.2 Map Program*

A map program called **geobase** was used in the 1987 IDC Workshop demonstration to show improvement in epicenter locations. The *SunView* source for this program is available only from Lamont-Doherty Geological Observatory. The **geobase** map program has the ability to plot world maps, regional maps, maps with contoured topography and bathymetry, epicenter maps, station maps, etc. In the 1987 demonstration this program was used to plot a map of the epicentral region, showing previous

seismicity and the error ellipses produced by the **locate** program (*Figure 3*).

#### *4.1.4.3 Record Section*

A record section program, **rsx**, also developed by Lamont-Doherty Geological Observatory, enables the analyst to plot a record section of waveforms from different stations, for a selected distance range and time interval, and to superimpose travel-time curves on the record section. Both waveform times and traveltime curves are reduced by the expected P-arrival time. The traveltime curves include P, pP, sP, PcP, S, LR, etc., so phase identification can be checked on the recordings, and by adjusting the depth, it is possible to see where depth phases might have been missed in the original analysis of the records. *Figure 4* shows an example of short-period signals with the initial P and depth phases.

### 4.1.5 Robert Herrmann's Computer Programs in Seismology

Over the last 15 years, R.B Herrmann, C.Y. Wang, and D. Russell have developed or modified an extensive library of computer programs at Saint Louis University. The programs are designed to be interactive and efficient tools for seismological research. To a great extent, the programs reflect current research areas. These programs and detailed documentation are available at the Center.

### 4.1.6 rdseed

**rdseed** is a program designed to read a tape (or other input file) in the format defined by the Federation of Digital Seismographic Networks (FDSN), popularly known as the Standard for Exchange of Earthquake Data (SEED). The version at the Center was written by Dennis O'Neill at IRIS, and has been modified by Mary Ann Brennan to produce version 2.8 output.

John Coyne

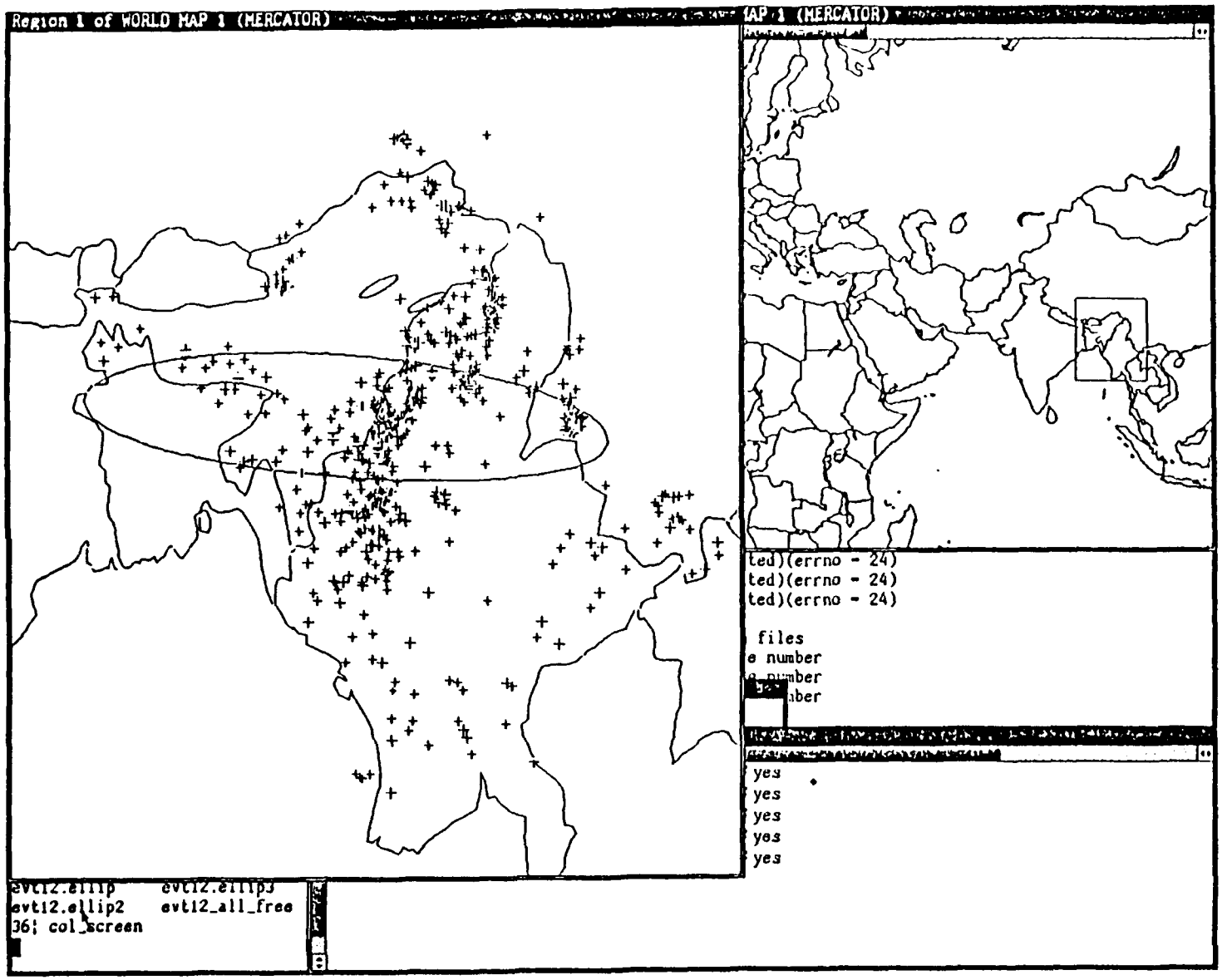


*Figure 3.* Map of Burma region, showing historic seismicity and error ellipses (95% confidence) for various relocation attempts for the Burma event. Large error ellipse is for original calculation, restricted to six stations in Scandinavia, small ellipses correspond to different *P* times. Area of inset shown on global map at right.

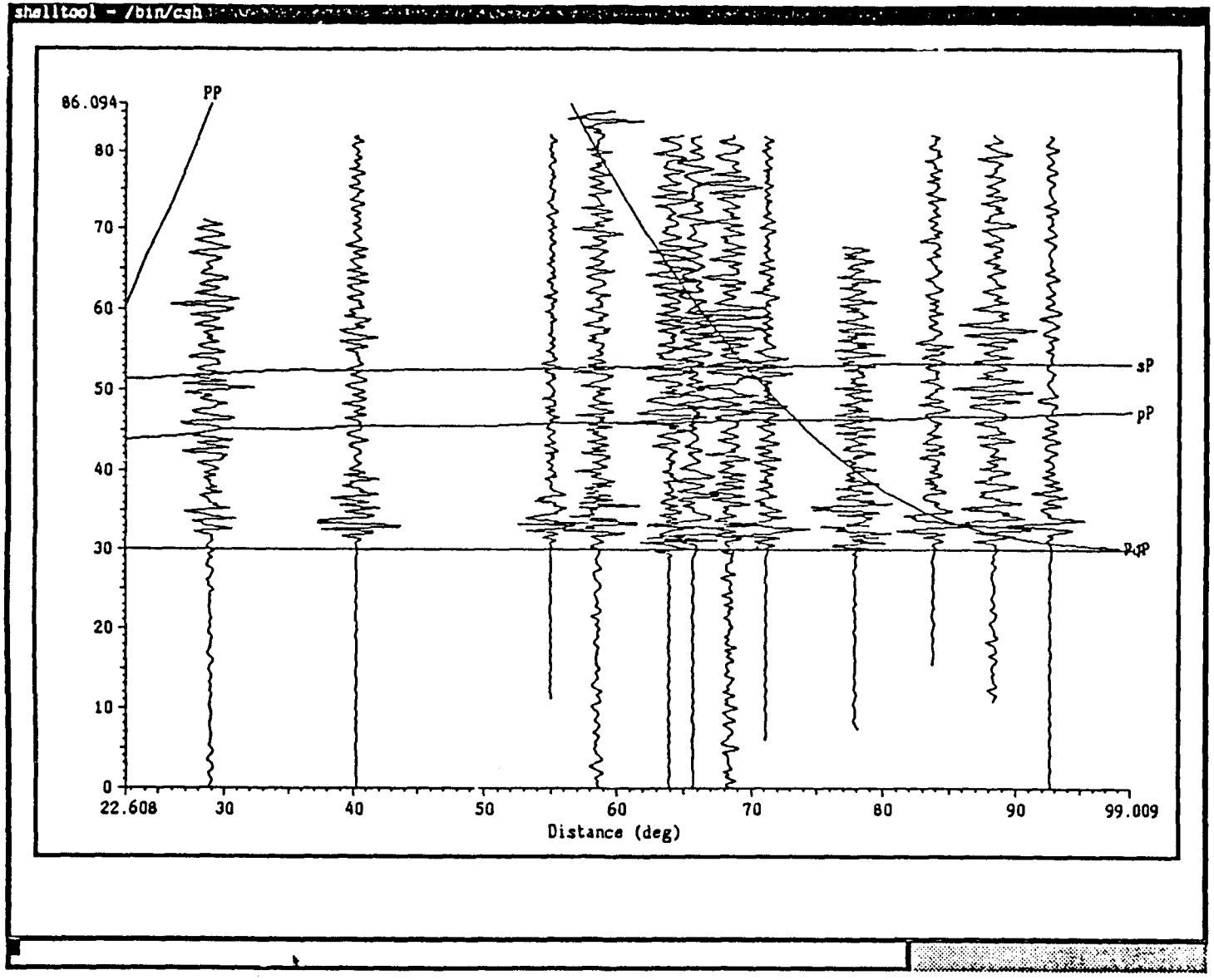


*Figure 4.* Reduced traveltime curves superimposed on waveforms for the Kurile Islands event at 04h 08m on 3 December 1984. The expected *P*-arrival time is at 30 seconds for all the waveforms.

# APPENDIX I

## Manual Pages

**NAME**

arseg – produce waveform segments from arrivals

**SYNOPSIS**

**arseg [ -vcCW ] -s segrules -i inp_prefix -o out_prefix [ -t wft_prefix ] [ -d wfd_prefix ]**

**DESCRIPTION**

**Arseg** produces **out_prefix**.wfreq and/or **out_prefix .wfdisc** that contain waveform requests and waveform segment index records. The segments of waveform data are chosen according to a list of segmentation rules supplied in the file **segrules**. These rules are applied to arrival times found in **inp_prefix**.arrival, thus obtaining time windows about these arrival times for which a search for available waveform data is conducted. Availability of waveform data is communicated to **arseg** via one or more wftape and/or wfdisc input files that are introduced on the command line with the **-t** and **-d** options. These two option flags may be repeated on the command line as many times as is necessary to fully define the "waveform universe" to be searched.

The format of each record in the segrules files is as follows:

pname ci co trb tra tdb tda

Where the fields are:

pname phase name for which waveform data is sought
ci channel id(s) to allow in the arrival records
co channel id(s) to search for if ci is found
trb required time before arrival time
tra required time after arrival time
tdb desired time before arrival time
tda desired time after arrival time

The channel id fields in the segrules file can be specified with "wild card" names. For example if s* is given, it will be expanded to sz,sn,se. If *z is given then sz,lz,mz,iz results. Once all expansions of this type are performed, redundant rules are eliminated from the list before proceding. The expanded list of rules can be obtained with the **-v** option.

Two time windows are specified for each rule. The first is a required window. Data coverage for this window must be present for a waveform request to be generated. If it is, the waveform data is requested for the desired window (before and after the arrival time). Thus if phase name *pname* on channel *ci* is found in the arrival file, and if waveform data for the window *atime-trb* to *atime+tra* is available, then a request for waveform data for the window *atime-tdb* to *atime+tda* will be generated.

The "wild card" scheme also applies to phase names. For example the pname P* means any phase name beginning with the letter P.

**OPTIONS**

**-v** Set verbose - prints segmentation rules and waveformsegment information.

**-c** Use a counter external file to control the assignment fo wfids in the newly created waveform index records.

**-C** Same as **-c** except also writes an output .counter file with updated nxwfid.

**-W** This option tells **arseg** to generate a wfdisc file which describes the

waveform segments in addition to the wfreq file it normally produces.

**FILES**

**inp_prefix**.arrival
**out_prefix**.wfreq
**out_prefix**.wfdisc
**wft_prefix**.wftape
**wfd_prefix**.wfdisc
**segrules**

**SEE ALSO**

cmpreq(1c), dareq(1c), detwo(1c), wfcopy(1c), vwave(1)

**DIAGNOSTICS**

You'll get a usage line echoed at you if you do not supply one of the required arguments. The easiest way to obtain a usage line is to type the command with no arguments.

**BUGS**

This program could be made to generate waveform copying scripts so that *wfcopy* could be used to perform physical segmentation of disc resident data. The scheme embodied in *cmpreq* should be subsumed by this program.

The most serious shortcoming of this program is that it does not deal with arrival files which contain parameters (not legal phase names) in any kind of reasonable way. This is because it uses an older version of indphs to look up the phase names and doesn't act very nice when the name is not found in the table. If **arseg** finds frequent use, it should be updated to fix this problem.

**NAME**

assoc_form – (css,database) corrects a bad assoc file format if possible

**SYNOPSIS**

**assoc_form [-r] -i** *inprefix* **-o** *outprefix*

**INPUT**

assoc

**OUTPUT**

assoc

**DESCRIPTION**

**Assoc_form** reads the specified **assoc** file, and prints it to another **assoc** file with Center external file field spacing. The read format depends only on white space between fields, so **assoc_form** may be used to convert from version 2.7 format to version 2.8 format. The **-r** option makes **assoc_form** revert to producing the version 2.7 format.

**-r** revert to version 2.7 output, deleting fields if necessary.

**-i** *inprefix*
reads file *inprefix*.**assoc** or, if *inprefix* is -, standard input.

**-o** *outprefix*
writes file *outprefix*.**assoc** or, if *outprefix* is -, standard output.

If you specify standard input or standard output, be sure to use pipes or redirect arrows for the shell to interpret.

**Assoc_form** uses getopt(3) to parse its arguments.

**EXAMPLE**

assoc_form -i old -o -

In this case, assoc_form will read a file named old.assoc and produce a version 2.8 assoc for display on your terminal.

**SEE ALSO**

wfdisc_form(1c), counter_form(1c), getopt(3)
Center for Seismic Studies
Database Structure
Version 2.8

**AUTHOR**

Mary Ann Brennan

"Center User's Manual"

**NAME**

beamform – optionally delays and sums waveforms to form a beam

**SYNOPSIS**

**beamform** *input_prefix channel_name*
[ **-n** *beam_prefix* ] [ **-c** *corr_file_name* ] [ **-p** ]

**DESCRIPTION**

**Beamform** forms a beam with waveforms pointed to in the *input_prefix*.wfdisc file in the current directory. Only waveforms whose channel is identical to *channel_name* are used. The beam is written in a .w file, and a new record is appended to the "beam.wfdisc" file in the current directory. By default, the name of the beam .w file is "beam.*channel_name.wfid*.w" (such as "beam.sz.3.w"). "wfid" is incremented every time a new record is appended to the "beam.wfdisc" file.

By default, all waveforms with the correct channel are summed without applying any delay. If the **-c** option is used, delays and weights are read from an ASCII file named *corr_file_name* in the current directory. The waveforms are weighted and delayed accordingly before summing.

If the **-p** option is used, a "plot.wfdisc" file is written in the current directory. It contains all the waveforms that were used and the beam, properly aligned for display purposes.

If no delays are applied, the reference waveform for the beam is that corresponding to the first record with the correct channel in the *input_prefix*.wfdisc file. If a correction file is used, the reference waveform is that for the first record with the correct channel in the *input_prefix*.wfdisc file and with non-zero weight.

**OPTIONS**

Options may appear in any order.

**-n** *beam_prefix*
*beam_prefix* is used instead of "beam" to form the name of the beam .w file. For example, if *beam_prefix* is "tele", *channel_name* is "sz" and the current wfid is "3", the name of the beam .w file will be "tele.sz.3.w".

**-c** *corr_file_name*
The file *corr_file_name* is read in the current directory. This file contains delays (in number of samples) and weights to apply to each waveform, specified by its station and channel. If a waveform has a weight of zero, it is not used. The selected waveforms are delayed and summed. The format of a record in the correction file is:

station channel delay weight

For example,

NRB1 sz -5 1.

The convention used for the sign of the delays is the following: if a waveform must be shifted towards increasing times to be properly aligned, its delay is positive; if it must be shifted towards decreasing times, its delay is negative.

**-p** A file named "plot.wfdisc" is written in the current directory. It contains records for all the waveforms that contributed to the beam, and for the beam

itself. The "time", "foff" and "nsamp" attributes are adjusted so that all waveforms have the alignment that was used to form the beam, and the beam is aligned correspondingly.

**FILES**

*input_prefix*.wfdisc
beam.wfdisc
plot.wfdisc
*corr_file_name*
".w" files for raw waveforms and beams

**CAVEATS**

The reference waveform for beamforming cannot be specified. It is automatically determined by the program as the first waveform used from the *input_prefix*.wfdisc file.

**BUGS**

**beamform** has not been tested for the case where waveforms used to form the beam have different sampling rates.

**AUTHOR**

Anne Suteau-Henson
Center for Seismic Studies
adapted from **beam(1)** by Andy Jurkevics

**NAME**

bps – (css, math, seismology, time) bandpass filter

**SYNOPSIS**

**bps [ -r ] [ -lf low ] [ -hf hi ] [ -rip ripple ] [ -l length ] [ -dt dt ] [ -gin ]**

**[ -gout ] [ -round ] [ -square ]**

**INPUT**

*Stdin* data stream to be filtered (see *-gin* ) if *-gin* not specified, expects ASCII input with at least one blank, tab or newline between each floating point number.

**OUTPUT**

*Stdout:* filtered data (see *-gout* ) if *-gout* not specified, writes ASCII output with one newline between each floating point number.

**DESCRIPTION**

*Bps* acts as a bandpass or band reject filter for digital waveform data. The data to be processed is read from *stdin* and the filtered data is written to *stdout.* If *-gin* and/or *-gout* is specified, the input and/or output waveform is in binary f4 format. Presently, *bps* assumes that all the data on *stdin* is to be filtered and passed to *stdout,* the user (or parent process) must supply a properly windowed waveform on *stdin.*

*Bps* filters the input using a Chebyschev recursive filter that has a small amount of ripple in the pass band. Double precision arithmetic is used to produce a sharp, short filter. The filter is applied forward and backward to produce zero phase shift. *Bps* automatically picks the length of the filter (number of coefficients) and the fractional height of the ripple to produce a filter with round shoulders that is adequate for most purposes. Options allow more precise control of the filter design.

DEFAULTS: -lf 0 -hf .9/(2*dt) -rip .05 -dt .05 -round

OPTIONS:

*-r* produces a band reject filter that has the edge of its reject region specified by *low* and *hi.*

*-lf low* specifies the low frequency edge of the pass band (in hertz). If only *low* is specified, a high pass filter results.

*-hf hi*
specifies the high frequency edge of the pass band (in hertz). If only *hi* is specified a low pass filter results.

*-dt dt* specifies the sampling rate in seconds.

*-gin* specifies .w file (binary waveform data) input.

*-gout* specifies .w file (binary waveform data) output.

*-square*
specifies a filter with square shoulders.

*-round*
specifies a filter with round shoulders.

The ripple and the length of the filter can be specified to allow one to design his own filter. In this case, *-square* should not be specified. The options are:

*-rip ripple*
specifies the fractional height of the ripple in the pass band. A value of .01 is recommended for band reject filters while .05 is recommended for bandpass

filters.

*-l length*
specifies length of the filter where length is odd and greater than one.

**EXAMPLES**

The command

**bps -lf .7** < *file*

will high pass filter the data in *file* with a low frequency edge of 0.7 Hz. Alternatively, a band reject filter to do this is:

**bps -r -hf .7** < *file*

As a rule of thumb, filters with smaller pass bands are sharper and faster to apply. Thus the second version is preferred.

The following commands will plot the impulse response of a filter designed by *bps:*

**bps** *arguments* < *spike.d* > *temp.file* **qdp -line -dx 0 .05 1** *spike.d* **-xa fix** *temp.file*

Where *arguments* are the arguments supplied to *bps* as described above, *spike.d* is an file containing an impulse with at least 50 zeros on either side of it, and *temp.file* is a temporary file containing the output.

**SEE ALSO**

Center for Seismic Studies Database
Structure, Relations, Attributes and
Tape Formats August 1984

**AUTHOR**

Ken Anderson
Lincoln Laboratory Applied Seismology Group
MODIFIED BY:
Mary Ann Brennan
Converted *-gin* and *-gout* options to use *.w* files.

**NAME**

counter_form – (css,database) corrects a bad counter file format if possible

**SYNOPSIS**

**counter_form [-r] -i** *inprefix* **-o** *outprefix*

**INPUT**

counter

**OUTPUT**

counter

**DESCRIPTION**

**Counter_form** reads the specified **counter** file and prints it to another **counter** file with Center external file field spacing. The read format depends only on white space between fields, so **counter_form** may be used to convert from version 2.7 format to version 2.8 format. The **-r** option makes **counter_form** revert to producing the version 2.7 format.

**Counter_form** looks for either a version 2.7 or version 2.8 *counter* file on input (i.e., either 7 or 20 blank-delimited fields) and produces the requested output format. If a version 2.7 file is converted to version 2.8, the additional fields will contain null (-1). If version 2.8 is converted to version 2.7 the additional fields are simply truncated and a warning is printed on standard error.

**-r** revert to version 2.7 output, deleting fields if necessary.

**-i** *inprefix*
reads file *inprefix*.**counter** or, if *inprefix* is -, standard input.

**-o** *outprefix*
writes file *outprefix*.**counter** or, if *outprefix* is -, standard output.

If you specify standard input or standard output, be sure to use pipes or redirect arrows for the shell to interpret.

**Counter_form** uses getopt(3) to parse its arguments.

**EXAMPLE**

counter_form -i old -o -

In this case, counter_form will read a file named old.counter and produce a version 2.8 counter for display on your terminal.

**SEE ALSO**

wfdisc_form(1c), assoc_form(1c), getopt(3)
Center for Seismic Studies
Database Structure
Version 2.8

**AUTHOR**

Mary Ann Brennan

**NAME**

css2sac – Database conversion program

**SYNOPSIS**

**css2sac -p db_prefix [-a,-b,-h]**

**OPTIONS**

-a - generate SAC ASCII file (default)
-b - generate SAC binary file
-h - show syntax of the command

**DESCRIPTION**

css2sac converts a Center for Seismic Studies (CSS) standard waveform database (version 2.7 or 2.8) to a suite of files readable by the LLNL Seismic Analysis Code program (SAC). A concordance between CSS waveform file names and SAC file names is written to the standard output. All work is performed in the current directory.

A CSS waveform database comprises one file with a name of the form db_prefix.wfdisc (containing CSS format information about the waveforms); one file with a name of the form db_prefix.origin (containing CSS format information about the event origin); and several files with names of the form db_prefix.###.w (containing CSS format waveforms), where ### is a number. This program intentionally ignores directory information stored in the db_prefix.wfdisc file.

A SAC file contains header information describing the source and receiver, along with other information, followed by waveform data. The SAC file format is completely described in the SAC user's manual.

css2sac reads the db_prefix.origin, db_prefix.wfdisc and dbprefix.###.w files and writes out one file for each waveform. The resultant files have names of the form db_prefix.saca### or db_prefix.sacb###, depending upon whether the -a or -b option was chosen. Numbers appended to the SAC format files are not necessarily the same as the numbers appearing as part of the input .w file names; they are assigned sequentially by the translator program. A cross reference file is written to standard output which gives the new and old names of the waveforms along with station and time information.

The following parameters are set in the SAC header; their values are taken from the CSS files db_prefix.origin and db_prefix.wfdisc: time increment between samples, event location, zero time of file, number of data points, station name, component name, and the generic name of the recording instrument. See the IRIS document describing the IRIS interim data distribution format for a more complete description. Note that receiver location is not available from the CSS files and is not set in the SAC header at the time of writing of this page.

**EXAMPLES**

css2sac -p kurile1 - converts the CSS database to SAC ASCII format
css2sac -p kurile1 -a - as above
css2sac -p kurile1 -b - converts the CSS database to SAC binary format
css2sac -p kurile1 -b >& dummy - as above, standard and diagnostic output sent to file

**DIAGNOSTICS**

Very forgiving, will skip missing or unreadable waveforms.

**FILES**

db_prefix.wfdisc - input, CSS format; describes waveforms in the database
db_prefix.origin - input CSS format; describes the event origin
db.###.w - input, CSS format; waveform files; ### represents a number
db_prefix.sac[ab]### - output, SAC format; ASCII or binary waveform files
/sail/CSS_data_recovery/source/css2sac - source files

**SEE ALSO**

sac2css
SAC User's Manual, v10.2
SAC Command Reference Manual, v10.2
IRIS Interim Data Distribution Format Specification, v1.0
Center for Seismic Studies Database Structure., v2.8

**BUGS**

None known.

**AUTHOR**

Michael Anthony Tiberio

**NAME**

firstloc – make trial origin from first arrival record

**SYNOPSIS**

**firstloc -i** *inprefix* **-o** *outprefix*

**INPUT**

arrival

**OUTPUT**

assoc origin

**DESCRIPTION**

**Firstloc** reads an **arrival** file and makes a trial **origin** from the first **arrival** location and time. It then produces an **origin** file and **assoc** file to be used with the **arrival** file by a location program such as **locex**(1c). An alternative is to use **trix**(1c) to create the trial **origin**, but then an **assoc** file must be created by hand – **assoc_form**(1c) reduces the tedium. For help in creating an **arrival** file by hand see **mkarrival**(1c).

**-i** *inprefix*
prefix of input **arrival** file, - means standard input

**-o** *outprefix*
prefix of output **origin** and **assoc** file, standard output not allowed.

If you specify standard input don't forget to use pipes or redirect arrows to inform the shell.

**SEE ALSO**

firstloc(1c),locex(1c),trix(1c),assoc_form(1c),mkarrival(1c)
Center for Seismic Studies
Database Structure
Version 2.8

**AUTHOR**

M.A. Brennan

**NAME**

fk – program for frequency-wavenumber analysis of array recordings

**SYNOPSIS**

**fk**

**INPUT**

Files *fk.in, hires.in, prefix.wfdisc,* and **.w,* which are described below.

**OUTPUT**

Contour plot of fk solution to the screen. Horizontal phase velocity and azimuth of most coherent energy. The output files are *output, scratch, fk.out,* and *fk.seg.* The first two files are written in the directory from where the program was run, while the latter two files are written in the directory where the data reside.

The output files are described as follows. *Output* - Contains the starting time that the job was run; echos back the information read from *hires.in;* lists the stations and their relative positions; writes the azimuth, velocity and power as determined by the analysis; and finally writes the ending time of the job. *Scratch* - writes the azimuth, velocity and power; and attempts to write the data date. *Fk.out* - writes the prefix to the local CSS database; epoch time of detection for centering analysis window; center frequency for bandpass filtering data; and the azimuth, velocity, and power determined by the analysis. *Fk.seg* - is a disc file with the information needed to reconstruct the resultant plot. The figure can be redrawn using the utility *recall* (1c).

**DESCRIPTION**

This program is a modification of routines in RONAPP (from NORSAR). A broad-band version of fk algorithm has been added.

**EXAMPLE**

The following is an example of the input file *fk.in:*

```
12345678901234567890123456789012345678901 <1>
/b/coyne/projects/find/threecomp                <2>
13                                              <3>
    epoch time      freq                        <4>
   506355097.953     5.000                      <5>
 lwndo                                          <6>
  20                                            <7>
  25                                            <8>
   1   0   NRA0      sz              <9>
   2   1   NRA1      sz              <10>
   3   1   NRA2      sz              <11>
   4   0   NRA3      sz              <12>
   5   1   NRB1      sz              <13>
   6   1   NRB2      sz              <14>
   7   1   NRB3      sz              <15>
   8   1   NRB4      sz              <16>
   9   1   NRB5      sz              <17>
  10   1   NRC1      sz              <18>
  11   1   NRC2      sz              <19>
  12   1   NRC3      sz              <20>
  13   1   NRC4      sz              <21>
  14   1   NRC5      sz              <22>
```

```
15  1  NRC6     sz          <23>
16  1  NRC7     sz          <24>
17  1  NRD1     sz          <25>
18  1  NRD2     sz          <26>
19  1  NRD3     sz          <27>
20  1  NRD4     sz          <28>
21  1  NRD5     sz          <29>
22  1  NRD6     sz          <30>
23  1  NRD7     sz          <31>
24  1  NRD8     sz          <32>
25  1  NRD9     sz          <33>
```

Note that the numbers in brackets on the right hand side are for use only in the following discussion and do not exist in the input file.

Line <1>
numbers used in helping to format the input; a blank line may be substituted,

Line <2>
directory of local CSS database,

Line <3>
prefix of local CSS database,

Lines<4 and 6>
description of the following line, a blank line may be substituted,

Line <5>
epoch time of detection for centering analysis window and center frequency for bandpass filtering data,

Line <7>
length of time window in samples,

Line <8>
Number of elements to follow.

Lines<9,...>
Element number, weights for seismograms, station names, and channels. If weight = 0, this element is omitted from the analysis, and if weight = 1, this element is included in the analysis.

The following is an example of the input file *nires.in:*

```
  NB   LB NEPS IFPR IFPL ICONV IHRES (1615)                          <1>
   1  120   2    0    0    1    0                      <2>
 NSIDE NCLEV  DK      XZERO    YZERO    XDIM     YDIM (2I5,5F10.0)
  41    4   0.060   -1.20    -1.20    16.0     16.0                  <4>
CONTOUR LEVELS IN DB (2513)                                                <5>
 1  3  5  7  9                                                        <6>
```

Note that the numbers in brackets on the right hand side are for use only in the following discussion and do not exist in the input file.

Lines<1,3,5>
description of the following line, a blank line may be substituted.

Line <2>

nb = number of blocks...no limit
lb = length of each block...max of 1000
neps = per cent of noise to be added to diagonal in covariance mat
ifpr = unknown, does not contribute to any computations
ifpl = 0/1 - do not/do...plot time traces
iconv = 0/1 - do not/do...compute conventional k-spectra
ihres = 0/1 - do not/do...compute high res k-spectra

Line <4>

nside = number of steps in each direction...max of 71
nclev = number of contours to be plotted in k-space...max of 25
dk = step length in wavenumber (c/km)
xzero,yzero = lower left hand corner of k-space area
xdim = plot dimension in x direction
ydim = plot dimension in y direction...max of 9 (inches)

Line <6>

Contour levels in dB. The number of contours is defined by nclev, given in line 4.

**SEE ALSO**

recall (1c)
Center for Seismic Studies Data Base
Structure, Relations, Attributes and
Tape Formats August 1984

**DIAGNOSTICS**

Intended to be self-explanatory.

**BUGS**

The day and hour recorded by scratch are incorrect. The program lacks a proper usage line, and some of the read statements may terminate the program with no explanatory message if an error occurs.

**AUTHOR**

Author of subroutine hires4 is R.T.Lacoss (1966). Modified by J.Capon (1970), numerous modifications at NORSAR (1970-81) in input/output. Some other routines were written by Dave Harris, while others are believed to have been written by Andy Jurkevics.

**NAME**

fseis – displays up to 10 filter bands of a single waveform

**SYNOPSIS**

**fseis** *database_prefix waveform_number*

**INPUT**

CSS version 2.7 formatted *.wfdisc*, and *.w* files. File *filter.info* contains the filtering information.

**OUTPUT**

A plot of the filtered waveforms.

**DESCRIPTION**

*fseis* filters and displays the waveform given by the *database_prefix* wfdisc file and the *waveform_number* in that file. Up to 10 filters may be used per display. The filters are applied forwards and backwards, producing a phase free output. The filter information must be in the users directory in the file *filter.info*. A time axis is drawn at the bottom of the plot, along with other pertinent information such as the start time of the plot, date, station name, database name, and scaling information.

*fseis* must be executed within a Sun window.

An example of the *filter.info* file is given below, where the 3 values on each line represent the low frequency cutoff, the center frequency of the filter, and the high frequency cutoff (all in Hertz).

```
 0.0  0.0  0.0
 8.0 12.0 16.0
 4.0  6.0  8.0
 2.0  3.0  4.0
 1.0  1.5  2.0
123456789-123456789-
```

First note that the values on the bottom line are for formatting purposes only; they are NOT in the actual file. Also note that a filter of 0. 0. 0. provides unfiltered output. *fseis* also checks to see that the requested filter is not above the Nyquist frequency. If it is, that filter is ignored, and an error message is printed.

**OPTIONS**

Prompts are given for the number of seconds to skip in the *.w* waveform file, number of seconds to plot, bandpass filtering, and scaling. The filtered waveform can be displayed either true to scale or scaled independently. If independent scaling is chosen, the individual scale factors are shown to the right of each trace.

**EXAMPLE**

The following command line will plot the filtered second waveform in the data base named *exmpl:*

```
fseis exmpl 2
```

**AUTHOR**

Jay J. Pulli
Center for Seismic Studies

**FILES**

${CSSHOME}/tables/filter.info

**BUGS**

It is assumed that the prefix of the *.wfdisc* and the *.w* files are the same.

**NAME**

lev2 – (css, gse, database) create level 2 waveform exchange file

**SYNOPSIS**

**lev2 -p** *db_prefix* [**-o** *orid*] [**-x**]
**-o** and **-x** are mutually exclusive

**INPUT**

wfdisc and optionally origin or extra

**DESCRIPTION**

**Lev2** reads **wfdisc** and waveform (**.w**) files and writes level 2 waveform exchange files. Optionally **lev2** will read either **origin** or **extra** external files and include the information as comments appended to the waveform identification section of a waveform exchange file. **Lev2** doesn't currently include the calibration section of waveform exchange files (no poles and zeros or frequency–amplitude–phase data). For some reason **lev2** considers the **origin** and **extra** options to be mutually exclusive. If you need both options, and there isn't a reason to leave it as is, this could be changed fairly easily. **Lev2** can read either integer or floating point binary waveforms. In the latter case, 7 digits of precision are retained in the level 2 file created, but the decimal point floats as needed.

**-p** *db_prefix*
required input file prefix for external files such as **wfdisc** or **origin** files

**-o** *orid*
optional **origin** id to specify **origin** information to include in waveform exchange file

**-x** optionally include **extra** file information if it exists for a waveform id

**SEE ALSO**

r2(1c)
Center for Seismic Studies
Database Structure
Version 2.8

**CAVEATS**

Doesn't create the calibration section

**AUTHOR**

M. Tiberio

**NAME**

mkarrival – makes an arrival file from a simple list of signal information

**SYNOPSIS**

**mkarrival**

**OUTPUT**

arrival

**DESCRIPTION**

**Mkarrival** is a purely interactive program that prompts you for the information it needs to create an **arrival** file. It reads from standard input and writes to standard output. It only needs *sta*, *chan*, *phase*, *date* and *time* to work. Place a blank between each value and hit return after each set of values for one **arrival** record. *Date* may be either in Julian form (*yyyydoy*) or in the form *yyyymmdd* where *mm* and *dd* are the two digit month and day of month. *Time* should be in the form *hh:mm:ss.sss*, you need not specify minutes or seconds or fractions. To finish **mkarrival**, type Ctl-D.

**Mkarrival** may be handy if you want to do a quick location using **arrival** information from a paper bulletin or other source that doesn't provide standard Center **arrival** files. Other tools are available to assist in this endeavor and are cited below.

**SEE ALSO**

assoc_form(1c), trix(1c), locex(1c), firstloc(1c)
Center for Seismic Studies
Database Structure
Version 2.8

**AUTHOR**

M. A Brennan

**NAME**

mkcss1 – (css, file, extra) aid for creating manual pages

**SYNOPSIS**

**mkcss1** *manfile descrfile*

**INPUT**

stdin and descrfile

**OUTPUT**

manfile.1

**DESCRIPTION**

**Mkcss1** is shell script to take some of the tedium out of writing command manual pages which conform to Center manual standards.

*manfile*
should be the prefix desired for the output manual page. **mkcss1** will add the suffix **.1** to this for Center command manual pages.

*descrfile*
should be the name of a file containing the paragraphs to be placed under the description heading.

**Mkcss1** uses a template to initialize the manual page then calls the awk script **get_date** to create a properly formatted date stamp. **Mkcss1** prompts for command names, one-line description, synopsis lines for commands, lists of input and output file suffixes and lists of key words to be italicized or made bold in the synopsis lines or in the description. After prompting for unformatted information from the user, **mkcss1** adds **troff** directives to the plain-text synopsis lines. The synopsis lines may contain constructs such as:

command_name [-opt1] [-opt2 value] file1 file2

Since the lists of bold and italic words received from the user (and some built-in lists) determine the typeface of items in the synopsis, the command name and option letters (**-opt1** or **-opt2**, i.e., literals) should be in the boldface list, and the non-literal words such as *file1* or *value* should be in the italics list. The built-in lists set relation names bold; attributes italic. The *descrfile* is added to the man page and filtered to produce the **troff** directives for the highlighting.

**Mkcss1** is meant to handle some basic man page formatting, ensures that headers and footers have a common form, and that some standard items are properly highlighted. Users are encouraged to provide an easily searched list of command line arguments (by using the **.TP** man macro) in the description even though it is not enforced by **mkcss1**.

**FILES**

${CSSHOME}/etc/Template1
${CSSHOME}/etc/get_date
${CSSHOME}/bin/igicase

**SEE ALSO**

get_date(1c), troff(1c), igicase(1c)

**DIAGNOSTICS**

Intended to be self explanatory.

**BUGS**

Has no intuition, output will require some hand editing to obtain perfection.

**AUTHOR**

Mary Ann Brennan

**NAME**

mkdirs – (css) make missing directory path components

**SYNOPSIS**

**mkdirs** *dirname* [ *dirname* ... ]

**DESCRIPTION**

**Mkdirs** checks if each component of the paths named on the command line exists and makes each missing component if possible. If any component directory can't be made, **mkdirs** prints a message and exits. Some paths may be made before the error is encountered. Paths that already exist may be named on the command line without dire consequences. If a path is an existing ordinary file, mkdir will quit without harming the file (and without processing other paths). The paths may be rooted (beginning with a "/"), or relative to the current directory. The exit status will be 0 if all is ok, -1 if there is a problem in making a path, or 2 if there isn't at least one path listed on the command line.

**AUTHOR**

M. A. Brennan

**NAME**

**plotarr, prwave, wdisp_this** – scripts for making hardcopies of waveforms

**SYNOPSIS**

**plotarr** *prefix origin lat lon depth tb ta*
**plotarr** *prefix –a aprefix tb ta*
**plotarr** *prefix –o oprefix tb ta*
**prwave** *prefix*
**wdisp_this** *prefix start_pt num_pts start_rec end_rec*

**INPUT**

wfdisc, waveforms, arrival window and either origin or arrival information

**OUTPUT**

hardcopies of waveforms

**DESCRIPTION**

This set of scripts can be used to automatically plot arrivals on the laserprinter, given a wfdisc, waveforms, a time window, and origin or arrival information. The script most commonly used is **plotarr**, which calls the other two scripts and the program **vwave(1)**. Note that there are 3 alternative ways to call **plotarr**, depending on whether you want to specify the arrival via origin information on the command line, or with an .arrival file, or an .origin file.

**plotarr origin info on command line**

In this mode, **plotarr** requires 7 command line arguments, a .wfdisc, and .w files. An example input line of **plotarr** is

plotarr 88313 1988/313/8:17:54.400 +36.575 +22.659 54.0 30. 60.

where prefix = wfdisc prefix
ORIGIN = the origin time of the event
lat = latitude (+=N & -=S)
lon = longitude (+=E & -=W)
DEP = depth of event
tb = time before the P in seconds.
ta = time after the P in seconds

The 7 command line arguments specify the .wfdisc prefix, origin information and time window around the first arrival. The script creates a virtual wfdisc about the first P-type arrival with a call to **vwave(1)**. This new .wfdisc will have the same prefix as the original .wfdisc, except there will be a "v" appended to the prefix. **plotarr** then calls **prwave**(1), which prints out the waveforms specified in the new .wfdisc. The new wfdisc will remain after **plotarr** exits.

Note that in this form **plotarr** takes the same arguments as the Boomer GET scripts, except that the GET scripts' time window specifies the data you want to dearchive, while the **plotarr** time window defines the time before and after the first arrival that you want displayed.

**plotarr with .arrival file information**

In this mode, **plotarr** requires 5 command line arguments, a .wfdisc, a .arrival, and .w files. An example input line of **plotarr** is

plotarr 88313 -a 88313b 30 60

where prefix = wfdisc prefix
−a specifies that an arrival file is to be used
aprefix = .arrival file prefix
tb = time before the P in seconds.
ta = time after the P in seconds

The command line arguments specify the .wfdisc prefix, the .arrival prefix, and the time window around the first arrival. The script creates a virtual wfdisc about the first P-type arrival with a call to **arseg**(1). This new .wfdisc will have the same prefix as the original .wfdisc, except there will be a "v" appended to the prefix. **plotarr** then calls **prwave**(1), which prints out the waveforms specified in the new .wfdisc. The new wfdisc will remain after **plotarr** exits.

**plotarr with .origin file information**

In this mode, **plotarr** requires 5 command line arguments, a .wfdisc, an .origin file, and .w files. An example input line of **plotarr** is

plotarr 88313 -o 88313b 30 60

where prefix = wfdisc prefix
−o specifies origin file is to be used
oprefix = .origin file prefix
tb = time before the P in seconds.
ta = time after the P in seconds

The command line arguments specify the .wfdisc prefix, the .origin prefix, and the time window around the first arrival. The script creates a virtual wfdisc about the first P-type arrival with a call to **vwave(1)**. This new .wfdisc will have the same prefix as the original .wfdisc, except there will be a "v" appended to the prefix. **plotarr** then calls **prwave**(1), which prints out the waveforms specified in the new .wfdisc. The new wfdisc will remain after **plotarr** exits.

**prwave**

**prwave**(1) is a script that takes one argument, a wfdisc prefix. The wfdisc is sorted according to the number of samples, time, station, and channel. The waveforms are then plotted on the laserprinter with **wdisp(1)**. The script **wdisp_this**(1) runs **wdisp(1)** in batch mode (-b option). **prwave**(1) will plot up to 30 waveforms per page on the laser printer. All points for each .wfdisc entry will be plotted. If there are more than 10,000 points in the waveform, multiple pages will be plotted, with the x value set to 10,000 for each page. If there are less than 10,000 points in the .wfdisc entry, then the x scale will be determined by the number of available points. Less than 30 waveforms per page will be plotted if 1) the number of samples in adjacent .wfdisc entries differs by more than 20% of the largerst value of *nsamp* in the wfdisc (this value is the variable *Tolerance* in the script), or 2) if the end of the .wfdisc is encountered. As **prwave**(1) runs, it will echo back where in the .wfdisc it currently is, and will identify where pages will be printed.

**prwave**(1) allows the user to have only 1 job at a time in the laser printer que. The motivation behind this is to prevent filling up the spooling area.

**NAME**

plotxy – a simple plot program

**SYNOPSIS**

**plotxy [plot | ps | both]**

**INPUT**

standard in

**OUTPUT**

UNIX plot file and/or postscript file

**DESCRIPTION**

*Plotxy* is a program for generating graphs from data files with a minimum amount of fuss. This program produces files which can be displayed on a graphics device or printed a laser printer. If the command line argument *plot* is given, a binary UNIX plot file is created, which will have the default name MYPLOT. This file can be displayed on a Sun workstation running suntools with the comand "sunplot MYPLOT", or the file may be printed on a laser printer with the command "plot -Ttek MYPLOT | ipr -t". Alternatively, the command line argument *ps* causes PostScript file to be produced, which will have the default name MYPLOT.ps. This file can be displayed on a terminal running NeWS with the command "psview MYPLOT.ps", or it can be printed on the laser printer with the command "ipr MYPLOT.ps". If the command line argument *both* is given, both types of output files will be produced. The main reason why there are two file formats is that the UNIX plot format does not support different line thicknesses.

In the simplest case, it is assumed that data points have been generated as x-y pairs in a file written with a formatted FORTRAN write statement (or perhaps saved in a COMO file); the program reads the file, and plots y as a function of x, interpolating with straight lines; axes are automatically assigned with reasonable limits and annotations. All this can be done with the three commands

```
READ
PLOT
STOP
```

Here a data file with the name XYDATA has been read format-free (that is with * instead of a format). An output file named MYPLOT has been constructed; it may be plotted in any of the standard ways (pen-plot, Versatec plotter, CRT). As documented in the rest of this write-up, it is possible to add embellishments of considerable complexity: for example many series on one plot, plotting of symbols at the points, cubic spline interpolation of continuous curves, logarithmic scales, error bars, titles, axis-labels and all the other common desiderata.

The program operates in a command mode; this means that you are not prompted at the console, but instead you type simple commands instructing the program which options are needed. Almost every option has a default value, so that if nothing is mentioned about a particular parameter the default is taken: for example the default plotting scales are linear in x and y. Once a particular option has been invoked, it remains in force until altered. The advantages of this approach are that great flexibility is available but a minimum of typing is required and no rigid order is demanded of the typist. The last factor makes the program very easy to use in batch mode, in constrast with prompting systems where one must remember the questions and the branches taken by the program during execution.

**wdisp_this**

**wdisp_this**(1) is a script that runs wdisp(1) in batch mode. An example input line of **wdisp_this** is

wdisp_this 88313 1 20 0 5000

where prefix = wfdisc prefix
where start_pt = starting point in wfdisc to plot
where num_pts = number of points in wfdisc to plot
where start_rec = line number of first wfdisc entry to plot
where end_rec = number of lines from wfdisc to plot

Note that these arguments are the same as when **wdisp** (1) is run once interactively.

**SEE ALSO**

Center for Seismic Studies
Database Structure
Version 2.8
arseg(1), vwave(1), wdisp(1)

**DIAGNOSTICS**

**CAVEATS**

The current defaults of this program are still experimental, and any feedback would be appreciated. Therefore, they are subject to change.

**AUTHOR**

*John Coyne*

## Basics

Upon execution the program prints the single prompt:
ENTER READ AND PLOT COMMANDS
Now you must type commands selected from the catalog below; each command begins in the 1st column of a new line; it may be followed by some literal or numerical parameters, which must be separated from the command word by a space. Any command may be abbreviated by its first four characters.

To read data from an external disk file there are a number of commands that define the attributes of the data to be input; an obvious example is the name of the disk file, defined by FILE, another the format of the numbers defined by FORMAT; other input attributes are things like whether this data set is to be connected with a smooth interpolating curve (SMOOTH) or to be plotted as individual points (SYMBOL). Having set up all the necessary specifications of the input, you actually perform the reading with the READ command. Another data series may be read from the same or a different file, simply by resetting the input attributes as required, and using READ again. All the parameters remain in force from the previous read unless they are specifically altered. Each of these data series with its different properties is accumulated in memory ready to be plotted.

Plotting is accomplished with PLOT. Actually all that is done by this command is to create the file MYPLOT which must be displayed with one described above. There are a number of parameters that apply to the whole plot, which may be set before invoking PLOT. For example, there are the x and y axis labels (XLABEL, YLABEL) and the plot title (TITLE). The physical size of the plot will default to 9 inches in x and 7 in y; the limits of the plot will default to values slightly larger than the extremes found in the series. These things can be over-ridden using XLIMIT and YLIMIT. When all the data are strictly positive, logarithmic scales can be set with LOGXY.

Before typing PLOT it is often wise to inspect the series and the way in which the data are going to be interpreted. This is done with STATUS, which provides a brief synopsis of each data series and the current parameter settings.

Additional graphs may be created by reading in more data and invoking PLOT again as often as necessary. To terminate the program just type STOP. After you have entered STOP, the program makes a file called MYPLOT (or something else if you used OUTPUT).

## Command Catalog

The commands are given their full English names here (though only four characters are needed). Parameters that may be omitted are enclosed in square brackets in this list. Lower case letters stand for numerical values, except where they obviously indicate names of things (e.g. filename). A list containing slashes denotes a set of possible items. The characters following the first blank after the command word itself are

termed the 'command field'.

AFFINE [a b c d]
Transforms the x and y coordinates of the next (and subsequent) data series to be read according to new(x) = a*x + b, new(y) = c*y + d. (This is an affine transformation).
Blank command field a=1, b=0, c=1, d=0

CANCEL [n]
Removes the last n data series read into memory. If no series has been read in, do nothing.
Blank command field n=1

CHARACTER h [angle]
Change the height of the lettering in titles, labels and axis-numbering to h inches. The new value applies to the next piece of text to be read, so that different height letters can appear in the title, the axis notations etc. The optional parameter angle specifies the angle at which text will be plotted in the next NOTE.
Default h=0.15, angle=0

DASH [s1 s2]
Plot the next data series to be read in as a dashed line, with visible segments s1 inches long and missing segments s2 inches long (note DASH is an input attribute applying to the next data to be read). To return to an unbroken curve, set s1=0.
Default s1=0, s2=0
Blank command field s1=0.2, s2=0.1

FILE filename
Defines the file name of the external disk file from which data are to be read; or the symbol *, which implies read from the console. The name must consist of 6 or fewer characters. After this command the next READ statement will begin at the beginning of the file.
Default =XYDATA
Blank command field = Rewind existing file

FORMAT (format specifier)
Defines a format for reading the next data series from an external disk file. The format specifier may be (1) a normal FORTRAN format specifier enclosed in parentheses (2) the character * meaning 'format-free' reading (3) the character B meaning a binary read. In each case the data are read with a single FORTRAN read statement of the appropriate type. Usually, if the numbers can be unambiguously read by a person without the need to skip certain columns or other tricks, there is no need to use an explicit format - the default * will work. Never use an I format because values are stored as REAL variables; thus a number written with I4 must be read with an F4.0 format. Always remember the space after the word FORMAT and the parentheses.
Default =*
Blank command field = *

FRAME [ON/OFF/NONE]

If ON causes two more sides to be added to the axes to complete a rectangular frame around the plot. OFF cancels the surrounding box and returns to the normal situation with two orthogonal axes. NONE specifies the total absense of axes and frame.
Default OFF
Blank command field = ON

HELP
Lists the four-letter abbreviation of all the commands. This may remind you of a name you have forgotten.

LNWT n
Specifies the line thickness for the next plot. The integer n may be any integer greater than 0. Each successive integer gives a progressively thicker line, where the increment is about 1/200 of an inch. Note that this option only works for PostScript files.
Default n=1

LOGXY [n]
Specifies the type of scales for the next plot. The integer n may be 0, 1, 2, 3, meaning: 0 both x and y are linear variables; 1 implies that x is logarithmic; 2 means only y is logarithmic; 3 means both x and y are logarithmic.
Default n=1
Blank command field n=3

MODE n [x0 dx]
Defines how the input data are grouped in the next and subsequent reads. The integer n may be 1, 2, 3, -3, 4: 1 implies data are simply consecutive y values with uniformly increasing x values beginning at x=x0 increment dx; 2 means data are x y pairs; 3 means data are x y z triples in which z is taken to be the uncertainty in y (thus a bar is plotted between y-z and y+z). -3 means use third member of data group as an uncertainty in the x-value. A symbol may be plotted at the actual value of y itself if SYMBOL is set; to insure the absence of a symbol put s=0 in SYMBOL. When MODE is 4 the x and y data must be read by separate READ commands, the x series being input first. The series length is that of the x series.
Default n=2
Blank field after n=1, x0=1, dx=1

NOTE (x y [IN]) text
NOTE (p q x y [IN]) text
Reads the characters of text to be plotted on the graph at the coordinates x,y. If the optional IN appears the coordinates refer to the bottom left corner of the first text character, measured in inches from the intersection of the axes; otherwise x,y are in the units of the graph. Notice that the parentheses surrounding the coordinates are mandatory. The height of the plotted characters is the value h in the most recent CHARACTER command. Similarly the angle the text makes with horizontal is the one previously set in CHARACTER. Up to 20 separate notes may be input. To clear the notes enter NOTE and a blank command field. If four coordinates instead of two appear in the parentheses, an arrow is drawn

with its tip at p,q and its tail near the text, which is plotted as before with x,y at the bottom left of the first character. The text is always horizontal with this option.
Blank field = delete old notes

OFFSET [dx dy]
When several similar data series are to be displayed together it is often convenient to introduce a displacement between them to clarify the picture. Thus if dy is nonzero at plotting time, the n-th series will be plotted with values of y + (n-1)*dy, where y is the input value. Similary with dx. When a logarithmic scale is used, the data are plotted as y*10**((n-1)*dy) to preserve equal apparent displacement on the graph. Notice all the series are displaced whenever OFFSET is invoked; for a more flexible method of offsetting data see AFFINE.
Default dx=0, dy=0
Blank command field dx=0, dy=0

OUTPUT filename
Defines the name of the plot file to be filename, which must be composed of 6 or fewer characters. This command may be used only once and must appear before the first PLOT command.
Default = MYPLOT

PLOT [x0 y0]
Creates the next complete graph containing all the data series that are currently in memory. Unless a SAVE command has been used, the plotted series are the ones read in since the last PLOT command or, if this is the first such command, all the series. A plot file is generated named MYPLOT, unless you have set a different name with OUTPUT. Usually PLOT is invoked with a blank command field but, if x0 and y0 are specified, the new graph is plotted with its origin at those coordinates in inches relative to the previous plot origin. The plot origin for these purposes is the place where the annotated axes cross, not the point (0, 0).

READ [n]
Performs the reading of the external disk file according to the specifications in force at this point. Each READ instruction is performed with a single FORTRAN READ statement with an implied DO; this means many data may appear on a single line in formatted files. With binary files only one binary record is read with every READ command. The integer n is the number of points to be read from the file, but if n is absent the file is read to the end of file (eof). When the eof is not reached, the file remains open and ready for further reading beginning at the next un-read record (i.e. the next line in formatted or COMO files); if the eof was reached, another read on this file will begin at the beginning. Up to 100 separate data series may be present at any one time. Note n must be explicit if FILE = *.

SAVE
After a PLOT command, the series in memory are normally erased ready for new data. To prevent this, the command SAVE must be entered before the next READ statement. If no additional data are to be read in, there is no need to use SAVE because the previous data are available for plotting in

this case.

SMOOTH [ON/OFF]
Decides whether continuous curves of y against x are interpolated with straight lines (SMOOTH OFF) or natural cubic splines (SMOOTH ON). This command is an input attribute, applying to the data to be read, not to the whole plot. SMOOTH ON will cancel a SYMBOL command and vice versa. SMOOTH OFF reverts to SYMBOL mode if that was the previous style of plotting (using the same symbol number and height as before). The series is re-ordered if necessary to make the x sequence an increasing one. Note that the automatic plot limits use the original data series, not the smoothed values, so that sometimes pieces of a SMOOTHed curve may be lost off the top or bottom of a graph even when you have let the program find its own limits.
Default = OFF
Blank command field = ON

SKIP [n]
Skips the next n records in the current file. With formatted files this means skipping n lines. The command examines the current read FORMAT to determine whether the current file is binary or formatted. Although skipping can be performed by including slashes in a format specification it is often more convenient to use SKIP.
Blank command field n=1

STACK
Causes the next complete graph (including axes, titles etc) to be drawn above the previous one with enough space to give a pleasing appearance. To stack several curves on one graph see AFFINE or OFFSET. This command is turned off internally after PLOT to prevent accidental plotting off the top of the paper. A more flexible way of organizing the relative positions of several complete graphs is by means of PLOT with origin parameters.

STATUS
Lists a convenient synopsis of the currently available plot series (their lengths, extreme values and other attributes), the current plot and reading parameters, and the number of words available for further data series. You should always use STATUS before plotting.

STOP
Closes the output file and brings program to an orderly halt. This must always be the last command of any run, otherwise part of your plot will be lost.

SYMBOL n s
Defines the next input series to be a set of discrete points with symbols rather than a curve. The height of symbol is s inches, the type of symbol defined by the integer n: 0 square; 1 triangle; 2 octagon; 3 diamond; 4 plus; 5 asterisk; 6 cross; 7 slashed square; 8 up-arrow; 9 hourglass. The value of n may be used to reset the input of continuous data: n=-1 means next data read will be continuous with straight line interpolation; n=-2 means go to cubic-splined curves.

Default n=-1, s=0

TITLE text
Specifies a title for the plot. This must be 80 or fewer characters. A blank command field cancels the previous title and leaves the next plot untitled.
Default text=blanks

XLABEL text
Specifies a label to be written under the x axis. See TITLE for other details.
Default text=blanks

XLIMIT xlength x1 x2
Defines the length of the x axis, xlength, in inches and the lower and upper limits of x: x1, x2. All plotted points will have values inside (x1, x2); those outside are omitted from the plot. If x1=x2=0, the x extremes will be chosen to encompass the values in the data series. This is a plot attribute, governing the behavior when PLOT is invoked.
Default xlength=9, x1=x2=0

YLABEL text
Same as XLABEL but for the y axis.
Default text=blanks

YLIMIT ylength y1 y2
Same as XLIMIT but for the y axis.
Default ylength=7, y1=y2=0

Defaults

AFFINE a=c=1, b=d=0
CHARSIZE 0.15
DASH s1=s2=0
FILE XYDATA
FORMAT *
FRAME OFF
LOGXY 0
MODE 2
OFFSET dx=dy=0
OUTPUT MYPLOT
SMOOTH OFF
SYMBOL n=-1, s=0
TITLE blanks
XLABEL blanks
XLIMIT xlength=9, x1=x2=0
YLABEL blanks
YLIMIT ylength=7, y1=y2=0

Friendly Advice and an Advanced Example

If you don't want to be fancy the cardinal rule is to prepare files

for input that represent what you want to plot in a direct manner (usually x-y pairs of coordinates). When the data you have is not in this form, the easiest thing to do is to doctor them with the editor. Either write out your data with formatted write in FORTRAN or, better still, simply keep a record of what went to the screen in a COMO file. Unless you really know what you are doing (most people don't) never use binary data files. Having got your data into x-y pairs, just read them format-free, which is the default. DO NOT make use of the FORMAT command of *plotxy* unless you must; the default format-free read works well and will take care of you unless you have data in peculiar arrangements (for example, no spaces between numbers or x and y coordinates in reverse order).

Now for a more complicated example of what can be done; it is intended for the advanced user and to show off the beautiful work of which *plotxy* is capable. Below is a listing of a file called ADMITS containing data; the first column is a frequency, the second the experimental result, the third its estimated error, the last the theoretical prediction. We wish to plot up these data as a function of frequency, putting error bars on the observational points and a smooth curve through the theoretical ones.

| OMEGA | ADMITTANCE | ERROR | THEORY |
|---|---|---|---|
| 0.5000 | 0.3328 | 0.2750E-01 | 0.3322 |
| 1.500 | 0.2365 | 0.2750E-01 | 0.2257 |
| 2.500 | 0.1909 | 0.2200E-01 | 0.1837 |
| 3.500 | 0.1595 | 0.1570E-01 | 0.1522 |
| 4.500 | 0.1369 | 0.1830E-01 | 0.1272 |
| 5.500 | 0.1190 | 0.1750E-01 | 0.1074 |
| 6.500 | 0.1037 | 0.1690E-01 | 0.9193E-01 |
| 7.500 | 0.8892E-01 | 0.1460E-01 | 0.7990E-01 |
| 8.500 | 0.7312E-01 | 0.1290E-01 | 0.7050E-01 |
| 9.500 | 0.5486E-01 | 0.1300E-01 | 0.6311E-01 |
| 10.50 | 0.3300E-01 | 0.1170E-01 | 0.5723E-01 |

First we skip the heading line. We read the data with a format that picks off the columns we require. The file is read twice: first for the data with their errors, next for the theoretical points. The first read picks off the frequencies, data and error bars; this is done with MODE 3 and an appropriate format. Then we set SMOOTH and read the file again with a format that picks the theoretical results and the frequencies. The data are positive and cover a wide range, so we try log y axis.

```
> plotxy
FILE ADMITS
FORMAT (3F15.0)
SYMBOL 2 .04
MODE 3
SKIP
READ
FORMAT (F15.0, 30X, F15.0)
SMOOTH ON
MODE 2
SKIP
```

```
READ
STAT

LOGXY 2
TITLE \ITA\Observed and theoretical admittance
XLABEL Radian frequency  \omega\  ks\sup{-1}
YLABEL Admittance  c  10\sup{6}m
XLIM 6 0 0
YLIM 4 0.01  1
FRAME
PLOT
STOP
```

Note that the x limits have been left unspecified and that we used STAT before plotting to verify the series and parameters are satisfactory. The italic font was selected in the title and this pertains to the whole graph. In the labels Greek letters and superscripts have been used.

## Cautions and Notes

This program is not bullet-proof in the sense that a few things you can do will cause it to crash. Examples include unintelligible formats or nonexistent input files. A common problem is with formats not matching the data; the program will usually detect this type of error, reject the whole series and then issue a warning. Mis-read data can result in incorrect values being stored; this may perhaps be detected before plotting by looking at the extreme values of each input series, something given by STATUS. Strange pictures result if you forget that AFFINE parameters are still in force. Also be sure to read the FORTRAN manual carefully about the rescanning of FORMAT statements if your input file is longer than the number of items in your FORMAT statement. Attempting to plot negative data on a log scale will not cause a crash - an error message is printed and the offending scale is made linear instead of a logarithmic. Some errors are harmless, like mis-spelled commands.

If you have explicitly set plot extremes with XLIM and YLIM and a data value falls outside the window, when SMOOTH is ON the program draws a piece of curve between the last captured point(s) and the edge of the graph in the direction of the invisible point. When SMOOTH is OFF the pen is simply lifted until onscale data are encountered. This allows you to insert breaks in your data records by using large values.

With this version of *plotxy* you can change the font in which the titles, labels, notes etc. are written. The names of the fonts are SIMPLEX, COMPLEX, ITALIC, DUPLEX; the default is the single-line SIMPLEX. To get any of the others in a text string (such as a title) enclose the first three letters of the name in back-slashes, e.g. \ITA\ of \DUP\ ahead of the text. The font remains in force until explicitly changed. The axis numerals are in the same font as the title. You may also get Greek letters by enclosing their names in back-slashes, as \GAMMA\ or \lambda\; upper case Greek appears when the English name is upper case. Superscripts are possible with the construct \sup{...}, so that x-squared is rendered x\sup{2}. (The superscripted expression is enclosed in curly

braces. These characters are garbled on line printer output.) Similarly with subscripts. There is a little problem with getting back-slashes inside the editor - you must either change the tab symbol, which is back-slash by default, or type a different character (e.g. @) and use the change command (C) to transform @ to \. For more information on the fancy character set see the write-up of the fancy SYMBOL routine.

**SEE ALSO**

plot(1G), plot(5), sunplot(1)

**DIAGNOSTICS**

Intended to be self-expanatory.

**CAVEATS**

The default physical size of the output is not exactly 9 by 7 inches. Hardcopies from the plot files and PostScript files are almost identical. For increases line thickness greater than 7, the line thickness does not necessarily increase with every integer increment. This is not critical, however, since each integer increment results in a very small increase in line thickness. In order to distiguish between lines, the integer increment should be at least 5.

**AUTHOR**

Loren Shure and Robert Parker
Modified by John Coyne

**NAME**

polarfilt – polarization filtering of three-component seismograms

**SYNOPSIS**

**polarfilt**

**INPUT**

Center for Seismic Studies formatted .arrival, .wfdisc and .w files.
Input parameters from pfilt.in, described below.

**OUTPUT**

Output consists of original and polarization filtered seismograms plotted on the screen.

**DESCRIPTION**

This program performs polarization filtering of three-component seismograms by passing rectilinear (body-wave) motions. A vector filtering is applied to the polarization ellipse in order to pass linear motion with a specified orientation. The signals are decomposed into short time windows and narrow frequency bands. The analysis is done seperately in each band and time window, with the results summed together. The processing is done in data segments at detection times as determined by the first record of the .arrival file. The sampling rate, number of samples, station, channel, and calibration information are obtained from the .wfdisc file.

**OPTIONS**

The segment length, frequency band, time and frequency resolution and orientation of linear pass motion are options.

**FILES**

The following is an example of the input file *polarfilt.in:*

```
12345678901234567890123456789012345678901234567890   <1>
/b/coyne/projects/find/polarfilt                      <2>
88230                                 <3>
    fc1     fc2   fcycles norder          <4>
    0.7     3.0     4.0   4          <5>
  seglen   tcycles  segdetect                       <6>
   30.0     4.0      6.0                  <7>
  apert     rect    azimuth  incidence    <8>
   20.0     1.0    318.9     18.5         <9>
 stname                                                    <10>
 NRA0                                                      <11>
```

Note that the numbers in brackets on the right hand side are for use only in the following discussion and do not exist in the input file.

Line <1>

numbers used in helping to format the input; a blank line may be substituted,

Line <2>

directory of local CSS database,

Line <3>

prefix of local CSS database,

Lines<4,6,8,10>

description of the following line, a blank line may be substituted,

Line <5>

fc1, fc2: frequency interval for analysis, fc1 < fc2 This inverval will be

broken into a number of sub-bands depending on the freq resolution. fcycles: resolution of frequency bands in # of cycles, use 2-6 norder: order of butterworth for bandpassing, use even order, 4 recommended (2 passes of filter made for zero phase)

Line <7>

seglen: length of time segment in seconds tcycles: resolution of time window in # of cycles, use 3-8 segdetect: locate detection time at 1/segdetect of seglen

Line <9>

apert: aperture parameter of form cos**apert for controling width of 'opening' to pass rectilinear motion. rect: parameter for scaling output according to degree of rectilinearity: (1-ev1/ev2)**rect. azimuth: azimuth of pass rectilinear motion from north in degrees. incidence: incidence of pass rectilinear motion from vertical in degrees.

Line <11>

stname - station name as specified in *.wfdisc* file.

**SEE ALSO**

Center for Seismic Studies Data Base
Structure, Relations, Attributes and
Tape Formats August 1984

**AUTHOR**

Andy Jurkevics

**NAME**

**r2** – Reads GSE Level II data files.

**SYNOPSIS**

**r2** [-i input_file] [-p db_prefix [-c][-n]] [-h]

**INPUT**

**R2** will accept input filename from the command line or use stdin if no input filename is given.

**OUTPUT**

**R2** will create a Center version 2.8 waveform database unless instructed to simply check the input data.

**DESCRIPTION**

*R2* reads its input and depending on what type of data section its reading will create .wfdisc and .w files and/or .extra files. Information in the WEX and CAL sections of a GSE Level II message are output into the .extra files. Data from WID and DAT sections make up .wfdisc and .w files respectively. On errors, *r2* will exit with a negative number if the error is due to some violation of the GSE format laid down in GSE/Japan,US/1. Positive numbered errors are command line argument errors, file open errors and the like. *R2* is very forgiving and can read data files with or without newlines. Files without newlines are assumed to have the maximum line length of 80 characters.

**OPTIONS**

-i input_file
names the GSE Level 2 input file (stdin default)

-p db_prefix
is the prefix of database to be created, if db_prefix isn't given it means check input for errors only, create no output

-c means read db_prefix.counter for value of nxwfid

-n supresses the creation of waveform files

-h help option, provides a syntax summary message

-c requires -p

**EXAMPLE**

```
% r2 -h          # r2 with -h argument gives a help message
usage: r2 [-i input_file] [-p db_prefix [-c][-n]] [-h]
input_file is GSE Level II file (stdin default)
db_prefix is prefix of database created
no prefix means check input for errors only, create no output
-c means read db_prefix.counter for value of nxwfid
-n supresses the creation of waveform files
-h prints this message
% cat file* | r2 -p       # r2 can check data from multiple files
% r2 -i file -p foo       # r2 will create a database foo
% r2 -i file -p foo -c    # r2 will read foo.counter for the value nxwfid
```

**AUTHOR**

Michael Anthony Tiberio

**REFERENCES**

GSE/Japan,US/1 Section 5

Center for Seismic Studies

Database Structure
Version 2.8
(Note that r2 was written for Database Version 2.7, but nothing used by r2 was changed from 2.7 to 2.8.)

**NAME**

recall – restores suncore vector segments saved in disc files

**SYNOPSIS**

**recall** *segment_file*

**INPUT**

segment file

**OUTPUT**

Screen displayed of the saved segment.

**DESCRIPTION**

*Recall* restores suncore retained (vector) segments which have been saved in disc files. The name of the retained segment file is given to recall as a command-line parameter. The resulting plot is scaled to the current dimension of the Suntools window.

**SEE ALSO**

fk (1c)

**NAME**

riffle – riffle or leaf through a series of raster screen image files

**SYNOPSIS**

**riffle** *table_file*

**INPUT**

A table containing the file names of the raster file images to be displayed.

**OUTPUT**

A display of the files listed in *table_file.*

**DESCRIPTION**

*Riffle* allows a rapid inspection of raster file images by sequentially displaying them each time the return key is struck. The order of the display is defined in *table_file* in the same directory. The raster file images are produced by the command *wpix.*

*Riffle* must be run within a Suntools window.

**SEE ALSO**

*wpix(1c)*

**NAME**

rdseed – Read an FDSN SEED format volume

**SYNOPSIS**

**rdseed inputfile -{a | c | d [list] | l | s | t | f file}**

**OPTIONS**

One of the following options must be provided:

**-a** retrieve the abbreviation dictionaries.

**-c** retrieve volume table of contents.

**-d** retrieve all or selected data, where selection is by list of starting record numbers.

**-l** list contents of each record in the volume.

**-s** retrieve all station and channel header information.

**-t** construct a list of all event start/stop times and starting record numbers.

**-f** *file* retrieve selected data, where seelection is by a list of starting record numbers given in *file*.

**DESCRIPTION**

**rdseed** reads a tape (or other input file) in the format defined by the Federation of Digital Seismographic Networks (FDSN), popularly known as the Standard for Exchange of Earthquake Data (SEED). According to the command line function option specified by the user, **rdseed** will read the volume and recover the volume table of contents (-c option), all or selected seismograms (-d option), the set of abbreviation dictionaries (-a option), or station and channel information and instrument response tables (-s option). Seismograms from the Center for Seismic Studies version are written in Center format **wfdisc** and **.w** file formats. Other Center files are also created. [Seismograms from the IRIS version are written in SAC binary format (Tull, 1987).]

Two additional options allow access to detailed information concerning the actual contents of the volume (rather than reading files purporting to contain such information from the volume, for which one uses the -c option). The first of these options (-t) writes out a list of data event start and stop times along with the starting records at which those data may be found. (For the purposes of this discussion, an **event** is defined as a set of station/channel/time continuous data records.) The other option (-l) is primarily a diagnostic tool; it writes a description of every record on the volume.

The source code is written in such a way that it will run, with recompilation, on both big-endian (e.g., Sun) and little-endian machines (e.g., VAX) under UNIX. This program has not yet been tested under VAX VMS.

**Recovering data from an FDSN SEED**

There are two necessary steps to recovering seismograms from a SEED tape.

The first step consists of finding out what is on the tape; one does this by using any of the command line options -c, -t, or -l, to list the station and channel names, starting times, and record numbers of the seismograms contained in the volume. Since the SEED writer implemented by the USGS can put table-of-contents information anywhere in a volume, and because the -t and -l options must scan the entire

volume, the wise user will redirect the output of these commands to files and run them in the background, as in examples 1-3 below. The times option (-t) and the list option (-l) exist to give the user the choice of performing a run-time determination of the contents of a volume to compare with the on-volume table.

Seismic data are recovered from SEED tapes in the second step. The command sequence to recover selected seismograms from a volume is

**rdseed inputfile -d record1 record2 ...**

where record1, record2, and so on are the starting record numbers taken from the volume table of contents created in the previous step. If the user wants **all** the data from a particular tape, no record numbers should be specified, i.e., the command sequence is

**rdseed inputfile -d**

Alternatively the data may be recovered using the **-f** *file* option by placing the desired record numbers in the *file* instead of on the command line as with the **-d** option. This is useful if you plan to retrieve a lot of data at once, awk scripts can create the *file* from the output of the **-l** [or **-t**, see bracketed comment below] option. In this way the only limit to the number of records is the disk space available, not the shell command line buffer size. [This follows the -d option convention regarding whether the just starting record numbers are needed or all record numbers for a seismogram. An earlier version required the latter, this man page suggests the former, I haven't determined which is correct. – MAB]

Seismogram files are written to the current directory with names of the form

yyyy,ddd,hh.mm.ss.ffff.SSSSS.CCC

where yyyy is the year, ddd is the Julian day, hh.mm.ss.ffff is the time of day of the start of the first record, SSSSS is the station name, and CCC is the component name for the particular seismogram being recovered. This seismogram file naming convention was chosen to provide unique names to output files without user intervention; however, the large number of files which can be generated to a single directory might cause problems for some operating systems. It is be possible to alter the name construction so that subdirectories of common starting time ranges or stations were created; output file name construction is performed in routine css_output_data.c.

**Recovering auxiliary data from an FDSN SEED volume.**

One may also retrieve the set of abbreviation dictionaries or the set of station information tables from an FDSN SEED volume. The former is accomplished with the command

**rdseed inputfile -a**

while the latter results from

**rdseed inputfile -s**

Output from these commands should be redirected to files, as in examples 6 and 7.

## DIAGNOSTICS

Various warnings and error messages are issued to the standard error device by the procedure. Typical response of the procedure to a warning condition is to write a message to the standard error device and then to continue execution. An error condition, on the other hand, will cause a message to be generated to the standard error device followed by immediate termination of the procedure.

## EXAMPLES

1. Reading the table of contents from a volume.

rdseed /dev/rmt8 -c > tape.contents &

reads the table of contents from the tape on device /dev/rmt8 into a file called

tape.contents; the job is run in the background. Output directed to "stderr", such as error messages, comes to the terminal. Table-of-contents entries have the format

AFI LPZ 1988,228,00:00:00.68 1 147

where the columns represent station name, channel name, start time, location flag (here, a blank), subsequence number, and starting record number.

2. Determining event start/stop times on a volume.

rdseed image -t > image.times &

reads a disk file called "image" and creates a table containing station and channel names, start and stop times of events, numbers of samples, sample rates, and starting record numbers for that file. Output is written to the file "image.times". The lines of the output table have the format

ANMO LPZ 1988,230,00:00:00.6800 1988,230,18:35:04.6800 1.00 66904 119

where the columns represent station name, channel name, start time, end time, sample rate in samples per second, number of samples, and starting record number for these data.

3. Creating a detailed list of the contents of a volume.

rdseed /dev/rmt11 -l > tape.list &

reads a tape on drive mt11 and writes a list of the contents of each record to a file called tape.list. The job is run in the background.

4. Reading all data from a tape.

rdseed /dev/rmt8 -d >& tape.extraction.list &

reads all seismograms from the tape on device /dev/rmt8 into the current directory, writes both "stdout" and "stderr" output to a file, and runs the job in the background.

5. Reading selected data from a tape.

rdseed /dev/rmt8 -d 2704 3826 15688

reads the seismograms beginning at records 2704, 3826, and 15688 into the current directory, writes various messages to the terminal, and runs in the foreground. HINT: if many seismograms are to be extracted at once use the **-f** option.

6. Reading the abbreviation dictionaries.

rdseed tape.image -a > tape.abbreviation.dictionaries

extracts the abbreviation dictionaries from a tape image stored on disk, sends the result to a file, and runs in the foreground.

7. Reading station information.

rdseed /dev/rmt8 -s > tape.station.information &

recovers station and channel location and response information from the tape on device /dev/rmt8, writes the information to a file, and runs in the background.

**FILES**

yyyy,ddd,hh.mm.ss.ffff.SSSSS.CCC - seismogram files as described above

**SEE ALSO**

Halbert, S. E., R. Buland, and C. R. Hutt (1988). Standard for the Exchange of Earthquake Data (SEED), Version V2.0, February 25, 1988. United States Geological Survey, Albuquerque Seismological Laboratory, Building 10002, Kirtland Air Force Base East, Albuquerque, New Mexico 87115. 82 pp.

O'Neill, D. (1987). IRIS Interim Data Distribution Format (SAC ASCII), Version 1.0 (12

November 1987). Incorporated Research Institutions for Seismology, 1616 North Fort Myer Drive, Suite 1440, Arlington, Virginia 22209. 11 pp.

O'Neill, D. (in preparation). RDSEED Technical Reference Manual.

Tull, J. (1987). SAC User's Manual, Version 10.2, October 7, 1987. Lawrence Livermore National Laboratory, L-205, Livermore, California 94550. ??? pp.

**BUGS**

Physical and logical block sizes are fixed at 32768 and 4096 bytes, respectively.

The -d and -f options requires that record numbers be in ascending order.

-l and -t options leave a few garbage lines at the end of the list.

Address bug reports to Dennis O'Neill at IRIS, 703-524-6222, or send ARPAnet mail to denio@iris.css.gov, or OMNET mail to d.oneill/iris. Please DO NOT "fix bugs" locally without telling the author about them. **Please DO NOT redistribute this program.** Address requests for the program to IRIS at the numbers given above.

**AUTHOR**

Dennis O'Neill, IRIS
revised for the Center for Seismic Studies by M. A. Brennan

**NAME**

sac2css – Database conversion program

**SYNOPSIS**

**sac2css -s sac_file -p db_prefix [-h]**

**OPTIONS**

-h - show syntax of command

**DESCRIPTION**

sac2css converts a file readable by the LLNL Seismic Analysis Code program to a set of files conforming to Center for Seismic Studies standard waveform file (version 2.8) format. All work is performed in the current directory. If Center data files with the given prefix exist, sac2css will append the new wave form index records to the existing wfdisc file. Otherwise, sac2css will create a new wfdisc file.

A SAC file contains header information describing the source and receiver, along with other information, followed by waveform data. The SAC file format is completely described in the SAC user's manual.

Center waveform data files include one file with a name of the form *db_prefix*.wfdisc; and one or more files containing binary waveform data. The waveform files are indexed by the wfdisc records, i.e., the waveform files are named in the wfdisc records. **Sac2css** creates waveform file names of the form *db_prefix.###*.w, where *###* is a number. In addition **sac2css** creates a Center origin file with a name that looks like *db_prefix*.origin. These files contain Center format information about the waveforms (in *db_prefix*.wfdisc) and the event origin (in *db_prefix*.origin), and the waveform data.

This program creates only one waveform file per invocation; therefore, multiple invocations are necessary to convert a suite of SAC binary files. A Unix C-shell script which will convert a suite of SAC binary files to a set of Center files is

```
foreach f (sacfile1 [sacfile2] ...)
    sac2css -s $f -p db_prefix
end
```

The first invocation will create the Center *db_prefix*.wfdisc file, while subsequent invocations will append to the *db_prefix*.wfdisc file.

**EXAMPLES**

sac2css -s kurile1.sacb001 -p kurile1 - converts SAC binary file to Center format

**DIAGNOSTICS**

Very forgiving, will skip missing or unreadable waveforms.

**FILES**

*sacfile* - input, SAC format; binary waveform file
*db_prefix*.wfdisc - output, Center format; describes waveforms in the Center files
*db_prefix*.origin - output Center format; describes the event origin
*db_prefix.###*.w - output, Center format; waveform file; ### represents a number

**SEE ALSO**

css2sac (not installed)
SAC User's Manual, v10.2
SAC Command Reference Manual, v10.2
IRIS Interim Data Distribution Format Specification, v1.0
Center for Seismic Studies Database Structure, v2.8

**BUGS**

None known.

**AUTHOR**

Michael Anthony Tiberio

**NAME**

threecomp – plot station or array three-component particle motion attributes as a function of time

**SYNOPSIS**

**threecomp**

**INPUT**

CSS version 2.7 formatted *.wfdisc* and *.w* files. Input parameters, station names and coordinates are read from the file *threecomp.in*, which is described below.

**OUTPUT**

The first display consists of three component waveforms of the first station in the analysis list. A detection time is picked, which determines the position of the particle-motion attributes figure. Up to five attributes may be chosen. The time given in this figure refers to the start time for the figure.

The file *threecomp.out* is produced, which echos the data read from *threecomp.in.*

**DESCRIPTION**

*Threecomp* computes ground particle-motion attributes as a function of time and frequency for a time segment selected by mouse pick. Three-component seismograms are bandpassed and time windowed and the 3x3 covariance matrix is formed for each window. If there are multiple three-component sensors in an array, the covariance matrices from all sensors are averaged. The eigen problem is then solved for the polarization ellipsoid. Parameters describing the ground particle-motions as a function of time are extracted from the polarization ellipse in each time window. When an array of three-component elements is used, the azimuth and horizontal phase velocity of the plane wave may be input from the file *threecomp.in* in order to improve the time alignment of the time windows at the various sensors before averaging. The sampling rate, number of samples, station, channel and calibration information are obtained from the *wfdisc* file.

*Suncore* graphics routines are used.

**OPTIONS**

The data segment length, frequency band, time resolution, number of three-component stations and the particle-motion attributes to output are options defined in the file *threecomp.in.*

**EXAMPLE**

The following is an example of the input file *threecomp.in:*

```
12345678901234567890123456789012345678901 <1>
/b/andy/noress/86017                       <2>
86017                                      <3>
   azim      vel                           <4>
   225.0     6.0                           <5>
  fcenter  fcycles                         <6>
    6.0     1.5                           <7>
  seglen   tcycles                         <8>
   40.0     4.0                           <9>
attributes:                                <10>
  1  6  10  9  14                          <11>
 nstns                                     <12>
  4                                        <13>
SITE    NS(KM)   EW(KM)                    <14>
NRA0     .003     .004                     <15>
```

```
NRC4    -.657    .208          <16>
NRC7     .548   -.447          <17>
NRC2     .341    .603          <18>
```

Note that the numbers in brackets on the right hand side are for use only in the following discussion and do not exist in the input file.

Line <1>
numbers used in helping to format the input; a blank line may be substituted,

Line <2>
directory of local CSS database,

Line <3>
prefix of local CSS database,

Lines<4,6,8,10,12,14>
description of the following line, a blank line may be substituted,

Line <5>
azim: fk azimuth in degrees for aligning windows if using array of 3-comp sensors and vel: horizontal phase velocity in km/sec for aligning windows,

Line <7>
fcenter: center frequency in Hz for bandpassing and fcycles: controls the frequency resolution; bandwidth = fcenter/fcycles,

Line <9>
seglen: time segment length in sec in which to do analysis and tcycles: controls the time resolution; window length = tcycles/fcenter,

Line <11>
indices of the particle-motion attributes to display; up to five can be plotted simultaneously. The indices are as follows:

1 - 3-component amplitude
2 - amplitude of eigenvalue 1
3 - amplitude of eigenvalue 2
4 - amplitude of eigenvalue 3
5 - horizontal amplitude
6 - rectilinearity
7 - planarity
8 - ratio of eigenvalue 1 to eigenvalue 3
9 - horizontal to vertical ratio
10 - vertical to horizontal ratio
11 - flatness
12 - incidence of eigenvector 1
13 - incidence of eigenvector 2
14 - incidence of eigenvector 3
15 - sine of azimuth of eigenvector 1
16 - sine of azimuth of eigenvector 2
17 - sine of azimuth of eigenvector 3
18 - azimuth of eigenvector 1
19 - azimuth of eigenvector 3
20 - back azimuth from Rayleigh motion
21 - Hmax/Hmin where H is horizontal
22 - azimuth of Hmin
23 - azimuth of Hmax

Line <13>

nstns: number of 3-component stations to combine in covariance average, if single station use nstns=1; if N 3-component stations in array, use nstns=N. A maximum of four stations is allowed.

Lines<15...>

stname - station name as specified in *.wfdisc* file, x, y - station coordinates in km relative to the center of the array; x = north/south and y = east/west.

**DIAGNOSTICS**

*STOP: 2* error opening the local CSS database

*STOP: 4* error opening .w file

*STOP: 5* invalid data storage type for .w file. Only VAX integer and IEEE integer are recognized. *Threecomp* does not check that the integer matches the given machine.

Other error messages are intended to be self-explanatory.

**AUTHOR**

Andy Jurkevics
Center for Seismic Studies

**NAME**

wdisp – (css, graph, database) view .w formatted waveforms on a tektronix 4014

**SYNOPSIS**

**wdisp** [ **-b** ] [ **-t** ] [ **-d** *decimation_factor* ] *prefix*

**INPUT**

CSS version 2.7 formatted *.wfdisc* and *.w* files.

**OUTPUT**

labeled waveform plot

**DESCRIPTION**

*Wdisp* reads the file *prefix.wfdisc*, and displays on a tektronix 4014 any of the *.w* (waveforms) described by the *.wfdisc* file.

In interactive mode (default), *wdisp* prompts the user for
a. "the first waveform to plot" (as numbered by *wfdisc)*
b. "number of waveforms to display"
c. "number of samples to skip before displaying waveform"
d. "number of samples to display"

After each screen is drawn the user is prompted to continue or quit. If the **-b** option is given on the command line, the prompts are not printed, but the answers are read and those needed for interpreting the plot are explicitly printed on the screen. This is convenient when wdisp is run from a script that plots directly to the Imagen laser printer (batch mode).

The **-t** option prompts for segment specification by time rather than by sample number. The **-d** *decimation_factor* option allows the user to specify that every *decimation_factor*'th point will be displayed on the plot. This can significantly speed up the drawing process and when done with a bit of forethought doesn't significantly affect the presentation (i.e. 10000 points per plot exceeds the display resolution anyway, so there is no reason to draw them all).

**OPTIONS**

**-b** batch mode, no prompts printed

**-t** time mode, segments specified by time not by sample number

**-d** *decimation_factor*
decimate by the given decimation factor

**BUGS**

Must run program in the directory which contains the *.wfdisc* file.
The **-b** option wasn't tested with the **-t** option set and may not work properly with it.